LIÈGE université
Arlon Campus Environnement

Doctoral dissertation submitted in partial fulfilment of the requirements for the degree of Doctor of Science

Hydrogeomorphological approaches to understanding flood hazards and flood-risk management in northwest Rwanda

Déogratias NAHAYO

March, 2026

Thesis committee:

Prof. Dr. Bernard Tychon (Promoter, University of Liège)

Prof. Dr. Matthias Vanmaercke (Co-Promoter, Katholieke Universiteit Leuven)

Prof. Dr. Umaru Garba Wali (Local Co-Promoter, University of Rwanda)

The cover photos illustrate flow measurements, river cross-section surveys, and the Rubagabaga small bridge, which was damaged during the flood event of 2–3 May 2023.

Doctoral dissertation submitted in partial fulfilment of the requirements for the degree of Doctor of Science

Hydrogeomorphological approaches to understanding flood hazards and flood-risk management in northwest Rwanda

Déogratias NAHAYO

March, 2026

Members of the Jury:

Prof. Dr. Pierre Ozer (Chair, University of Liège)

Prof. Dr. Bernard Tychon (Promoter, University of Liège)

Prof. Dr. Matthias Vanmaercke (Co-Promoter, Katholieke Universiteit Leuven)

Prof. Dr. Umaru Garba Wali (Jury member, University of Rwanda)

Dr. Olivier Dewitte (Jury member, Royal Museum for Central Africa)

Dr. Emmanuel Rukundo (Jury member, Rwanda Water Resources Board)

Prof. Dr. Joost Wellens (Secretary, University of Liège)

Academic year 2025–2026

To my wife Marie Claire Uwakunzwe;

To my children:

Pascaline Uwayo;

Noeline Nuwayo;

Angelo Nduwayo;

To you;

Acknowledgements

My heartfelt thanks go to the individuals and institutions whose invaluable support made this Ph.D. journey—spanning over five years—possible. This thesis could not have been completed without their generous assistance during in-country fieldwork and throughout my time at the University of Liège.

I extend my heartfelt appreciation to my Promoter, Prof. Bernard Tychon, whose role went far beyond academic supervision. His day-to-day invaluable guidance, insightful feedback, and continuous encouragement were matched only by the care and support he offered throughout this journey. More than a supervisor—he was a mentor and a father figure—and his presence was instrumental in shaping both the quality of this work and my personal growth.

I am equally grateful to my Co-Promoter, Prof. Matthias Vanmaercke, for his constructive input, thoughtful suggestions, and support throughout the research process. His contributions have greatly enriched the scientific depth of this thesis.

Special thanks also go to my Local Co-Promoter, Prof. Umaru Garba Wali, for his close supervision, practical insights, and unwavering support on the ground. His involvement has been essential to the successful implementation of the research activities.

Beyond the above, I am deeply grateful to my three supervisors for their invaluable guidance during Ph.D. research reviews, committee meetings, and throughout the manuscript preparation and submission process until its acceptance. I also sincerely thank Dr. Olivier Dewitte for his constructive feedback, and Prof. Serge Schmitz, director of the SPHERES research unit, for facilitating the additional scholarship that supported this work.

I extend my sincere appreciation to the academic and administrative staff of the Faculty of Science, especially those from the Department of Science and Environmental Management at the Arlon campus—Nathalie Fossion, Thomas Barthel, Solofotiana Randresihaja, Moussa Eljaroudi, Joost Wellens, Djaby Bakary, Antoine Dennis, Jonathan Peereman, Hein Koufanou, Marie Lang, Antoine Corine, Françoise Dasnoy, and Sandrine Péché—for fostering a collaborative and intellectually stimulating environment.

I extend my heartfelt gratitude to the registration staff at the University of Liège, especially Madam Virginie Lemoine, who processed my initial registration and managed my file with care. I am also deeply thankful to the team at Partenariat, Coopération et Développement

(PACODEL), particularly Alexia Gusu and Clara Frognet, for facilitating my journey from Rwanda to Belgium and back, and for ensuring the timely provision of my scholarship.

My deepest thanks go to my Ph.D. colleagues—Bassolo Cyrille Baki, Ameni Mokhtar, Wièmé Somé, Dior Diallo, Marie Lang, Ingrid Jacquemin, Achraf Mamassi, Shahla Yadollahi, Thi Thanh Thao Nguyen, Gratien Kiki, and Abdoul-Hamid Mohamed Sallah—with whom I shared many meaningful moments over the years. I'm especially grateful for their friendship and support whenever it was needed.

I extend my deepest thanks to Gaspard Ndagijimana, whose initiative in contacting Prof. Bernard Tychon led to the launch of the Landslides and Flood Hazards and Vulnerability in Rwanda: Towards Applicable Land Management and Disaster Reduction (LAFHAZAF) project. I am equally grateful to those who contributed to its development and finalization—Bernard Tychon, Emmanuel Rukundo, Matthias Vanmaercke, Olivier Dewitte, Aurélia Hubert-Ferrari, Sabine Henry, Florence De Longueville, Caroline Michellier, and Jean d'Amour Dusabimana. Without their dedication, this project would not have been selected or successfully implemented.

This Ph.D. research journey would not have been possible without the support of the INES-Ruhengeri drivers—Vincent Nsengiyumva, Jérôme Kubwimana, Valens Hitimana, Dieudonné Dusingizimana, Jean Baptiste Kwizera—whose assistance was invaluable during the construction of hydrometric and weather stations, the installation of water level sensors and rain gauges, and the execution of flow measurement fieldwork.

I also extend my sincere gratitude to the field assistants—Charles Habumuremyi, Jean Marie Vianney Ndabamenye, Mudakemwa, Rusimbukande, Faustin Kamonyo, Ngerageze, and Simon Ntawuhebake—for their dedication to data collection, equipment maintenance, and day-to-day guardian services. Their commitment was instrumental to the success of this research. I am equally grateful to my colleagues Jean d'Amour Dusabimana, Aphanie Murhunzi and Noël Hakuzwiyaremye for their valuable support during data collection and the topographic surveys of river cross-sections and flood extents.

My sincere thanks go to Father François Regis Bagerageza—parish priest of Busengo Parish, Father Protogène Hategekimana—headteacher of Groupe Scolaire Saint Jérôme, Father Vincent Twizeyimana—parish priest of Ruhengeri Cathedral, Sister Victoire Uwamariya—headteacher of Groupe Scolaire Notre Dame de la Conception de Muramba, and Anastase Hitimana—

headteacher of Groupe Scolaire de Rusongati—for generously providing the land for the installation of weather stations and rain gauges.

I am grateful to acknowledge the mutual collaboration and supports shared with my fellow Ph.D. colleagues—Pascal Sibomana and Clémence Idukunda—throughout this project.

My deepest gratitude goes to my family—my mother Bernadette Nyiramahane, my mother-in-law Josephine Nyirabariyanga, my uncle Apollinaire Nkundakozera, my siblings, especially Father Juvénal Nsengiyumva, my wife Marie Claire Uwakunzwe, and my children Pascaline Uwayo, Noëline Nuwayo, and Angelo Nduwayo—as well as to my relatives and friends, particularly Tharcisse Ndagijimana, Donatien Nshimyimana, Jérôme Nsengiyumva, Gratien Nizeyimana, Bernard Nsengiyumva, Faustin Niyibizi, Théophile Muhire, Aloys Uwimana, Jean Clément Murenzi, Isaac Newton Niyobubasha, Pauline Uwajeneza, Laurent Nsabimana, and Théoneste Bizet. I am deeply thankful for their unwavering moral support, the joyful moments we shared during fieldwork in the country, and the warm welcome I received in Belgium.

I would like to express my sincere gratitude to the Académie de Recherche et d'Enseignement Supérieur (ARES) for their generous financial support, which made this research journey possible. I also thank the University of Liège for granting admission and coordinating the thesis activities with professionalism and commitment. I am equally grateful to the Unité de Recherche Sphère—led by Serge Schmitz—for providing supplementary financial support that helped bring this Ph.D. research to completion.

Finally, I gratefully acknowledge my home institution—Institut d'Enseignement Supérieur de Ruhengeri (INES-Ruhengeri)—for granting me permission to conduct this Ph.D. research and for providing essential logistical and financial support. I also extend my sincere thanks to the Royal Museum for Central Africa, the University of Namur, and the University of Rwanda for their partnership in this project; to the manuscript reviewers and editors; and to the National Council for Science and Technology (NCST), Rwanda Water Board (RWB), and Rwanda Meteorological Agency (Meteo-Rwanda) for their valuable assistance with data collection.

Abstract

Flood hazards and flood-risk management in tropical mountainous regions are constrained by scarce or missing hydrometeorological data, a limitation that hampers understanding of the factors governing rainfall-runoff responses. This thesis investigates the role of topography, soil characteristics, and land use/land cover in shaping flood dynamics, using short-term rainfall-streamflow observations and statistical and numerical approaches in two contiguous agricultural catchments of the Mukungwa watershed in northwest Rwanda: Nyamutera (44 km²) and Gaseke (109 km²).

Firstly, cost-effective river monitoring systems were deployed to generate high-resolution rainfall-runoff datasets, enabling detailed analysis of storm-events variability. Event-based assessments revealed contrasting runoff coefficients and peak discharges between the steep Nyamutera and the floodplain-connected Gaseke catchments, reflecting the role of topography, soil properties, land use/land cover, and water storage connectivity in shaping hydrological responses. The findings highlight clear contrasts in the hydrogeomorphic behaviour of the two catchments, which likely reflect differences in topography, soil properties, and storage capacity. Together, these results advance understanding of flood hazards and rainfall-streamflow dynamics in tropical mountainous environments and underscore a shift away from purely empirical approaches toward process-based hydrological interpretation. . These insights contribute to the development and application of hydrological models in similar data-limited mountainous catchments.

Secondarily, the applicability of the Natural Resources Conservation Service- Curve Number method was tested through storm-based simulations using a developed custom Python-based hydrological modelling framework. Event-based calibration and validation reveal contrasting model behavior between the two catchments rather than uniformly poor performance. In Nyamutera, NSE values are generally low during both calibration and validation, indicating limited skill in reproducing peak magnitudes and runoff volumes, even though KGE often remains acceptable and hydrograph timing is reasonably captured. In Gaseke, calibration results are more stable, with better agreement between observed and simulated peaks for many events; however, validation shows increased scatter, highlighting event-specific deviations likely linked to variable floodplain storage and routing dynamics rather than systematic model failure. Peak-flow and runoff volume errors were frequently substantial, highlighting challenges in capturing flood magnitudes and hydrograph dynamics. These results emphasize the importance of locally calibrated, event-based, process-informed models for flood hazard assessment and

their potential to support rainfall-driven early warning systems in mountainous tropical catchments.

Thirdly, the “Génie Rural à 4 paramètres Journaliers” (GR4J)-based approach was applied to reconstruct historical streamflows and derive flood early-warning thresholds. Catchment-specific calibration revealed a rapid rainfall response in Nyamutera and dampened peaks in Gaseke, attributable to floodplain buffering. These contrasting behaviours were consistent with expectations and linked to differences in topography, soil properties, land use/land cover, and water storage connectivity. Logistic regression fused with physical criteria identified antecedent rainfall windows of 5–6 days for Nyamutera and 7–11 days for Gaseke as critical for forecasting flood risks.

Overall, this research advances understanding of rainfall-runoff dynamics in tropical mountainous catchments, demonstrates the value of short-term monitoring and tailored modelling frameworks, and delivers practical tools for flood hazard management and early warning in data-limited regions worldwide.

Résumé

Les aléas d'inondation et la gestion des risques associés dans les régions montagneuses tropicales sont fortement contraints par la rareté, voire l'absence, de données hydrométéorologiques, ce qui limite la compréhension des facteurs contrôlant les réponses pluie-débit. Cette thèse analyse l'influence de la topographie, des propriétés des sols ainsi que de l'occupation et de la couverture du sol sur la dynamique des crues. L'étude repose sur des observations hydrologiques de courte durée, centrées sur les relations pluie-débit, et sur des approches statistiques et numériques appliquées à deux sous-bassins versants agricoles et contigus du bassin de la Mukungwa, au nord-ouest du Rwanda: Nyamutera (44 km²) et Gaseke (109 km²).

Premièrement, des systèmes de suivi des cours d'eau à coût réduit ont été déployés pour enregistrer des jeux de données pluie-débit à haute résolution, permettant une analyse détaillée de la variabilité des événements pluvieux. Les analyses événementielles ont révélé des coefficients de ruissellement et des débits de pointe contrastés entre le bassin escarpé de Nyamutera et celui de Gaseke, connecté à une plaine inondable, illustrant l'influence de la topographie, des propriétés des sols, de l'occupation et de la couverture du sol, ainsi que de la connectivité des zones de stockage de l'eau sur les réponses hydrologiques.

Les résultats révèlent des contrastes marqués dans le comportement hydrogéomorphologique des deux bassins versants, liés à des différences de topographie, de propriétés des sols et de capacité de stockage. Ensemble, ils améliorent la compréhension des aléas d'inondation et des dynamiques pluie-débit en milieu tropical montagneux, tout en mettant en évidence une transition des approches empiriques vers une interprétation hydrologique fondée sur les processus. Ces résultats contribuent au développement et à l'application de modèles hydrologiques dans des bassins versants montagneux présentant des caractéristiques similaires, où les données restent limitées.

Deuxièmement, l'applicabilité de la méthode du « *Natural Resources Conservation Service-Curve Number (NRCS-CN)* » a été évaluée au moyen de simulations événementielles, réalisées à l'aide d'un cadre de modélisation hydrologique personnalisé conçu en Python. La calibration et la validation événementielles mettent en évidence des comportements de modèle nettement contrastés entre les deux bassins, plutôt qu'une performance uniformément faible. Dans le bassin de Nyamutera, les valeurs de NSE demeurent généralement faibles en calibration comme en validation, traduisant une capacité limitée à reproduire les débits de pointe et les volumes écoulés, bien que le KGE reste souvent satisfaisant et que le calage temporel de l'hydrogramme

soit globalement correct. Dans le bassin de Gaseke, la calibration est plus stable, avec une meilleure correspondance entre les débits de pointe observés et simulés pour de nombreux événements; toutefois, la validation présente une dispersion accrue, révélant des écarts propres à certains événements, probablement liés à la variabilité du stockage en plaine inondable et aux dynamiques de routage, plutôt qu'à une défaillance systématique du modèle. Les erreurs fréquentes sur les débits de pointe et les volumes de ruissellement soulignent les difficultés à reproduire fidèlement l'ampleur des crues et la dynamique des hydrogrammes.

Ces résultats mettent en évidence la nécessité de recourir à des modèles événementiels localement calibrés et guidés par les processus hydrologiques, pour l'évaluation des aléas d'inondation. Ils soulignent également le potentiel de tels modèles pour soutenir des systèmes d'alerte précoce déclenchés par les précipitations dans les bassins versants tropicaux de montagne.

Troisièmement, l'approche basée sur le modèle « *Génie Rural à 4 paramètres Journaliers* » (GR4J) a été appliquée pour reconstruire les débits historiques et définir des seuils d'alerte précoce aux crues. La calibration spécifique à chaque bassin a révélé une réponse rapide aux précipitations dans le bassin de Nyamutera et des pics atténués dans le bassin de Gaseke en raison du stockage en plaine inondable. La régression logistique, combinée à des critères physiques, a identifié des fenêtres de précipitations antécédentes de 5–6 jours pour Nyamutera et de 7–11 jours pour Gaseke comme critiques pour la prévision des risques d'inondation.

Dans l'ensemble, cette recherche améliore la compréhension des dynamiques pluie-débit dans les bassins tropicaux de montagne, démontre la valeur d'un suivi de courte durée et de cadres de modélisation adaptés, et fournit des outils pratiques pour la gestion des risques d'inondation et l'alerte précoce dans les régions à données limitées à l'échelle mondiale.

Contents

List of Figures

List of tables

List of abbreviations, symbols and acronyms

ADCPs	Acoustic Doppler Current Profilers
AIC	Akaike Information Criterion
AMC	Antecendent Moiture Condition
ARES	Académie de Recherche et d'Enseignement Supérieur
AUC	Area under the curve
BBC	British Broadcasting Corporation
BFI_{max}	long-term ratio of baseflow to total streamflow—Maximum Baseflow Index
BIC	Bayesian Information Criterion
BS	Bias score
C	Runoff coefficient
Ca	Mean Annual Runoff coefficient
Cav	Average runoff coefficient
Cd	Design runoff coefficient
Cp	Peak runoff coefficient
CSI	Critical success index
CSI*	Composite critical success index
Cwb	Temperate oceanic climate with dry winters and warm summers — often referred to as a subtropical highland climate
DE	Differential Evolution
E	Evapotranspiration
Es	Actual evapotranspiration from the production store
F1	Harmonic mean of precision and detection
Fa	Infiltration after Initial Abstraction

FAO	Food and Agriculture Organization of the United Nations
FAQ	Frequently Asked Questions
FAR	False alarm ratio
FDCs	Flow duration curve
F_{max}	Maximum floodplain storage
FN	False negative
FNR	False negative rate
FP	False positive
FPR	False positive rate
FT	Fused threshold
GSA	Global sensitivity analysis
HEC-HMS	Hydrologic Engineering Center-Hydrologic Modeling System
HSS	Heidke skill score
Ia	Initial abstraction
IDF	Intensity-Duration_Frequency
INES	Institut d'Enseignement Supérieur
K	Muskingum storage constant
Ka	Actual evapotranspiration coefficient
Kc	Crop evapotranspiration coefficient
KGE	Kling-Gupta efficiency
KS	Kolmogorov-Smirnov statistic
KU	Katholieke Universiteit
lm	Maximum length or the distance from the remotest point of the catchment to the outlet in m
L_T	Logistic threshold

LULC	Land use/land cover
Meteo_Rwanda	Rwanda Meteorological Agency
MINEMA	Ministry of Emergency Management
NASA POWER	National Aeronautics and Space Administration Prediction Of Worldwide Energy Resources
NCST	National Council for Science and Technology
NEH	National Engineering Handbook
NSE	Nash-Sutcliffe Efficiency index
NW	Northwest Rwanda
P	Precipitation
PBIAS	Percent bias
P_d	Direct rainfall contribution (effective rainfall to routing)
P_e	Effective Precipitation
PEPD	Percent Error in Peak Discharge
P_{erc}	Percolation from the production store
Ph.D.	Doctor of Philosophy
P_n or Pe	Effective precipitation
POD	Probability of detection
P_T	Physical threshold
p-value	Probability value
PWRMSE	Peak Weighted Root Mean Squared Error
PWVP	Peak-Weighted Variable Power
Q_d	Direct Flow
QGIS	Quantum Geographical Information System
Qr	Routed Flow

R	Routing store (channel & groundwater reservoir)
RMCA	Royal Museum for Central Africa
RMSE	Root mean squared error
ROC	Receiver operating characteristic
R^2	Coefficient of determination
RWB	Rwanda Water Resources Board
S	Storage/Soil moisture storage
S1	First order sensitivity
S2	Second order sensitivity
SAR	Sum of Absolute Residuals
SCS-CN	Natural Resources Conservation Service-Curve Number
S-curve	Summation curve
SDCs	Specific discharge curves
SDRCs	Stage-Discharge Rating Curves
S_{mm}	Potential Maximum Retention in mm
SSR	Sum of Squared Residuals
ST	Total order sensitivity
Tc	Time of Concentration
TD	Digital pressure Transducer
T_L or L	Lag Time
TN	True negative
TNR	True negative rate
TP	True positive
TPR	True positive rate

UH	Unit hydrograph
UR	University of Rwanda
USACE HEC	United States Army Corps of Engineers – Hydrologic Engineering Center
USDA	United States Department of Agriculture
VE	Volume error
w	weight
X	Muskingum weighting factor X
X_1	Production/soil store capacity
X_2	Groundwater exchange coefficient
X_3	Routing store capacity
X_4	Unit hydrograph time base
Y	Average land slope
α	Variability ratio
β	Bias ratio
σ	Standard deviation

Chapter 1 General introduction

1.1 Background and context

The hydrological dynamics of mountainous tropical regions are uniquely influenced by steep topography, dense drainage networks, significant relief, and intense convective and orographic precipitation, alongside human-induced factors including deforestation, land degradation, urbanization, population growth, and varied agricultural practices (Muhire & Ahmed, 2015; Walker et al., 2024). The interplay of diverse physical and anthropogenic factors results in unique hydrological responses, frequently characterized by accelerated runoff and pronounced spatial variability, features less commonly observed in lowland environments (Buytaert, Celleri, et al., 2006; Pandeya et al., 2021; Viviroli et al., 2007). Monitoring these hydrological systems is further hindered by the limited availability of high-temporal-resolution rainfall and streamflow data, combined with the swift hydrological responses characteristic of mountainous tropical regions (Sidle et al., 2006). In light of the fragile equilibrium between water resource availability and vulnerability to hydrological hazards, deepening knowledge of rainfall-runoff processes in mountainous tropical regions is critical for informed and sustainable watershed management (Borga et al., 2011; Immerzeel et al., 2010). Consequently, enhanced insight into rainfall-runoff dynamics in tropical mountainous regions is vital for refining flood prediction models and promoting resilient water resource management, especially amid shifting climate regimes and land use/land cover (LULC) change.

This research is conducted within the framework of the *Landslides and Flood Hazards and Vulnerability in NW Rwanda: Towards Applicable Land Management and Disaster Risk Reduction* (LAFHAZAV) project. Hosted by the University of Liège in partnership with the Royal Museum for Central Africa, the University of Namur, the Institut d'Enseignement Supérieur de Ruhengeri (INES-Ruhengeri), the University of Rwanda, and Rwanda Polytechnics, the project aims to strengthen the capacity of Rwandan researchers and stakeholders to prevent and mitigate the impacts of floods and landslides on local communities. Its objectives are to (i) understand and quantify the role of land use, land management, and land-cover changes in triggering floods and landslides, (ii) assess population vulnerability to these hazards, (iii) develop reliable and applicable tools for hazard and risk assessment, and (iv) foster partnerships among local, national, and international actors involved in disaster risk reduction. This thesis contributes to these goals by applying hydrogeomorphological approaches to analyze flood hazards and inform flood-risk management in northwest Rwanda.

1.2 Global flood hazards and their impact

Floods are among the most frequent and widespread natural hazards worldwide, affecting more people than any other geophysical disaster (Smith & Ward, 1998). In recent years, tens of millions of people have been displaced by disasters, with weather-related hazards—including floods—accounting for the majority of these movements. Over the past decade, an average of about 24 million people were displaced each year by disasters, and in 2023 alone floods caused nearly 9.8 million displacements globally, highlighting the large human impact of flood events (UNHCR, 2025). In addition to displacement, disaster-related mortality remains high, with tens of thousands of deaths recorded annually across all hazard types, many of them linked to flood events (UNDRR, 2023). These figures underscore the continued global significance of floods as a major hazard to lives and livelihoods. . Despite this global prevalence, flood occurrence and impacts vary substantially by region. A global database of flood events from 1998 to 2008 showed that most floods were triggered by heavy rainfall (64%), followed by monsoon rains (11%) and tropical cyclones (6%), though regional patterns in flood frequency and magnitude remained poorly differentiated (Adhikari et al., 2010). Today, nearly 80% of the world's population resides in flood-prone areas, and roughly one-third of the Earth's land surface is considered vulnerable to flooding (Henrike, 2012; Kundzewicz et al., 2014; Rentschler et al., 2022; Singh & Kumar, 2013). Weather-driven flood events are most prevalent in tropical and subtropical regions, which encompass many developing countries. While developed nations typically benefit from advanced infrastructure, robust healthcare systems, and comprehensive flood warning mechanisms (Alderman et al., 2012; Cools et al., 2016; Keoduangsine et al., 2014), developing countries often face financial and institutional constraints that hinder the implementation of effective flood protection measures (Geekiyanage et al., 2025). As a result, vulnerable populations in these regions are disproportionately affected by flood events. The African tropics, in particular, face heightened flood risk due to a combination of high population densities in flood-prone areas, increasing climate variability, and limited investment in flood management infrastructure. Therefore, flood management must rely on structural measures (e.g., dams, levees) that directly control flows and non-structural measures (e.g., land-use planning, early warning systems) that reduce vulnerability and exposure, particularly in contexts where knowledge gaps or poor understanding of hydrological processes persist (BA Notes, 2023; Conitz et al., 2021; Oladokun et al., 2023; Yasitli, 2021). While structural approaches provide immediate protection, they can be costly and disruptive, whereas non-structural strategies are more sustainable and adaptable, making integrated approaches essential for long-term resilience (BA Notes, 2023; Conitz et al., 2021).

1.3 Hydrological vulnerability and flood risk in tropical mountainous catchments

Flood risks in tropical mountainous catchments, such as those in northwest Rwanda, pose a serious threat to lives, infrastructure, and livelihoods. These risks stem from the combined effects of steep terrain, volcanic and tropical soil types (e.g., Andosols and Ferralsols) that develop deep profiles in some landscapes but become significantly shallower on steep slopes, land-use and land-cover (LULC), climate variability, and rapid hydrological responses driven by intense, concentrated rainfall and limited catchment water-storage capacity (Arango-Carmona et al., 2025; Dufatanye Umwali et al., 2024; Hahirwabasenga et al., 2024; Muñoz-Villers & McDonnell, 2013; Roohi, Dehghani, et al., 2025; Uwitonze, 2016). Moreover, the absence of long-term hydrological monitoring at the small to medium-catchment scale, hinders accurate flood forecasting and effective planning (Buytaert, Celleri, et al., 2006; Buytaert & De Bièvre, 2012). The vulnerability is further exacerbated by deforestation, expansion into marginal lands, and high population density (Douglas et al., 2008). This study addresses these critical challenges by integrating short-term field observations with hydrogeomorphological analysis and data-driven modeling, providing a practical framework for identifying dominant runoff-generating mechanisms. By focusing on terrain, soil properties, and LULC, it delivers a nuanced understanding of flood generation in high-risk environments. The application of statistical and numerical tools supports local capacity in hazard mapping, early warning, and infrastructure design (UNDRR, 2022). By evaluating traditional flood-modeling tools and their ability to represent physical hydrological processes in mountainous catchments, this research strengthens the scientific basis for hazard and flood-risk management and supports resilience-building efforts in the African tropics and other similarly vulnerable regions.

1.4 Flood hazards in Rwanda: climate, challenges and the need for enhanced risk management

Rwanda's climate is strongly shaped by its elevation and complex topography. Altitudes range from approximately 900 m in low-lying areas such as the Bugarama plain (southwestern province) to more than 4,500 m in the Vorcanoes highlands. The relatively low elevations of the Eastern Province, the Bugarama lowlands, and the central plateau around Kigali contrast sharply with the higher terrain of the Congo-Nile Divide and the Volcanoes National Park in the northwest. This pronounced topographic gradient gives rise to substantial spatial variability in temperature and rainfall patterns across the country, with cooler and wetter conditions prevailing in the highlands and warmer, drier conditions dominating the eastern and southwestern lowlands (McSweeney et al., 2010; MIDIMAR, 2015).

According to the Köppen–Geiger climate classification, northwest Rwanda is classified as a highland temperate climate (Cwb), characterized by relatively mild temperatures due to elevation and generally humid conditions associated with the regional rainfall regime (Beck et al., 2018; McSweeney et al., 2010). The region has two rainy seasons, from February to May and from September to mid-December, and two dry seasons, from mid-December to January and from mid-May to August (Ministry of Environment-Rwanda, 2018). Annual rainfall usually falls between 1,200 and 1,600 mm, but intense, short-lived convective storms can occur locally, producing heavy downpours that have a strong impact on runoff, especially in steep areas. Based on the Global Precipitation Measurement–Integrated Multi-satellitE Retrievals for GPM (GPM IMERG), the mean annual rainfall between 2000 and 2023 in Rwanda declines to slightly below 1000 mm in the east, while it gradually increases to more than 1400 mm in the center (Kigali), the south (Nyungwe National Park), and the western riverine areas of Lake Kivu (GPM IMERG, n.d.). Figure 1-1 shows the mean annual rainfall totals per 0.1° grid cell (≈11 km) for the period 2000–2023. The map illustrates the spatial distribution of rainfall across the country and includes major lakes, principal rivers, and the boundaries of the study catchments (Nyamutera (44 km²) and Gaseke (109 km²)).

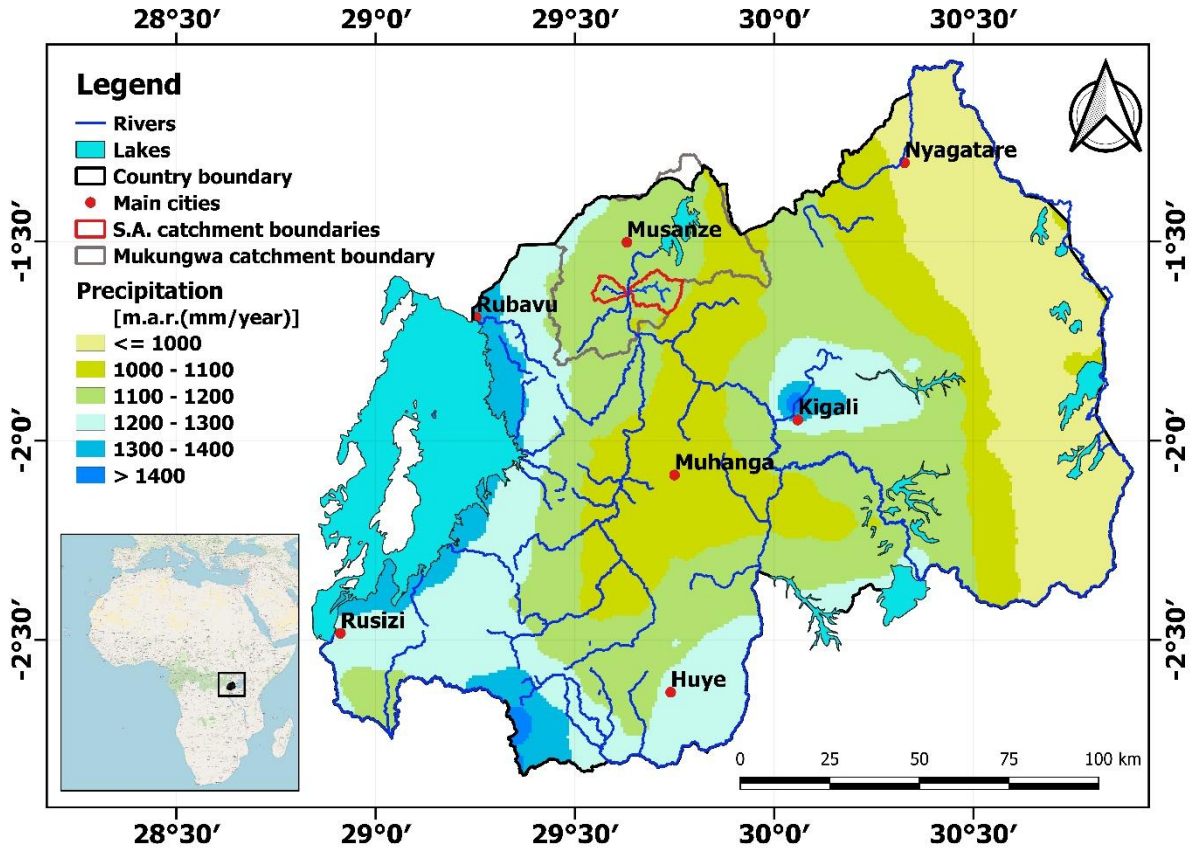

Figure 1-1 Spatial distribution of mean annual rainfall (mm/year) across the country, incorporating major lakes, principal rivers, and the study area (S.A.) catchment boundaries(red color)—Nyamutera and Gaseke, including the Mukungwa watershed boundary (gray color).

Temperatures are influenced by elevation, with average yearly values typically ranging from 15 to 20 °C, becoming cooler as altitude increases (Cui et al., 2021).

(Rwanda Water Resources Board, 2025) reports that Mukungwa basin is roughly receiving over 1,315 mm of rainfall annually, corresponding to a total volume of approximately 2,323 hm^3, corresponding to an average surface flow of 28.7 m^3/s (≈900 hm^3 per year) for the entire catchment. Extrapolating the above information to the study catchments, Nyamutera and Gaseke, the expected mean flows based purely on catchment area and rainfall would be roughly 1.84 m^3/s and 4.53 m^3/s, respectively. However, precipitations in the region is highly convective and variable (Muhire & Ahmed, 2015), making actual flows lower and subjected to spatiotemporal variabilities. Additionally, estimated catchment streamflow also ignores slope and other geomorphological controls, underscoring the need for rainfall-runoff modeling to better understanding the realistic hydrological responses.

In tropical regions such as Africa, flash floods and river floods occur with increasing frequency due to a combination of climate variability and human-driven factors, including intense rainfall, LULC change, and the absence of sufficient flood control infrastructure (Thanvisitthpon et al., 2024).

Rwanda, located in East Africa's tropical highlands, is particularly vulnerable to flood risks. Between 1974 and 2008, floods in Rwanda claimed 159 lives and displaced nearly two million people (UNEP, 2011, 2022). Floods have also become a primary trigger for water-related conflicts, as reported by the Ministry of Emergency Management (MINEMA) and the United Nations Environment Programme (UNEP) (UNEP, 2011, 2022; Zimmerman & Byizigiro, 2012). Table 1-1 illustrates the districts affected by flood events between 1988 and 2017.

Table 1-1 Districts affected by flood events from 1988 to 2017(Mind'je et al., 2019).

Year	Number of people killed	The number of people affected	Properties damaged	District/province affected (see below: number for district / letter for province)
1988	48	21, 678	1,225 houses, 19 bridges, 7 roads cut off	10, 14, 15, 20, 25
2000	0	1,000	200 houses, roads, cropland	3, 25
2001	12	3,000	100 houses, 60 schools, cropland	7, 10, 15, 20, 25
2002	69	20,000	Not available	4, 7, 10, 28
2003	0	7,016	Not available	7, 12, 19
2005	27	25,003	5,000 houses, 3,000 croplands	7, 15, 23
2007	45	7,310	1,570 houses, 562 homeless families,	7, 18, 25
2008	15	3,000	4,000 ha of crops, 500 homeless families, bridges, roads	N, S, W
2009	Not available	Not available	Infrastructure and cropland destroyed	6, 12, 25
2010	3	Not available	1 industrial site, house, and cropland	K
2011	1	Not available	19 houses, 152 ha of lands	2, 18, 19, 22, 30
2012	26	Not available	201 houses, 411 ha of land	1, 4, 7, 12, 15, 20, 25, 28
2013	15	64	593 houses, 411 ha of land	4, 10, 12, 15, 18, 23, 24, 25, 26

2014	18	Not available	6 houses, 206 ha of cropland, water supply infrastructure	7, 11, 18, 20, 21, 23, 24, 29
2015	24	3,425	34 houses, 1,111 of cropland	1, 10, 14, 15, 17, 25, 26, 27, 28, 29
2016	54	2,317	222 collapse, 448 ha of cropland	2, 10, 15, 18, 23, 25, 26, 29
2017	7	5,850	640 homeless families, 1,036 ha of crops, farms	1, 5, 8, 9, 13, 16, 17, 21, 28, 29

Note: Each superscript shown in brackets corresponds to the adjacent names of the districts, cities, or provinces listed in the last column of the Table1.1 ([1]Bugesera, [2]Burera, [3]Gakenke, [4]Gasabo, [5]Gatsibo, [6]Gisagara, [7]Gicumbi, [8]Huye, [9]Kamonyi, [10]Karongi, [11]Kayonza, [12]Kicukiro, [13]Kirehe, [14]Muhanga, [15]Musanze, [16]Ngoma, [17]Ngororero, [18]Nyabihu, [19]Nyagatare, [20]Nyamagabe, [21]Nyamasheke, [22]Nyanza, [23]Nyarugenge, [24]Nyaruguru, [25]Rubavu, [26]Ruhango, [27]Rulindo, [28]Rusizi, [29]Rutsiro, [30]Rwamagana, [K]Kigali city, [W]Western province, [S]Southern province, [N]Northern province).

Over the past three decades, northwestern Rwanda has experienced recurring floods that have caused substantial socio-economic and infrastructural damage. For instance, in Rubavu District, floods from the Sebeya river have impacted multiple schools, including GS NDA Nyundo, École d'Arts de Nyundo, GS Sanzare, Petit Séminaire St. Pie X de Nyundo, GS Rubavu II, and CS Kayanza, damaging laboratories, equipment, classrooms, and libraries, and forcing temporary suspension of classes during relocation and repair efforts (Africa Press, May 5, 2023).

On the night of 3–4 April 2023, intense rainfall triggered flooding in Musanze town and surrounding catchments in northwest Rwanda. The floodwaters caused local disruptions, particularly in small catchments such as Kabwa and Gaseke. In the Gaseke catchment, the event temporarily affected infrastructure, including the hydrometric station established as part of this thesis to monitor rainfall-runoff dynamics. Such events underscore the vulnerability of mountainous tropical catchments to extreme rainfall and highlight the importance of accurate hydrometric monitoring for improved flood risk assessment and management.

Even more severe flooding occurred on the night of 2–3 May 2023, causing over 130 fatalities nationwide (Africa-Press, 2023; Cyuzuzo Samba & Cecilia Macaulay, 2023). Among the monitored catchments of this thesis, the Nyamutera River basin experienced significant flooding, highlighting the acute vulnerability of tropical mountainous catchments in Rwanda. These events emphasize the urgent need for improved flood monitoring, forecasting, and risk management strategies.

After the flooding on the night of 2–3 May 2023, field assessments revealed extensive damage to public infrastructure, including 14 national roads, 13 district roads, 8 water treatment plants, 12 power stations, and 12 medium-voltage lines. The hydrological monitoring network was also impacted: two stations (Giciye and Nyabarongo) were completely lost, while two others (Nyamutera and Rubagabaga) sustained severe damage. Agricultural lands were widely affected, with substantial crop loss and land degradation.

As Rwanda continues to experience rapid urbanization and increasing climate variability, flood risk remains a pressing challenge for national disaster management strategies.

This thesis adopts hydrogeomorphological approaches to better understand flood hazards and support improved flood risk management in northwest Rwanda, a region characterized by complex topography, diverse LULC, and high vulnerability to flooding. By integrating hydrological processes (such as rainfall, runoff, and streamflow) with catchment physiography, the research aims to develop tools for assessing rainfall-runoff dynamics, identifying flood-prone areas, and evaluating the transferability of hydrological models across sub-catchments. These efforts are expected to contribute to more reliable flood predictions and enhanced management practices, thereby increasing regional resilience to flood hazards.

Specifically, the study focuses on identifying key factors influencing rainfall-runoff responses and flood event occurrences, with particular emphasis on topography, soil types, and LULC. Furthermore, by evaluating hydrological models and tools such as the Rational Method, SCS-CN, and Muskingum routing models, the thesis seeks to improve flood prediction accuracy and offer insights into the most effective flood management strategies for the region.

1.5 Conceptual and theoretical frameworks

1.5.1 Introduction

Rainfall-Runoff (RR) processes in tropical mountainous environments are governed by the interaction of steep terrain, intense convective rainfall, shallow and highly weathered soils, and land cover dynamics (Muñoz-Villers & McDonnell, 2012a; Muñoz-Villers & McDonnell, 2013). These factors jointly shape a hydrological regime that is often rapid and unpredictable (Ye et al., 2023). In the northwestern highlands of Rwanda, specifically within the Nyamutera and Gaseke catchments, this interplay results in rapid runoff responses, marked by short response times, high runoff coefficients, and increased flood risk (Munyaneza et al., 2014). In such settings, runoff generation is highly variable across both space and time, driven by factors including slope gradient, soil saturation, land use practices, and the density of the drainage network (De Vente & Poesen, 2005). In this context, storm-event sensitivity refers to the rapid

transformation of rainfall into streamflow, typically characterized by brief lag times and limited infiltration. Furthermore, convective rainfall patterns and orographic influences associated with the Congo-Nile Divide contribute to pronounced spatial variability in precipitation, with annual totals exceeding 1,500 mm in many regions (NISR, 2023). Consequently, rainfall events in the region are typically short and intense, promoting overland flow, particularly on slopes exceeding 25%, where deforestation and agricultural expansion have reduced vegetation cover (Karamage, Shao, et al., 2016; Karamage et al., 2017; Nambajimana et al., 2019). These landscapes present optimal conditions for investigating storm runoff generation and routing, while simultaneously posing unique challenges for hydrological monitoring and modeling (Muñoz-Villers & McDonnell, 2012a; Ye et al., 2023).

The conceptual framework underpinning this study is based on event-based hydrological analysis, which isolates individual rainfall events to examine how precipitation interacts with initial abstraction, soil properties, and topographic structure to produce streamflow (Blöschl et al., 2013). Although a growing body of research has advanced our understanding of rainfall-runoff dynamics in tropical and mountainous regions, significant knowledge gaps remain, particularly concerning the fine-scale mechanisms of runoff generation and event-specific flood responses in data-scarce environments (Buytaert, Célleri, et al., 2006; Lørup et al., 1998).

For Rwanda and similar regions in the African highlands, there is limited event-scale analysis linking rainfall characteristics to streamflow responses in small- to medium-sized headwater catchments. In particular, integrated studies that connect hydrogeomorphological indicators, such as relief ratio, flowpath length, drainage density, and floodplain extent, to runoff response metrics and flood generation mechanisms remain scarce (Montgomery & Dietrich, 2002).

1.5.2 Conceptualizing flood hazard and risk in mountainous tropical regions

Understanding flood risk in mountainous tropical environments requires an integrative framework that bridges physical landscape processes with human dimensions of vulnerability and decision-making (Arango-Carmona et al., 2025; Awah et al., 2024). This framework integrates hydrological events and geomorphological processes, shaped by terrain characteristics and socio-environmental factors, to advance the understanding of flood risk generation dynamics. The following subsections examine this complexity through four interlinked perspectives: (1) hydrogeomorphological approaches to flood hazard and risk assessment, (2) the amplification of flood risk through human-induced modifications to the natural environment, (3) the limitations of conventional environmental impact assessments in

steep terrains, and (4) the added value of integrating geomorphic insights into flood risk management strategies.

Together, these elements establish a theoretical foundation for analyzing flood dynamics and informing risk reduction in steep, data-scarce regions such as northwest Rwanda (Beven, 2012; Merz & Blöschl, 2003).

Floods in tropical highlands, such as those in Rwanda's northwestern mountains, are not random disturbances, but the outcomes of dynamic geomorphic systems. With slopes often exceeding 20%, shallow to very deep and well drained soils, and convective rainfall patterns that can surpass 1,800 mm annually (Sebaziga et al., 2020), the region's physical terrain is highly conducive to flash floods, mass wasting, and sediment-loaded flows.

These processes are particularly intense in catchments like Nyamutera and Gaseke, where high-relief terrain interacts with volcanic soils and dense agricultural land use to exacerbate surface runoff and slope instability (Verdoodt & Van Ranst, 2006).

Framing floods as geomorphological processes expands the scope of flood hazard assessments beyond river discharge and inundation models. It demands attention to hillslope-channel coupling, sediment transport, and landscape thresholds, especially in regions where shallow landslides and channel avulsions co-occur during intense storm events (Montgomery & Dietrich, 1994). Such events often have cascading effects, including channel siltation, infrastructure damage, and longer-term changes in valley morphology.

However, the physical hazard alone does not define flood risk. In Rwanda's densely populated highlands, human vulnerability, such as shaped by poverty, land pressure, informal settlements, and inadequate infrastructure, amplifies the consequences of even moderate hydrometeorological triggers (Nyssen et al., 2010; Ramos & Martínez-Casasnovas, 2010). Agricultural terraces, road construction, and encroachment into flood-prone areas all modify surface hydrology and sediment pathways, often increasing risk unintentionally.

This coupled human-physical system requires an integrated, interdisciplinary approach. Environmental impact assessments (EIAs), while increasingly mandated, often fail to capture terrain-sensitive hazards in sufficient detail, particularly in small and intermediate watersheds. Embedding geomorphic analysis into flood risk management, using tools such as slope stability mapping, sediment budgeting, and event-based rainfall-runoff modeling, can improve the predictive capacity and relevance of risk assessments in such contexts.

In sum, conceptualizing flood hazards in mountainous tropical settings like NW Rwanda requires moving beyond traditional hydrological paradigms. Integrating geomorphological

insights with other contributing factors offers a more effective basis for developing context-specific adaptation strategies.

1.5.3 Hydrogeomorphological perspectives on flood hazard and risk assessment

The dynamics of river systems are inherently complex, and the application of hydrological and hydraulic concepts alone is insufficient to capture the full range of physical parameters that govern their behavior (Knighton, 2014; Montgomery & Buffington, 1997). Traditional hydrology and hydraulics often overlook the temporal and spatial variability of channel forms and sediment fluxes, thereby limiting their explanatory power, especially in environments where water and sediment adjust co-dependently (Charlton, 2007; E. W. Lane, 1955). In this context, hydrogeomorphology provides a critical complement to hydrology and hydraulics in river management, as it integrates geomorphic processes and their interactions with mineral elements such as soils, rocks, and sediments (Charlton, 2007; Fryirs & Brierley, 2022).

Hydrogeomorphology is an interdisciplinary field that explores the close relationship between water and landscapes. It focuses on how water movement—through rainfall, river flow, floods, and groundwater—shapes the Earth's surface, creating and transforming landforms such as river channels, floodplains, and deltas, while these same landforms regulate how water moves and is stored within catchments (Knighton, 2014; Leopold et al., 1995; Montgomery, 2001). The field integrates concepts from hydrology, geomorphology, soil science, and ecology to develop a holistic understanding of water–land interactions (Fryirs & Brierley, 2022; Wohl, 2021).

A central emphasis of hydrogeomorphology is the study of dynamic processes, including erosion, sediment transport, and channel adjustment, examined across timescales from individual storm events to long-term landscape evolution (Leopold et al., 1995; Montgomery & Buffington, 1997). Both surface and subsurface water systems are considered integral to these processes, as exchanges between rivers and groundwater strongly influence streamflow regimes, sediment mobility, and ecosystem functioning (Montgomery & Buffington, 1997; Wohl, 2021).

An important concept within the discipline is the presence of feedback mechanisms, whereby water-driven modification of landforms alters flow pathways, hydraulic conditions, and sediment transport processes, which in turn reshape subsequent geomorphic development (Phillips, 2003; Wohl et al., 2015). These insights have practical value for river restoration, flood-risk management, watershed planning, and assessments of landscape responses to climate variability and land-use change (Brierley et al., 2006; Jansson et al., 2005). Therefore, the

application of hydrogeomorphological approaches supports the identification of flood-prone areas, the estimation of flood magnitude and duration, and the assessment of how land-use or infrastructure changes may influence flood risk (S. N. Lane et al., 2011). Consequently, hydrogeomorphology provides a foundational framework for flood hazard assessment, risk mapping, and the planning of effective mitigation strategies (Montgomery, 2001; Yang et al., 2007).

Several authors have discussed expressions of flood risk, with the most common formulation defining risk as the product of hazard, vulnerability, and exposure (De Moel et al., 2009; Sieg et al., 2023; UNISDR, 2012). This emphasizes that risk depends not only on physical flood processes but also on the susceptibility and presence of populations or assets exposed to those hazards.

In mountainous tropical regions, characterized by steep slopes, intense storms, and vulnerable infrastructure, this framework is particularly valuable. Hydrogeomorphological approaches primarily quantify hazard by analyzing flood frequency, magnitude, and spatial patterns, while also providing insights into how terrain and LULC influence vulnerability and exposure. This integrated approach supports more effective flood risk management by highlighting areas where physical flood processes intersect with social and environmental vulnerabilities, thereby guiding targeted mitigation and adaptation strategies in these complex landscapes.

1.5.4 Anthropogenic influences on flood risk amplification

The relationship between humans and the environment is marked by a duality: while seeking protection from natural hazards, societies also intensify their exposure through land-use changes and infrastructural expansion (Dulawan et al., 2024). In mountainous regions, this tension is particularly acute, as limited flat terrain fosters the clustering of settlements and infrastructure in geomorphologically active zones (Dulawan et al., 2024; Rijal et al., 2024). Roads, urban areas, and hydropower developments often alter natural hydrological pathways, amplifying the potential for flooding, erosion, and slope instability (Montgomery, 1994).

This spatial overlap between human development and geomorphic activity frequently leads to risk amplification, especially when physical terrain processes are not adequately considered in planning (Dulawan et al., 2024). Where both natural and socio-economic systems operate at high intensity and compete for limited space, the consequences of poor integration can be severe (Dulawan et al., 2024; Rijal et al., 2024). Effectively addressing these risks requires moving

beyond reactive responses toward proactive land-use strategies that incorporate geomorphic risk evaluations from the outset.

1.5.5 Limitations of conventional environmental impact assessment in mountainous landscapes

Environmental Impact Assessments (EIAs) provide a regulatory framework for evaluating the potential effects of development projects on environmental systems (Engida, 2010). While traditionally centered on ecological and pollution-related impacts, there is growing recognition of the need to integrate geomorphological processes, such as flooding, sediment transport, and slope instability, into these assessments (Cavallin et al., 1994; Rodriguez-Bachiller & Glasson, 2004). EIAs typically compare projected impacts against a no-project baseline, capturing both direct and indirect environmental changes (Wathern, 2013).

However, conventional EIAs often treat geomorphology as static, focusing on preserving catchment physiography rather than accounting for active terrain dynamics (Cavallin et al., 1994). This limited perspective can obscure critical feedbacks between development and geomorphic processes, especially in flood-prone mountainous regions (Cavallin et al., 1994). Consequently, the neglect of process-based hazards undermines the effectiveness of environmental safeguards and results in inadequate risk mitigation measures.

To enhance flood resilience in topographically complex environments, it is essential to incorporate geomorphic process understanding into both EIA procedures and broader flood risk management frameworks. This study responds to that need by linking field-based hydrometric observations (rainfall, streamflow, and runoff response) with terrain analysis to characterize flood-generating mechanisms in the study area. Such empirical insights are crucial for evaluating the applicability of simplified hydrological models, like the rational and NRCS-CN methods, in data-scarce mountainous regions.

By contextualizing hydrological model performance within the catchment's physical setting, the research advances a process-based understanding of flood hazards. This approach not only improves the reliability of flood prediction for infrastructure design but also supports the development of early warning systems and spatial planning strategies that are better aligned with local hydro-geomorphological realities.

1.5.6 Integrating geomorphological hazard assessment into flood risk management

Hydrogeomorphological approaches offer a critical framework for understanding how landscape characteristics control flood generation and propagation, particularly in mountainous tropical catchments (Lombana et al., 2024). From a hydrogeomorphological perspective,

factors such as slope gradients, relief ratios, drainage density, floodplain morphology, and bedrock position strongly influence the spatial and temporal distribution of runoff, thereby shaping the frequency, magnitude, and duration of flood events (Kameyama et al., 2025; Masaoka et al., 2021). These physical controls influence both surface and subsurface flow pathways, mediating the partitioning between direct runoff and baseflow and determining catchment responsiveness to intense convective rainfall (Arnaud-Fassetta et al., 2009; Kameyama et al., 2025; Quesada-Román et al., 2022). Insights derived from hydrogeomorphological analyses therefore provide a mechanistic understanding of rainfall-runoff processes, enabling the identification of sensitive zones prone to rapid hydrological responses or flood accumulation. By integrating geomorphic indicators, stream network characteristics, and catchment-specific physiography into flood hazard assessment, hydrogeomorphological approaches support a more robust evaluation of flood risk. This integration allows for the mapping of high-risk areas, the assessment of potential impacts on lives, infrastructure, and property, and the design of context-sensitive mitigation and management strategies. In data-limited, steep, and heterogeneous mountain environments, such as the catchments of northwestern Rwanda, these approaches bridge the gap between empirical observations and predictive modeling, providing a transferable framework for proactive flood-risk management.

1.6 Rainfall-runoff dynamics in tropical mountainous catchments

Rainfall-runoff dynamics in tropical mountainous regions are characterized by rapid and nonlinear responses shaped by a complex interplay of climatic, geomorphic, and land use factors. High-intensity, short-duration convective storms that are common in tropical highlands, frequently interact with steep slopes, shallow soils, and variable LULC to produce swift overland flow and elevated runoff coefficients (Adhikari et al., 2010; Blöschl et al., 2007). These effects are further influenced by human activities such as deforestation, intensive agriculture on steep terrains, and road construction, which reduce infiltration and increase hydrological connectivity, whereas terracing promotes infiltration and can help mitigate these impacts (Bruijnzeel, 2004; Niehoff et al., 2002).

Steep terrain and limited soil depth restrict infiltration, while shallow or fractured bedrock facilitates lateral subsurface stormflow and rapid saturation. Consequently, infiltration-excess and saturation-excess runoff mechanisms can operate concurrently within the same catchment (Beven, 2012; Bonell, 1993). Return flow from upslope areas and shallow interflow further contribute to fast streamflow responses, especially during events preceded by high antecedent

moisture (Bruijnzeel, 2004). These conditions present substantial challenges for rainfall-runoff modeling, particularly in data-scarce environments, where lumped models often fail to capture the coexistence of multiple runoff generation mechanisms (Blöschl & Zehe, 2005; Chow et al., 1988).

Temporal variability adds further complexity to hydrological behavior in these settings. Short lag times and closely spaced rainfall events during the rainy season can lead to cumulative soil saturation and elevated peak flows (T. Liu et al., 2022; Mind'je et al., 2021). Event-based rainfall-runoff is therefore highly sensitive to antecedent moisture conditions, storm sequencing, and rainfall intensity, factors that introduce significant nonlinearity into stream response and necessitate fine-resolution, event-scale monitoring and modeling (Beven, 2012; Merz & Blöschl, 2003).

These dynamics are clearly observed in the tropical highlands of northwest Rwanda, where volcanic terrain, deeply dissected valleys, and thin, heterogeneous soils create sharp spatial contrasts in runoff generation (Bamutaze et al., 2010; Munyaneza, 2014). When forested hillslopes are converted to cropland or informal settlements, the loss of canopy increases surface erosion. Terracing and fragmented land can improve infiltration and slow runoff, but they may also redirect concentrated flows, occasionally triggering landslides that deposit sediments in rivers and change their morphology (Mind'je et al., 2023; Rukundo et al., 2018). As a result, rapid flow concentration into valley bottoms elevates flood risks and complicates conventional flood hazard assessment.

To address these challenges, this study adopts a hydrogeomorphological approach that integrates event-scale runoff analysis, terrain characteristics, and physically based modeling tools (e.g., Rational Method, NRCS Curve Number, Muskingum routing). This framework improves understanding of runoff generation processes across geomorphically distinct sub-catchments and provides a foundation for flood-risk assessment and hydraulic infrastructure design in data-scarce tropical upland environments.

1.7 Rainfall-runoff interactions in steep tropical catchments

Rainfall-runoff processes in steep tropical catchments are strongly influenced by the interplay of intense convective precipitation, complex topography, and heterogeneous land cover (Muhire & Ahmed, 2015). In such environments, steep slopes and high relief ratios promote rapid overland flow, reducing infiltration and increasing the speed at which rainfall is converted to streamflow (Beven, 2012). Subsurface flow pathways, including shallow subsurface flow along soil-bedrock interfaces, often contribute significantly to the hydrograph, particularly during

moderate rainfall events, while direct surface runoff dominates during high-intensity storms. LULC and soil characteristics further modulate these responses: forested or well-vegetated areas tend to enhance infiltration and delay peak flows, whereas degraded soils or impervious surfaces accelerate runoff and peak discharges (Nyssen et al., 2010; Ramos & Martínez-Casasnovas, 2010). The combination of short, high-intensity rainfall events with steep, dissected terrain often leads to flash floods, highly variable runoff coefficients, and rapid streamflow responses, posing challenges for flood prediction and hydraulic design. Understanding these rainfall–runoff interactions through both field measurements and modeling approaches is therefore essential for developing robust, context-specific flood management strategies in tropical mountain catchments (Buytaert, Célleri, et al., 2006; Mugiraneza et al., 2020; Viviroli et al., 2007).

1.8 Dominant runoff generation mechanisms

In the steep, tropical highlands of northwest Rwanda, runoff generation is governed by a dynamic interplay of Hortonian infiltration-excess and saturation-excess flow mechanisms, both of which operate concurrently across varying spatial and temporal scales (Buda, 2013; Tamer et al., 2025). High-intensity rainfall events often exceed the infiltration capacity of volcanic soils, particularly where land degradation has reduced permeability, promoting infiltration-excess overland flow (Bamutaze et al., 2010). However, prolonged antecedent moisture conditions often result in the saturation of shallow soils, particularly in depressions or low-lying areas, thereby enhancing overland flow through return flow (Bruijnzeel, 2004). Shallow subsurface stormflows are also significant, particularly where deep, permeable soils overlie less conductive subsoil layers, facilitating lateral downslope flow before surfacing (Beven, 2012; Bruijnzeel, 2004). In tropical mountain catchments, variation in slope, land use, and soil depth creates complex runoff patterns. Capturing these mixed processes requires spatially distributed hydrological models (Blöschl et al., 2007) to improve flood prediction and water resource management.

1.9 Event-based dynamics and temporal variability

Hydrological responses in tropical mountainous catchments, such as those in NW Rwanda, are strongly shaped by event-based dynamics and temporal variability in rainfall, antecedent soil moisture, and storm sequencing (Mind'je et al., 2019). Successive storms in short succession reduce infiltration due to soil saturation, increasing runoff volumes and shortening lag times (Mind'je et al., 2019). This clustering intensifies streamflow peaks and flood magnitudes, especially under closely spaced, high-intensity rainfall (Mind'je et al., 2019, 2021).

Furthermore, variations in the rainfall-streamflow lag with storm intensity and wetness conditions underscore the need for high temporal resolution in hydrologic analysis (Beven, 2012; Blöschl et al., 2007). Event-based monitoring is therefore essential for capturing the non-linear runoff response and for calibrating models to simulate floods realistically. Models that fail to incorporate event-scale variability and soil moisture memory effects risk underestimating peak flows and misinforming flood-risk assessments in data-scarce tropical regions (Farmani et al., 2025; Y. Liu et al., 2025; Staudinger et al., 2025).

1.10 Rainfall-runoff relationships and hydrological model applications

Hydrological models are simplified representations of real-world hydrological systems, including surface runoff, soil moisture, wetlands, groundwater, and estuarine dynamics. These models aid in understanding, predicting, and managing water resources by approximating complex processes through system-based concepts (Beven, 2006, 2012; Singh & Woolhiser, 2002). Broadly, hydrological models are categorized into two classical types: deterministic models and stochastic models (Karamouz et al., 2010a). However, models cannot fully substitute for hydrological realities; therefore, field-based observations remain essential for validating model outputs and assessing predictive reliability (Gupta et al., 2009).

1.11 Hydrological modeling approaches

Hydrological models are often described along a continuum of complexity, spanning from empirical to conceptual to physical based appoaches (Chow et al., 1988; Seibert & Bergström, 2022). This perspective aligns naturally with the distinction between deterministic and sthocastic models. Deterministic models use mathematical formulations in which outputs are fully determined by a given set of inputs and parameters, without incorporating randomness; each simulation yields a single outcome, assuming no uncertainty in the inputs or model structure (Beven, 2012). These models are particularly useful for predicting system behavior and exploring how variations in one variable influence others, based on an assumed exact relationship between inputs and outputs (Clark et al., 2011; Todini, 2007).

Within deterministic frameworks, models are commonly classified into three categories, which mirror the continuum of complexity. Empirical models (black-box) rely primarily on observed data to define statistical relationships between inputs and outputs, without explicitly representing the internal hydrological processes of a catchment (Singh & Woolhiser, 2002; Sivapalan et al., 2003). Their simplicity and low data requirements make them attractive in data-scarce environments or for event-scale assessments. Examples include the Rational Method and the Unit Hydrograph technique (Chow et al., 1988).

Conceptual models (grey-box) represent catchments using spatially averaged state variables, such as soil moisture or storage, combining physical understanding with empirical calibration (Beven, 2012; Sivapalan et al., 2003a). The NRCS-Curve Number (CN) method is a prominent example, capturing catchment response through simplified storage assumptions and empirically derived lookup tables, while often being implemented semi-distributedly across sub-basins or hydrologic response units (Mishra & Singh, 2003; USDA NRCS, 2004). Conceptual models are particularly suitable for situations where spatially detailed data are limited, yet some physical insight is required.

Physically based distributed models (white-box) aim to explicitly simulate hydrological processes using fundamental physical equations—such as the Saint-Venant equations for unsteady flow—applied at fine spatial scales across grid cells or hydrological response units (Beven, 2012; Blöschl & Sivapalan, 1995). These models can provide detailed representations of catchment dynamics, but they demand extensive data, high computational resources, and careful handling of spatial heterogeneity and scale effects.

In contrast, stochastic models explicitly incorporate randomness to represent uncertainties in inputs, boundary conditions, and model parameters, thereby producing probabilistic forecasts rather than single deterministic outcomes (Olcese et al., 2022; M. Pandey et al., 2025). By capturing the inherent variability of hydrological systems, these models are well suited for analyzing rainfall–runoff variability, generating synthetic time series, and supporting risk-based assessments (e.g., Markov chain models).

By framing hydrological models along this continuum—from empirical to physically based, deterministic to stochastic—it becomes easier to understand the trade-offs between model complexity, data requirements, and process representation. Event-based approaches, such as the Rational Method or the NRCS-CN model, provide rapid assessments of storm-scale responses under limited data, whereas continuous conceptual models like GR4J allow reconstruction of historical streamflow and exploration of catchment water balance dynamics. Finally, routing schemes such as Muskingum link runoff generation to downstream propagation, highlighting how different modelling approaches can be applied complementarily to capture both short-term flood responses and longer-term hydrological dynamics within data-constrained mountainous catchments (Chow et al., 1988; Subramanya, 2008).

Model classification frameworks, such as that proposed by (Clark et al., 2011), provide a structured way to compare hydrological models in terms of their architecture, process

representation, and data requirements. Complementarily, model evaluation frameworks (Gupta et al., 2009) emphasize the need to assess not only statistical performance, but also the adequacy of model structure and underlying assumptions. Figure 1-2 summarizes these classifications, highlighting how different modeling approaches treat randomness as well as the spatial and temporal variability of hydrological processes.

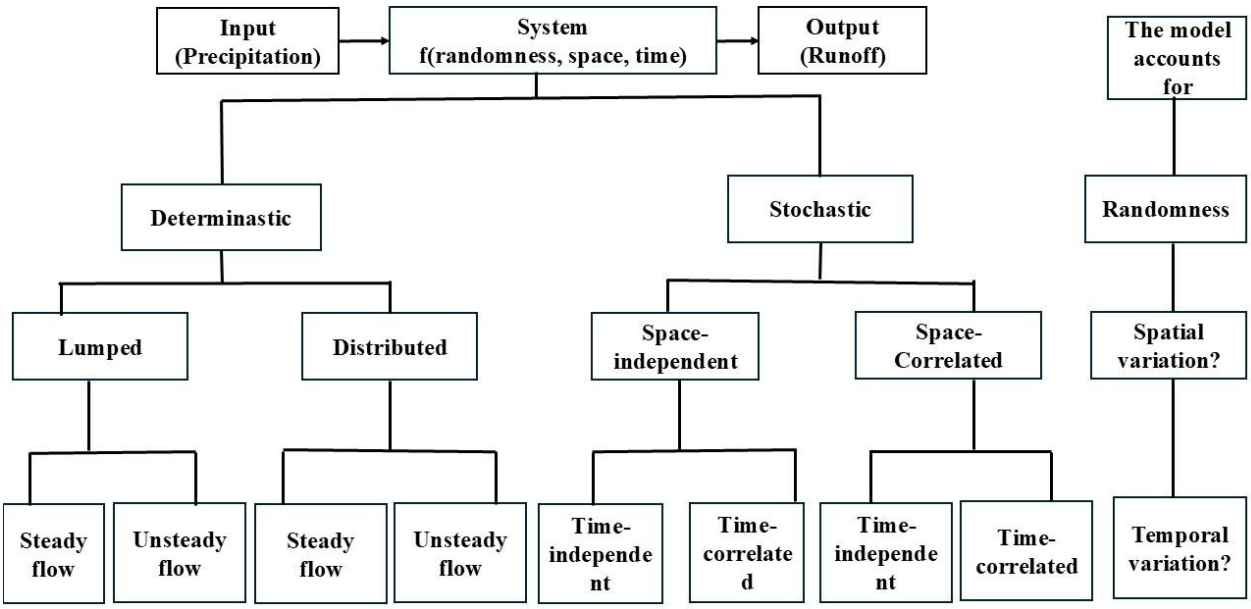

Figure 1-2 Hydrological models classification based on the way they treat the randomness and space and time variability of hydrological phenomena (Chow et al., 1988).

1.11.1 Limitations of traditional rainfall-runoff models

In the steep and highly heterogeneous terrains of northwest Rwanda, traditional lumped rainfall–runoff models often perform poorly because their simplifying assumptions of homogeneous catchment properties and uniform hydrological responses fail to capture the complex topography, land use, and soil variability typical of tropical mountain environments (Mind'je et al., 2019, 2021). These limitations lead to inaccuracies in predicting runoff timing and magnitude, particularly during storms where soil saturation varies locally across the landscape. The lack of high-resolution hydrometeorological and soil data further reduces the effectiveness of lumped models in such contexts (Beven, 2012; Blöschl et al., 2007). Consequently, there is increasing emphasis on the analysis of rainfall-streamflow responses in small and medium catchments using process-based or semi-distributed models that explicitly account for topographic controls, land-cover heterogeneity, and event-based dynamics. These

approaches provide more realistic representations of hydrological behavior, thereby improving flood forecasting and water management in data-scarce tropical catchments.

1.11.2 Hydrological modelling approaches in data-limited mountainous catchments

Hydrological modeling plays a pivotal role in understanding rainfall-runoff dynamics and assessing flood hazards, particularly in data-scarce tropical mountainous regions (Arciniega-Esparza et al., 2022). In this study, several hydrological models are applied. Each model fulfils a specific role within an integrated modelling framework and spanning a continuum from empirical to process-based approaches. In general, empirical models rely on simplified relationships derived from observations, often without an explicit representation of underlying hydrological processes (Seibert & Bergström, 2022). They are particularly useful in data-scarce environments or for rapid event-scale assessments. In contrast, process-based models simulate key components of the hydrological cycle—such as soil moisture storage, evapotranspiration, percolation, and runoff generation—through conceptual or physically interpretable reservoirs and fluxes, providing a more mechanistic representation of catchment behaviour over longer timescales (Ali et al., 2024).

Within this conceptual spectrum, the Rational Method—from its empirical formulation to its physical interpretation—and the Natural Resources Conservation Service-Curve Number (NRCS-CN) approach—implemented through a composite objective function within a custom Python-based hydrological framework—are applied as event-based rainfall–runoff models (Beven, 2012; Soulis et al., 2009). They primarily characterise short-duration storm responses and peak runoff generation under data-limited conditions, making them ideal for analysing rapid flood events (Fan et al., 2019; Mishra & Singh, 2003). In contrast, the *Génie Rural à 4 paramètres Journaliers* (GR4J) model is implemented as a continuous rainfall-runoff model, calibrated against observed rainfall and streamflow to both reconstruct historical streamflow and represent catchment water-balance dynamics over extended periods (Perrin et al., 2003a). This continuous simulation framework enables antecedent moisture conditions, seasonal storage effects, and low- to high-flow variability to be explicitly captured, supporting the identification of practical antecedent rainfall windows that can guide early warning systems. The Muskingum method, although not a rainfall–runoff model in itself, serves as a hydraulic routing scheme to simulate flow translation and attenuation along river reaches following runoff generation (Chow et al., 1988; Subramanya, 2008, 2009).

Taken together, these models are applied in a complementary manner, allowing short-term flood responses, long-term catchment behaviour, and channel routing effects to be analysed within a

coherent, integrated modelling framework. This distinction between empirical and process-based approaches clarifies the conceptual roles of each model and justifies their combined use for a comprehensive understanding of rainfall–runoff dynamics in tropical mountainous catchments.

1.12 Research rationale and thesis structure

1.12.1 Knowledge gaps and justification of the study

Although hydrological processes in mountainous regions have been extensively studied in temperate and well-instrumented catchments (Buytaert et al., 2006; Buytaert & De Bièvre, 2012; Viviroli & Weingartner, 2004), tropical mountainous environments, particularly in sub-Saharan Africa, remain markedly underrepresented in the hydrological literature (Conway & Schipper, 2011; McMillan, 2020; McMillan et al., 2011). In northwest- Rwanda, detailed hydrometeorological datasets are scarce, limiting the development of robust models for rainfall-runoff dynamics, baseflow contributions, and flood forecasting. The lack of long-term, high-resolution data constrains analysis of interannual variability and extreme events, issues that are increasingly critical under climate change (Mugiraneza et al., 2020; Viviroli et al., 2011).

Well-established techniques such as baseflow separation, event-based hydrograph analysis, and conceptual rainfall-runoff modeling are widely applied in global hydrology (Danielescu et al., 2018). However, their integrated application and local calibration in steep, data-poor tropical catchments, where short, intense convective storms and complex subsurface flows dominate, remain largely unexplored (Evin et al., 2024; Hrour et al., 2025). Systematic studies examining how geomorphological features (e.g., slope gradients, relief ratios, and floodplain morphology) interact with rainfall variability to shape runoff generation and flow regimes in such environments are scarce (Buytaert, Célleri, et al., 2006; Viviroli et al., 2011). Moreover, much of the existing hydrological research in East Africa emphasizes large river basins, leaving small headwater catchments under-studied despite their critical role in downstream flow regulation and sediment transfer (Amoussou et al., 2021; Jacobs et al., 2018). Comparative analyses across neighboring catchments with differing physiographic and LULC characteristics are uncommon, limiting the generalizability of regional hydrological understanding (Viviroli & Weingartner, 2004).

Although the importance of rainfall-runoff modeling for flood management is well established, the systematic development and use of high-resolution rainfall-streamflow datasets remain limited (Huang et al., 2019). Moreover, the robustness of widely used empirical and lumped conceptual models to such high-resolution inputs is not fully understood, particularly with

respect to their physical interpretability in flood-hazard applications (Fathi et al., 2025; Li et al., 2024; Xie et al., 2024). Spatial-variability analyses further indicate that finer data resolution can influence streamflow predictions, yet comprehensive assessments across diverse catchments are still scarce (He et al., 2025; Kim et al., 2024). Additionally, only few studies have explicitly connected observed hydrological responses to real-world needs such as flood-risk management, hydraulic design, or climate-adaptation planning in under-researched tropical catchments (Arciniega-Esparza et al., 2022). Consequently, there remains a pressing need for empirical studies that deliver high-quality field observations (Bouaziz et al., 2021; Kanishka & Eldho, 2020) and context-sensitive, transferable modeling frameworks (Blöschl et al., 2013; Blöschl & Sivapalan, 1995; Sivapalan et al., 2003a), while advancing the shift from empirical formulations toward physically grounded interpretations of runoff generation (Beven, 2006; Fan et al., 2019; Fan & Bras, 1998).

This thesis addresses these gaps by integrating short-term, event-scale field observations with statistical and numerical analyses to identify the dominant factors influencing rainfall-runoff responses and flood occurrences in the mountainous catchments of northwestern Rwanda. Through three complementary studies, it tests the reliability of simple yet robust hydrological tools, the Rational Method, NRCS-CN, and GR4J models, under data-scarce tropical conditions. The approach is novel in combining localized field calibration, multi-event validation, and model-based reconstruction to deepen hydrological understanding and render it more physically interpretable for flood management applications. Collectively, this research provides a transferable framework for improving runoff prediction, hydraulic design, and early-warning system development in poorly gauged, topographically complex mountain regions.

1.12.2 Research question

Flood hazards in the mountainous areas of northwestern Rwanda is the major concern, stemming from complex interactions among rainfall, topography, soil properties, and LULC changes (Kim et al., 2025). These hydrogeomorphic factors significantly influence rainfall-runoff processes and, in turn, the frequency and magnitude of flood events. Despite the increasing incidence of damaging floods in the area, the understanding of how these variables interact to drive flood risks, particularly at the scale of small to medium-sized catchments is limited.

This knowledge gap is exacerbated by the scarcity of long-term and high-resolution streamflow data, which hampers the development of reliable flood prediction models and risk management strategies. In such data-limited environments, there is a pressing need to evaluate whether short-

term field observations, supplemented by statistical and numerical analyses, can be used effectively to identify the key drivers of flood response. The central research question is: *"To what extent can short-term rainfall and streamflow observations, combined with statistical and numerical analyses, help improve our understanding of the factors controlling rainfall-runoff responses and flood events in mountainous tropical catchments?"*

Addressing this question provides insight into how rainfall and catchment characteristics influence hydrological responses, especially during extreme events, and aims to support practical flood-risk assessment and management in data-limited mountainous catchments. .

1.12.3 Research objectives and hypotheses

a. Research objectives

This research aimed to accurately assess the key factors controlling rainfall-runoff responses, including topography, soil characteristics, and LULC. These factors were evaluated using short-term rainfall-streamflow observations, along with the temporal and spatial extents of flood events, supported by statistical and numerical approaches. The analysis focused on two small and contiguous catchments of the Mukungwa watershed in northwest Rwanda. Specifically, this study was guided by four key objectives:

1. To collect and provide detailed short-term rainfall and streamflow observations from two contiguous small catchments characterized by contrasting topography, soil types, and LULC conditions.
2. To identify and analyze the main factors influencing rainfall-runoff (RR) response during flood events, focusing on topography, soil characteristics, and LULC.
3. To develop statistical and numerical tools aimed at enhancing the understanding of flood hazards and risks, thereby supporting the design of more effective flood management strategies informed by RR dynamics and catchment characteristics.
4. To estimate probable maximum flood (PMF) events and evaluate their potential impacts on lives, properties, and hydraulic infrastructure within the study area.

b. Research hypotheses

Four central hypotheses guided this research, each reflecting the study's objectives and focusing on how hydrogeomorphological factors shape flood responses in mountainous catchments.

1. Short-term rainfall and streamflow observations from small catchments with contrasting physiography and LULC conditions can reliably capture the variability of rainfall-runoff dynamics.

2. Differences in runoff responses during storm events in mountainous tropical catchments can be explained by variations in topography, soil properties, and hydrogeomorphological controls, as revealed through short-term rainfall and streamflow observations.
3. Statistical and numerical tools based on rainfall-runoff relationships, topography, soil characteristics, and LULC data can improve the understanding of flood hazard patterns and inform better flood management strategies.
4. Rainfall-runoff simulations can be used to estimate probable maximum floods (PMFs), which will identify the spatial and magnitude patterns of flood risk to infrastructure and communities in the study area.

1.12.4 Thesis structure

This thesis is organized into five chapters that together develop a hydrogeomorphological understanding of rainfall-runoff dynamics and flood risk management in the tropical mountainous catchments of northwest Rwanda.

Chapter one introduces the research by establishing the background and global context of flood hazards, then narrows the focus to the significance of flood risk in tropical mountainous regions and the specific challenges in Rwanda. It also presents a critical review of literature on rainfall-runoff processes in tropical mountain regions, storm-event hydrology, and the application of the Rational Method, NRCS-CN, GR4J rainfall-runoff models, as well as alternatives and complementary modeling approaches. It identifies key knowledge gaps, particularly the limited evaluation of event-based modeling in steep, data-scarce catchments.

Chapter two introduces the study area, focusing on the Nyamutera and Gaseke catchments, and presents the hydrometeorological datasets available for the study. It also explains the data-processing procedures, such as storm-event extraction, baseflow separation, runoff coefficient estimation, and the integration of field measurements with modeling analyses. The chapter investigates the spatiotemporal variability of rainfall-runoff dynamics in the catchments through event-based observational analysis, examining hydrological response patterns and the influence of geomorphic factors on streamflow variability. Flow duration curves and specific discharge metrics are then introduced to characterize baseflow and peak flow regimes, followed by an evaluation of event-based runoff coefficients. Finally, the chapter analyses rainfall-runoff relationships to derive design runoff coefficients and evaluates the applicability of the Rational Method, from its empirical formulation to its physical interpretation, for estimating peak discharge in support of flood hazard assessment in steep, data-scarce environments.

Chapter three evaluates storm-based RR modeling approaches for flood risk assessment. It focuses on the performance of the NRCS-CN method in estimating direct runoff and flood design parameters, using event-scale modeling, parameter calibration, and predictive techniques. It also integrates model calibration, validation for transferability, and sensitivity analysis to identify influential variables and parameters.

Chapter four builds upon the preceding analyses of rainfall-runoff dynamics and event-based modeling by addressing the reconstruction of historical streamflows to improve flood early warning in tropical mountainous environments. The chapter focuses on the application of the GR4J rainfall-runoff model in northwestern Rwanda, providing methodological insights into streamflow reconstruction under data-limited conditions. Specifically, it supports the estimation of probable maximum flood (PMF) events and evaluates how reconstructed streamflows can inform flood early-warning thresholds and assess potential impacts on lives, properties, and hydraulic infrastructure within the study area. The chapter demonstrates how model-based approaches can bridge observational gaps, guide the development of effective flood-warning strategies, and contribute to climate-resilient water management in the region.

Finally, chapter five concludes the thesis by summarizing the key findings and scientific contributions. It discusses limitations and provides recommendations for future research and practical applications in flood hazard mitigation across tropical mountainous regions.

Figure 1-3 illustrates main key components of the thesis.

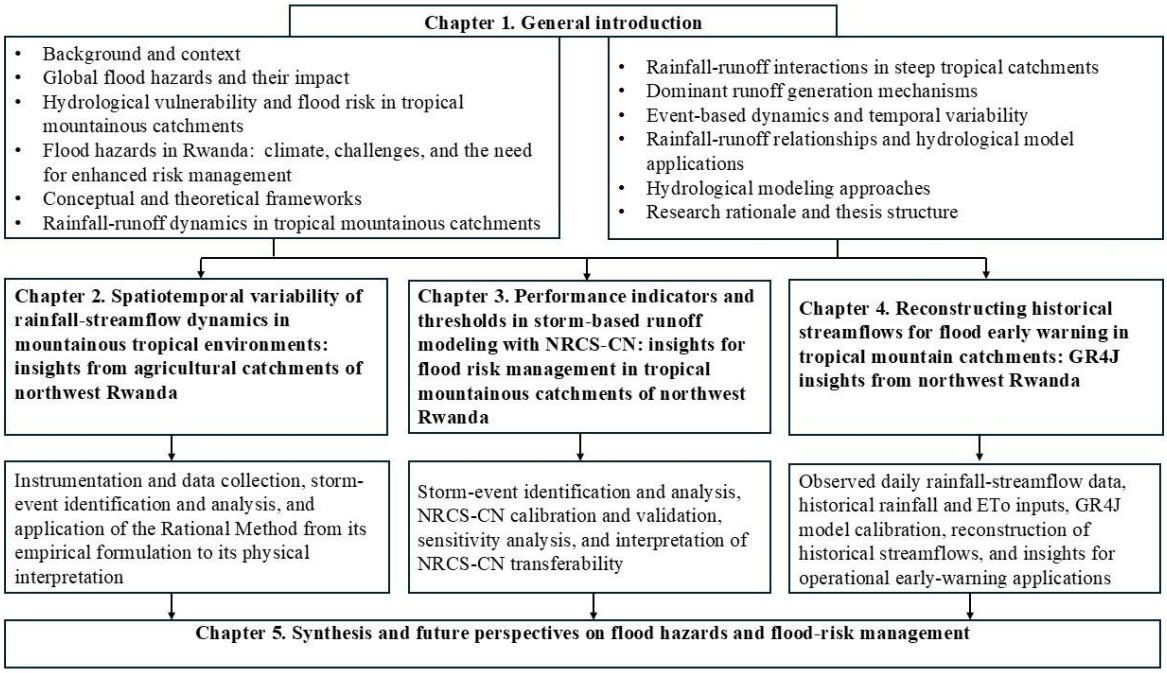

Figure 1-3 Conceptual flowchart summarizing the key components of each chapter and the overall organizational structure of the thesis.

Chapter 2 Spatiotemporal variability of rainfall-streamflow dynamics in mountainous tropical environments: insights from agricultural catchments of northwest Rwanda

This chapter was adapted from a paper published in *Hydrological Processes*. © 2026 John Wiley & Sons Ltd. It is cited as follows:
Nahayo, D., Tychon, B., Rukundo, E., Dewitte, O., Wali, U. G., & Vanmaercke, M. (2026). Spatiotemporal Variability of Rainfall-Streamflow Dynamics in Mountainous Tropical Environments: Insights From Agricultural Catchments of Northwest Rwanda. *Hydrological Processes*, *40*(1), e70360. *https://doi.org/10.1002/hyp.70360*

Abstract

Accurate rainfall–streamflow observations are essential for understanding runoff generation and flood hazards in mountainous regions. Yet such information remains scarce in many areas, especially for small and medium-sized catchments in tropical environments of developing countries. This study develops high-resolution rainfall-streamflow datasets and evaluates the spatiotemporal variability of rainfall-runoff dynamics to assess the applicability of the rational method, from its empirical formulation to its physical interpretation, for flood-hazard management in the Nyamutera (44 km²) and Gaseke (109 km²) catchments of the mountainous Mukungwa watershed in northwestern Rwanda.

To address data scarcity, cost-effective stream monitoring stations were installed to record flow depths, complemented by three automatic rain gauges and two weather stations that record rainfall and other weather parameters at 15-minute intervals. Periodic discharge measurements were conducted to establish stage-discharge rating curves, which were used to derive continuous streamflow records from April 2022 to May 2023.

Analysis of 40 storm-event responses revealed marked contrasts between the catchments: Nyamutera produced higher runoff coefficients (0.05–0.40; mean = 0.20; annual mean = 0.18) than Gaseke (0.02–0.35; mean = 0.10; annual mean = 0.11), reflecting its steeper slopes and lower storage capacity. Design runoff coefficients for the 100-year event were 0.55 and 0.51, and recorded peak discharges reached 131 and 122 m³/s, respectively. These values reflect Nyamutera's faster, more concentrated flow pathways, in contrast to the more attenuated response observed in Gaseke.

The results highlight differences in runoff behavior between the two catchments, likely reflecting their contrasting topography, soil properties, and storage capacity. Although the monitoring network captured most dynamics, uncertainties remain in monitoring very low flows, extreme peaks, and high rainfall variability. This study suggests additional monitoring techniques that could help capture these conditions. The developed approach provides a practical, transferable framework for rainfall-streamflow characterization in similarly data-limited mountainous environments.

Keywords: flood prediction, baseflow separation, runoff coefficient, tropical mountainous catchments, stage-discharge rating curves

2.1 Introduction

Flooding happens when rivers or streams overflow their banks, usually after heavy rainfall or high river discharge, and can submerge areas that are normally dry (Goyal, 2016; Subramanya, 2008). Rainfall that is intense or lasts for several hours often leads to rapid runoff in mountainous catchments. As a result, peak flows can be high, creating hazards for local communities and infrastructure (Kundzewicz & Takeuchi, 1999; Smith & Ward, 1998). Understanding how rainfall translates into runoff is essential, as it can help guide flood hazard management in areas with scarce hydrological data such as northwestern (NW) Rwanda.

In mountainous catchments, the generation of runoff is shaped by the interplay of topography, soil characteristics, and land use/land cover (LULC) (Birch et al., 2021; Haile et al., 2009; Muñoz-Villers & McDonnell, 2012b). Together, these factors determine whether rainfall soaks into the ground, moves as subsurface flow, or runs off the surface. The temperate tropical mountains of NW Rwanda experience steep slopes, heavily weathered soils, and intense convective storms, which often lead to very rapid runoff and pronounced peak flows (Bruijnzeel, 2005). These conditions highlight why it is crucial to study rainfall-runoff events for effective flood hazard management.

Rainfall-runoff processes in tropical Africa are highly complex. Nevertheless, hydrological design and flood estimation often rely on simple empirical methods (Clark et al., 2016). For example, the rational method assumes a constant runoff coefficient and that the catchment responds instantaneously, which may not capture all the variability in real storms (Clark et al., 2016; Smithers, 2012). Such simplifications may overlook critical variations in event-scale runoff behavior driven by topography, soil properties, and geomorphic connectivity. Despite growing research, little attention has been paid to understanding how runoff coefficients at the scale of individual storms relate to the physical and geomorphological characteristics of mountainous tropical African catchments (Abebe et al., 2020; Jacobs et al., 2018; Zenebe et al., 2013), limiting the effectiveness of conventional flood management practices.

Flooding frequently threatens mountainous tropical areas, reflecting a complex mix of rainfall patterns, terrain characteristics, and land-use practices (Bruijnzeel, 2005; Jongman et al., 2015). In temperate tropical mountains, rainfall intensity and duration, steep topography, soil characteristics, and river morphology govern runoff responses and the frequency of flood events (Birch et al., 2021; Haile et al., 2009; Muñoz-Villers & McDonnell, 2012b). LULC changes, including deforestation, agricultural expansion, population pressure in both rural and urban areas, have further altered watershed hydrology, increasing surface runoff and exacerbating flood risk (FAO, 2021; UNEP, 2022; Weng, 2011). Across the African tropics, these conditions

tend to trigger repeated and worsening floods, which makes it especially important to study rainfall-runoff dynamics to guide effective flood management strategies (Doocy et al., 2013; Jongman et al., 2015; Mind'je et al., 2019; Tehrany et al., 2015).

The mountainous catchments of NW Rwanda lie in the African tropics and remain relatively under-studied. In this region, intense rainfall, steep slopes, dense population, and expanding agricultural activity can combine to increase flood hazards (Hahirwabasenga et al., 2024; Nambajimana et al., 2019). In these catchments, where population pressure is high—particularly in flood-prone zones—floods occur frequently and rank among the most damaging hydrological disasters (Nyandwi et al., 2016, 2017). They often lead to loss of life, displacement of communities, and damage to both infrastructure and farmland (Nyandwi et al., 2016, 2017). The combination of steep slopes and high-intensity rainfall renders small (<250 km²) and medium-sized (250–2,500 km²) catchments particularly susceptible to rapid flood generation (Letsinger et al., 2021). In 2018 and 2023, severe flood events caused widespread damage, highlighting the urgent need for improved flood management. For instance, Samba & Macaulay (2023) reported via BBC News that floods and landslides in Rwanda claimed over 130 lives. Assessing flood hazards remains difficult, in part due to the complex nature of hydrological processes and the scarcity of streamflow records. Without sufficient data, reliable prediction and mitigation planning become more uncertain (Blume et al., 2007; Taye et al., 2023a). Therefore, examining the variability of event-based runoff coefficients and their physical controls is critical for both accurate flood assessment and process-based hydrological interpretation.

Accurate hydrological data are essential, yet Rwanda's streamflow monitoring network is still sparse, especially for smaller catchments. The Mukungwa catchment (1,767 km²), encompassing the Nyamutera (44 km²) and Gaseke (109 km²) subcatchments, has just one operational hydrological station at Nyakinama (Rwanda Water Resources Board, 2025). This station is unable to fully capture the flood dynamics further downstream, making it difficult to characterize extreme events across the catchment. The catastrophic floods of 2–3 May 2023 in Nyamutera, which resulted in 11 fatalities near the catchment outlet, underscore the urgent need for improved monitoring. In this context, we focus on rainfall-streamflow dynamics in the Gaseke and Nyamutera catchments. These catchments differ in area, slope, and floodplain extent, and frequent extreme rainfall events, combined with limited rainfall and streamflow data, make conventional flood prediction especially challenging.

Small mountainous catchments in NW Rwanda, such as Gaseke and Nyamutera, often experience flooding during extreme rainfall, which makes accurate forecasting challenging.

However, in such data-scarce environments, simple empirical approaches like the rational method can provide a practical way to estimate peak discharges (Chow et al., 1988). While flood estimation plays a crucial role in hydrological analysis, guiding infrastructure design and flood hazard assessment, the rational method remains a widely used approach due to its simplicity, relying on rainfall intensity, catchment area, and runoff coefficients to estimate peak discharge (Chow et al., 1988; Goyal, 2016; Raghunath, 2006; Yazdanfar & Sharma, 2015). It is defined as:

$$Q_p = \frac{C_d * i_{T_c,p} * A}{3.6} \quad (2.1)$$

where Q_p is the peak discharge (m^3/s), C_d is the design runoff coefficient, $i_{T_c,p}$ is the design rainfall intensity (mm/h) corresponding to the time of concentration T_c for a given exceedance probability p (for a given design return period T years (T=1/p), $i_{T_c,p}$ is directly read in the local Intensity-Duration-Frequency (IDF) curves, A is the drainage area in km^2, and 1/3.6 is the conversion factor (Goyal, 2016; Raghunath, 2006).

Despite its practicality, the rational method assumes uniform rainfall distribution, constant runoff coefficients, and negligible baseflow, simplifications that often fail in complex, steep environments constrained by limited resources and scarce data (McCuen, 2005; Schneider & McCuen, 2006; Viessman & Frost, 2003). Given these limitations, accurate runoff assessment requires distinguishing direct runoff from baseflow, necessitating effective hydrograph separation techniques. While advanced methods such as hydrochemical tracers and environmental isotopes offer precise separation, they are often resource-intensive (Collischonn & Fan, 2013; Ladouche et al., 2001; Mul et al., 2008)**.** Other practical approaches, such as graphical hydrograph analysis, are also used, but automated filters offer a more reproducible and efficient alternative (Blume et al., 2007; Collischonn & Fan, 2013). Among these, the Eckhardt filter is widely adopted due to its general applicability, encompassing several other filtering techniques as special cases (Collischonn & Fan, 2013; Danielescu et al., 2018; Eckhardt, 2005; Fatchurohman et al., 2018; Royem A. A. et al., 2012).

By integrating financially sustainable hydrometeorological monitoring techniques, this study enhances the accuracy of hydrological models and supports more effective flood management. It applies automated baseflow separation and rainfall-runoff modelling to refine flood estimation in two steep contiguous catchments, Nyamutera and Gaseke, contributing to more reliable flood prediction and mitigation efforts. From the above, the following research question was raised:

"How can the rational method be reliably applied for flood hazard assessment and hydraulic design in mountainous, data-scarce catchments such as NW Rwanda, accounting for climate-driven spatiotemporal variability in runoff and the influence of physiographic factors including slope, soil properties, relief, floodplains, and LULC"? Specifically, this study aims to: (i) provide high-resolution rainfall and streamflow datasets from direct field observations to support hydrological analysis in data-scarce mountainous catchments, (ii) characterize the spatiotemporal variability of rainfall-runoff responses and quantify the influence of geomorphic and hydrological controls on event-scale runoff dynamics, and (iii) explore the potential use of the rational method for representing rainfall-runoff processes and informing flood hazard assessment in small, data-limited tropical catchments.

2.2 Materials and methods

2.2.1 Description of the study area

The study was conducted in the Nyamutera and Gaseke catchments, located in the lower Mukungwa watershed (Figure 2-1). Characterized by hilly terrain, the catchments span elevations from approximately 1,400 to 2,600 m above sea level. Both catchments drain into the Mukungwa River, which is fed by a network of permanent and seasonal tributaries (Rwanda Water Resources Board, 2025). These two catchments are part of the Nyabarongo catchment, which itself is a sub-basin of the Akagera River within the Nile Basin.

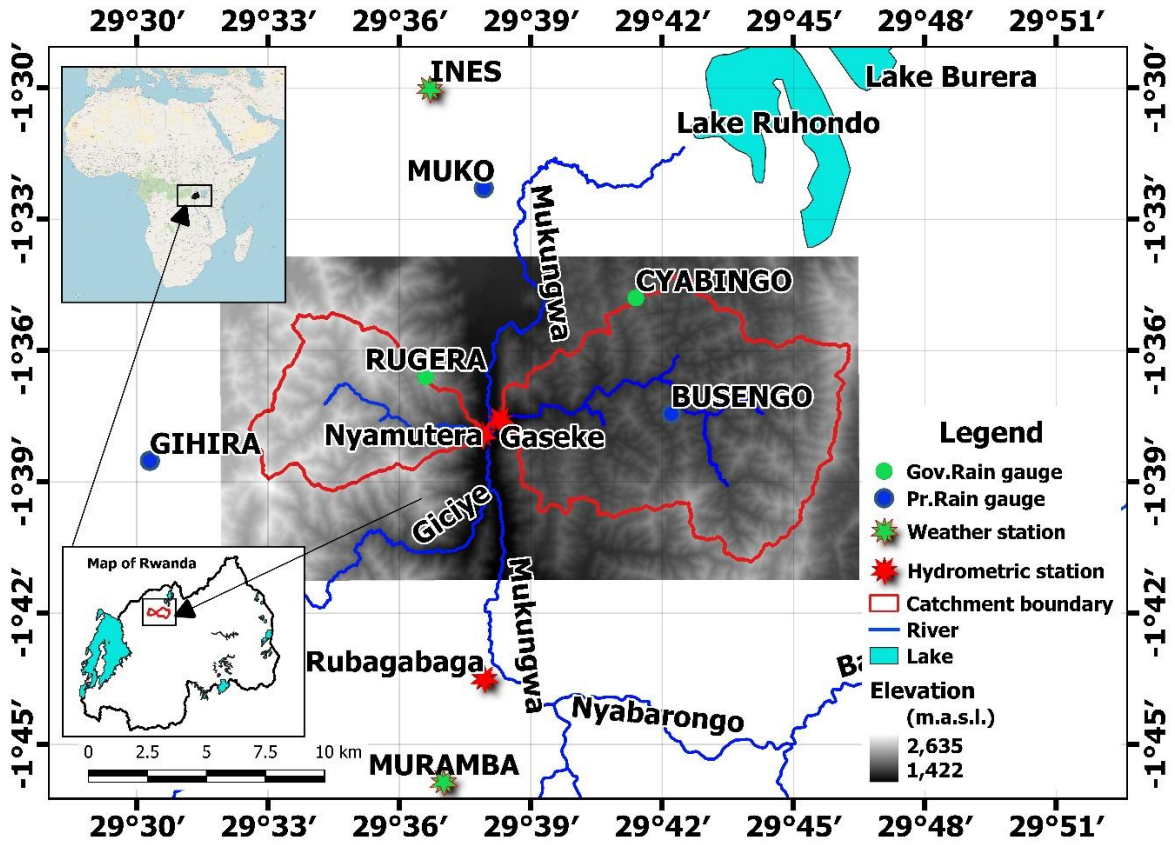

Figure 2-1 Elevation map of the Nyamutera and Gaseke catchments (gray), showing the locations of head sensors (red stars), government rain gauges (green dots) project rain gauges (blue dots), and weather stations (green stars), hydrometric stations (red stars).The arrows indicate, the study area in Rwanda and the country location in Africa, respectively. The acronym 'm.a.s.l.' stands for 'meters above sea level.

According to the Köppen–Geiger climate classification, the study area falls within the tropical highland climate zone (Cwb), characterized by mild temperatures and humid conditions throughout the year (Beck et al., 2018). The region has two rainy seasons, from February to May and from September to mid-December, and two dry seasons, from mid-December to January and from mid-May to August (Ministry of Environment-Rwanda, 2018). Annual rainfall usually falls between 1,200 and 1,600 mm, but intense, short-lived convective storms can occur locally, producing heavy downpours that have a strong impact on runoff, especially in steep areas. Temperatures are influenced by elevation, with average yearly values typically ranging from 15 to 20 °C, becoming cooler as altitude increases (Cui et al., 2021). Across the broader Mukungwa catchment, long-term climate records show that it receives around 1,315 mm of rainfall each year, which amounts to roughly 2,563 hm^3 of water. This rainfall generates an average surface flow of about 28.7 m^3/s, equivalent to approximately 900 hm^3 annually (Ministry of Environment-Rwanda, 2018). These climatic characteristics contribute to rapid hydrological responses in small mountainous catchments such as Nyamutera and Gaseke.

The dominant soil type is Andosols which covers the northern and northeastern parts of the area. Other common soil types include Nitosols, Acrisols, Alisols, Lixisols, Ferralsols, and Cambisols. Except for Cambisols, all these soils generally have high infiltration rates, contributing to significant groundwater recharge in the region (over 300 mm/year, or nearly 25% of the annual rainfall) (Rwanda Water Resources Board, 2025).

The lithology of the Nyamutera catchment is dominated by granitic and gneissic rocks, followed by alluvium and volcanic rocks. In contrast, the Gaseke catchment is primarily composed of schists and quartz mica-schists, with minor pegmatite and alluvial deposits in valley bottoms and terraces (Baudet et al., 1989; Theunissen et al., 1991), as described in the Figure 2-2.

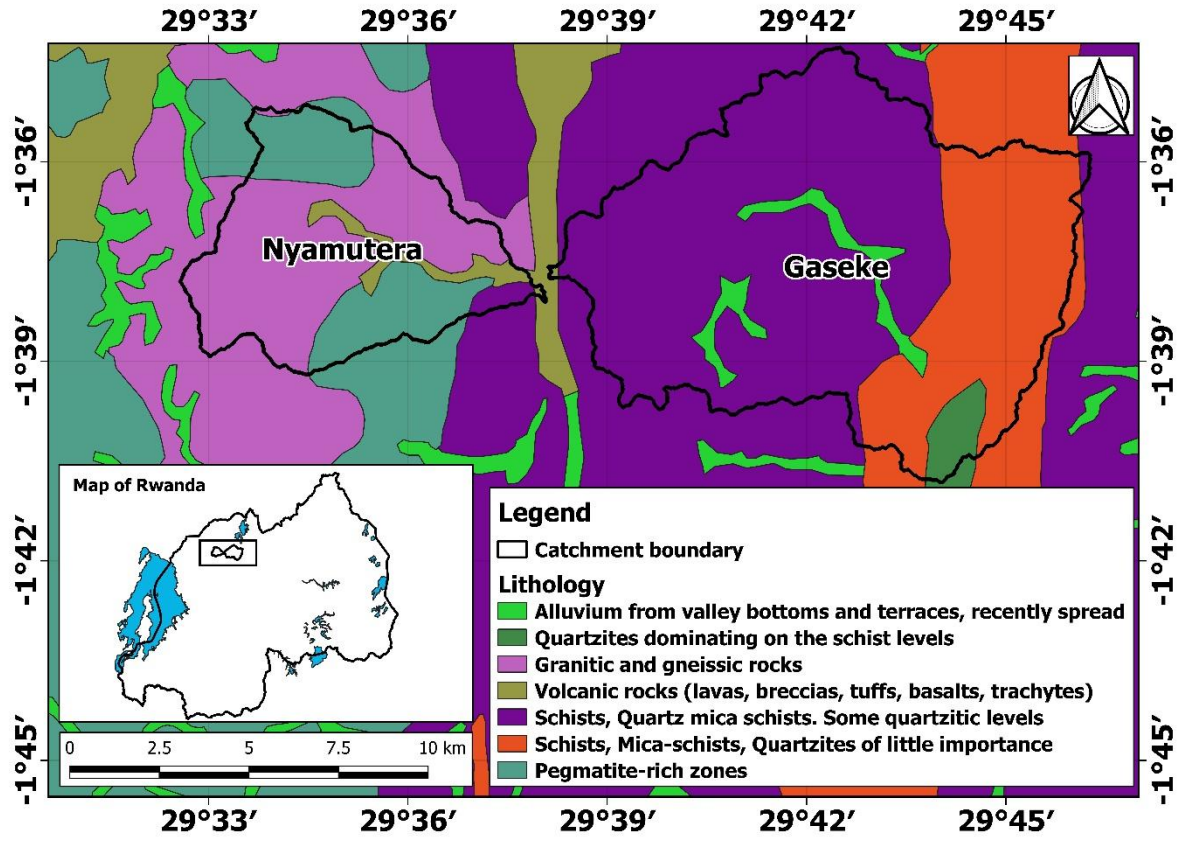

Figure 2-2 Lithology map of Nyamutera and Gaseke catchments (Theunissen, K. et al., 1991).

The land use and land cover (LULC) in the study area include scattered plantations, open agricultural land, and closed agricultural systems. Open agricultural land refers to sparsely vegetated croplands dominated by seasonal crops (e.g., beans, maize, potatoes), with minimal tree cover and limited permanent infrastructure, conditions that increase exposure to rainfall and soil erosion (Karamage, Zhang, et al., 2016). Closed agricultural systems, by contrast, are more intensively managed and characterized by intercropping of permanent crops (such as bananas) with seasonal crops, often under partial canopy cover (Ruticumugambi et al., 2024). Most agricultural land consists of individually owned smallholdings, while government-owned

parcels are limited and typically located on marginal hillslopes. Other LULC classes consist of scattered built-up areas, and settlements concentrated in small commercial centers (Rwanda Water Resources Board, 2025). Agricultural land dominates the study area, followed by forest plantations, with grasslands covering the smallest portion, and a floodplain of about 168 hectares crossed by the Gaseke river (Figure 2-3). These distinctions in land use and ownership are important for understanding flood vulnerability and guiding local flood control strategies.

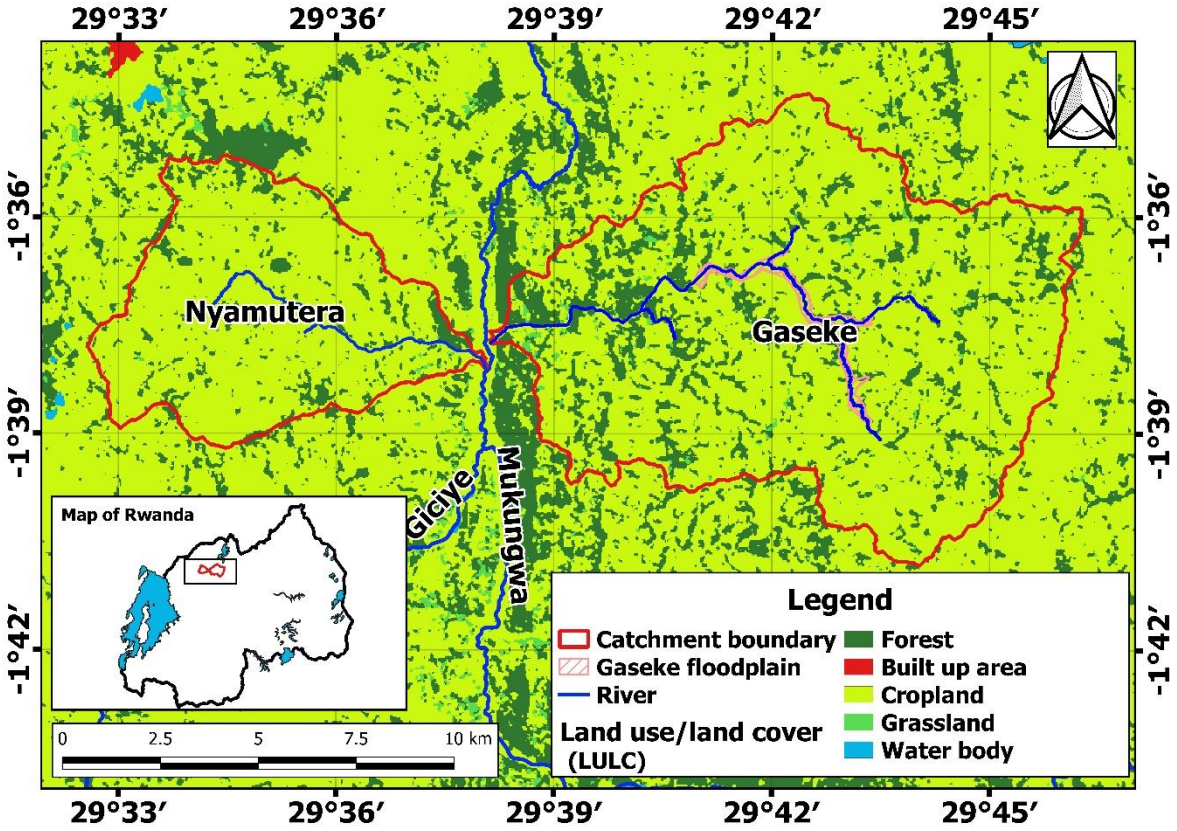

Figure 2-3 Land use/land cover (LULC) map of the study area in 2021 (Source: Rwanda Water Resources Board).

2.2.2 Construction of the hydrometric stations, flow depth and rainfall data collection

Two hydrometric stations were constructed near the outlets of the Nyamutera and Gaseke rivers using reinforced concrete structures. Each station was equipped with a galvanized iron intake pipe, bent at a right angle at the base to facilitate efficient water entry. The lower end of the pipe was perforated and embedded in concrete to house a digital pressure transducer (TD-diver), which recorded water column height and temperature at 15-minute intervals. To correct atmospheric pressure fluctuations, a barometric pressure transducer (Baro-diver) was installed at the Rubagabaga station (Figure 1), capturing atmospheric pressure and temperature on an hourly basis. These readings were used to adjust the raw water level data collected by the TD-

divers across the Mukungwa catchment. The TD-divers determine water column height by measuring the pressure exerted by the water column through an integrated sensor, with data regularly retrieved and processed for analysis.

To maintain accuracy, the transducers and their enclosures were regularly cleaned to prevent sediment buildup from high flows (Zenebe et al., 2013). The Baro-diver, positioned at a lower elevation than the Nyamutera and Gaseke stations, adjusted water pressure readings from all TD-divers in the catchment. Barometric pressure corrections followed the international formula (Ahlheim et al., 1989; Roedel, 2000).

$$p(h) = \frac{p_0}{\left(\frac{T(h)+0.0065h}{T(h)}\right)^{5.255}} \quad (2.2)$$

where p_0 is the reduced pressure at the location of the baro-diver, p(h) is the corrected barometric pressure at the considered location (Nyamutera or Gaseke hydrometric stations), T(h) is the temperature in Kelvin, h (in meters) is the difference in elevation between the baro-diver and two hydrometric stations, and 0.0065 is the vertical gradient of the temperature of 0.65K per 100m.

Alongside automatic measurements, staff gauges were installed at each station, with flow depths recorded daily at 07:00, 12:00, and 17:00 to compare Diver readings with manual observations. Flow assessments were carried out using either the float method or flow probe techniques. The float method estimates surface velocity by timing a floating object, such as a tennis ball, over a known distance (Raghunath, 2006; Subramanya, 2008). To ensure accurate discharge calculations, measurements were taken in river sections exhibiting relatively uniform cross-sections and steady flow conditions (Raghunath, 2006; Subramanya, 2008). At the designated control section, the free water surface width (B) was divided into six equal intervals, and velocity was measured along a 10-meter stretch both upstream and downstream. Each measurement was repeated three to five times to minimize random variations. The mean surface velocity (Vs) was then converted to the average velocity (V) using Prony's equation (Dos Santos & Tavares, 2015; Jha et al., 2022; Koutalakis & Zaimes, 2022; Zenebe et al., 2013).

$$V_s = 1.2V \; or \; V = 0.8V_s \quad (2.3)$$

Unlike the float method, the flow probe directly determines average velocity through the rotation of its propeller.

Additionally, the channel cross-section (A in m^2) of each river was surveyed at each field measurements of water depths and velocities, and the instantaneous discharge (Q in m^3/s) was

calculated as the product of the cross-sectional area (A) and the average flow velocity (V) (Subramanya, 2009).

$$Q = A \times V \quad (2.4)$$

Besides the head sensors (TD-Divers), the catchments were equipped with three automatic rain gauges (Gihira, Muko, and Busengo) and two complete weather stations (INES and Muramba) to collect rainfall and other meteorological data. Measurements are recorded every 15 minutes and can be conveniently accessed online at *https://ng.fieldclimate.com* (n.d.) (Figure 1). Rainfall distribution across the two catchments was estimated using the Thiessen polygon method, which interpolates spatial data between the ground rain gauges (Di Piazza et al., 2011; Garnero & Godone, 2014). Note that the above cost-effective hydrometric and rain gauge tools were selected due to their low cost compared to radar-based systems for water level and discharge monitoring.

2.2.3 Conversion of flow depths to the river discharge time series

The instantaneous river discharges (Q) and flow depths (d) measured during field surveys were used to develop stage-discharge rating curves (SDRCs) (Zenebe et al., 2013):

$$Q = a * d^b \ , \quad (2.5)$$

where a and b are the fitting parameters. These curves enabled the conversion of continuously recorded flow depth data into river discharge records at 15-minute intervals.

Due to terrain constraints, field discharge measurements during the study period did not extend to bankfull conditions. According to the International Organization for Standardization (ISO), SDRCs should not be extrapolated beyond twice the largest measured discharge, except as a last resort (Braca, 2008; Pappenberger et al., 2006; Rowiński, 2013). Based on this guideline, SDRCs were extrapolated but calibrated using the Manning equation, incorporating field measurements, observations, and literature recommendations (Braca, 2008; Chow et al., 1988). The SDRCs derived from measurements were applied to flow depths for which the computed values closely aligned with those obtained from the Manning equation (≤20% discrepancy); for flow conditions beyond this range, hydraulic computations reverted to the SDRCs derived from the Manning equation (Darienzo et al., 2021; François Birgand, 2012). The river cross-sections and riverbed slopes were obtained through a field survey using a differential global positioning system (DGPS). The Manning equation is defined as:

$$Q = \frac{A}{n} R^{2/3} S^{1/2} \ , \quad (2.6)$$

where Q is the discharge, n is the Manning's roughness coefficient, S is the riverbed slope, A is the cross sectional area, and R is the hydraulic radius (Karamouz et al., 2010b; Subramanya, 2009).

2.2.4 Hydrograph, hyetograph, and S-curve analysis

High-resolution time series data of rainfall and streamflow at 15-minute intervals were analyzed to characterize the rainfall-streamflow response of the Nyamutera and Gaseke catchments. Hydrographs and hyetographs were plotted together to visualize the temporal relationship between precipitation inputs and streamflow outputs during storm events. Cumulative rainfall and streamflow volumes were calculated and plotted as S-curves, enabling clear identification of key hydrological time parameters (A. Pandey et al., 2021). The lag time (TL) was computed as the temporal difference between the peak rainfall and the peak streamflow, providing a measure of the catchment's hydrological response speed. The time of concentration (Tc) was derived by applying a scaling factor (Tc ≈ 1.67 × TL), as shown in Equation 8, consistent with methodologies established in recent hydrological research (McCuen, 2017).

$$T_L = 0.6T_c \quad (2.7)$$

These parameters were visually annotated on hydrographs and S-curves to support interpretation of flow dynamics (Gericke & Smithers, 2014a). This approach facilitates detailed event-based analysis of rainfall-streamflow processes and provides critical input for hydrological modeling and flood forecasting (Gericke & Smithers, 2014a; Sultan et al., 2022).

2.2.5 Hydrograph separation and runoff coefficient estimation

Accurate flood assessment requires distinguishing between direct runoff and baseflow (Blume et al., 2007). Baseflow separation techniques help isolate overland flow contributions, thereby improving the reliability of runoff coefficients in flood estimation (Collischonn & Fan, 2013). One widely used approach is Eckhardt's automated filtering method, defined as:

$$b_t = \frac{(1-BFI_{max})\alpha b_{t-1} + (1-\alpha)BFI_{max}Q_t}{1-\alpha BFI_{max}} \quad (2.8)$$

where b is baseflow (m³/s), Q is streamflow, t represents time, α is the groundwater recession constant (ranging from 0 to 1), and BFI_{max} is the long-term ratio of baseflow to total streamflow (also between 0 and 1). The recession constant (α) is derived from recession analysis, while BFI_{max} is estimated based on the catchment's predominant geological characteristics (Collischonn & Fan, 2013; Danielescu et al., 2018; Eckhardt, 2005).

This method is applied in three steps: (i) selecting one or more recession segments to estimate α, (ii) using the estimated α to run the backward filter and determine BFI_{max}, and (iii) applying Eckhardt's filter (Collischonn & Fan, 2013; Eckhardt, 2005).

Given the geological makeup of the study area, which may feature various aquifer types across the subcatchments (Baudet, D et al., 1989; Theunissen, K et al., 1991), BFI_{max} was assumed to range between 0.25 and 0.80 (Collischonn & Fan, 2013). Through trial and error and visual analysis of recession curves, α was set to 0.99, yielding BFI_{max} (parameter estimated based on the predominant geological characteristics of the catchment) values of 0.52 for Gaseke and 0.75 for Nyamutera. The hydrograph separation was then carried out using the Sephydro online tool (Danielescu et al., 2018).

The event-based runoff coefficient (C), average event-based runoff coefficient (Cav), and annual runoff coefficient (AC) were determined as the ratios of direct runoff to total rainfall for a storm event, the average of event-based runoff coefficients, and total annual direct runoff to total annual rainfall, respectively (Blume et al., 2007; Negatu et al., 2022).

Furthermore, the peak runoff coefficients (Cp) for both catchments were fitted to the Normal, Lognormal, Gumbel, and Log-Pearson III distributions to estimate the design runoff coefficient (Cd) for hydraulic structure design across multiple return periods (2, 5, 10, 25, 50, and 100 years) (Froehlich, 2016; Hajani & Rahman, 2018; Kidanie et al., 2022a; Shah & Pan, 2024, 2024; V. P. Singh et al., 2018). These distributions were chosen due to their widespread use and suitability in hydrological frequency analysis: Normal and Lognormal for symmetric and positively skewed data, respectively (Chow et al., 1988; Vivekanandan, 2018); Gumbel for extreme event modeling (Subramanya, 2008; Vivekanandan, 2018); and Log-Pearson III, recommended by the U.S. Water Resources Council, for its flexibility in handling skewed and heavy-tailed flood data (Vivekanandan, 2018). Using different distributions helps ensure that C_d estimates are robust, supporting the design of hydraulic structures capable of handling floods with various return periods.

Because the number of storm events was limited, parametric bootstrapping was used to capture the uncertainty in design runoff coefficients (Efron & Tibshirani, 1993; Kundzewicz & Robson, 2004; Singh et al., 2018). Design values were re-estimated from the fitted probability distributions, with the 2.5th and 97.5th percentiles defining 95% confidence intervals. This approach provides a statistically robust estimate of parameter uncertainty, even for small sample sizes (Kundzewicz & Robson, 2004). Nevertheless, the accuracy of these Cd values could be further improved by incorporating reliable historical flood records, which are currently unavailable.

While the Nash-Sutcliffe Efficiency index (NSE) is widely used in hydrological modeling, its sensitivity to peak flows and limitations in reflecting low-flow performance warrant complementary metrics (Jain Sharad Kumar & Sudheer, 2008; James et al., 2023; Mir &

Dubeau, 2015; Swamynathan, 2017; Tufféry, 2017). Therefore, additional indicators, including RMSE and R^2 for error magnitude and explained variance, the Kolmogorov-Smirnov statistic (KS stat) and p-value for distributional similarity, the Kolmogorov-Smirnov (KS) statistic, p-value, Akaike Information Criterion (AIC) and Bayesian Information Criterion (BIC) for model selection, were used, where necessary, to provide a more robust and multi-faceted evaluation (Pachepsky et al., 2016; Zhan et al., 2019). Some of their equations are given below:

$$NSE = \frac{\sum_{i=1}^{n}(Q_o(i)-Q_m(i))^2}{\sum_{i=1}^{n}(Q_o(i)-\bar{Q}_O(i))^2} \quad (2.9)$$

$$RMSE = \sqrt{\frac{1}{n}\sum_{i=1}^{n}(Q_o(i) - Q_m(i))^2} \quad (2.10)$$

$$R^2 = \frac{\sum_{i=1}^{n}(Q_o(i)-\bar{Q}_O(i))(Q_m(i)-\bar{Q}_m(i))^2}{\sum_{i=1}^{n}(Q_o(i)-\bar{Q}_o(i))^2 \sum_{i=1}^{n}(Q_m(i)-\bar{Q}_m(i))^2} \quad (2.11)$$

Where Q_o is observed value at time step i, Q_m is modelled value at time step i, $\bar{Q}_O$ and $\bar{Q}_m$ are the means of observed and modelled values, respectively, and n is the number of observations. Note that the KS stat, p-value, AIC, and BIC are calculated based on a statistic test and their corresponding probability distributions.

2.2.6 Hydrological response characterisation using flow duration and specific discharge curves

To characterize the hydrological response of the Nyamutera and Gaseke catchments, flow duration curves (FDCs) were developed using daily streamflow records. To facilitate inter-catchment comparison, streamflow values were standardized by catchment area to compute specific discharge (L s^{-1} km^{-2}). Daily flow values were ranked in descending order and assigned exceedance probabilities based on their position in the record length. These probabilities were then plotted against the corresponding specific discharge values to construct the FDCs, enabling evaluation of flow regime variability across low, medium, and high flows. This approach follows standard procedures in hydrological analysis (Merz et al., 2006; Smakhtin, 2001; Vogel & Fennessey, 1994).

2.2.7 Coupling SCS-CN optimization with Lorenz-based runoff distribution metrics

To investigate the influence of initial soil water content on event-based runoff generation, linear regression analyses were performed between initial abstraction (Ia) and the runoff coefficient (C) for each catchment, based on rainfall-runoff events. Ia values were estimated through SCS-CN model calibration (Mishra & Singh, 2003) using a custom Python framework developed to optimize rainfall-runoff event simulations. The initial curve number (CN) was derived from 2023 Sentinel-2 imagery (10 m resolution) using Esri Land Cover data (arcgis.com, 2024).

This framework introduces a dual-objective calibration approach that combines peak-weighted root mean square error (PW-RMSE) and percent error in peak discharge (PEPD) to better capture both hydrograph shape and peak response (USACE HEC, 2025). Differential evolution was used as the optimization algorithm for its robustness in handling nonlinear, multi-parameter hydrologic models (USACE HEC, 2025). This framework enables automated event-specific calibration to estimate Ia values in data-scarce regions, providing a practical alternative to soil moisture measurements, which remain difficult to obtain even in well-instrumented catchments. To evaluate catchment sensitivity, we analyzed statistical significance, slope magnitude, explained variance (R^2), and distributional similarity (p-value) (Berghuijs et al., 2016).

To further assess variability in runoff generation, we used Lorenz-based runoff distribution, which describes how total runoff volume is built up across individual rainfall-runoff events, offering an intuitive way to assess whether a catchment produces runoff frequently or mainly during a few dominant storms. Rather than focusing on discharge magnitudes alone, this approach highlights the relative contribution of small versus large events to the annual runoff total. A Lorenz curve close to the line of equality indicates that runoff is generated progressively by many events, reflecting frequent hydrological connectivity and limited threshold behavior (Berghuijs et al., 2016). In this context, Lorenz curve-based analysis was applied to the distribution of direct runoff volumes, yielding Gini indices as indicators of concentration versus dispersion (Berghuijs et al., 2016). These hydrologic metrics were interpreted in relation to geomorphic variables, slope, relief, and centroid flowpath length, extracted from 12.5 m digital elevation models (Laudon et al., 2022). This enabled scale-independent comparison of runoff generation dynamics and timing, revealing functional differences in catchment behavior under varying rainfall conditions (Detty & McGuire, 2010a; McGlynn et al., 2003; Wörman et al., 2002). Overall, this integrative approach quantifies how terrain and landscape structure mediate rainfall partitioning and runoff generation efficiency.

2.3 Results

2.3.1 Rainfall data

Between May 3, 2022, and May 2, 2023, the total annual rainfall recorded at the Gihira, Muko, and Busengo rain gauge stations was 1,708 mm, 1,739 mm, and 2,216 mm, respectively. For the same period, rainfall estimated using NASA POWER satellite data totaled 1,811 mm (NASA Prediction Of Worldwide Energy Resources, 2024). In comparison, nearby government-operated stations recorded 2,566 mm at Rugera and 1,491 mm at Cyabingo. The most intense daily rainfall events occurred on April 2 at Rugera (86.8 mm) and on April 3, 2023,

when Gihira recorded 97.4 mm, Muko 65.2 mm, Busengo 80.8 mm, and Cyabingo 80.4 mm, corresponding with a major flood event in the Gaseke catchment. To address gaps in daily precipitation records from the government rain gauges from April 2022 to May 2023, missing values, 44 days for Rugera and 21 days for Cyabingo including the dates of flood events, were estimated using corresponding data from the NASA POWER dataset (Figure 2-4).

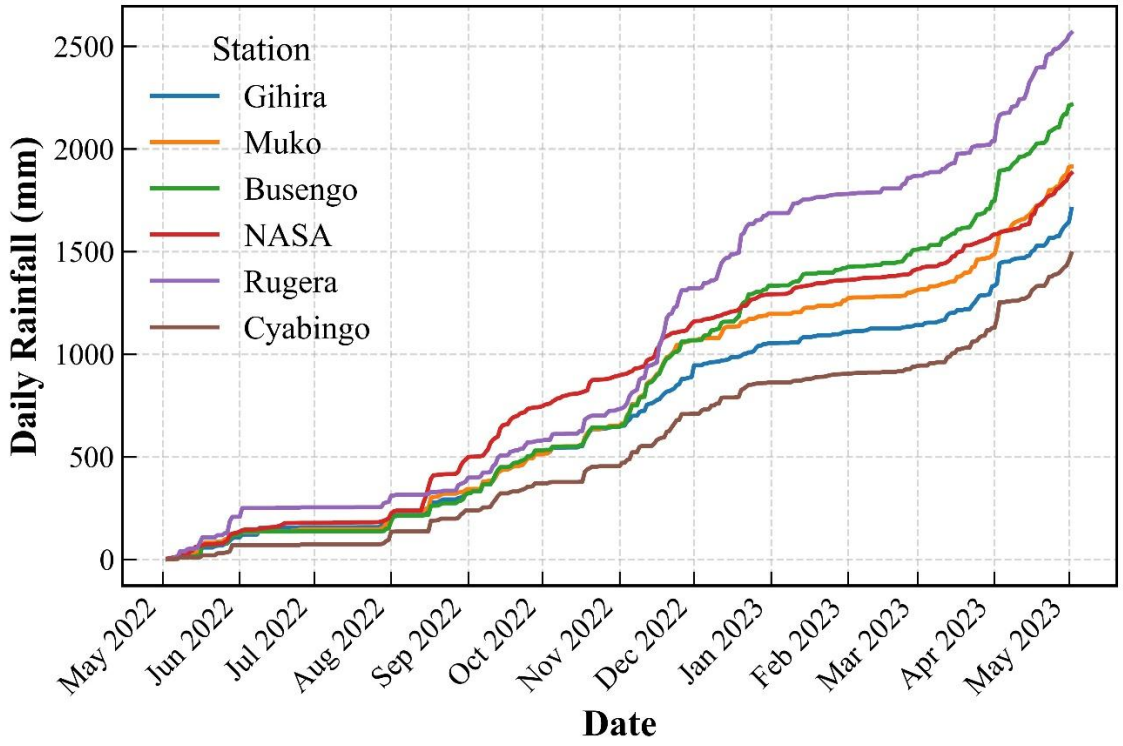

Figure 2-4 Cumulative rainfall data recorded at the Gihira, Muko, Busengo, Rugera, and Cyabingo rain gauges, along with NASA Power rainfall data.

2.3.2 Stage-discharge rating curves, flow regimes, and specific discharges

Figure 2-5 presents the fitted stage-discharge rating curves (SDRCs) based on field observations (blue dashed lines) and their extrapolation to bankfull conditions using the Manning equation (red dashed lines) for Nyamutera (a) and Gaseke (b). Uncertainties associated with the observed SDRCs are also indicated in the legend. Statistical metrics used to assess the uncertainty in the SDRCs indicate RMSE values of 1.572 for Nyamutera and 1.992 for Gaseke. The corresponding NSE and R^2 values are 0.912 and 0.867, respectively. The fitted SDRC

parameters *a* and *b* derived from observations were 26.91 and 2.41 for Nyamutera, and 5.02 and 2.11 for Gaseke, respectively.

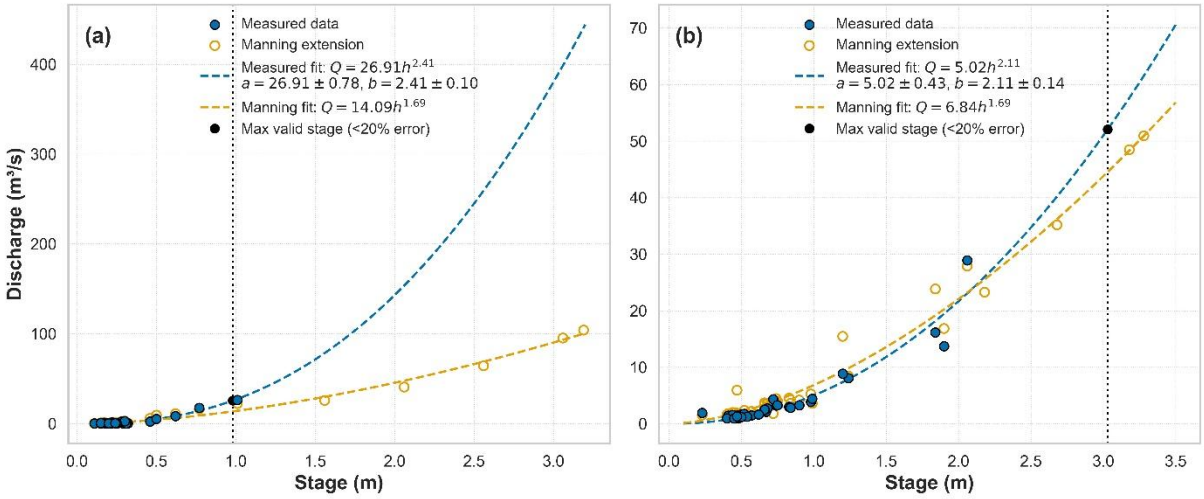

Figure 2-5 The plots above present the stage-discharge rating curves (SDRCs) developed from measured stages and discharges (dashed blue) and those extrapolated to bankfull conditions using Manning's equation (dashed red) for (a) Nyamutera and (b) Gaseke.

Note: The green dashed lines indicate the maximum stage threshold beyond which the SDRCs derived from measurements should not be applied. Q is the discharge (m³/s), d is the stage (m), a and b are the SDRC parameters with their uncertainties (a=26.91±0.78, b= 2.41±0.10 for Nyamutera, and a=5.02±0.43, b= 2.11±0.14 for Gaseke).

For the Manning-based stage-discharge rating curves (SDRCs), roughness coefficients (*n*) were estimated as 0.03 for Nyamutera and 0.05 for Gaseke. The corresponding rating curve parameters *a* and *b* were 14.09 and 1.69 for Nyamutera, and 6.84 and 1.69 for Gaseke, respectively. The maximum water depths to which the measured SDRCs apply were 0.98 m (corresponding to 25 m³/s) for Nyamutera and 2.03 m (60 m³/s) for Gaseke. SDRC uncertainty was quantified using 95% confidence intervals (legend of Figure 2-5), and the errors between observed and Manning SDRCs are reported in Table 2-1.

Table 2-1 Stage-discharge rating curve error estimates for the Nyamutera and Gaseke catchments.

Catchment	Stage/measured (m)	Discharge/measured (m³/s)	Discharge/Manning (m³/s)	Errors(%)
Nyamutera	0.26	0.71	0.76	7.65
	0.28	2.16	2.29	5.82
	0.19	0.32	0.32	1.25
	0.77	17.53	16.28	7.10
	0.2	0.35	0.41	16.74
	0.2	0.56	0.51	8.71
	0.22	1.29	1.52	17.74
	0.3	2.74	2.85	4.18

	0.2	0.31	0.36	15.03
Gaseke	0.48	1.07	1.08	1.12
	1.24	7.90	8.45	6.88
	0.98	4.81	5.25	9.24
	0.9	4.02	4.19	4.20
	0.84	3.47	3.61	3.92
	1.9	19.45	16.84	13.39
	2.18	25.99	23.27	10.46
	2.68	40.19	35.18	12.45
	3.03	52.07	44.53	14.46

Note: In the Gaseke catchment, stage and discharge values beyond the measured range were extrapolated, limited to ≤ 20% deviation from Manning-based estimates.

Flow duration curves (FDCs) and their corresponding specific discharges are also illustrated in Figure 2-6. These FDCs indicate that Gaseke exhibits higher specific discharge at the lowest flows (e.g., Q5 = 1.4 L/s/km²) compared to Nyamutera (Q5 = 0.9 L/s/km²). At Q10 and throughout intermediate flow conditions, Nyamutera shows greater specific discharge (Q10 = 2.9 L/s/km²; Q50 = 4.1 L/s/km²; Q90 = 18.4 L/s/km²) than Gaseke (Q10 = 1.7 L/s/km²; Q50 = 3.6 L/s/km²; Q90 = 12.2 L/s/km²). At the high-flow end (Q95), Gaseke reaches a specific

discharge of 30.3 L/s/km², slightly exceeding Nyamutera's 27.6 L/s/km². These patterns are consistent across both total and specific discharge metrics.

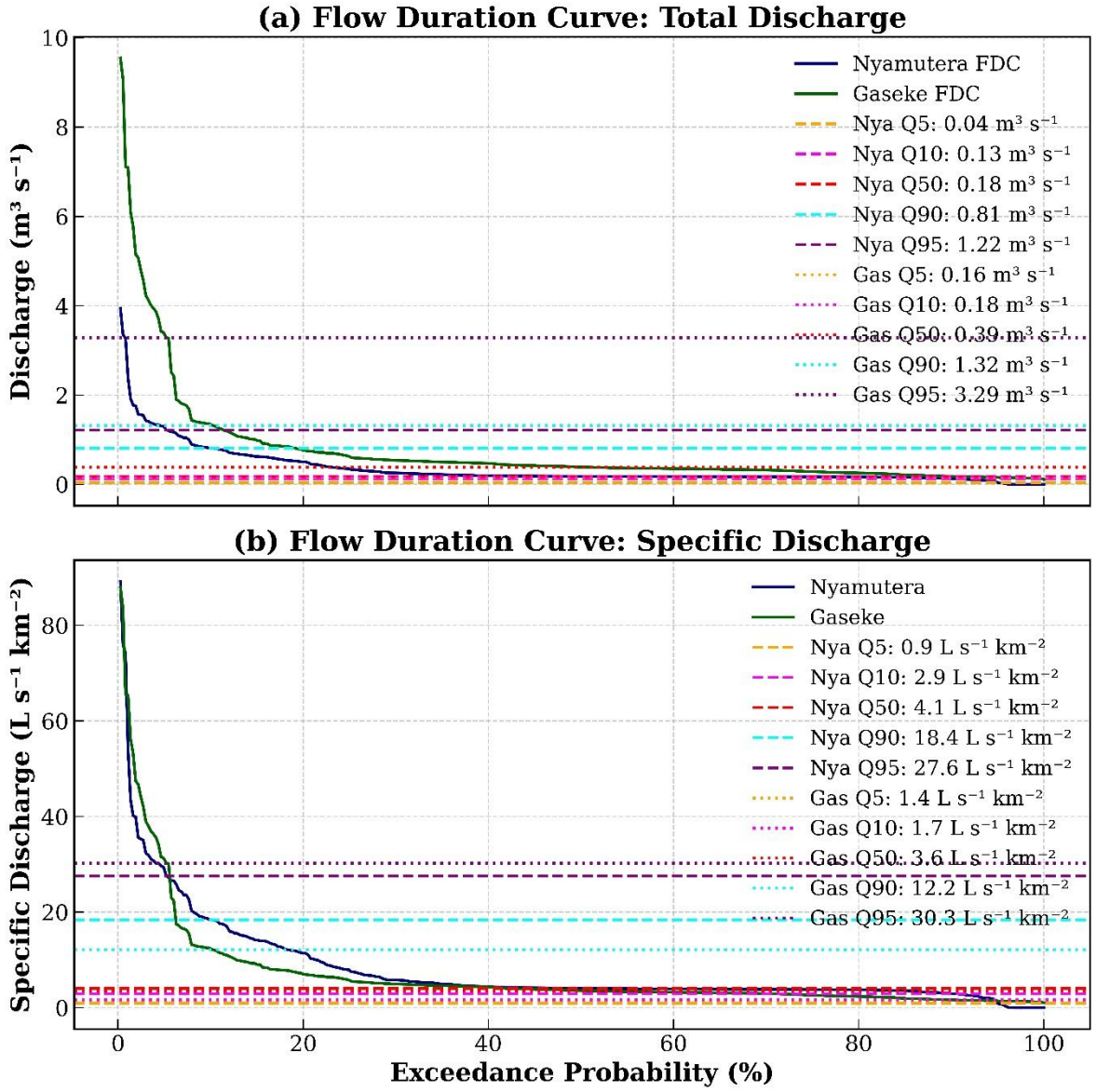

Figure 2-6 The flow duration curves (a) with the specific discharges (b) in Nyamutera and Gaseke.

2.3.3 Runoff dynamics and catchment response parameters

As outlined in the methodology, Eckhardt's digital baseflow filter was applied to separate baseflow from total streamflow for 40 recorded rainfall-runoff events, 16 in the Nyamutera catchment and 24 in the Gaseke catchment. The total annual streamflow was 886 mm in Nyamutera and 446 mm in Gaseke. Of this, the annual direct runoff was estimated at 242 mm (27%) in Nyamutera and 217 mm (49%) in Gaseke, while baseflow contributions amounted to 644.1 mm (73%) and 229 mm (51%), respectively.

Event-based lag times (TL) in Nyamutera and Gaseke ranged from 0.5-3.5 and 1.25-6 hours, respectively, while times of concentration (Tc) ranged from 0.83-5.84 and 2.09-10.02 hours. The mean TL and Tc values were 1.43 and 2.39 hours in Nyamutera, and 3.77 and 6.32 hours in Gaseke, respectively. A summary of event-based runoff coefficients (C), annual runoff coefficients (AC), peak discharges per event (Qmax), TL and Tc for both catchments is provided in Table 2-2. An asterisk ([a]) indicates events during which the hydrometric station was damaged before the storm concluded.

Event-based hydrological characteristics in Nyamutera (3 May 2022–2 May 2023) and Gaseke (4 April 2022–3 April 2023) catchments, Event-based hydrological characteristics in Nyamutera (3 May 2022–2 May 2023) and Gaseke (4 April 2022–3 April 2023) catchments.

Table 2-2 Event-based hydrological characteristics in Nyamutera (3 May, 2022 – 2 May, 2023) and Gaseke (4 April, 2022 – 3 April, 2023) catchments, including direct runoff (DRO), precipitation (P), runoff coefficient (C), maximum discharge (Qmax), lag time (TL), and Time of concentration (Tc).

Catchment	Date	Storm Duration (h)	DRO (mm)	P (mm)	C	Qmax (m^3/s)	T_L (h)	Tc (h)
Nyamutera	07-08 Apr 2022	3	2.5	21.21	0.1	30.9	0.5	0.83
	15-16 Apr 2022	3.25	2.16	6.37	0.3	15.84	0.75	1.25
	19-20 Apr 2022	13.5	6.97	30.89	0.2	29.09	1	1.67
	21-22 Apr 2022	3.75	1.2	4.48	0.3	14.26	0.75	1.25
	23-24 Apr 2022	14.25	13.7	34.32	0.4	28.07	2.25	3.76
	29-30 Apr 2022	9.25	4.55	15.74	0.3	11.82	1	1.67
	01-02 May 2022	3.5	3.51	14.3	0.3	15.82	0.75	1.25
	17-18 May 2022	6	6.19	23.44	0.3	20.37	0.5	0.83
	28-31 May 2022	15.25	7.85	30.67	0.3	11.46	2	3.34
	12-13 May 2022	7.75	3.75	34.5	0.1	14.35	3.25	5.43

	20-22 Dec 2022	9.75	4.13	21.69	0.2	31.7	2.25	3.76
	03-04 Apr 2023	11.75	3.67	79.82	0.1	32.77	1.75	2.92
	18-19 Apr 2023	9.75	1.97	19.96	0.1	9.73	3.5	5.84
	22-23 Apr 2023	6.75	2.97	24.86	0.1	17.38	0.75	1.25
	23-26 Apr 2023	9	2.83	29.52	0.1	11.24	0.5	0.83
	30 Apr–02 May 2023	2.5[a]	25.5	68.06	—	130.8	—	—
Average	—	—	—	—	0.2	—	1.43	2.39
Annual	—	—	—	1715	0.2	—	—	—
Gaseke	8-Apr-22	4.25	0.66	12	0.1	5.02	2	3.34
	19-20 Apr 2022	9.75	3.45	35	0.1	23	1.75	2.92
	23-24 Apr 2022	11	3.21	24.8	0.1	12.25	4.5	7.51
	01-02 May 2022	3.5	2.74	31.2	0.1	18.07	3	5.01
	28-29 May 2022	4	1.09	23.4	0.1	9.64	2.25	3.76
	01-02 Aug 2022	16	1.05	54.6	0	5.82	5	8.35
	17-18 Aug 2022	9.75	1.52	44.4	0	11.15	4.25	7.1
	29-30 Aug 2022	4	0.45	7.8	0.1	3.61	6	10.02
	31 Aug-01 Sep 2022	7.5	0.68	26.2	0	3.62	1.25	2.09
	11-12 Sep 2022	7	1.4	46.2	0	7.56	4.25	7.1
	13-14 Sep 2022	1.75	1	17.2	0.1	8.35	4.5	7.51
	18-19 Sep 2022	8.28	1.44	26.2	0.1	10.26	4.5	7.51
	20-Oct-22	2.75	0.58	25	0	8.95	5.25	8.77

	10-11 Nov 2022	11.5	3.91	41.8	0.1	29.31	5	8.77
	12-13 Nov 2022	8.75	8.32	71.4	0.1	53.81	3.75	6.26
	17-18 Nov 2022	8	1.32	14.4	0.1	17.51	4.75	7.93
	18-19 Nov 2022	5	4.42	26.2	0.2	24.59	3.5	5.84
	19-20 Nov 2022	3.25	3.73	21.6	0.2	22.02	1.75	2.92
	20-21 Nov 2022	8.5	6.25	24.6	0.3	26.52	5.25	8.77
	22-23 Nov 2022	10	2.51	12.8	0.2	13.58	2.25	3.76
	25-26 Nov 2022	2.25	3.39	9.6	0.4	23.25	4	6.68
	26-27 Nov 2022	2.25	7.68	40.6	0.2	46.83	4.25	7.1
	31-Mar-23	4.25	0.78	34.6	0	7.43	3.75	6.26
	02-03 Apr 2023	4.25[a]	1.85	63.2	—	121.9	—	—
Average	—	—	—	—	0.1	–	3.77	6.32
Annual	—	—	—	1985	0.1	—	—	—

Note: The Em dash (—) indicate no need of value.

[a] indicates the hydrometric station has been destroyed before the accomplishment of the storm event.

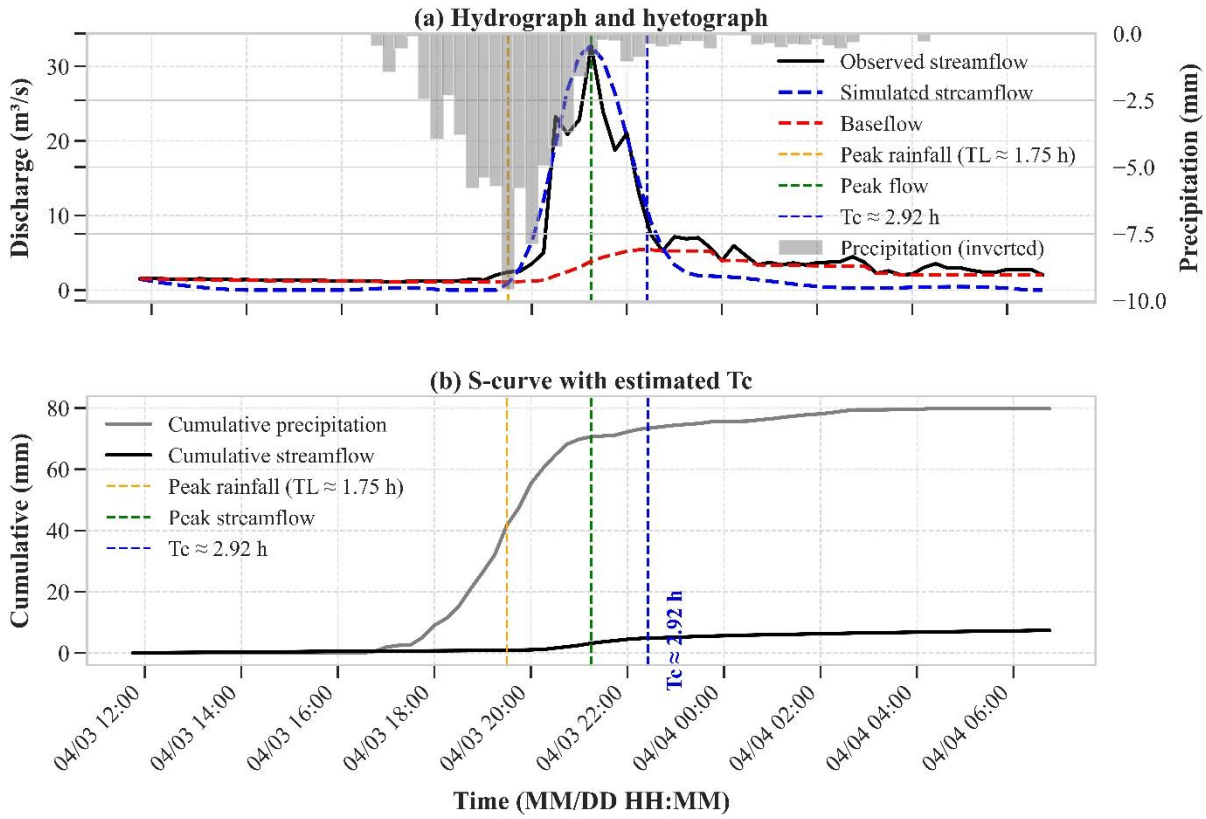

Figure 2-7 Example of hydrograph separation and lag time estimation for rainfall–runoff event #12 in Nyamutera catchment. Panel (a) shows the event hydrograph with precipitation (gray bars), observed streamflow (black line), simulated streamflow (dashed blue line, and baseflow (dashed red line). Panel (b) presents the corresponding S-curve.

2.3.4 Event-based relationships between initial abstraction and runoff coefficient

Figure 2-8 shows that initial abstraction (Ia) is inversely related to the event-based runoff coefficient (C) in both catchments. In Nyamutera, the regression equation was Ia = -13.75 C + 5.27 (R^2 = 0.31, p = 0.032), while Gaseke exhibited a steeper relationship: Ia = -19.92 C + 7.76 (R^2 = 0.27, p = 0.011).

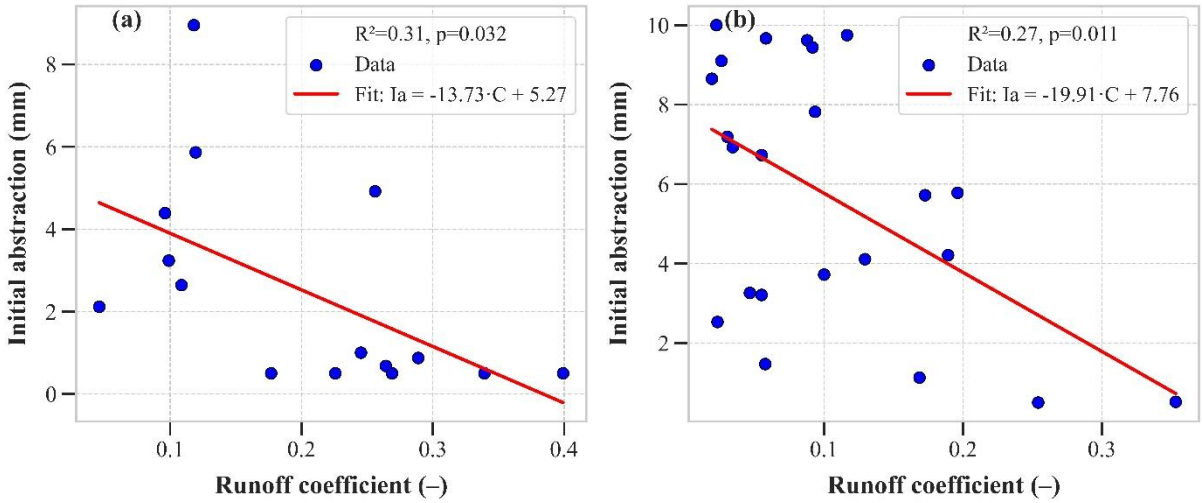

Figure 2-8 Scatterplots of initial abstraction versus runoff coefficient, with fitted regression lines, for Nyamutera (a) and Gaseke (b).

Lorenz curve analysis (Figure 2-9) indicated a Gini index of 0.065 for Nyamutera and 0.151 for Gaseke, reflecting differing distributions of runoff contributions across events.

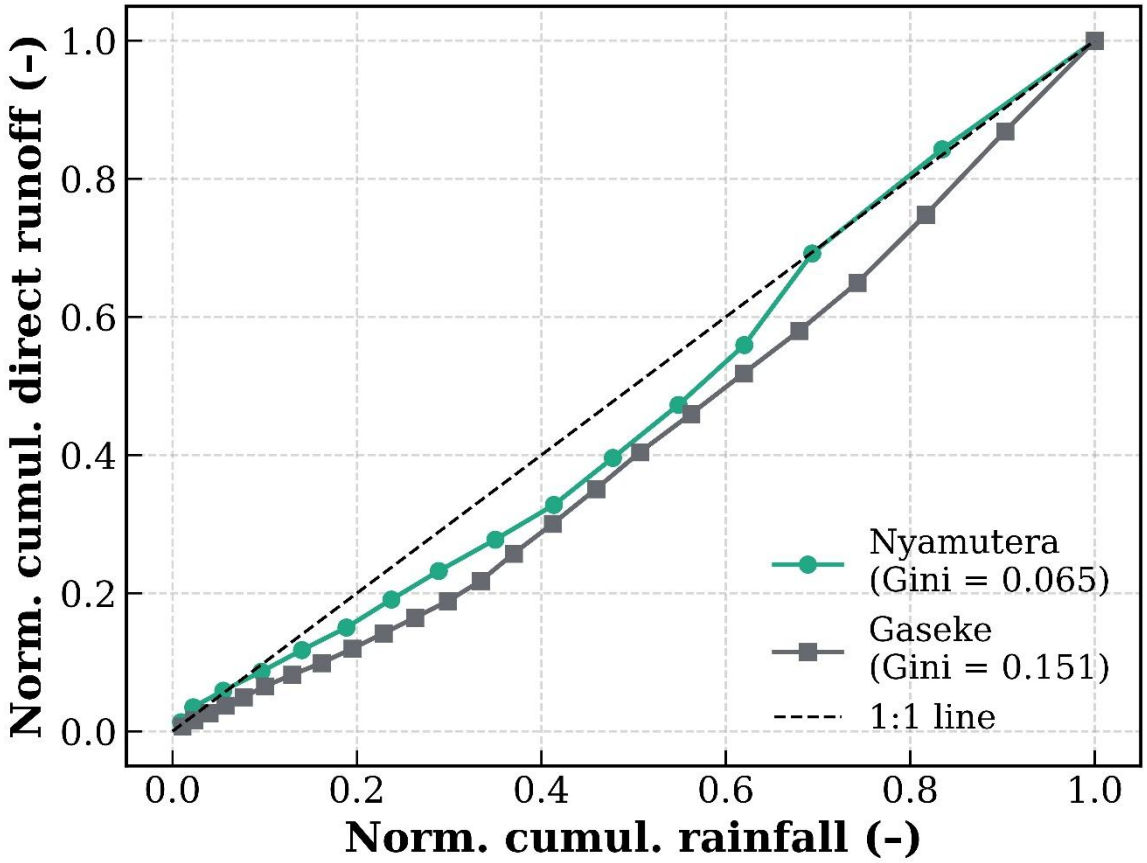

Figure 2-9 Lorenz-based runoff distribution metrics illustrating contrasting runoff responses shaped by geomorphic characteristics and floodplain extent, as indicated by the Gini indices.

2.3.5 Relationship between direct runoff, baseflow and runoff coefficient

Regression analyses were performed to evaluate the relationships between runoff coefficient (C) and event-based direct runoff and baseflow for the Nyamutera and Gaseke catchments (Figure 2-10, panels (a) and (b)). All relationships were statistically significant ($p < 0.05$). In Nyamutera, the coefficient of determination (R^2) was 0.31 for direct runoff ($p = 0.032$) and 0.40 for baseflow ($p = 0.011$). In Gaseke, higher R^2 values were observed: 0.38 for direct runoff ($p = 0.002$) and 0.48 for baseflow ($p < 0.001$).

Seven data points (3.63, 0.66, 6.19, 8.32, 4.13, 6.25, and 3.76 mm) were annotated to indicate key runoff and baseflow events observed in both catchments. Scatter plots with fitted regression lines and 95% confidence intervals illustrated these relationships for each catchment.

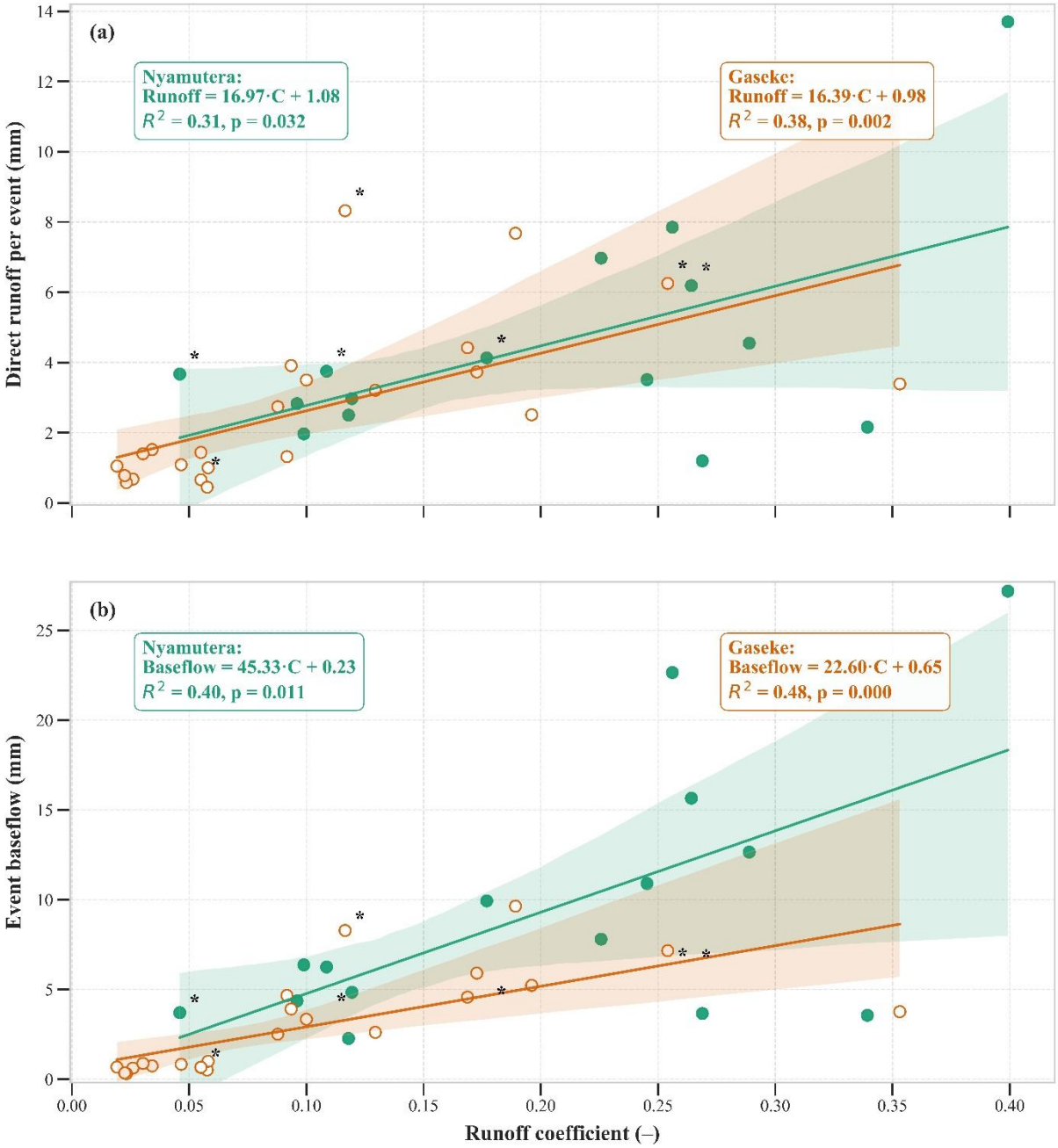

Figure 2-10 Relationships between event-based runoff coefficient (C) and (a) direct runoff and (b) baseflow in the Nyamutera and Gaseke catchments.

Note: Linear regression lines with 95% confidence intervals highlight differences in runoff-generation behavior. Key events are marked with asterisks and detailed in Table 2.5.

2.3.6 Recorded floods in the study area during the study period

Floods in northwestern Rwanda typically occur during the main rainy seasons, which span from mid-September to December and from mid-March to mid-May. During the study period, two notable flood events were recorded: 3–4 April (Q_p = 122 m³/s) and 2–3 May, 2023 (Q_p = 131 m³/s), affecting the Gaseke and Nyamutera catchments, respectively (Table 2-3).

Table 2-3 Results of computations of discharge during the flood events of the nights of 03–04 April for Gaseke, and 02–03 May 2023 for Nyamutera.

Catchment	d_{bf} (m)	P_{bf}(m)	A_{bf}	R_{bf}(m)	n_c	S	Q_{bf} (m^3/s)
Nyamutera	3.19	18.19	35.60	1.96	0.03	0.00314	104.08
	d_{ovt} (m)	P_f (m)	A_f	R_f (m)	n_f		Q_f (m^3/s)
	1.13 (1.13)	164.98	78.38	0.48	0.1		26.75
Total							130.83
Catchment	***d_{bf} (m)***	***P_{bf}(m)***	***A_{bf}***	***R_{bf}(m)***	***n_c***		***Q_{bf} (m^3/s)***
Gaseke	3.28	17.24	31.05	1.80	0.05		50.93
	d_{ovt} (m)	P_f (m)	A_f	R_f (m)	n_f	S	Q_f (m^3/s)
	0.40 (1.37)	222.5	159.77	0.72	0.1	0.00307	70.99
Total							121.92

Note: water depth to the bankfull (dbf), river overtopping depth (dovt; the value in bracket indicates the maximum water depth of the flooded area), wetted perimeter to the bankfull (Pbf), wetted perimeter of the flooded area (Pf), cross-sectional area of the channel to the bankfull (Abf), cross-sectional of the flooded area (Af), hydraulic radius of the main channel (Rbf), hydraulic radius of the flooded area (Rf), the Manning n of the main channel (nc), Manning n of the flooded area (nf), slope (S), total discharge of the main channel (Qbf), discharge of the flooded area (Qf).

2.3.7 Design runoff coefficient estimates across return periods

As outlined in the methodology, four probability distributions, Normal, Lognormal, Gumbel, and Log-Pearson III, were evaluated for estimating the design runoff coefficients (Cd) (Kidanie et al., 2022b). The best-fitting distribution was selected based on a combination of statistical metrics, including the KS stat, p-value, AIC, BIC. Among these, the Gumbel distribution and Lognormal distributions provided the best overall fits. Based on these distributions, the estimated design runoff coefficients for 2, 5, 10, 25, 50, and 100-year return periods were 0.19, 0.28, 0.35, 0.43, 0.49, and 0.55 for Nyamutera, and 0.08, 0.15, 0.22, 0.32, 0.41, and 0.51 for Gaseke. These results are summarized in Tables 2-4 and 2-5 and illustrated in Figure 2-11.

Table 2-4 Design runoff coefficients (Cd) and 95% confidence intervals derived from 10,000 parametric bootstrap realizations for the Nyamutera and Gaseke catchments across selected return periods.

Catchment	Return_period (years)	Cd best	Cd boot mean	Cd–boot–lower–2.5%	Cd–boot–upper–97.5%
Nyamutera	2	0.19	0.19	0.14	0.24
	5	0.28	0.28	0.21	0.36
	10	0.35	0.34	0.25	0.45
	25	0.43	0.42	0.30	0.56
	50	0.49	0.47	0.34	0.64
	100	0.55	0.53	0.37	0.72
Gaseke	2	0.08	0.08	0.05	0.10
	5	0.15	0.15	0.10	0.22
	10	0.22	0.21	0.13	0.33
	25	0.32	0.31	0.17	0.51
	50	0.41	0.40	0.21	0.70
	100	0.51	0.50	0.25	0.91

Note: Cd best represents the best-fit values from the fitted probability distributions, while Cd boot mean and the 2.5–97.5th percentiles quantify parameter uncertainty.

Table 2-5 Goodness-of-fit statistics for four probability distributions (Log-Pearson III, Lognormal, Gumbel, and Normal) fitted to event-based runoff coefficients (Cd) in the Nyamutera and Gaseke catchments.

Nyamutera											
Distribution	**KS-Stat**	**p-value**	**AIC**	**BIC**	**Score**	**2-yr**	**5-yr**	**10-y**	**25-yr**	**50-yr**	**100-yr**
Gumbel	0.1792	0.6572	-22.6517	-21.2356	0.0103	0.19	0.28	0.35	0.43	0.49	0.55
Normal	0.201	0.5158	-22.672	-21.2559	0.4	–	–	–	–	–	–
Lognormal	0.2007	0.518	-19.9559	-17.8318	0.4612	–	–	–	–	–	–
Log-Pearson III	0.1787	0.6608	4.3726	6.4968	0.6	–	–	–	–	–	–
Gaseke											
Distribution	**KS-Stat**	**p-value**	**AIC**	**BIC**	**Score**	**2-yr**	**5-yr**	**10-y**	**25-yr**	**50-yr**	**100-yr**
Lognormal	0.1011	0.9542	-56.8578	-53.4513	0.0017	0.08	0.15	0.22	0.32	0.41	0.51
Gumbel	0.1736	0.4427	-53.3349	-51.0639	0.3679	–	–	–	–	–	–
Normal	0.1852	0.3639	-45.0446	-42.7736	0.4836	–	–	–	–	–	–
Log-Pearson III	0.1006	0.9559	23.8284	27.2349	0.6	–	–	–	–	–	–

Note: The best-fitting distribution for each catchment was identified based on the lowest Akaike Information Criterion (AIC) and Bayesian Information Criterion (BIC) values and the highest p-value from the Kolmogorov–Smirnov (KS stat) test. Design runoff coefficients for return periods of 10, 25, 50, and 100 years were subsequently estimated using the best-fitting distributions (Gumbel for Nyamutera, and Lognormal for Gaseke).

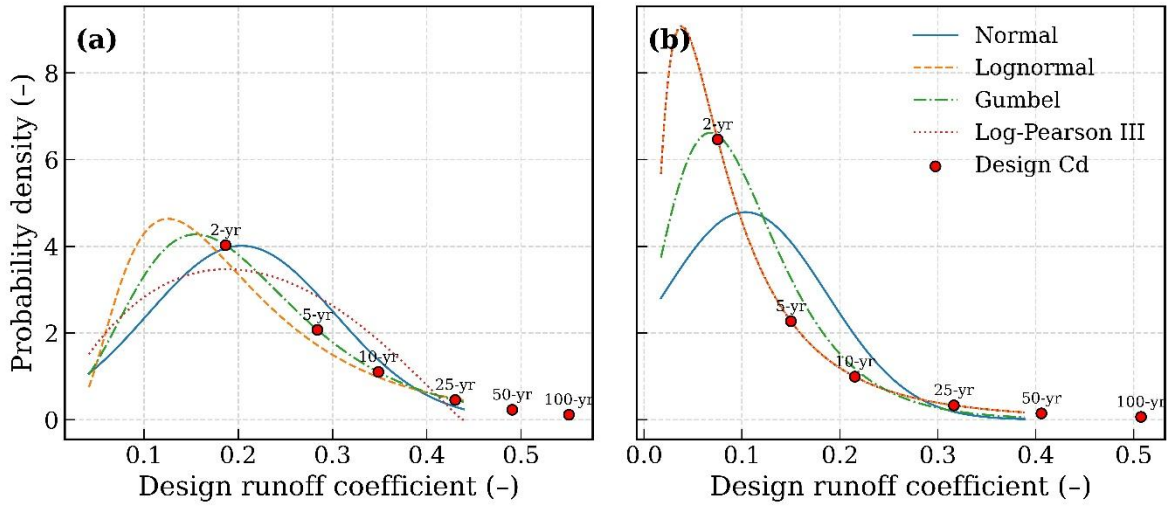

Figure 2-11 Probability distribution fits (Lognormal, Log-Pearson III, Gumbel, and Normal) to the observed runoff coefficient data for the Nyamutera (a) and Gaseke (b) catchments.

Note: The Gumbel and Lognormal distributions provided the best fit based on KS statistic, p-value, AIC, and BIC criteria for Nyamutera and Gaseke, respectively. Cd means design runoff coefficient.

2.4 Discussion

2.4.1 Reliability of the collected rainfall and streamflow data

Interpreting the collected rainfall data requires attention to potential uncertainties. As described in the methodology, rainfall data for the Nyamutera catchment were obtained through spatial interpolation using the Thiessen polygon method, based on three rain gauges located outside the catchment (Gihira, Muko, and Busengo). However, this region is characterized by convective precipitations influenced by orographic effects due to its mountainous terrain (Muhire & Ahmed, 2015). Such rainfall events are typically of short duration, with high intensities, and often occur during the afternoon and evening in the main rainy seasons (March-May and September-December) (Muhire & Ahmed, 2015). Given their localized nature and high spatial variability, these rain gauges may not always accurately capture the rainfall responsible for generating runoff within the Nyamutera catchment. In the Gaseke catchment, a similar limitation exists: The Thiessen polygon method relied on a single rain gauge at Busengo to establish the rainfall-streamflow relationship. Relying on a single gauge may not adequately reflect the spatial variability of rainfall influencing streamflow at the Gaseke outlet. Nevertheless, a comparison between the annual cumulative rainfall from this study, government rain gauges, and NASA POWER satellite data revealed consistent cumulative patterns, suggesting that the overall rainfall estimates lie within a reasonable range (Figure 4). However, gaps in the daily records from government rain gauges were filled using values from the NASA POWER dataset. This highlights the limitations in the temporal completeness of the government data and underscores the utility of satellite products in supplementing ground-based observations (Figure 2-4).

Additionally, it is important to interpret the estimated streamflows and derived runoff coefficients, obtained after hydrograph separation, with a critical perspective. From January 20 to February 12, 2023, the Nyamutera TD-Diver experienced a malfunction, during which small negative differences in water column readings were observed between the TD-Diver and the Baro-Diver. Consequently, streamflow values were set to zero for that period, as the issue occurred during the extended dry season when manual streamflow measurements were practically impossible due to minimal water flow. Furthermore, the TD-Diver was not installed at the deepest point of the river cross-section, which affected data accuracy. To reduce measurement uncertainty, manual depth readings were taken at the deepest points of the channel and averaged to derive corresponding discharge estimates (Zenebe et al., 2013). As a result, baseflows during this period were not accurately captured. However, this limitation has minimal

impact on the estimation of runoff volumes, though it may lead to underestimation of the corresponding baseflows.

2.4.2 Geomorphological and hydrological controls on runoff generation

An inverse relationship between initial abstraction (Ia) and event-based runoff coefficient (C) in both catchments indicates that abstraction losses decline as runoff efficiency increases (Figure 2-8), with Gaseke showing a stronger sensitivity than Nyamutera (reflected in a steeper slope). This contrast aligns with prior findings linking lower Ia to higher antecedent wetness and faster hydrologic connectivity (Mishra, Pandey, et al., 2008; Mishra & Singh, 2003). The differing responses are tied to geomorphological contrasts: Nyamutera's steep slope (0.41) and high relief (1186 m) promote rapid runoff, whereas Gaseke's moderately terrain (slope = 0.37), longer flowpaths (11.67 km), and extensive floodplain (~168 ha) enhance storage and delay runoff (Yeshaneh et al., 2014) (Table 2-6 and Figure 2-3). Consequently, Gaseke exhibits a sharper Ia–C regression, reflecting disproportionate runoff once storage is exceeded.

Table 2-6 Geomorphological characteristics of the Nyamutera and Gaseke catchments, including flowpath metrics, basin relief, shape indices, and drainage density.

Catchment	Area (km²)	Longest Flowpath Length (km)	Longest Flowpath Slope (m/m)	Centroid Flowpath Length (km)	Centroid Flowpath Slope (m/m)	10–85% Flowpath Length (km)	10–85% Flowpath Slope (m/m)	Basin Slope (m/m)	Basin Relief (m)	Relief Ratio	Elongation Ratio	Drainage Density (km/km²)
Nyamutera	44	14.29	0.08	6.91	0.08	10.72	0.07	0.41	1186	0.08	0.52	0.22
Gaseke	109	21.57	0.04	11.67	0.02	16.18	0.02	0.37	902	0.04	0.55	0.21

Note: Catchment delineation and geoprocessing using the Hydrologic Engineering Center-Hydrologic Modelling System (HEC-HMS 4.12) with a digital elevation model of 12.5 m resolution (DEM 12.5).

A Lorenz curve analysis further supports these differences: Nyamutera's low Gini index (0.065) suggests evenly distributed runoff across events, while Gaseke's higher index (0.151) points to a concentration of runoff in fewer intense storms (Figure 2-9). This pattern is consistent with variable source area theory, where slope, connectivity, and subsurface properties shape runoff dynamics (Beven, 2012; Beven & Freer, 2001). Gaseke's floodplain likely amplifies this effect by storing water during moderate events and attenuating peak flows (Acreman & Holden, 2013a; Bullock & Acreman, 2003). Together, the Ia–C relationship and Lorenz analysis highlight how geomorphic structure controls both runoff magnitude and distribution,

emphasizing the need to integrate geomorphological metrics into hydrological modeling in tropical mountain regions.

The contrasting runoff behavior of the Nyamutera and Gaseke catchments emphasizes the key influence of soil, vegetation, and topography on rainfall-runoff dynamics in temperate tropical mountain regions (Roa-García et al., 2011; Wamucii et al., 2021). The Nyamutera catchment, with its steep, rugged terrain underlain by granitic and gneissic rocks, has shallow lateritic soils that promote rapid surface runoff whenever rainfall exceeds the soil's infiltration capacity (X. Han et al., 2021; Roa-García et al., 2011). By contrast, the Gaseke catchment, primarily composed of schists and quartz-mica schists with minor pegmatite and alluvial deposits in valley bottoms and terraces, exhibits moderately steep slopes, a thicker soil mantle, and a well-connected floodplain (~168 ha). These features contribute to a delayed peak response and greater baseflow, consistent with saturation-excess overland flow and subsurface stormflow dynamics (Muvundja et al., 2022; Uwihirwe et al., 2020).

The differences in event-based runoff coefficients between Nyamutera and Gaseke can also be understood through the theoretical framework that connects soil, vegetation, and topography heterogeneity to the probabilistic patterns of baseflows (Botter et al., 2007). In this setting, the runoff coefficient captures the combined effects of soil infiltration, vegetation-mediated storage, and interconnected features like floodplains on the catchment's stormflow behavior (Cai et al., 2021; Gnecco et al., 2018). By adopting this perspective, we gain a clearer understanding of how runoff forms in tropical mountain environments and can place our findings within the wider framework of hydrological theory (Kumar et al., 2025).

These differences highlight how the geomorphic setting influences the way rainfall is divided between quick flow and baseflow. Similar patterns have been observed in other tropical mountain regions, where factors such as relief and soil depth together determine when saturation occurs and how hillslopes connect to valley bottoms (Muñoz-Villers & McDonnell, 2012b; Muñoz-Villers & McDonnell, 2013). In both catchments, variations in event-based runoff coefficients reflect how rainfall intensity, antecedent moisture, and local storage capacity interact to determine the effective contributing area during storm events (Detty & McGuire, 2010b). Future work should explore and build upon this framework in mountainous tropical regions, where the unpredictable nature of convective rainfall has a strong impact on rainfall-runoff patterns (Bruijnzeel, 2004, 2005; Muñoz-Villers & McDonnell, 2012b).

Although the rational method is commonly used for empirical design flood estimation, the variation in event-based runoff coefficients observed in this study provides valuable insights into the dominant hydrological processes, serving as a conceptual link between empirical design

approaches and physically based models. In the Nyamutera catchment, high runoff coefficients during short, intense storms suggest a threshold-driven shift toward infiltration-excess runoff, which is further intensified by steep slopes and surface compaction resulting from intensive cultivation. In Gaseke, moderate runoff coefficients under similar rainfall suggest that the catchment absorbs and stores water efficiently, releasing it gradually through the baseflow (François et al., 2024). This highlights how, in humid tropical mountain environments, the event-based runoff coefficient reflects the cumulative impact of soil properties, vegetation, and terrain on the catchment's response (Mango et al., 2011; Smithers, 2012).

By examining how runoff coefficients vary with catchment form and function, this study demonstrates that the rational method, when calibrated using event-scale data, can move beyond its empirical roots and provide a process-based perspective. This aligns with calls in tropical hydrology to integrate engineering methods with physical understanding (Beven & Freer, 2001; Hrachowitz et al., 2013a; Näschen et al., 2018; Ogden et al., 2013), especially in data-limited regions where process-based models are hard to parameterize.

In addition, the catchments lie in a region that is strongly affected by soil erosion, largely linked to agricultural activities (Hishamunda et al., 2024; Karamage, Zhang, et al., 2016). Landslides are also frequent, occasionally triggering extreme sediment flows that locally disrupt flow connectivity and influence flood behavior (Dewitte et al., 2021). The occurrence of landslides is further shaped, and in some cases worsened, by land management practices and cultivation on steep slopes (Maki Mateso et al., 2023; Sibomana et al., 2025). These processes related to erosion and slope stability alter runoff pathways, landscape connectivity, and colluvial storage, ultimately impacting the hydrological functioning of the river systems (L. Jacobs et al., 2016). Such cascading earth-surface processes play a significant role in catchment response and warrant further focused investigation (Yanites et al., 2025).

2.4.3 Spatial variability of rainfall and contrasts in runoff responses and flow regimes

The study area experiences convective rainfall strongly shaped by orographic effects due to its mountainous terrain. This spatial variability in rainfall adds complexity to hydrological analysis, as steep topography causes rapid changes in rainfall patterns that directly affect the magnitude and timing of streamflow at catchment outlets. Microclimatic factors like elevation and slope orientation can intensify rainfall variability (Buytaert, Celleri, et al., 2006). As a result, using rainfall data from a single station (e.g., Busengo for Gaseke) or from outside the catchment (e.g., Gihira, Muko, and Busengo for Nyamutera) may fail to represent spatial variability, particularly during short, high-intensity convective storms (Figure 2-1).

Flow duration curve (FDC) analysis underscores contrasting runoff regimes between the Nyamutera and Gaseke catchments, primarily governed by geomorphology and rainfall-runoff interactions. Gaseke, with its larger area (109 km²), moderately slopes (0.02-0.04 m/m), elongated shape, and extensive floodplain (~168 ha), exhibits higher low-flow discharges (Q_5 = 1.4 L/s/km² for Gaseke vs. 0.9 L/s/km² for Nyamutera) and a more storage-dominated response. Its longer centroid flowpaths (11.67 km) and lower relief (902 m) promote delayed runoff and sustained baseflows, reflecting findings from humid tropical basins where shallow groundwater connectivity and topographic storage maintain low flows (Bonell, 1998; Bonneau et al., 2018; De Hamer et al., 2008; McDonnell, 2003; Tetzlaff et al., 2009). Similar hydrologic buffering by floodplains has been documented by Samal et al. (2015) and Abdel-Fattah et al. (2017).

In contrast, Nyamutera (44 km²) exhibits steep slopes (0.08 m/m), high relief (1186 m), and short flowpaths (6.91 km), driving rapid runoff generation and higher specific discharge under moderate flows (Q_{90} = 18.4 L/s/km² vs. 12.2). During peak events (Q_{95}), however, Gaseke surpasses Nyamutera (30.3 vs. 27.6 L/s/km²), likely due to floodplain spillover and area-driven accumulation (Jencso et al., 2009; Yeshaneh et al., 2014). These contrasts underscore how slope, relief, and drainage structure govern flow regimes (Itsukushima, 2021; McGuire et al., 2005; Montgomery et al., 2002; Tague & Band, 2004), with Nyamutera's steep slopes and short flowpaths driving a rapid, surface runoff-dominated regime, while Gaseke's moderately gradients and floodplain storage promote delayed, baseflow-supported responses, an insight critical for hydrological modeling and flood risk analysis (Beven & Freer, 2001).

The fitted SDRCs reveal distinct hydrological responses between the catchments. Nyamutera's higher scaling factor ($a = 26.91 \pm 0.78$) and steeper curve indicate faster runoff due to its steeper terrain, while Gaseke's lower scaling factor ($a = 5.02 \pm 0.43$) corresponds to its moderately slopes and delayed flow. Despite similar discharge exponents ($b = 2.14 \pm 0.10$ vs. 2.11 ± 0.14), Nyamutera's slightly higher value suggests a more uniform response across flow conditions. The narrow uncertainty ranges confirm the robustness of the SDRC fits and the reliability of the flow regime representation (Figure 2-5).

Hydrograph analysis and modeling metrics align with the conceptual understanding of catchment behavior. SDRCs calibrated with Manning-based estimates performed well in both catchments, but Nyamuntera's dynamic flow regime limited calibration to depths ≤ 0.98 m (max measured stage: 1.01 m), likely overestimating high flows due to measurement challenges at high velocities. In contrast, Gaseke's SDRC was validated up to 3.23 m, supported by deeper field measurements (up to 2.06 m), allowing more reliable modeling of extreme events (Figure

2-5). These limitations highlight the potential for modeling errors in steep upland catchments with rapid flow dynamics (Habets et al., 1999; Westerberg et al., 2016).

The bootstrap 95% confidence intervals widened with increasing return period, reflecting the greater uncertainty associated with the upper tail of the distributions. These intervals were generally narrower for Nyamutera (e.g., 0.37–0.72 for the 100-year Cd) than for Gaseke (0.25–0.91 for the 100-year Cd), consistent with the stronger variability in hydrological response observed in the Gaseke basin (Table 2-7).

Table 2-7 Design runoff coefficients (Cd) and 95% confidence intervals derived from 10,000 parametric bootstrap realizations for the Nyamutera and Gaseke catchments across selected return periods.

Catchment	Return_period (years)	Cd best	Cd boot mean	Cd–boot–lower–2.5%	Cd–boot–upper–97.5%
Nyamutera	2	0.19	0.19	0.14	0.24
	5	0.28	0.28	0.21	0.36
	10	0.35	0.34	0.25	0.45
	25	0.43	0.42	0.30	0.56
	50	0.49	0.47	0.34	0.64
	100	0.55	0.53	0.37	0.72
Gaseke	2	0.08	0.08	0.05	0.10
	5	0.15	0.15	0.10	0.22
	10	0.22	0.21	0.13	0.33
	25	0.32	0.31	0.17	0.51
	50	0.41	0.40	0.21	0.70
	100	0.51	0.50	0.25	0.91

Note: Cd best represents the best-fit values from the fitted probability distributions, while Cd boot mean and the 2.5–97.5th percentiles quantify parameter uncertainty.

Rainfall analysis revealed strong spatiotemporal variability in event characteristics, leading to contrasting streamflow responses between catchments due to terrain effects. Lorenz curve analysis (Figure 2-9) effectively illustrated these differences by normalizing cumulative rainfall and runoff, allowing scale-independent comparisons of hydrologic behavior. This approach, previously used to distinguish runoff regimes across climatic and physiographic settings (McGlynn & McDonnell, 2003; Sivapalan et al., 2003), supports the interpretation that Nyamutera exhibits more surface-dominated flow, while Gaseke reflects storage-based buffering.

The hydrograph separation of 15 storm events in Nyamutera (1 April 2022–28 April 2023) and 23 events in Gaseke (1 April 2022–1 April 2023) shows clear differences in how the two catchments respond to rainfall. In Nyamutera, streamflow rose quickly even though baseflow made up a large share of total discharge (67%) and direct runoff contributed only 33%. This

pattern suggests that the catchment's steep slopes and granitic–gneissic terrain encourage infiltration during lower-intensity storms, while fractured volcanic bedrock helps store and transmit water through subsurface pathways, possibly enhancing geological connectivity within the catchment (Douinot et al., 2022; Kosugi et al., 2006). In contrast, Gaseke showed an almost even balance between direct runoff (47%) and baseflow (53%), suggesting a more tempered hydrological response (Cai et al., 2021; François et al., 2024). Together, these patterns imply that Nyamutera is mainly influenced by infiltration-driven subsurface flow, while Gaseke's landscape promotes evapotranspiration and retains more surface water (Cai et al., 2021; Decharme & Colin, 2025; Wohl, 2021). Developing strategically positioned retention ponds upstream of Nyamutera could help moderate flood peaks, particularly given its steep terrain, limited storage, and quick runoff response.

These results emphasize the critical influence of catchment physiography and hydrogeology on flow regimes in steep tropical headwaters. They demonstrate the importance of considering both geomorphological structure and SDRC accuracy in streamflow modeling, especially in complex terrains affected by floodplain dynamics or measurement constraints. Supporting evidence from Fan and Bras (1998) and Milly and Shmakin (2002) indicates that landscape structure and catchment organization fundamentally shape hydrological responses in tropical mountains, enabling improved predictions of flow partitioning and water availability under climate variability and land-use change scenarios.

2.4.4 Temporal variability of rainfall-runoff relationships across storm events

A comparative analysis of runoff coefficients (C) and flow components between the Nyamutera and Gaseke catchments reveals distinct hydrological responses linked to geomorphic characteristics. Regression analyses (Figure 2-10, panels a and b) show statistically significant relationships between C and both event-based direct runoff and baseflow, with stronger coefficients of determination in Gaseke (R^2 = 0.38 and 0.48) than in Nyamutera (R^2 = 0.31 and 0.40), supported by lower p-values (0.002 to <0.001 in Gaseke vs. 0.032 to 0.011 in Nyamutera).

Event-based analysis reveals contrasting baseflow dynamics between Nyamutera and Gaseke catchments. Nyamutera shows higher baseflow at low runoff (3.67 mm at C ≈ 0.046, Event#12) than Gaseke (0.66 mm, Event#1), reflecting its steeper slopes and permeable granitic-gneissic lithology facilitating rapid subsurface flow (Gardner et al., 2020). Both catchments exhibit increased baseflow at moderate runoff (≈0.116), linked to antecedent wetness (Nyamutera Event#8, Gaseke Event#15). Notably, Gaseke shows a pronounced baseflow increase at higher

runoff (6.25 mm at C ≈ 0.20–0.26, Event#19), attributed to floodplain activation and slower groundwater release from schist and alluvial deposits (Beven, 2012).

Lithological contrasts explain differing baseflow sensitivities: Nyamutera's steeper baseflow vs. runoff coefficient slope (45.32) versus Gaseke's lower slope (22.6) suggests more reactive groundwater response in Nyamutera's sandy soils over fractured bedrock (McDonnell, 2003), while Gaseke's slower response stems from less permeable schists and floodplain storage (Blöschl et al., 2019; Neal et al., 2012). Conversely, similar slopes in direct runoff vs. runoff coefficient (Nyamutera 16.97; Gaseke 16.39) indicate that lithology influences baseflow generation more than surface runoff, which is driven largely by rainfall intensity and saturation thresholds (Blöschl et al., 2019; Neal et al., 2012; Sivapalan et al., 2003a).

Together, these findings underscore the interplay of lithology, geomorphology, and rainfall-runoff processes: Nyamutera's steep, sandy terrain yields rapid baseflow response at low runoff, whereas Gaseke's larger floodplain and schist-dominated geology foster delayed baseflow activation. Both catchments share similar direct runoff behaviors, highlighting the dominant role of rainfall and soil saturation in surface runoff generation (Table 2-8).

Table 2-8 Comparative geomorphic and hydrologic characteristics integrating flow duration curve analysis and event-based baseflow-runoff dynamics.

Aspect / Metric	Nyamutera	Gaseke	Interpretation
Catchment area (km²)	44	109	Gaseke is more than 2× larger: more cumulative discharge
Centroid flowpath length (km)	6.91	11.67	Longer flowpaths in Gaseke delay runoff: more infiltration
Centroid flowpath slope (m/m)	0.08	0.02	Nyamutera much steeper: faster runoff
Basin relief (m)	1186	902	Nyamutera has greater elevation drop: higher energy flow
Relief ratio	0.08	0.04	Nyamutera's terrain is more rugged
Elongation ratio	0.52	0.55	Gaseke slightly more elongated
Drainage density (km/km²)	0.22	0.21	Similar stream network density
Floodplain area (ha)	–	~168	Gaseke has significant floodplain storage potential
Low-flow (Q5 specific discharge)	0.9 L/s/km²	1.4 L/s/km²	Gaseke sustains higher low flows: flatter terrain + storage
Q10 specific discharge	2.9 L/s/km²	1.7 L/s/km²	Nyamutera loses runoff faster: steep terrain
Moderate-flow (Q50 specific discharge)	4.1 L/s/km²	3.6 L/s/km²	Nyamutera yields more per unit area in moderate rainfall
High-flow (Q90 specific discharge)	18.4 L/s/km²	12.2 L/s/km²	Nyamutera shows quick response, sharper runoff under high rain
Q95 specific discharge (extreme flow)	27.6 L/s/km²	30.3 L/s/km²	Gaseke peaks during extremes: floodplain saturation effect

Baseflow at C = 0.0460 (Event #12)	3.67 mm	C = 0.0550 (Event #1): 0.66 mm	Nyamutera produces more baseflow at low runoff: steep flowpaths promote rapid subsurface drainage.
Baseflow at C = 0.2642 (Event #8)	6.19 mm	C = 0.1165 (Event #15) : 8.32 mm	Both catchments show strong baseflow; in Gaseke, floodplain storage appears to enhance sustained discharge despite lower C.
Event baseflow at C = 0.1769 (Event #11)	4.13 mm	Present (moderate C range)	Moderate baseflow in both suggests wet antecedent conditions activating subsurface and near-surface pathways.
Event baseflow at C = 0.2541 (Event #19)	–	6.25 mm	Gaseke shows a post-threshold response, indicating floodplain activation once runoff exceeds a certain level.
Event baseflow at C = 0.1086 (Event #10)	3.75 mm	–	Nyamutera displays a typical wet-season response, with moderate baseflow generated at mid-low C.
Regression slope (Runoff vs C)	16.97	16.39	Both catchments exhibit similar runoff responses to C increases, with Nyamutera's slope marginally steeper
Regression slope (Baseflow vs C)	45.32	22.60	Nyamutera's steeper terrain and lithologic characteristics result in a faster baseflow response
Hydrologic behaviour	Quick response; high runoff at low C	Storage-dominated initially; sharp rise post-threshold	Distinct flow regimes shaped by geomorphology

Gaseke's larger catchment area (109 km² vs. 44 km² in Nyamutera) and substantial floodplain (~168 ha) promote enhanced water storage and flow attenuation, contributing to stronger runoff–baseflow coupling (Tockner & Stanford, 2002; Zhou et al., 2021). Its moderately longest flowpath slope (0.04 m/m vs. 0.08 m/m) and lower relief (902 m vs. 1186 m) favor slower runoff concentration and greater infiltration, sustaining baseflow and reinforcing the observed statistical relationships (Beven, 2012; Dunne & Black, 1970). In contrast, Nyamutera's steeper slopes and higher relief lead to more rapid runoff and greater flow variability, consistent with its comparatively weaker, yet still significant, correlations. Despite similar drainage densities and elongation ratios, differences in slope and floodplain extent emerge as dominant controls on runoff–baseflow dynamics (McCarthy & Gale, 2001).

Runoff coefficients (C) ranged from 0.05 to 0.40 in Nyamutera (mean = 0.20) and from 0.02 to 0.35 in Gaseke (mean = 0.10), with corresponding average annual coefficients (AC) of 0.18 and 0.11, respectively. The higher minimum values observed in Nyamutera reflect its limited storage capacity and steeper terrain, whereas Gaseke's broader range and higher maximum indicate more variable responses, likely due to floodplain buffering. The ratio of maximum to minimum runoff coefficients (C), 8.7 in Nyamutera and 17.5 in Gaseke, further underscores these contrasts, although all values remain within expected ranges for humid, mountainous environment (Merz et al., 2006), highlighting the influence of physiographic and antecedent

moisture conditions on runoff generation (Tables 1 and 5). Seasonal increases in C were also observed during the rainy season, likely associated with enhanced baseflow contributions.

For all recorded storm events, lag time (TL) ranged from 0.5 to 3.5 hours in Nyamutera and from 1.25 to 6 hours in Gaseke, while time of concentration (Tc) ranged from 0.83 to 5.84 hours in Nyamutera and from 2.09 to 10.02 hours in Gaseke. Overall, TL and Tc in Gaseke were nearly twice those in Nyamutera, likely influenced by differences in catchment area, slope, floodplain extent, other geomorphic characteristics, and rainfall distribution (Beven, 2012; Chow et al., 1988; McGuire et al., 2005). Larger and flatter catchments with floodplains tend to exhibit slower hydrologic response times due to greater storage capacity and lower channel gradients (Blöschl & Zehe, 2005; Sivapalan et al., 1990, 2003b).

2.4.5 Analysis of design runoff coefficients based on return periods

The evaluation of probability distributions for estimating design runoff coefficients (C_d) revealed that the Gumbel and Lognormal distributions consistently provided the best fit for Nyamutera and Gaseke, respectively, as indicated by the lowest AIC and BIC values and the highest p-values from the Kolmogorov-Smirnov (KS) goodness-of-fit test (Table 4 and Figure 11).

Desing runoff coefficient estimates derived from the Gumbel and Lognormal distributions increased with return period, capturing the enhanced runoff generation expected during extreme events. In Nyamutera, C_d values rose from 0.19 for a 2-year return period to 0.55 for a 100-year event, while Gaseke ranged from 0.08 to 0.51 for the similar periods. Higher Cd values are consistent with lower infiltration and greater saturation during extreme storm events. Nyamutera shows smaller uncertainty, which is expected given its steep slopes and quick drainage, while the wider variability in Gaseke aligns with the effects of its floodplain storage. The parametric bootstrap captured these uncertainties well despite the small dataset, emphasizing the value of providing confidence bounds when deriving design runoff coefficients in complex tropical catchments (Kundzewicz & Robson, 2004). The convergence of C_d values at higher return periods suggests a threshold effect, where intense rainfall overwhelms subsurface storage and activates rapid surface runoff pathways, including floodplain contributions (Merz et al., 2006; Merz & Blöschl, 2009). The obtained design runoff coefficients (Cd) are intended as guideline values, given the absence of the historical flood event records for the study period. Since the Gumbel and Lognormal distributions focus on extreme events, adding a modest safety factor (such as 1.05 × Cd) helps guard against possible underestimation in hydraulic and flood-risk design. Furthermore, these findings underscore the

importance of considering geomorphic and catchment-specific hydrological contexts when applying statistical models to estimate design runoff coefficients. The dominance of the Gumbel and Lognormal distributions further highlights the nonlinear and variable nature of storm-event hydrological responses, reinforcing the value of event-based analysis for infrastructure sizing and flood risk assessment in tropical mountainous environments (Serrano-Notivoli et al., 2022; Zheng et al., 2023).

2.4.6 Broader implications for tropical hydrology

Findings from the two Rwandan catchments add to the recognition that humid tropical uplands do not behave uniformly; instead, they show highly mixed and locally variable runoff-generation mechanisms. This contrasts with the traditional rational method, which treats the runoff coefficient as a fixed value based mainly on soil type, slope, and LULC characteristics (Chow et al., 1988; Subramanya, 2008, 2009). The results suggest that event-based runoff coefficients are shaped by several interacting factors, including rainfall intensity, antecedent moisture, soil depth, vegetation cover, and the underlying catchment geomorphology. Even subtle differences in slope, soil depth, or floodplain extent can lead to noticeably different hydrograph responses under comparable rainfall conditions. These patterns carry important implications for flood prediction and hydrological modelling in tropical Africa, where standard design practices that rely on fixed runoff coefficients often overlook the inherent heterogeneity of individual catchments (Grimaldi & Petroselli, 2015; Smithers, 2012). Our results align with those of (Pathiraja et al., 2012), who showed that variations in antecedent moisture and nonlinear rainfall-runoff behaviour lead to substantial event-to-event differences in runoff, and therefore in runoff coefficients. Their work highlights why design approaches based on a single fixed coefficient often fail to capture real catchment dynamics. (Descheemaeker et al., 2006) similarly found that event-scale runoff coefficients in tropical highlands respond strongly to slope, land cover, and land management practices, underscoring the limitations of using uniform coefficients in heterogeneous landscapes.

Taken together, these studies emphasize the value of understanding how soil properties, geomorphology, and LULC patterns influence rainfall-runoff conversion. Such insight helps bridge empirical design practices with more physically based hydrological reasoning, ultimately improving the transferability and reliability of flood estimates in data-scarce and poorly gauged basins. This perspective is particularly important when establishing design runoff coefficients that reflect local catchment conditions rather than relying on generalized

values. The need is especially acute in mountainous settings, where intense convective storms often trigger rapid runoff responses and heightened flood hazards.

2.4.7 Future perspectives in flood monitoring strategies

The study area in NW Rwanda highlights the urgency of improving flood monitoring and early warning systems. Significant flood events, such as the Gaseke flood (3–4 April, 2023, peak flow: 122 m^3/s) and the Nyamutera flood (2–3 May, 2023, peak flow: 131 m^3/s), both occurring during the night, caused multiple fatalities, destruction of property, and the loss of key infrastructure, including hydrometric stations.

These events emphasize the critical need for enhanced flood monitoring, particularly during nighttime when response efforts are most constrained.

To address the challenges of flood monitoring in resource-limited and hydrologically complex regions like NW Rwanda, several practical and scalable strategies are proposed. These include deploying automated rain and streamflow gauges at small to medium catchment scales, equipped with sensors for real-time data transmission to centralized monitoring centers, and using Acoustic Doppler Current Profilers (ADCPs) for low-flow measurements. Satellite-based rainfall estimates derived from microwave links between mobile phone network antennas are increasingly recognized as reliable alternatives for capturing real-time precipitation and flood information.

Finally, strong institutional coordination among key agencies is crucial for implementing an integrated and effective flood preparedness and response strategy. Collaborative efforts should focus on enhancing preparedness, communication, and evacuation protocols, especially concerning night-time flood risks.

2.5 Conclusion

The mountainous terrain of NW Rwanda, particularly the Vunga corridor where the Nyamutera and Gaseke catchments converge, is highly susceptible to hydro-geomorphologic hazards, notably floods. In this study, we generated high-resolution rainfall-streamflow data and examined how runoff patterns vary across space and time. We also explored how geomorphological and hydrological features influence event-scale runoff behavior and evaluated whether the rational method can realistically represent rainfall-runoff processes and support flood-hazard planning in such complex landscapes.

The findings revealed that the C values ranged from 0.02 to 0.35 in Gaseke and 0.05 to 0.40 in Nyamutera, with respective ACs of 0.11 and 0.18. The observed temporal variability in C values highlights important discussion points. Notably, the ratio between the largest and smallest

values, 8.7 for Nyamutera and 17.5 for Gaseke, suggests that the presence of a floodplain in the Gaseke catchment significantly influences rainfall-runoff responses, gradually altering the relationship between rainfall and runoff.

Design runoff coefficients increased with return period and were consistently higher for Nyamutera than for Gaseke, reflecting contrasting hydrological responses. These Cd values serve as foundational guidelines for the engineering design of hydraulic structures and for strategic flood risk management. The results indicate that variations in slope, floodplain extent, antecedent soil moisture, rainfall distribution, and soil storage capacity give rise to distinct runoff generation processes. Nyamutera shows a rapid, infiltration-excess dominated response, while Gaseke exhibits more sustained baseflow and saturation-excess behavior. These observations highlight that the runoff coefficient in the rational method is not just an empirical fitting parameter, but rather reflects the combined influence of soil, vegetation, topography, and storage connectivity on runoff at the event scale.

Conceptually, this study contributes to tropical hydrology by showing that even simple empirical models can provide meaningful insights into underlying processes when interpreted in a physically grounded context. Methodologically, it presents a framework for calibrating and interpreting rational method coefficients in data-scarce regions, supporting more reliable flood design and hydrological predictions. More broadly, the findings reinforce the emerging perspective that tropical mountain hydrology is governed by mixed flow generation mechanisms, with their relative importance shaped by geomorphic setting and antecedent wetness conditions.

However, data limitations, such as sparse rain gauge coverage, the absence of historical flood event records, and inadequate monitoring of both extreme low and peak flows, posed significant challenges. Addressing data limitations requires expanding rain gauge and affordable sensor networks, leveraging satellite-based microwave link rainfall estimates for improved precipitation monitoring, and employing ADCPs for low-flow measurements.

This study further demonstrates that field-based rainfall-streamflow measurements are instrumental in identifying the distinct hydrological behaviours of each catchment. These insights are essential for improving flood prediction and informing the development of effective early warning systems tailored to local conditions.

By addressing key data gaps and proposing context-appropriate solutions, this research strengthens the practical application of the rational method in flood-prone, data-scarce mountainous regions. It sets a foundation for scalable physical approaches to flood hazard

management and resilience building, not only in NW Rwanda but also in similarly mountainous terrains worldwide.

Chapter 3 Performance indicators and thresholds in storm-event runoff modeling with NRCS-CN: insights for flood risk management in tropical mountainous catchments of northwest Rwanda

-

This chapter has been prepared for submission to a peer-reviewed journal, after incorporating feedback from my thesis defense as well as input from co-authors. The tentative title is *"Performance indicators and thresholds in storm-event runoff modeling with NRCS-CN: insights for flood risk management in tropical mountainous catchments of northwest Rwanda."*

Literature, methodology and formulas presented in previous chapters have been intentionally omitted here to avoid redundancy.

Abstract

The Natural Resources Conservation Service-Curve Number method is widely used for rainfall-runoff estimation, yet its performance in steep tropical catchments is constrained by slope insensitivity, limited consideration of storm duration, and minimal treatment of antecedent moisture. This study examines storm-based runoff in two contiguous mountainous catchments—Nyamutera (44 km²) and Gaseke (109 km²)—and investigates threshold behaviors that are critical for flood-risk management in northwest Rwanda.

Thirty-eight storm events recorded between April 2022 and May 2023 were simulated using a custom Python-based hydrological modeling framework, enabling detailed analysis of rainfall–runoff dynamics in the two catchments. Curve Numbers were derived from recent land-use and land-cover data based on Sentinel-2 imagery, complemented by field observations, while event-specific lag times were estimated from hydrograph analysis. An event-based modeling framework combining NRCS–Curve Number losses, the SCS unit hydrograph, and Muskingum routing was applied to simulate runoff response. Model parameters were optimized using a Differential Evolution algorithm with a composite performance metric, and transferability and parameter sensitivity were assessed using jackknife cross-validation and Sobol' sensitivity analysis.

Lag time analysis reveals contrasting flood controls: in the steep, storage-limited Nyamutera catchment, flood response is shaped by a combination of travel time, lag time, and channel routing effects, with no single factor dominating peak flows. In contrast, in the larger, floodplain-connected Gaseke catchment, flood response is strongly controlled by lag time, which explains most of the variability compared to other parameters.

Reliable flood simulation in mountainous tropical catchments requires event-specific calibration. In steep, compact basins like Nyamutera, peak flows are highly sensitive to abstraction, channel storage, and routing, whereas in catchments with longer flowpaths and floodplain influence like Gaseke, lag time and travel through the system primarily govern flood dynamics. While the NRCS-CN method captures general flood responses, parameter transferability is weak in steep headwaters and remains event-dependent even in floodplain-influenced catchments. These results highlight the importance of tailoring models to local hydrogeomorphic conditions to improve flood hazard assessment and support rainfall-driven early warning in data-scarce tropical regions.

Keywords: Rainfall-runoff modeling, Curve Number method, Tropical mountainous catchments, Storm-event analysis, Flood risk assessment

3.1 Introduction

Rainfall-runoff (RR) relationships play a critical role in hydrological modeling and supports effective strategies for managing water and land resources at global scales (D'Asaro et al., 2014; Shi & Wang, 2020). However, accurate runoff prediction is hindered by the complex spatiotemporal variability of rainfall, influenced by both natural factors (e.g., soil characteristics, topography, rainfall intensity) and anthropogenic pressures, including land use/land cover (LULC) changes linked to urban growth, agricultural expansion, deforestation, and infrastructure deficiencies (Abdi & Meddi, 2021; Cristiano et al., 2017; C. Kim & Kim, 2020). To address these complexities, several conceptual-lumped, semi-distributed or distributed hydrological models were developed (Lin et al., 2020), but their applicability depends on various conditions, including required data inputs and modeling purposes. Among the various event-based hydrological models, the Natural Resources Conservation Service Curve Number (NRCS-CN) method—originally known as the Soil Conservation Service Curve Number (SCS-CN)—is widely applied in data-scarce and ungauged catchments because it requires minimal input data and can be implemented flexibly in either lumped or semi-distributed form. Its driving concept lies in the curve number (CN), a key parameter that represents runoff potential based on hydrologic soil groups (HSG), land use/land cover (LULC), surface characteristics, and antecedent moisture conditions (AMC) (Ahmadisharaf et al., 2018; Ajmal et al., 2015; Shi & Wang, 2020).

The method was developed for temperate agricultural watersheds in the United States, but now is widely applied in different regions such as the African tropics, including semi-arid areas such as Ethiopia, and humid regions like Rwanda and neighboring areas (Taye et al., 2023b; Tuyishime & Choi, 2025). In Rwanda, like in other regions, the method was employed for flood peak flow predictions and flood risk management, soil and water management, and rainwater harvesting for agriculture purposes (Benimana et al., 2015; Taye et al., 2023b; Tuyishime & Choi, 2025). Although the NRCS-CN method is widely applied in ungauged or data-scarce catchments, only a subset of studies have rigorously evaluated its predictive performance across different hydrological contexts, highlighting the need for careful calibration and validation (Jeon et al., 2014; Khattab et al., 2025; Michel et al., 2005; Muche et al., 2019). Among these, a few studies proposed various enhancements, including empirical CN adjustments and soil moisture accounting, to improve model performance under specific catchment conditions (Jain et al., 2006; Mishra, Jain, et al., 2008; Petroselli et al., 2019; R. K. Sahu et al., 2012; Shi et al., 2017; Shi & Wang, 2020; Soulis & Valiantzas, 2012). Nevertheless, such ad-hoc adjustments

often depart from established guidelines, potentially undermining both the consistency and practical applicability of the method (Rezaei-Sadr & Sharifi, 2018; Taye et al., 2023b). Its structural limitations also persist, notably the reliance on the 5-day antecedent moisture condition (AMC), which can destabilize model outputs (Hawkins et al., 2015; Rezaei-Sadr & Sharifi, 2018).

Moreover, since the method was originally developed and validated for gentle slopes (~5%), its reliability may decline in steep terrains unless adjusted with site-specific corrections (Sahu et al., 2012; Shi & Wang, 2020). In African tropical regions such as Ethiopia, (Taye et al. (2023) found that National Engineering Handbook (NEH) table–derived CN values were about 21% greater than field-based estimates. Nevertheless, the method remains widely used due to its operational simplicity and ease of implementation.

In northwest Rwanda—where rainfall is strongly shaped by orography and steep, variable terrain—storm-runoff responses are fast and spatially heterogeneous (Muhire & Ahmed, 2015). Several recent studies in Rwanda have applied the NRCS-CN method for event-scale runoff estimation and infrastructure design, often using CNs derived from land-cover maps or regional tables even when formal calibration/validation was limited (Iradukunda et al., 2024; Uwizeyimana et al., 2019). These applications reflect the method's pragmatic value under data scarcity, but also highlight the need to interpret results in light of local hydrogeomorphology and, where possible, to support CN-based designs with event-based calibration or uncertainty envelopes (Ntwali et al., 2016; Uwizeyimana et al., 2019). Given the prevalence of terrain-driven and convective flood events (Muhire & Ahmed, 2015), there is a clear need for locally calibrated and storm-based modeling approaches to inform flood hazard assessments. Accordingly, this study is guided by the following research question: *"Can a storm-based, locally calibrated NRCS–CN modeling framework provide reliable and transferable runoff predictions across multiple events in steep, poorly gauged tropical catchments?"* Specifically, this study investigates the applicability of the NRCS-CN method in two contiguous mountainous catchments in NW Rwanda, Nyamutera (44 km²) and Gaseke (109 km²), using observed rainfall and streamflow data from April 2022 to May 2023. Therefore, the specific objectives of this study are to: (i) simulate storm-based rainfall-streamflow responses in mountainous tropical catchments using a custom Python modeling framework that integrates NRCS–CN loss estimation, unit hydrograph transformation, and Muskingum routing; (ii) estimate and calibrate key model parameters to reproduce observed hydrographs, applying performance thresholds to systematically evaluate model behavior; and

(iii) validate the model and assess the applicability and transferability of the NRCS–CN approach to other mountainous catchments with hydrological and geomorphic characteristics comparable to those of northwest Rwanda.

To address the challenges of simulating storm-driven runoff in steep, data-scarce tropical catchments, this study presents a flexible Python-based NRCS-CN modeling framework. The framework integrates multi-event rainfall-runoff simulation with calibration, validation, and sensitivity analysis using performance-based thresholds, enabling robust reproduction of hydrographs, including peak flows and runoff variability. By combining methodological rigor with a physically informed structure, the approach supports the assessment of model applicability and transferability to other poorly gauged mountainous catchments beyond the study area.

3.2 Materials and methods

3.2.1 Streamflow data and rainfall collection as main input for hydrological modeling

Streamflow data were extracted from the Nyamutera and Gaseke river outlets using gauging stations previously described in chapter 2 (Nahayo et al., 2026), and based on continuous data collection as illustrated on the pictures of Appendix 0-1. A total of 38 storm events were analyzed: 15 in the steep, floodplain-absent Nyamutera catchment and 23 in the less steep, floodplain-connected Gaseke. The geomorphological characteristics of the catchments were estimated using the Hydrologic Engineering Center-Hydrological Modeling System (HEC-HMS), and the extent of the Gaseke floodplain was extracted using Quantum Geographic Information System (QGIS) (Nahayo et al., 2026). Event-based rainfall-runoff simulations were then performed with the custom Python-based hydrological framework, driven by rainfall data from the Gihira, Muko, and Busengo gauges, along with streamflow records from previous storm events. Furthermore, the calibrated hydrographs were evaluated using performance metrics including Kling-Gupta efficiency (1-KGE), percent error in peak discharge (PEPD), Nash-Sutcliffe efficiency (NSE), root mean squared error (RMSE), and volume error (VE).

3.2.2 Lag-time and imperviousness estimation for understanding rainfall-runoff response

Lag time is a key control on flood response in steep, data-scarce tropical catchments (Sultan et al., 2022). In this study, it was characterized using complementary metrics: (i) the time from the rainfall centroid to peak discharge, (ii) rainfall onset to peak discharge (time-to-peak), and (iii) hydrograph rise onset to peak discharge (rise time) (Nagy et al., 2022; Shook et al., 2024).

Centroid-to-peak lag is commonly used to represent catchment storage and routing processes, whereas time-to-peak and hydrograph rise time more directly quantify the speed and intensity of runoff, making them particularly relevant for flood-hazard assessment and early-warning applications (Nagy et al., 2022; Sultan et al., 2022). However, centroid-based lag metrics can yield non-physical negative values when the event centroid occurs after the discharge peak, especially in flashy or multi-peaked events (Gericke & Smithers, 2014b; Shook et al., 2024). To avoid this limitation, peak-referenced response metrics such as time-to-peak and hydrograph rise time are preferred (Shook et al., 2024). These metrics are strictly non-negative and directly quantify the speed and intensity of runoff generation, providing more robust and interpretable indicators of catchment responsiveness that are especially relevant for flood-hazard assessment and early-warning applications. Additionally, incorporating initial discharge further embeds physically meaningful controls on timing and magnitude, particularly in data-scarce mountainous basins (Nagy et al., 2022; Shook et al., 2024). Together, these measures offer a robust framework for simulating storm-driven runoff and evaluating flood onset, propagation, and warning potential in catchments such as Nyamutera and Gaseke.

Recent studies have demonstrated empirical relationships between catchment response timing (e.g., lag time) and both antecedent wetness and storm intensity using regression and other statistical approaches. For example, (Knapp et al., 2025) showed that antecedent discharge and precipitation intensity jointly influence runoff response dynamics, supporting the inclusion of both variables in lag-time models. (Zhao et al., 2023a); and (Zwartendijk et al., 2023) similarly highlighted the utility of statistical models incorporating antecedent hydrological conditions (e.g., baseflow or soil moisture proxies) and storm characteristics to explain variability in lag times and hydrologic response. These findings provide the basis for the formulation of the lag-time regression model adopted in this study (Knapp et al., 2025).

In this study, the shortest positive lag times (L, hours) which capture the critical delay between rainfall and runoff response, were selected and related to antecedent hydrological conditions and storm forcing using a multivariate log-linear regression model. Initial discharge (Q_0, $m^3\ s^{-1}$) was used as a proxy for catchment wetness, while maximum event rainfall (P, mm) represented storm intensity (Sultan et al., 2022; Talei & Chua, 2012; Zhao et al., 2023b). The regression model is expressed in logarithmic form as:

$$lnL = a + blnQ_o + clnP \quad (3.1)$$

where a, b, and c are regression coefficients estimated using ordinary least squares. No sign constraints were imposed on the coefficients, allowing both positive and negative sensitivities

to be identified from the data. The model was subsequently expressed in its operational power-law form as:

$L = \alpha {Q_0}^b P^c$, with $\alpha = e^a$ (3.2)

In this formulation, α represents a scaling constant defining the baseline lag time under unit discharge and rainfall conditions, while b and c quantify the elasticity of lag time with respect to antecedent discharge and storm magnitude, respectively. Positive values of b or c indicate that lag time increases with increasing Q_0 or P, whereas negative values indicate a reduction in lag time with increasing forcing (Talei & Chua, 2012; Zhao et al., 2023b). Larger absolute values of these exponents indicate stronger sensitivity of lag time to rainfall-runoff controls. In this study, regression coefficients were estimated without sign constraints, allowing lag time to either increase or decrease with antecedent discharge and rainfall magnitude depending on catchment response characteristics.

Furthermore, since the study area consists of mountainous agricultural catchments with scattered settlements and small commercial centers, the impervious fraction was estimated at 15% for both catchments based on field observations (Dams et al., 2013; W. S. Han & Burian, 2009). While this estimate carries some uncertainty, it provides a reasonable basis for rainfall-runoff modeling and helps limit parameter calibration, reducing the risk of overfitting.

3.2.3 Lumped event-based rainfall-runoff modelling framework

A lumped, Python-based hydrological modeling framework was developed to simulate event-scale runoff responses by integrating NRCS-Curve Number loss estimation, the SCS unit hydrograph, and Muskingum channel routing. Model parameters were optimized using a Differential Evolution algorithm, guided by a composite objective function that combines normalized peak-weighted root mean squared error, peak discharge error, and the Kling-Gupta Efficiency (KGE). The framework also incorporates calibration, Jackknife cross-validation (to account for the limited number of storm events), and Sobol' sensitivity analysis (Shin & Choi, 2018; Wan et al., 2015). This approach enables event-scale parameter estimation, evaluation of model performance across multiple storms, and assessment of hydrological responses under varying rainfall and antecedent moisture conditions (Rozalis et al., 2010; Shin et al., 2013).

The NRCS-CN method remains widely used for estimating direct runoff from storm rainfall and is underpinned by the water balance equation (Soulis et al., 2009):

$P = P_e + I_a + F_a$ (3.3)

where P is total precipitation, P_e is direct runoff, I_a is initial abstraction (e.g. interception and surface storage), and F_a is infiltration after I_a. Empirical studies have suggested that the initial

abstraction (I_a) can be approximated as a fixed fraction of potential retention (S), typically *Ia=0.2S.* However, several authors argue that this assumption may not be realistic, as I_a can vary considerably depending on land use and land cover, storm characteristics, and catchment properties, ranging from 0.05 to 0.2S. This variability underlies the simplified form of the NRCS runoff equation commonly used in hydrological modeling. (Farran & Elfeki, 2020; USDA NRCS, 2004). Based on the above simplified form, this can lead to:

$$P_e = \frac{(P-0.2S)^2}{(P+0.8S)} \; for \; P > I_a, and \; P_e = 0 \; for \; \leq I_a \quad (3.4)$$

The retention parameter *S* is linked to watershed characteristics through the CN, which is a dimensionless index reflecting LULC, hydrologic soil group (HSG), and antecedent soil moisture condition (AMC):

$$S = 25.4(\frac{1000}{CN} - 10) \quad (3.5)$$

CNs range from 30 (for highly permeable, vegetated soils under dry conditions) to nearly 100 (for impervious surfaces). CN values are typically referenced to average soil moisture conditions (AMC II), but can be adjusted for dry (AMC I) or wet (AMC III) conditions using the following formulae (Mishra & Singh, 2003; D. K. Singh & Singh, 2019):

$$\mathrm{CN(I)} = \frac{\mathrm{CN\ (II)}}{2.281-0.0128\ \mathrm{CN(II)}} \quad (3.6)$$

$$\mathrm{CN(III)} = \frac{\mathrm{CN\ (II)}}{0.427-0.00573\ \mathrm{CN(II)}} \quad (3.7)$$

In this study, CN values corresponding to average antecedent moisture conditions (AMC II) were adopted for event-based simulations. CN(II) values were derived from 2023 land use/land cover (LULC) data, classified from 10 m Sentinel-2 imagery in QGIS (Esri Land Cover (arcgis.com), 2024). Although the NRCS-CN method was originally developed for very small watersheds (≤15 km²), it was applied here to larger small catchments (44 km² and 109 km²) using area-weighted composite CN values derived from a 2023 LULC map based on 10 m Sentinel-2 imagery. (Nguyen & Bouvier, 2019; Phiri et al., 2020).

$$CN_w = \frac{\sum CN_i * A_i}{\sum A_i} \quad (3.8)$$

where CN_i and A_i are the curve number and area of the i^{th} grid, respectively. This approach accommodates spatial variability in LULC and soil characteristics across the study area.

3.2.4 Channel routing and composite objective function calibration strategies

HEC-HMS offers eight objective functions, which were evaluated and ranked based on their ability to capture hydrograph magnitude, shape, and timing. These include Peak-Weighted

RMSE (pwRMSE), Percent Error in Peak Discharge (PEPD), Peak-Weighted Variable Power (pwVP), Time-Weighted RMSE, Root Mean Square Error (RMSE), Sum of Absolute Residuals (SAR), Sum of Squared Residuals (SSR), and Mean of Squared Residuals (MSR) (USACE HEC, 2025). The ranking showed that peak-sensitive metrics, particularly pwRMSE and PEPD, outperformed others, regarding peak flow reproductivity, hydrograph shape and timing, which are the most important for flood modeling purposes. The pwRMSE offered a balanced evaluation of peak magnitude, hydrograph shape, and timing, while PEPD focused on peak discharge accuracy. Therefore, selecting pwRMSE and PEPD ensures robust assessment of flood dynamics in steep, high-risk catchments, like those of the NW Rwanda (Halwatura & Najim, 2013; Sahu et al., 2023) (Appendix 0-2). The pwRMSE and PEPD objective functions are defined as follows:

$$pwRMSE = \sqrt{\frac{\sum_{i=1}^{n} w_i (Q_o - Q_m)^2}{\sum_{i=1}^{n} w_i}} \quad (3.9)$$

$$PEPD = 100. \frac{(Q_{op} - Q_{mp})}{Q_{op}} \quad (3.10)$$

Here, Q_o and Q_m represent the observed and simulated discharges at time step i, respectively. Q_{op} and Q_{mp} denote the observed and simulated peak discharges. The weight w_i, which emphasizes errors near the hydrograph peak, is typically a function of the observed discharge and is calculated as:

$$w_i = \left(\frac{Q_o(i)}{Q_{omax}}\right)^{\beta} \quad (3.11)$$

where Q_{omax} is the maximum observed discharge, and β is an exponent (typically ranging from 1 to 3) that controls the sharpness of weighting near the peak.

In parallel, a Python-based framework was developed that integrates multiple performance metrics into a single composite objective function. The framework implements an adaptive, variance-aware objective function for flood model calibration, combining peak discharge error, pwRMSE, PEPD, and KGE into a single dynamically weighted metric. Peak errors were assigned greater weight for extreme floods, while pwRMSE, PEPD, and Kling-Gupta efficiency (KGE) shared the remaining weight (40%, 40%, and 20%, respectively), emphasizing hydrograph magnitude and timing while retaining correlation information. Following recommendations for condition-adaptive, multi-objective calibration approaches (Efstratiadis

& Koutsoyiannis, 2010; Gupta et al., 1998), the composite objective function (J) for this study was formulated as:

$$J = 0.4 * \frac{pwRMSE(Q_o, Q_m)}{max(Q_o)} + 0.4 * \frac{PEPD(Q_o, Q_m)}{100} + 0.2 * (1 - KGE) \quad (3.12)$$

All components of the objective function were normalized using relative error formulations to ensure comparable magnitudes and to prevent any single metric from dominating the optimization. The composite objective function integrates relative pwRMSE, peak discharge error (PEPD), and the loss term (1 − KGE), with greater weight assigned to flood peak representation. The pwRMSE emphasizes hydrograph shape by penalizing errors near peak flows, while PEPD directly quantifies bias in peak discharge estimates. Together, these metrics provide a robust evaluation of high-flow behavior, which is essential for flood-risk analysis and infrastructure design (Jie et al., 2016; Moriasi et al., 2007). KGE further incorporates correlation, bias, and variability, offering a balanced multi-objective calibration criterion well suited to steep, data-scarce tropical catchments (Althoff & Rodrigues, 2021; Gupta et al., 2009; Knoben et al., 2019).

Beyond PEPD and pwRMSE, model performance was further assessed using the following metrics:

$$VE = \frac{\sum_i^n (V_m(i) - V_o(i))}{\sum_i^n V_o(i)} X100 \quad (3.13)$$

$$KGE = 1 - \sqrt{(r-1)^2 + (\alpha - 1)^2 + (\beta - 1)^2} \quad (3.14)$$

In the Equations 3.12–3.14, Q_o and V_o are observed discharge and volume values at time step i, Q_m and V_m are modelled discharge and volume values at time step i, respectively, and n is the number of observations.

The correlation coefficient r indicates how well the simulated peaks and timing match the observed hydrograph (Hu & Shrestha, 2020). The variability ratio $\alpha = \frac{\sigma_s}{\sigma_o}$ assesses how well the spread of simulated values matches observations, and the bias ratio $\beta = \frac{\mu_s}{\mu_o}$ evaluates how well the mean of simulated values corresponds to the observed mean (Cheng et al., 2023). Here μ and σ denote the mean and standard deviation, with subscripts s and o referring to simulated and observed values, respectively. Note that although VE is widely used in water-supply studies to assess runoff balance, in flood modeling it is generally secondary to peak- and timing-based metrics such as NSE, KGE, or PEPD (*Hydrological Model FAQ*, 2025; Ismail Dhaqane et al., 2023).

3.2.5 Event-based rainfall-runoff model calibration

The NRCS-CN rainfall-runoff model was calibrated using an event-based approach, whereby each storm event was analyzed individually rather than merging all rainfall and discharge data into a single continuous simulation (Assaf et al., 2025; Filipova et al., 2019). This approach was chosen to better capture the pronounced variability in hydrological response observed between storms, which arises from differences in rainfall intensity, duration, temporal rainfall patterns, and antecedent catchment conditions (Filipova et al., 2019). By treating storm events separately, the calibration process could more realistically represent how the catchment responds under contrasting hydrometeorological situations.

For each storm event, the associated rainfall and streamflow records were extracted to capture the complete hydrological response, including the rising limb, peak discharge, and recession of the hydrograph (Odey & Cho, 2025). By treating each storm as an independent event, the model is able to focus on the specific rainfall-runoff dynamics of that event, without interference from unrelated dry periods or low-flow conditions (Odey & Cho, 2025). This approach is particularly appropriate for mountainous tropical catchments, where short-duration storms often produce rapid and highly variable runoff responses (Mohammadpour Khoie et al., 2025).

Catchment characteristics that are not expected to change over short time periods were specified in advance of model calibration. These included the Curve Number (CN), which reflects the runoff generation potential associated with land use, land cover, and soil properties; the proportion of impervious surfaces, representing rapid runoff contributions from built-up areas; the catchment lag time, which describes the delay between rainfall and the resulting runoff response; and the initial discharge at the start of each event, capturing antecedent flow conditions in the channel (Shi et al., 2017; Subramanya, 2008).

Values for these parameters were derived from field measurements, spatial analyses, and previous hydrological assessments (e.g., 2023 Sentinel-2 LULC map (10-m resolution) for CN values, literature for impervious fraction, and hydrograph analysis for lag times). To maintain physical realism and limit the risk of overfitting, they were held constant during calibration rather than treated as adjustable parameters. This approach helped reduce parameter interaction and ensured that model calibration focused on processes that are more directly related to event-scale hydrological response.

Calibration focused on three key parameters that play a central role in controlling how rainfall is transformed into runoff and how flood waves move through the channel during individual storm events. The first parameter, the initial abstraction (Ia), accounts for the portion of rainfall that is lost at the beginning of an event due to processes such as interception by vegetation,

temporary storage in surface depressions, and early infiltration before surface runoff is generated (Farran & Elfeki, 2020; Soulis & Valiantzas, 2012).

The Muskingum method represents channel storage through two parameters: *K*, which controls flood wave translation and attenuation, and *X*, which defines the relative contribution of inflow and outflow to channel storage. When only a single observed hydrograph is available, *X* is initially assumed and storage is computed over successive time steps; linearity in the resulting storage relationship indicates an appropriate value of *X*. In this study, *K* and *X* were iteratively optimized using Differential Evolution (DE) to achieve linear storage behavior. Flood routing was then performed using a finite-difference approximation of the continuity equation combined with the linear storage formulation (Blöschl et al., 2019; Chow et al., 1988; Subramanya, 2008, 2009), as expressed below:

$$S_1 - S_2 = K[(I_1 - I_2) + (1 - X)(Q_1 - Q_2)] \quad (3.15)$$

where S is the storage, I is the inflow, Q is the outflow, and the subscripts 1 and 2 denote successive time steps.

This formulation leads to a recursive routing equation in which the outflow at each time step is expressed as a weighted sum of current and previous inflows and the previous outflow:

$$Q_2 = C_0 I_2 + C_1 I_1 + C_2 Q_1 \quad (3.16)$$

The routing coefficients C_0, C_1, and C_2 are functions of storage-time constant K, the weighting factor X and the computational time step Δt, and are defined as follows:

$C_0 = \frac{-KX+0.5\Delta t}{D}$, $C_1 = \frac{KX+0.5\Delta t}{D}$, $C_2 = \frac{K-KX-0.5\Delta t}{D}$, where $D = K - KX + 0.5\Delta t$

satisfying the continuity constraint $C_0 + C_1 + C_2 = 1$ to ensure mass conservation. Numerical stability was maintained by enforcing $2KX < \Delta t \leq K$ (Blöschl et al., 2019; Chow et al., 1988; Subramanya, 2008, 2009).

To ensure hydrological realism during calibration, all parameters were restricted to physically meaningful ranges informed by established theory and standard modeling practice. For instance, the initial abstraction (Ia) was treated as a free calibration parameter and constrained between 0.5 and 10 mm to avoid unrealistically low runoff thresholds or excessive initial losses during event-scale simulations. These bounds were defined a priori and independently of CN, rainfall depth, or lag time, allowing event-specific variability while ensuring realistic runoff initiation in steep tropical environments (Calero Mosquera et al., 2022; Ekwule & Agunwamba, 2024). Bounds for K were constrained using event-specific lag times, with K allowed to vary between the half of the minimum observed lag time and 1.2 times the mean lag time, converted to seconds. This approach ensures physically realistic routing behavior consistent with observed

flow translation through the channel network (Alhumoud & Almashan, 2019). X was bounded between 0 and 0.5, representing pure storage and pure translation, respectively. Consistent with classical hydrologic theory, where X values for natural river channels typically fall between 0.1 and 0.3 (Chow et al., 1988; Subramanya, 2008, 2009). The imperviousness fraction was set to 15% based on the field observations—agricultural catchments, comprising sparse settlements and small commercial centers—and based carefully on value ranges from literature (Rose et al., 2017; Shuster et al., 2005).

Parameter optimization was carried out using the Differential Evolution (DE) algorithm, a global optimization method well suited to hydrological models with complex and non-linear behavior. Instead of starting from a single initial parameter set, the algorithm works with a population of candidate solutions, allowing it to explore a wide range of possible parameter combinations (Storn & Price, 1997). Through successive iterations, these candidate solutions are progressively refined by comparing simulated discharge with observed discharge and favoring parameter sets that produce better agreement. The optimization was designed to reduce discrepancies in both the timing and magnitude of the simulated hydrographs, ensuring a realistic representation of runoff dynamics. A sufficiently large population size and number of iterations were chosen to support convergence toward a stable and reliable solution, and a fixed random seed was used to ensure that the results could be reproduced (RRMPG, 2025; Storn & Price, 1997).

After calibration, the model was run again using the optimized parameter set for each storm event to produce simulated discharge hydrographs. Model performance was then evaluated using a set of complementary metrics, each designed to highlight a different aspect of the hydrological response (NSE, KGE, RMSE, PEPD, and VE). Together, these metrics ensured that good statistical performance was not achieved at the expense of accurately reproducing key flood characteristics, such as peak magnitude and event-scale water balance.

3.2.6 Jackknife (leave-one-out) validation

To evaluate the robustness and predictive reliability of the rainfall-runoff model, a jackknife (leave-one-out) validation approach was adopted. This validation strategy is particularly suitable for event-based hydrological studies, where the number of observed storm events is limited and where hydrological responses can vary substantially between events (Dinh & Aires, 2022; Gudmundsson & Seneviratne, 2015).

The fundamental principle of the jackknife approach is to test the model's ability to reproduce runoff for a storm event without having been calibrated using that event. In practice, this means

that one storm event is temporarily excluded from the dataset, and the model is calibrated using all remaining storm events (Dinh & Aires, 2022; Mueller et al., 2023). The calibrated model is then applied to simulate the excluded storm independently. This procedure is repeated sequentially so that each storm event serves once as an independent validation case (Haddad et al., 2013).

This approach provides a rigorous test of model generalization because it mimics a real-world prediction scenario: model parameters are inferred from past events and then used to simulate a new, unseen event. By repeating this process for all storm events, the validation results are not dependent on a single arbitrary calibration-validation split, but instead reflect model performance across the full range of observed hydrological conditions (Biondi et al., 2012).

During each jackknife iteration, model parameters were optimized using the training storm events (i.e., all events except the one withheld) (Biondi et al., 2012; Parajka et al., 2005). Parameter optimization aimed to achieve a balanced model performance across multiple storms rather than a perfect fit to any single event. An aggregated objective function was used to evaluate a set of model parameters (Ia, K, and X) by minimizing the average discrepancy between observed and simulated discharge across all calibration datasets. This approach ensures that the optimized parameters are robust and transferable, reflecting general hydrological behavior rather than being tuned to specific events (Biondi et al., 2012; Parajka et al., 2005).

Once the optimal parameter set was obtained for a given iteration, the model was applied to the withheld storm event without further adjustment. The simulated discharge hydrograph for the validation event was then compared against observed discharge data. Model performance was evaluated using several complementary metrics (NSE, KGE, RMSE, PEPD, and VE) that quantify overall goodness of fit, timing and magnitude of peak discharge, and event-scale runoff volume (Knoben et al., 2019; Parajka et al., 2005). These quantitative metrics were supplemented by visual inspection of observed and simulated hydrographs plotted together with the corresponding rainfall input, enabling assessment of response timing, peak attenuation, and recession behavior.

Briefly, Jackknife validation assesses model reliability by repeatedly calibrating the model on all but one storm event and then testing its ability to reproduce the excluded event, thereby providing a robust measure of predictive performance under independent conditions..

3.2.7 Global variance-based sensitivity analysis and uncertainty quantification

A global sensitivity analysis (GSA) using the variance-based Sobol' method (Sobol′, 2001) was conducted to identify which hydrological parameters most strongly influence key model

performance metrics, focusing on the lag time (L), initial abstraction (Ia) and Muskingum routing parameters (K and X) (Mrokowska & Osuch, 2011). The Sobol' method is particularly well-suited for capturing both linear and nonlinear parameter effects, which has contributed to its widespread use in environmental and hydrological research (Georg et al., 2025; Razavi & Gupta, 2015; Saltelli et al., 2007). To enhance computational efficiency and navigate the high-dimensional parameter space, a surrogate model was employed to approximate system behavior and facilitate estimation of sensitivity indices (Nearing et al., 2016; Sun et al., 2023).

Quasi-random Sobol' sequences were generated using the Saltelli algorithm from the SALib package, enabling efficient and accurate sampling for multi-dimensional sensitivity analysis (J. Herman & Usher, 2017; Sobol′, 2001). Using surrogate-assisted GSA, first-, total-, and second-order sensitivity indices were calculated to quantify direct effects, interactions, and their joint impact on model output variability (Pianosi et al., 2016; Saltelli et al., 2007). This approach enables efficient, data-driven assessment of parameter sensitivities, supports identification of dominant parameters, and enhances model interpretability (Razavi & Gupta, 2015). The logical framework of the methodology is summarized in Figure 3-1.

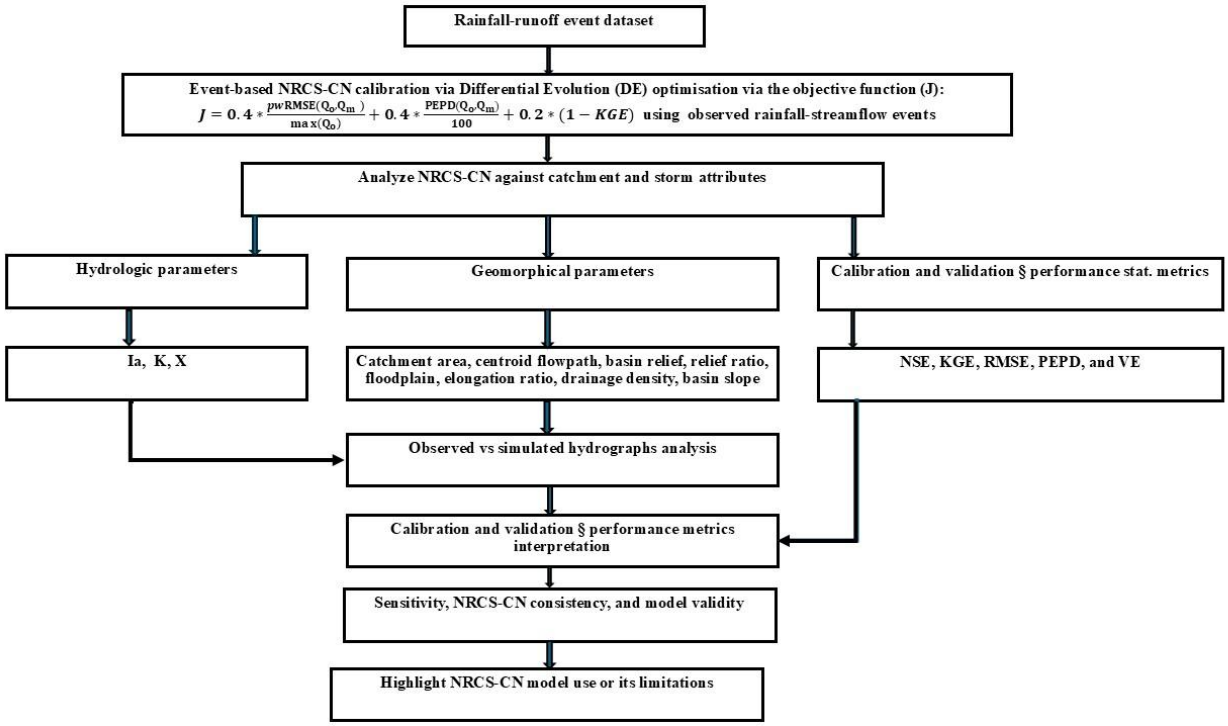

Figure 3-1. Flowchart of the methodological approach applied in the present study.

Note: CN (curve number), pwRMSE (peak-weight root mean squared error), PEPD (percent error in peak discharge), KGE (Kling-Gupta efficiency), Ia (initial abstraction), K and X (Muskingum routing parameters), NSE (Nash-Sutcliffe efficiency), and VE (Volume error). CN

values were derived from LULC data, lag times from event-based hydrograph analysis, and imperviousness percentages from field observations and literature sources.

3.3 Results

3.3.1 Catchment hydrogeomorphology and observed lag-time responses

Table 3-1 presents multiple lag-time estimates, including time-to-peak, centroid-to-peak lag, rise time, and the lag time adopted for flood-hazard assessment.

Table 3-1. Comparison of event-based lag-time estimation methods—time-to-peak, centroid-to-peak lag, and rise time—and the shortest positive lag time adopted for flood-hazard assessment.

Catchment	Event	Time-to-peak L(h)	Centroid-to-peak L(h)	Rise time L (h)	Adopted L (h)	Q_0 (m3/s)	P_{max} (mm)
Nyamutera	E1	0.50	2.43	0.25	0.25	0.70	12.45
	E2	0.75	7.81	0.75	0.75	0.57	1.69
	E3	1.00	1.05	5.50	1.00	1.74	3.31
	E4	0.75	0.98	3.25	0.75	5.44	1.60
	E5		10.51	3.75	3.75	4.26	2.87
	E6		7.04	5.25	5.25	4.92	4.32
	E7		9.88	3.75	3.75	4.26	2.87
	E8	0.50	21.73	2.50	0.50	2.09	4.03
	E9	2.00	0.89	2.75	0.89	4.77	3.40
	E10	3.25	7.94	3.25	3.25	0.75	11.70
	E11		8.52	0.25	0.25	0.75	4.05
	E12	1.75	2.29	2.00	1.75	1.51	9.59
	E13	3.50	10.21	4.00	3.50	2.21	4.26
	E14	0.75	3.17	2.25	0.75	0.90	4.55
	E15	0.50	5.22	4.75	0.50	1.43	2.59
Gaseke	E1	2.00	4.50	2.50	2.00	1.27	8.40
	E2	1.75	5.40	5.00	1.75	1.73	5.40
	E3	4.50	8.33	12.50	4.50	1.16	2.80
	E4	3.00	8.05	3.50	3.00	2.21	19.80
	E5	6.25	5.47	7.25	5.47	1.14	5.80
	E6	14.50	6.29	17.00	6.29	1.07	10.80
	E7	4.25	4.71	6.75	4.25	0.75	10.00
	E8		1.31	6.50	1.31	0.79	1.60
	E9	6.50	6.39	7.00	6.39	1.12	5.40
	E10	7.25	4.93	8.25	4.93	0.65	7.20
	E11	4.50	5.93	5.00	4.50	0.90	8.40
	E12	4.50	4.17	8.25	4.17	0.60	2.40
	E13		2.11	5.75	2.11	0.94	10.00
	E14	5.00	8.82	2.75	2.75	0.92	6.40
	E15	3.75	10.42	2.50	2.50	1.63	23.40
	E16		-0.15	1.25	1.25	8.02	3.20
	E17	3.50	4.91	4.75	3.50	5.87	6.60
	E18	1.75	8.58	3.00	1.75	7.21	8.80
	E19	5.25	5.45	5.50	5.25	6.55	2.20

	E20	2.25	1.81	2.50	1.81	8.21	1.20
	E21	4.00	7.99	5.00	4.00	4.88	3.20
	E22	4.25	12.74	4.25	4.25	5.94	21.20
	E23	3.75	4.88	2.50	2.50	0.26	20.80

Figures 3-2 presents the observed versus predicted lag-time regression analyses for Nyamutera and Gaseke, highlighting the contrasting hydrological responses. In Nyamutera, lag time tends to increase with both antecedent discharge and rainfall magnitude, with antecedent discharge exerting a statistically significant influence (b = 0.78, p = 0.035), explaining a moderate portion of the variability (R^2 = 0.32). In contrast, Gaseke shows near-zero regression coefficients (b = -0.09, c = 0.06) and very low explanatory power (R^2 = 0.05), indicating that event-scale rainfall and baseflow contribute little to the observed lag-time variability.

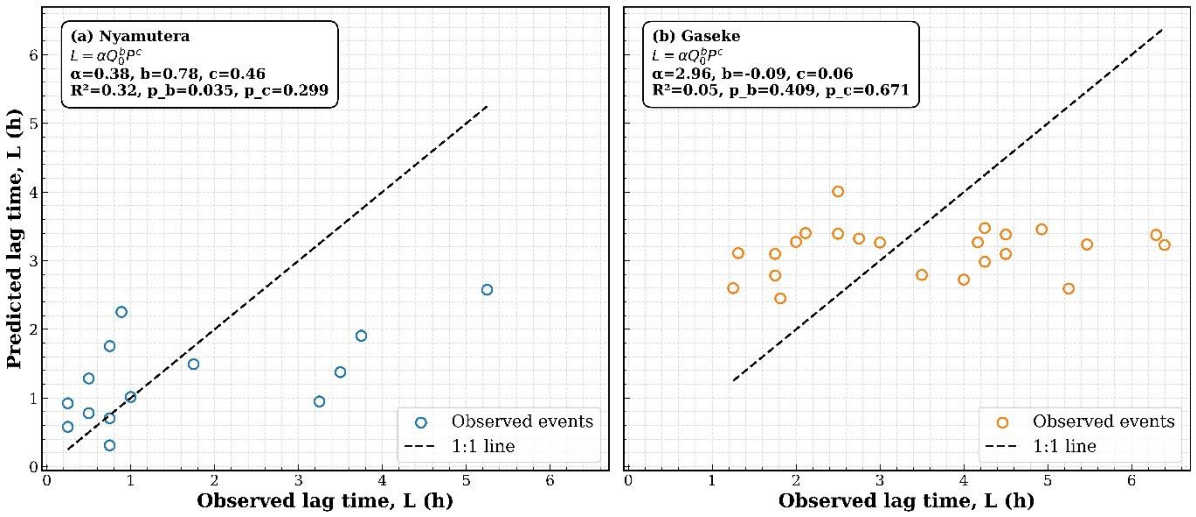

Figure 3-2 Observed versus predicted lag times derived from the operational lag-time model.

Note: The dashed line in the regression plots represents the 1:1 relationship between observed and predicted lag times.

3.3.2 Calibration and cross-validation of storm-event hydrological response

Curve Number (CNII) values of 74.16 for Nyamutera and 75.34 for Gaseke, derived from a 2023 Sentinel-2 LULC map (10-m resolution), along with an imperviousness fraction of 15%, were assumed constant during model calibration and validation. Calibration and leave-one-out cross-validation results highlight the contrasting hydrological behavior of the Nyamutera and Gaseke catchments (Appendix 0–3). Nyamutera (44 km²; steep, limited storage) responds strongly to individual events. Initial abstraction (Ia) ranges from 0.5 to 10 mm, Muskingum storage constants (K) vary between ~450 and 7,700 s, and weighting factors (X) are generally low (0–0.5). Model performance is moderate for smaller storms (NSE up to 0.67; KGE up to

0.62) but declines markedly for larger or more complex events (NSE down to −33.22; KGE down to −0.44), with RMSE between 2.3 and 11.96 m³/s. Peak discharge and volume errors are often substantial (up to 79–89%), reflecting a strong sensitivity to antecedent moisture and the timing of rainfall. During jackknife cross-validation, errors generally increase and NSE and KGE decrease (down to −33.85 and −0.64, respectively), underscoring the event-specific nature of model skill in this steep, storage-limited basin.

By contrast, Gaseke (109 km²; moderate slope, floodplain-connected with ~168 ha storage) exhibits more consistent responses. Ia is consistently near 10 mm, K values are high (~14,000–15,000 s), and X is close to zero, reflecting storage-dominated flow and longer travel times. Calibration metrics vary across events (NSE ≈ −33.22 to 0.89; KGE ≈ −3.89 to 0.86), RMSE is moderate (≈1.1–11.7 m³/s), and peak discharge and volume errors fluctuate widely (up to 264% and 416%, respectively). Validation results are generally in line with calibration, indicating that floodplain storage and catchment geomorphology dominate storm responses rather than event-specific rainfall patterns.

Overall, these results indicate that Nyamutera's steep, storage-limited catchment requires event-specific parameterization due to its sensitivity to antecedent wetness and storm characteristics. In contrast, Gaseke's larger, floodplain-connected system allows for more transferable parameters, with runoff timing and magnitude largely controlled by geomorphic structure. Jackknife cross-validation emphasizes these contrasts and highlights the key role of catchment-scale storage and connectivity in shaping flood responses.

Table 3-2. Summary of calibration and jackknife cross-validation performance metrics for Nyamutera and Gaseke catchments.

Catchment	***Area (km²)***	***Basin Slope (m/m)***	***Upstream Floodplain (ha)***	***Median Ia (mm)***	***Median K (s)***	***Median X***	***Median NSE***	***Median KGE***	***Median RMSE (m³/s)***	***Median Peak Error (%)***	***Median Volume Error (%)***
Nyamutera	*44*	*0.41*	*–*	*10*	*1564*	*0.33*	*−0.36*	*0.02*	*5.58*	*58.4*	*78.5*
Gaseke	*109*	*0.37*	*168*	*10*	*15068*	*0.0*	*−1.01*	*0.05*	*4.3*	*36.0*	*50.1*

Note: Values represent median performance across all events. Geomorphological characteristics are provided for context: Ia = initial abstraction; K = Muskingum storage constant; X = Muskingum weighting factor, NSE = Nash-Sutcliffe efficiency; KGE = Kling-Gupta efficiency; RMSE = root-mean-square error, peak and volume errors expressed as

percent deviation from observed values, and metrics represent the median across all storm events (see Appendix 0-3 for full event-wise results).

3.3.3 Event Classification and Visualization

Figure 3-3 presents two panels showing observed, calibrated, and validation peak discharges for the Nyamutera (panel a) and Gaseke (panel b) catchments. Observed events are color-coded by severity—light gray for minor, medium gray for moderate, and dark gray for major events—allowing visual assessment of model performance across different event magnitudes. Calibrated and validation discharges are overlaid in blue and green, respectively. Events with peak discharge errors exceeding ±25% are emphasized using error bars, highlighting cases where the model substantially over- or underestimates observed flood peaks. This visualization provides a clear comparison of model accuracy and bias for individual events across both catchments.

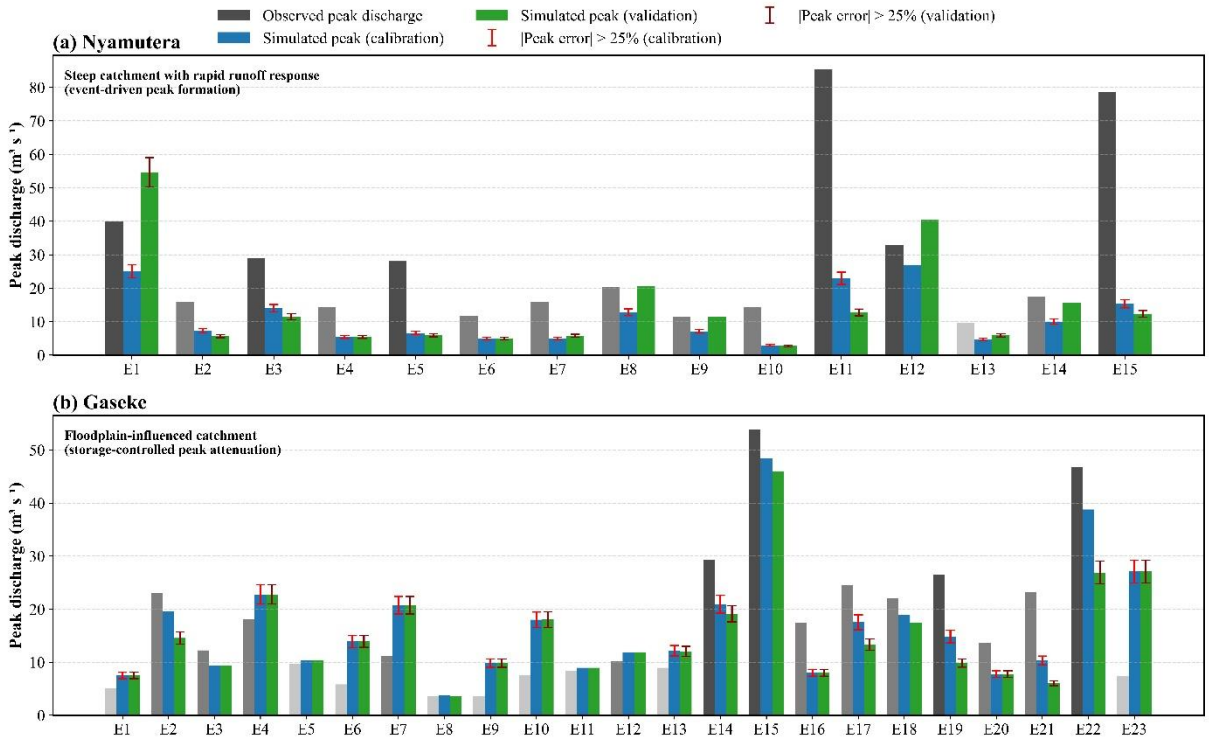

Figure 3-3 Observed, calibrated, and validated peak discharges for (a) Nyamutera and (b) Gaseke.

Note: Observed events are color-coded by severity (light gray: minor, medium gray: moderate, dark gray: major). Calibrated and validation discharges are shown in blue and green, respectively. Events with model errors exceeding ±25% are marked with I-bar symbols

indicating over- or under-prediction. This figure highlights model performance and bias across individual events of varying magnitudes.

3.3.4 Catchment-specific parameter sensitivities from Sobol' analysis

The Sobol' global sensitivity analysis (GSA) reveals clear differences in parameter importance between the Nyamutera and Gaseke catchments. These differences are consistent across performance metrics and are further supported by correlation analysis and parameter ranking.

For the Nyamutera catchment, sensitivity is shared among several factors, with Muskingum storage coefficient (K) and lag time showing the highest overall influence on model performance. Based on the mean Sobol' indices across all metrics, K ranks first (mean ST ≈ 0.45), followed by lag time (mean ST ≈ 0.40), Muskingum weighting factor X (mean ST ≈ 0.15), and initial abstraction (Ia) (mean ST ≈ 0.05).

Metric-specific results indicate that lag time dominates NSE sensitivity, with total-order indices approaching unity (ST ≈ 0.98). In contrast, K exhibits the highest sensitivity for KGE and RMSE, with ST values of approximately 0.75, indicating a strong influence on both efficiency and error magnitude. For peak-related and volume-based error metrics (PEPD and VE), sensitivity is more distributed, with lag time and X contributing notably to peak errors, while K shows the strongest influence on volume errors.

Correlation analysis aligns with the Sobol' results, showing positive correlations between K and efficiency metrics (particularly KGE) and negative correlations with RMSE, PEPD, and VE. The influence of Ia is comparatively low across all metrics, with consistently small Sobol' indices and weak correlations.

Overall, the Nyamutera results indicate that no single parameter exclusively controls model performance; instead, sensitivity is distributed among routing, timing, and loss-related parameters.

In contrast, the Gaseke catchment displays a markedly different sensitivity structure. Lag time is the dominant factor across all metrics, accounting for the largest share of variance in model performance. The mean total-order Sobol' index for lag time is approximately 0.67, substantially higher than for any other parameter.

For NSE and KGE, lag time shows very high sensitivity, with ST values exceeding 0.90. Lag time also remains the primary contributor to RMSE, PEPD, and VE, although the relative contribution decreases slightly for error-based metrics. The Muskingum storage coefficient (K)

ranks second in overall importance (mean ST ≈ 0.19), followed by initial abstraction (Ia) (mean ST ≈ 0.11) and Muskingum weighting factor X (mean ST ≈ 0.06).

Correlation results support this pattern, with lag time exhibiting the strongest relationships with both efficiency and error metrics. Other parameters show comparatively weak correlations and low Sobol' indices, indicating a limited contribution to output variability.

Overall, the Gaseke results show a highly concentrated sensitivity structure, with model performance primarily controlled by a single parameter. These results are summarized in Table 3-3 and Figures 3-4 and 3-5 below.

Table 3-3. Mean first-order (S_1) and total-order (ST) Sobol sensitivity indices for key hydrological model parameters in the Nyamutera and Gaseke catchments. Dominant influence indicates the relative importance of each parameter in controlling flood hydrograph simulations, highlighting contrasting controls between the two catchments.

Catchment	**Parameter**	**Mean S_1**	**Mean ST**	**Dominant Influence**
Nyamutera	Ia (mm)	0.05	0.055	Low
	Lag (h)	0.368	0.399	Moderate
	K (s)	0.416	0.452	High
	X	0.121	0.146	Moderate
Gaseke	Lag (h)	0.641	0.672	Very High
	Ia (mm)	0.086	0.114	Low
	K (s)	0.189	0.191	Moderate
	X	0.052	0.059	Very Low

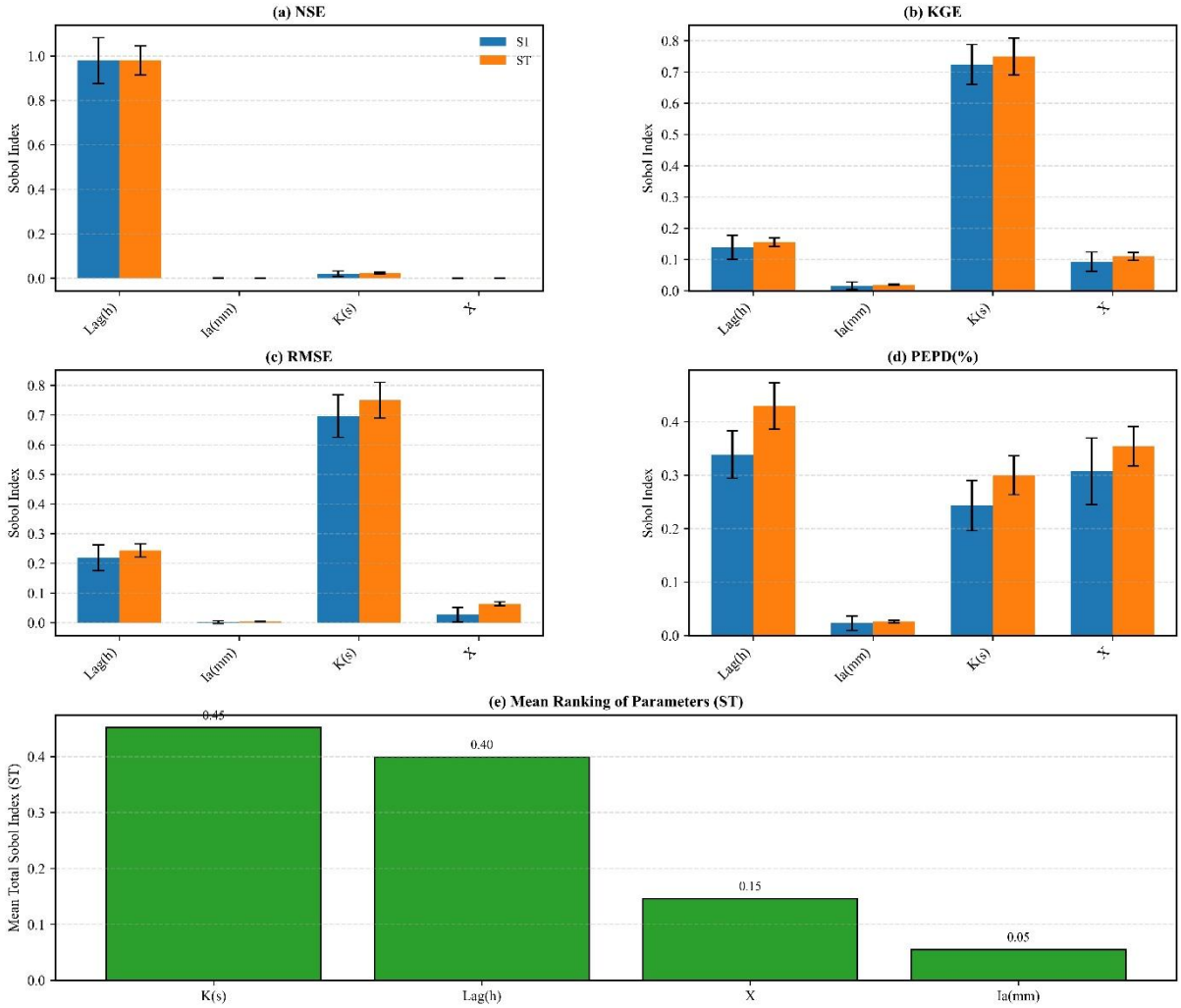

Figure 3-4 Sobol sensitivity analysis of model parameters for the Nyamutera catchment.

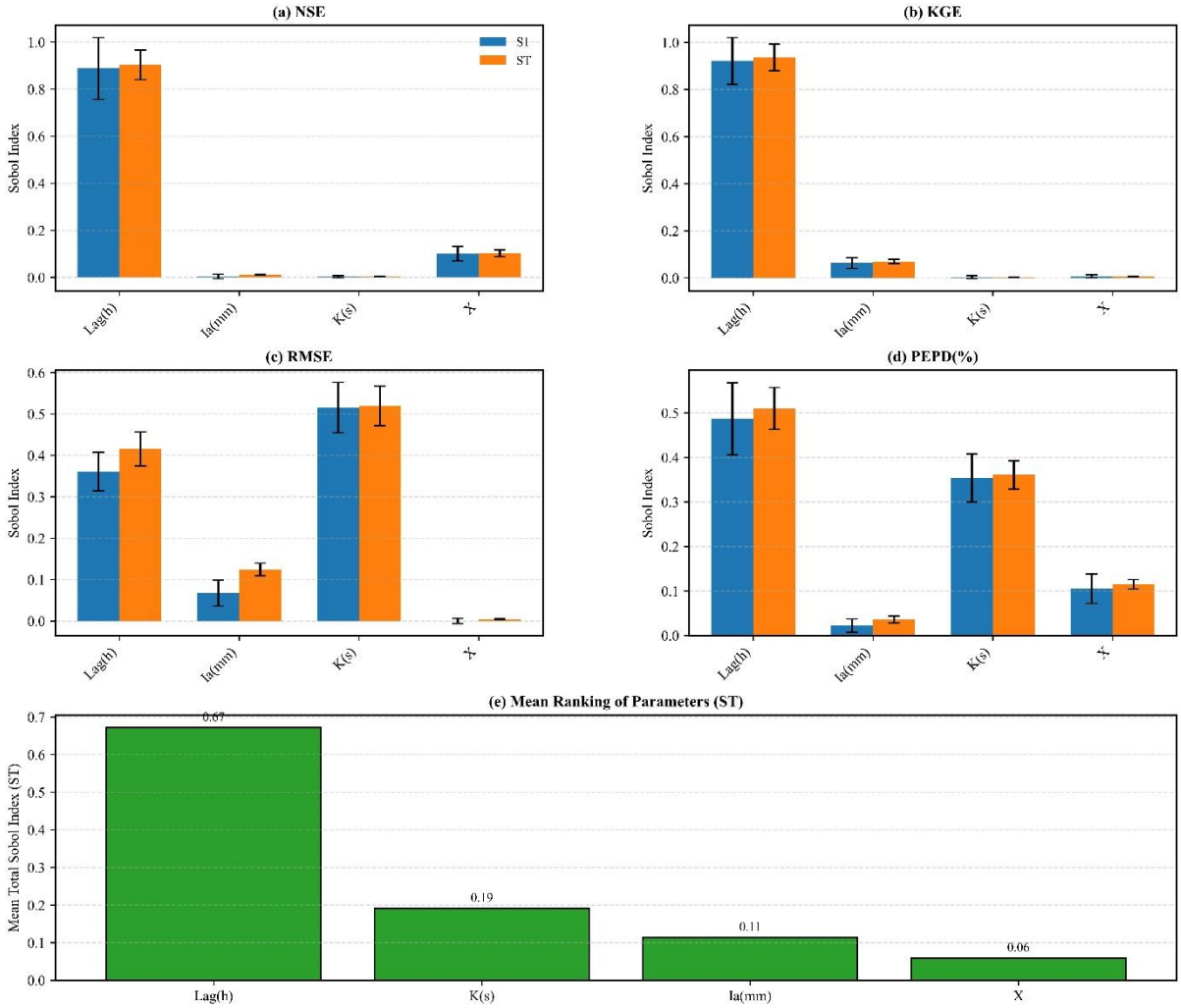

Figure 3-5 Sobol sensitivity analysis of model parameters for the Gaseke catchment.

Note: Panels (a)–(d) show first-order (S1, blue) and total-order (ST, orange) Sobol indices for NSE, KGE, RMSE, and PEPD (%), respectively, with confidence intervals. Panel (e) presents the mean ST indices across all metrics, ranking the parameters by their overall influence on

model output variability. Higher ST values indicate greater parameter sensitivity in controlling the rainfall-runoff response of the Nyamutera catchment.

These findings suggest different calibration priorities: in Nyamutera, focus on initial abstraction and channel routing parameters, whereas in Gaseke, lag time and initial abstraction (Ia) require more careful adjustment.

3.4 Discussion

3.4.1 Catchment morphometry and floodplain effects on event-based lag-time

The regression results reveal fundamentally different controls on event-scale lag time in the two catchments, reflecting contrasts in geomorphology, storage capacity, and hydrological connectivity.

In the Nyamutera catchment (44 km²; basin slope = 0.41; limited storage), lag time shows a strong positive dependence on antecedent discharge (b = 0.78, p = 0.035), while the influence of rainfall magnitude is secondary and not statistically significant (c = 0.46, p = 0.299). This pattern suggests that, in this small and steep basin, pre-event wetness plays a key role in regulating response timing. When antecedent discharge is high, subsurface flow paths are more connected and hillslopes may temporarily store additional water, slowing the transfer of runoff to the stream channels. The low baseline coefficient ($\alpha = 0.38$) indicates an inherently rapid response under dry conditions, consistent with Nyamutera's steep slopes, high relief, and limited capacity for long-term storage. Although the model explains a moderate fraction of the observed variability ($R^2 = 0.32$), a substantial portion of the variance remains unexplained, suggesting the influence of additional controls such as rainfall temporal structure, spatial heterogeneity of runoff generation, and localized flowpath activation (Arash et al., 2025; Garzon et al., 2023). These results confirm the Sobol' sensitivity results suggesting that Nyamutera's hydrological response is largely controlled by the Muskingum storage coefficient K (ST = 0.45) and lag time (ST = 0.40), while the weighting factor X (ST = 0.15) and initial abstraction Ia (ST = 0.05) play a comparatively minor role, consistent with the catchment's steep slopes and its tendency for rapid, event-driven runoff.

In contrast, the Gaseke catchment (109 km²; basin slope = 0.37; floodplain-connected with approximately 168 ha of storage) exhibits negligible sensitivity of lag time to both antecedent discharge and rainfall magnitude (b = −0.09, c = 0.06), accompanied by very low explanatory power ($R^2 = 0.05$). Despite a substantially larger baseline coefficient ($\alpha = 2.96$), reflecting longer flow paths and inherently slower catchment response, event-scale hydrometeorological variables explain little of the observed lag-time variability. This behavior indicates that

floodplain storage and hydraulic attenuation primarily control runoff timing, effectively decoupling lag time from short-term rainfall characteristics. Here, antecedent wetness, defined as the initial moisture condition of the catchment (approximated by baseflow or pre-event discharge), influences runoff generation on hillslopes and small tributaries but has only a minor effect on the volume of water stored in the floodplain. This is because floodplain storage is largely constrained by its physical capacity and hydraulic characteristics, such as area, slope, and downstream conveyance, which limit how much water can accumulate regardless of prior wetness. As a result, the lag between rainfall and peak discharge is controlled more by floodplain dynamics than by the antecedent hydrological conditions of the catchment (Bennett et al., 2018; Nied et al., 2017). The weak and only marginally significant regression coefficients suggest that lag time in the Gaseke catchment is primarily governed by structural and geomorphic controls rather than storm-scale dynamics. This pattern is confirmed by the Sobol' sensitivity analysis, which indicates that lag time overwhelmingly governs the model response (mean total-order index, ST = 67%), far surpassing the influence of the Muskingum storage coefficient K (ST = 19%), initial abstraction Ia (ST = 11%), and the weighting factor X (ST = 6%).

These contrasting responses align with widely reported differences between storage-limited headwater catchments and floodplain-integrated systems. In steep basins with limited internal storage, antecedent moisture conditions often exert a strong influence on runoff timing, as subsurface connectivity and transient storage vary markedly between events. Conversely, in larger catchments with extensive floodplain storage, distributed retention and delayed routing dampen event-scale variability, smoothing hydrograph responses and reducing the predictive power of simple regression-based lag-time models (Blöschl et al., 2019; Blume et al., 2007; Borga et al., 2014; Bullock & Acreman, 2003).

The lag-time model exhibited limited predictive skill, likely reflecting the complex and event-specific runoff response of the catchment (Figure 3-2). Owing to this strong event-to-event variability, a detailed sensitivity analysis of lag time was not undertaken. Nevertheless, lag time was retained in the Sobol' sensitivity analysis because of its critical role in shaping the rainfall-runoff response at the catchment outlet. Future work should place greater emphasis on this

influential factor, particularly as additional high-resolution rainfall and streamflow data become available from the low-cost monitoring system.

Table 3-4 presents the summary of the interpretation of hydrogeomorphical control.

Table 3-4. Interpretation of hydrogeomophological controls across catchments.

Aspect	**Nyamutera**	**Gaseke**
Dominant control	Antecedent wetness	Floodplain storage
Storage type	Hillslope & channel	Floodplain & channel
Lag-time variability	High, event-specific	Low, buffered
Model explanatory power	Moderate	Very low
Transferability	Low	Limited

Overall, the contrasting regression structures demonstrate that lag-times in steep, storage-limited catchments remain sensitive to antecedent hydrological conditions, whereas larger, floodplain-connected systems substantially reduce this sensitivity through internal buffering and delayed routing. These findings highlight the importance of explicitly accounting for geomorphic storage and hydrological connectivity when interpreting, comparing, or regionalizing lag-time relationships in mountainous tropical catchments (Dwivedi et al., 2025; Zuecco et al., 2018).

3.4.2 Hydrological response and model performance in contrasting catchments

The calibration and leave-one-out cross-validation results reveal clear differences in hydrological behavior and model performance between Nyamutera and Gaseke, reflecting contrasts in catchment size, slope, storage capacity, and floodplain connectivity.

In the steep, storage-limited Nyamutera catchment (44 km²), calibrated parameters show substantial variability across storm events. Initial abstraction (Ia) ranges from 0.5 to 10 mm, capturing responses under both dry and wet antecedent conditions: higher Ia values (e.g., events E1 and E4) correspond to dry pre-event states, whereas lower values indicate near-saturated soils or highly responsive surfaces. The Muskingum storage coefficient (K) spans roughly 450 to 7,721 s, reflecting how event magnitude and flow path length influence channel routing, while the weighting factor X remains low (0–0.5), consistent with rapid, channel-dominated flow typical of steep basins.

Model performance during calibration is moderate. NSE values reach up to 0.67 (E1) but drop below zero for more complex events, illustrating the difficulty in simultaneously reproducing peak and volume. RMSE values are generally low to moderate, yet peak discharge and volume errors can be substantial, highlighting Nyamutera's sensitivity to rainfall timing and antecedent

wetness. Leave-one-out validation further emphasizes this event-specific behavior: performance generally declines, with increased peak discharge errors and persistently high volume errors, demonstrating that parameters such as Ia and K strongly influence model skill on an event-by-event basis. Overall, Nyamutera exhibits a highly event-driven response, controlled by steep slopes and limited storage capacity.

By contrast, the larger, floodplain-connected Gaseke catchment (109 km^2, with ~168 ha upstream floodplain) shows a more homogeneous hydrological response. Initial abstraction is consistently around 10 mm for most events, suggesting a relatively uniform pre-event storage effect. Muskingum storage coefficients are large (~14,000–15,000 s) and X values are near zero, indicating that flow routing is dominated by storage processes rather than channel conveyance. Calibration metrics are mixed: NSE values are often negative or near zero, and KGE values vary, reflecting the model's limited ability to capture short-term fluctuations, as the floodplain and distributed storage attenuate the hydrograph. RMSE values remain moderate, and peak and volume errors fluctuate across events, indicating that runoff timing and magnitude are primarily governed by catchment structure rather than individual storm characteristics. During validation, performance is broadly consistent with calibration, demonstrating that Gaseke's response is largely dictated by structural and storage properties, rather than by antecedent discharge or rainfall intensity.

Overall, the contrast between the two catchments highlights important insights. Event-scale sensitivity dominates in steep, storage-limited Nyamutera, requiring event-specific parameterization for accurate predictions. In Gaseke, the floodplain and larger area buffer hydrological responses, producing smoother hydrographs and more transferable parameter sets. High K values and low X in Gaseke indicate slow routing and storage-controlled behavior, whereas lower K and more variable X in Nyamutera reflect rapid, event-driven flow. The leave-one-out validation effectively underscores these differences: Nyamutera shows strong dependence on event-specific conditions, while Gaseke demonstrates that structural and geomorphic controls largely govern lag times and peak flows. Collectively, these results emphasize the importance of catchment-specific hydrological characteristics in shaping both model calibration and predictive performance, reinforcing that steep, storage-limited basins require careful event-wise calibration, whereas floodplain-connected catchments allow for

more generalizable parameter sets (Garzon et al., 2023; Knapp et al., 2025; O'Sullivan et al., 2012; Padiyedath Gopalan et al., 2019) (Table 2-3).

3.4.3 Model performance under exploratory thresholds

Applying the exploratory performance thresholds (NSE ≥ 0.5, KGE ≥ −0.41, |PEPD| ≤ 25%, and |VE| ≤ 25%) reveals clear and systematic differences in model behavior between the Nyamutera and Gaseke catchments, reflecting their contrasting hydrological and geomorphic controls.

In Nyamutera, model performance is highly event-dependent. During calibration, only E1 achieves NSE ≥ 0.5, while KGE is generally more favorable, indicating that hydrograph timing and shape are often captured even when peak and volume reproduction are poor. Peak-flow errors are acceptable in roughly two-thirds of events, showing the model can often capture the timing and magnitude of peaks reasonably well. However, storm volume errors remain consistently high, with only E12 meeting the volume-error criterion. This reflects the catchment's steep slopes, rapid runoff response, and the strong influence of event-specific parameters such as initial abstraction (Ia) and Muskingum routing coefficient (K) on runoff generation and translation. Small variations in rainfall losses or channel storage can lead to large differences in cumulative runoff, making volume reproduction particularly challenging.

Leave-one-out validation reinforces this pattern. Peak timing remains moderately well captured in some events, but volumetric errors remain high across all storms, confirming limited parameter transferability. This behavior is characteristic of flashy mountainous catchments, where runoff is strongly controlled by rainfall intensity and antecedent wetness (Li et al., 2012).

In contrast, Gaseke exhibits more stable and consistent model behavior. Most events satisfy the KGE criterion during calibration, indicating good capture of hydrograph timing and shape. Peak-flow errors are generally small, and volumetric performance is substantially improved: nearly half of the events meet the volume-error threshold during calibration, with several maintaining acceptable performance during cross-validation. These results reflect the catchment's structural characteristics: a larger area (109 km²), moderately slopes, longer flowpaths, and a ~168 ha upstream floodplain buffer runoff generation, allowing cumulative storage and attenuation effects to dominate. Lag time is identified as the primary control in Gaseke, consistent with Sobol' sensitivity results. Once adequately represented, the model is resilient to variability in individual storm characteristics.

Overall, these findings highlight the influence of catchment structure on both parameter sensitivity and model performance. In the rapid responding and steep Nyamutera catchment,

rainfall losses and routing dominate, making storm-volume reproduction highly event-specific. By contrast, floodplain-connected larger Gaseke shows smoother, storage-controlled responses, allowing more transferable parameter sets and better overall model performance (Gupta et al., 2009; Moriasi et al., 2007; Patil & Stieglitz, 2015; Ponce & Hawkins, 1996).

3.4.4 The NRCS-CN sensitivity analysis across storm-based rainfall-runoff events

The sensitivity analysis of the NRCS-CN-based rainfall-runoff model reveals clear contrasts in the controls of flood response between Nyamutera and Gaseke catchments.

In Nyamutera, the Muskingum storage constant (K), and lag time emerge as the dominant factor influencing peak flows, with a mean first-order Sobol index (S_1) of 0.42 and 0.37 and a total-order index (ST) of 0.45 and 0.40, respectively, while the Muskingum weighting factor (X) and initial abstraction (Ia) play minimum influences. This highlights the pivotal role of rainfall losses and flow timing in regulating the effective runoff volume available to generate peak discharge.. The fact that X has a measurable sensitivity indicates that channel routing and flood-wave translation are non-negligible processes shaping the hydrograph.

These sensitivity patterns are consistent with the catchment's physical attributes. Nyamutera is small and steep (44 km²), with short flowpaths (longest 14.3 km, centroid 6.9 km), steep slopes (0.07–0.08 m/m), and high relief (1,186 m). The limited catchment storage reduces natural buffering capacity, causing peak flows to be primarily controlled by runoff translation and channel routing rather than by rainfall losses. Consequently, parameters governing flow timing and routing storage (lag time and Muskingum K) dominate peak flow formation, while initial abstraction exerts only a minor influence on hydrograph shape despite geological heterogeneity. (Pohl et al., 2015; Zhang et al., 2024).

In contrast, Gaseke exhibits a markedly different sensitivity profile. Lag time dominates the flood response, with $S_1 \approx 0.64$ and ST ≈ 0.67, far surpassing all other parameters. Initial abstraction (Ia) still contributes ($S_1 \approx 0.09$, ST ≈ 0.11), whereas Muskingum storage K ($S_1 \approx 0.19$, ST ≈ 0.19) and X ($S_1 \approx 0.05$, ST ≈ 0.06) play only minor roles. The near-negligible sensitivity of X suggests that attenuation effects are largely captured by the lag time parameter, reflecting the catchment's longer flowpaths (longest 21.6 km, centroid 11.7 km), moderately slopes (0.02–0.04 m/m), moderate relief (902 m), and the presence of a 168-hectare floodplain that naturally slows runoff and extends hydrograph duration (Herman et al., 2013). The

schistose lithology with minor alluvial deposits allows moderate infiltration, explaining why Ia retains a secondary role in controlling flood peaks.

These contrasting sensitivity patterns clearly illustrate how geomorphology and geology shape flood processes. In steep, floodplain-free catchments like Nyamutera, rainfall losses and channel routing are the primary drivers of peak flows, whereas in gently sloping, floodplain-rich catchments like Gaseke, flow attenuation is dominated by lag time. For model calibration and flood prediction, this suggests prioritizing K and lag timewith minor adjustment of X and Ia in Nyamutera, while focusing primarily on lag time with minimal adjustment needed for K, Ia and X.

Overall, this analysis highlights that identical rainfall events can trigger very different flood responses depending on catchment characteristics, emphasizing the need for tailored modeling approaches in mountainous tropical environments (Beven, 2012; Patil & Stieglitz, 2015; Pohl et al., 2015; Ponce & Hawkins, 1996; Veeck et al., 2020; Zhang et al., 2024).

3.4.5 Implications and limitations of the NRCS-CN method for flood modeling in mountainous terrain

The combined sensitivity and performance analyses reveal important limitations of the NRCS-CN approach when applied to storm-based flood modeling in mountainous tropical catchments. In both Nyamutera and Gaseke, flood response is governed less by static runoff generation and more by catchment-controlled flow timing, storage, and routing processes, which are only indirectly represented in the NRCS-CN framework.

In Nyamutera, the sensitivity analysis indicates that channel storage (K) is the dominant control on flood response, followed closely by lag time, while the routing weight X plays a moderate role and initial abstraction (Ia) has a relatively minor influence (mean ST: K = 0.45, Lag = 0.40, X = 0.15, Ia = 0.05). This suggests that the timing and translation of runoff through the channel network largely govern peak flows, rather than rainfall losses alone. Even though Ia contributes less, it still modulates early-event runoff, reflecting the importance of antecedent moisture and infiltration heterogeneity. The NRCS-CN approach, with its simplified representation of losses, can struggle to fully capture these dynamics, particularly in Nyamutera's steep, compact, and floodplain-absent terrain, where channel routing and storage dominate the shaping of flood peaks.

These limitations are reflected in the event-based performance results. In Nyamutera, the model struggles to consistently reproduce observed flows. NSE values remain poor across both calibration and validation, even though KGE often indicates acceptable performance. This contrast suggests that, while the model can generally capture the timing and overall shape of

hydrographs, it frequently under- or overestimates peak magnitudes and total runoff volumes. Such behavior is typical of small, steep headwater catchments, where even minor variations in abstraction or routing thresholds can lead to large differences in flood response. The catchment's short flowpaths and steep slopes provide limited natural buffering, amplifying sensitivity and reducing the transferability of calibrated parameters between events. Sensitivity analysis supports this interpretation: channel storage (K) and lag time exert the greatest influence on model outputs (mean ST = 0.45 and 0.40, respectively), while routing weight X and initial abstraction (Ia) have smaller, yet still meaningful, effects (mean ST = 0.15 and 0.05). This hierarchy highlights the critical role of flow translation and storage in shaping flood peaks, with early losses and threshold-controlled runoff playing a secondary, but noticeable, role (Li et al., 2012; Patil & Stieglitz, 2015).

By contrast, Gaseke exhibits a very different pattern. Lag time emerges as the dominant control on flood response (mean ST = 0.67), while channel storage (K), initial abstraction (Ia), and routing weight (X) play supporting roles (mean ST = 0.19, 0.11, 0.06, respectively). This distribution reflects the catchment's longer flowpaths, moderate slopes, and a substantial floodplain, which collectively slow runoff and stretch hydrographs. Calibration results confirm that the model reproduces hydrograph timing and peak magnitudes relatively well, with observed and simulated peaks closely aligned for most events. Overall volumetric performance is also superior to Nyamutera, although some individual events are still under- or over-predicted, highlighting the event-dependent variability inherent in flood modeling (Fleischmann et al., 2016; Garzon et al., 2023).

However, validation results reveal that peak-flow accuracy can deteriorate sharply for some events, even when the overall hydrograph shape is reasonably well captured. This pattern reflects the influence of event-specific variability in floodplain storage and delayed release, which strongly affects peak flows in a floodplain-influenced catchment like Gaseke. Because the NRCS-CN approach lacks a dynamic representation of these processes, a single parameter set cannot consistently reproduce all events. Thus, while Gaseke appears more "model-friendly" than Nyamutera in general, its apparent robustness masks underlying structural limitations under varying hydrological conditions.

Taken together, these findings reinforce the insights from the sensitivity analysis. In steep, compact basins like Nyamutera, model behavior hinges on abstraction thresholds and channel routing, making storm volumes and peak flows difficult to reproduce consistently. In larger, floodplain-influenced basins like Gaseke, hydrograph timing dominates performance, allowing better reproduction of flow dynamics but still challenging peak prediction under variable

storage conditions. These contrasts illustrate that the NRCS-CN method, in its event-based form, is better suited to damped catchments with longer response times than to highly responsive mountainous headwaters. However, the lag-time model showed limited predictive skill, likely reflecting the complex and event-specific runoff response of the catchment (Figure 3-2).

These results are consistent with previous studies highlighting the challenges of applying NRCS-CN in data-scarce and geomorphologically complex regions (Kang & Yoo, 2023; Yu et al., 2025). While recent work suggests that coupling NRCS-CN with machine learning approaches can improve predictive skill (Raj et al., 2024), such hybrid models introduce additional complexity, require extensive training data, and may reduce transparency and robustness. In contrast, the findings of this study emphasize that explicit consideration of geomorphic controls and routing dynamics—rather than further refinement of static runoff estimation alone—is essential for improving flood modeling in mountainous tropical catchments.

3.4.6 Applicability and transferability of the NRCS-CN method in mountainous tropical catchments

The combined calibration, validation, and sensitivity results from Nyamutera and Gaseke provide clear insights into where the NRCS-CN method is applicable—and where its transferability becomes limited—in mountainous tropical environments. Across both catchments, flood response is governed less by static runoff generation and more by terrain-driven flow timing, storage, and routing, processes that the NRCS-CN framework represents only indirectly.

The sensitivity analysis and model performance reveal striking contrasts between the two catchments. In Nyamutera, flood response is strongly influenced by channel storage (K, mean ST = 0.45) and lag time (mean ST = 0.40), with routing weight (X, mean ST = 0.15) and initial abstraction (Ia, mean ST = 0.05) playing smaller but still relevant roles. This hierarchy highlights the critical role of flow translation and storage in shaping peak flows, while early losses and threshold-controlled runoff contribute to a lesser extent. Model performance reflects these sensitivities: NSE values are consistently low across calibration and validation, indicating poor agreement with observed peak magnitudes and total runoff volumes, whereas KGE often remains acceptable, suggesting that the model generally captures hydrograph timing and overall shape. The steep slopes, short flowpaths, and absence of a floodplain in Nyamutera amplify

sensitivity to small changes in abstraction or routing parameters, resulting in event-dependent variations and poor transferability of calibrated parameters between storms.

By contrast, Gaseke exhibits a markedly different pattern. Lag time dominates flood response (mean ST = 0.67), with channel storage (K = 0.19), initial abstraction (Ia = 0.11), and routing weight (X = 0.06) playing secondary roles. The catchment's long flowpaths, moderate slopes, and a substantial 168-hectare floodplain combine, reducing the sensitivity of flood timing to parameter variability.

The model generally reproduces hydrograph timing and peak magnitudes well across most events, and volumetric performance is superior to Nyamutera, although some individual events are still under- or over-predicted. This event-dependent variability reflects the influence of dynamic floodplain storage and delayed runoff release, processes that the NRCS-CN method cannot explicitly capture. As a result, while Gaseke appears more "model-friendly," its apparent robustness masks underlying structural limitations under changing hydrological conditions (Fleischmann et al., 2016).

Together, these results underscore how catchment geomorphology and hydrological processes fundamentally shape flood behavior and model sensitivity. In steep, compact headwater catchments like Nyamutera, threshold-controlled losses and rapid routing dominate, limiting predictive performance. In contrast, floodplain-influenced systems like Gaseke shift dominance to lag time, smoothing flood peaks and enhancing model reproducibility, yet still challenge NRCS-CN representations under event-specific conditions. This comparison highlights the need for tailored modeling strategies that account for both geomorphic controls and process heterogeneity when predicting floods in mountainous tropical regions (Fleischmann et al., 2016; Garzon et al., 2023).

Overall, these findings indicate that the NRCS-CN method can provide useful first-order estimates of flood response, particularly in catchments with slower, attenuated hydrographs. However, its predictive reliability and transferability are limited in environments where topography, channel routing, and storage processes strongly influence flood behavior. In steep, rapidly responding tropical catchments, small differences in abstraction or routing thresholds can lead to large variations in peak flows, challenging the method's applicability. For flood-risk management and hydraulic design in such settings, more physically informed modeling approaches—ones that explicitly capture travel times, channel and floodplain storage, and dynamic retention processes—are likely necessary to improve robustness and ensure more

reliable predictions across a range of storm events (Beven, 2012; Blöschl et al., 2013; Ponce & Hawkins, 1996).

3.4.7 Pathways for model enhancement and implications for flood risk management

The results from Nyamutera and Gaseke show that improving flood prediction in mountainous tropical catchments requires moving beyond static runoff estimation toward models that explicitly represent terrain-controlled flow timing and storage. While the NRCS-CN framework remains attractive for its simplicity and low data requirements, its limitations become evident in environments where flood response is governed by steep slopes, short response times, and variable floodplain attenuation.

One promising pathway for improvement lies in combining CN-based runoff estimation with simplified, physically informed peak-flow approaches such as the Rational method, applied in a context-dependent manner (Nahayo et al., 2026). When adapted to account for catchment slope, flowpath length, and travel time, this hybrid approach can provide a pragmatic alternative for steep tropical basins where detailed hydraulic data are unavailable. While such methods do not explicitly resolve flood wave propagation, they offer a transparent way to link runoff generation to peak discharge and timing, thereby addressing key weaknesses of the CN framework in reproducing flood peaks and response times. Retaining the empirical efficiency of the CN method while embedding physically meaningful timing constraints allows flood estimates to better reflect terrain-controlled dynamics without increasing data demands.

Additional refinements could focus on improving the representation of flow translation and channel storage dynamics, which dominate flood response in Nyamutera. Incorporating approaches that better capture the effects of rapid routing and storage processes may enhance the model's ability to reproduce peak flows and total runoff volumes, rather than focusing primarily on variable initial abstraction. Likewise, topography-driven storage representations—for example, indices linked to floodplain extent or channel–floodplain connectivity—could improve the simulation of delayed responses in floodplain-influenced systems such as Gaseke (Beven, 2012; Blöschl et al., 2013). These enhancements directly address the dominant sensitivities identified in this study, namely abstraction thresholds, channel storage, and travel time (Cortés-Salazar et al., 2023).

By contrast in Gaseke, model refinements should prioritize the accurate representation of floodwave translation and the buffering effects of the floodplain, which largely control peak timing and hydrograph elongation. Adjustments to routing and storage parameters, rather than

initial abstraction, are likely to yield the greatest improvement in predictive performance across diverse storm events (Ekwule & Agunwamba, 2024).

From a flood risk management perspective, these results highlight critical limitations in steep, compact catchments like Nyamutera. Here, small inaccuracies in representing channel routing and flow translation can translate into large errors in peak-flow predictions, while early losses and initial abstractions play a secondary but still relevant role. As a result, flood peaks may be substantially under- or overestimated for individual events, limiting the reliability of hazard assessments and highlighting the challenges of representing routing and storage processes within simplified modeling frameworks.

In contrast, in floodplain-influenced catchments like Gaseke, neglecting variable attenuation and travel time can misrepresent both flood timing and magnitude, with direct consequences for early warning and infrastructure design.

Overall, the results point toward the need for geomorphologically informed, hybrid modeling strategies. Retaining the efficiency of the NRCS-CN approach while embedding process-based routing and storage components offers a practical pathway toward more robust flood prediction in data-scarce tropical regions. By aligning model structure with catchment characteristics—emphasizing channel routing and storage in steep, compact basins like Nyamutera, and prioritizing flow travel time and floodplain retention in more extended basins like Gaseke—flood risk assessments can achieve greater reliability and interpretability. Tailoring model representations in this way strengthens the scientific foundation for infrastructure planning and flood management, ensuring that predictions of peak flows and runoff volumes better reflect the actual hydrological behavior of mountainous tropical catchments (Beven, 2012; Blöschl et al., 2013; Viglione et al., 2009).

3.5 Conclusion

This study assessed the applicability of the NRCS-CN loss method and UH transformation coupled with Muskingum routing, for event-based rainfall-runoff modeling in two contiguous and contrasting mountainous catchments in northwest Rwanda. A total of 38 storm events were analyzed: 15 in the steep, floodplain-absent Nyamutera catchment and 23 in the less steep, floodplain-connected Gaseke.

Event-based calibration and validation results demonstrate that the NRCS-CN framework exhibits limited and highly event-dependent performance in both Nyamutera and Gaseke catchments. In Nyamutera, the model struggled to capture peak flows, with all calibration events exhibiting poor NSE values and none of the validation events reaching the NSE ≥ 0.5

threshold, reflecting the catchment's steep slopes and rapid runoff response. In Gaseke, calibration performance was somewhat better, with few events approaching satisfactory NSE values, but validation again showed limited success, as event-specific variability in floodplain storage and flow timing prevented consistent reproduction of observed hydrographs. These outcomes indicate that calibration success does not translate into reliable predictive skill under independent storm conditions.

Peak-flow simulations further underscore the model's limitations. While a few calibration events in Gaseke showed reasonably low peak errors, most events in both catchments exhibited substantial discrepancies, which often worsened during validation, particularly for large floods. Total runoff volumes were consistently misrepresented, frequently deviating by more than ±50%, indicating that the model systematically underestimates event runoff rather than failing in isolated cases.

The observed performance patterns are consistent with the sensitivity analysis. In Nyamutera, flood response was largely governed by channel storage (K) and lag time, with routing weight (X) and initial abstraction (Ia) playing secondary roles, reflecting how the catchment's short, steep flowpaths and limited buffering amplify the influence of flow translation and storage processes on peak discharge. This sensitivity explains the model's instability under validation, where small changes in event conditions led to large deviations in simulated discharge. In Gaseke, flood response was clearly dominated by lag time, reflecting the influence of floodplain storage and slower channel routing. This allowed the model to achieve reasonable calibration fits for several events, yet transferability remained limited, as event-to-event differences in floodplain attenuation and storage dynamics could not be fully captured by a single parameter set.

Overall, the NRCS-CN method was able to capture certain features of flood hydrographs during calibration, such as general timing or shape, but consistently struggled to reproduce peak magnitudes and total runoff volumes simultaneously, with performance deteriorating further under validation. This highlights the method's limited transferability across events in mountainous tropical catchments with complex flow dynamics. These findings suggest that in mountainous tropical catchments where runoff dynamics are strongly shaped by geomorphology and internal storage processes, static abstraction-based modelling approaches have limited predictive reliability. Hydrological modelling studies of small mountainous basins demonstrate that fast hydrological responses and the need to resolve key processes at fine spatiotemporal scales challenge model performance (Bouaziz et al., 2021; Evin et al., 2024), and that simplified or static process representations often yield greater uncertainty and

inconsistent performance across flow regimes (e.g., multi-model analyses of process formulation impacts). The persistent uncertainty in streamflow predictions even with advanced data integration underscores the importance of explicitly accounting for geomorphic storage and heterogeneous flow paths in such complex catchments (Bouaziz et al., 2021; Van Kempen et al., 2021).

While the NRCS-CN method provides useful first-order estimates of flood response in mountainous tropical catchments, its transferability is highly catchment-dependent. In steep, compact headwater basins like Nyamutera, rapid runoff and limited buffering make peak flows highly sensitive to channel routing and lag time, causing calibrated parameters to perform poorly across events. In contrast, catchments with longer flowpaths, moderate slopes, and substantial floodplains, such as Gaseke, show better transferability, although event-specific variability in floodplain storage still limits consistent performance. These findings highlight the need for modeling approaches that explicitly represent dynamic abstraction, travel time, and storage processes to improve predictive reliability in such complex terrains (Bahremand, 2016; Seibert & Bergström, 2022).

To improve flood prediction in steep tropical catchments, we recommend a hybrid approach that combines CN-based runoff estimation with simplified, physically informed peak-flow methods, such as the Rational method, applied according to catchment-specific characteristics. By accounting for factors like slope, flowpath length, and travel time, this approach preserves the CN method's efficiency while offering a practical, context-sensitive way to simulate peak flows and timing (Nahayo et al., 2026). It provides a transparent, low-data-demand solution to overcome the main limitations of the CN framework in reproducing flood response dynamics in data-scarce, high-relief environments.

Model performance is further constrained by data scarcity, short observation periods, and uncertainty in event delineation, which amplify parameter equifinality and reduce calibration transferability. Nonetheless, the consistency between performance metrics and sensitivity results suggests that the observed limitations primarily reflect structural constraints of the NRCS-CN method rather than data issues alone. For flood risk assessment and hydraulic design in steep tropical basins, these findings underscore the need for modeling approaches that

explicitly consider event-specific storage, routing, and geomorphologically controlled flow timing, even when data availability is limited.

Chapter 4 Reconstructing historical streamflows for flood early warning in tropical mountain catchments: GR4J insights from northwest Rwanda

This chapter has been prepared for submission to a peer-reviewed journal, after incorporating feedback from my thesis defense as well as input from co-authors. The tentative title is "*Reconstructing historical streamflows for flood early warning in tropical mountain catchments: GR4J insights from northwest Rwanda*."

Literature, methodology and formulas presented in previous chapters have been intentionally omitted here to avoid redundancy.

Abstract

Reliability of flood early warning in data-scarce mountainous tropics is constrained by the absence or incompleteness of hydrometeorological records. This study applies the *"Génie Rural à 4 paramètres Journaliers"* (GR4J)-based approach to reconstruct historical daily streamflows in two contiguous catchments of the Mukungwa watershed in northwest Rwanda: Nyamutera (44 km²) and Gaseke (109 km²), and advances flood risk management by proposing flood early warning thresholds. The model was driven by observed rainfall-streamflow data (2022–2023), long-term rainfall from neighboring gauges, and satellite-derived potential evapotranspiration records (2010–2023). Model parameters were calibrated through multi-start differential evolution using a composite objective function incorporating Nash-Sutcliffe efficiency, Kling-Gupta efficiency, peak-weighted root mean squared error, and percent error in peak discharge. Equal weights of 0.25 were assigned to each metric, with an additional 15.47 mm parameter capturing floodplain buffering and sustained baseflows in Gaseke. Rainfall thresholds for flood early-warning were derived by fusing logistic regression and physical criteria. Calibration highlighted catchment-specific behavior: Nyamutera (NSE = 0.213, KGE = 0.506, RMSE = 1.355 m³/s, PWRMSE = 2.165 m³/s, and PEPD ≈ 0 %) responded rapidly to rainfall, while Gaseke (NSE = 0.451, KGE = 0.694, RMSE = 1.56 m³/s, PWRMSE = 2.942 m³/s, and PEPD ≈ 0 %) showed dampened peaks due to floodplain storage. The fused thresholds showed that 5–6-day and 7–11-day antecedent windows were identified for flood-risk forecasting in the Nyamutera and Gaseke catchments, respectively.

Finally, logistic regression performance metrics showed robust and consistent skill across both catchments, with probabilities of detection ranging from 0.57 to 0.80 and low false alarm ratios (0.00–0.25). High precision (0.75–1.00), near-perfect specificity (≈1.0), and overall accuracy exceeding 0.99 indicate strong discrimination between flood and non-flood conditions. Skill-based indices, including the critical success index (0.50–0.67), F1-score (0.67–0.80), and Heidke skill score (0.67–0.84), further support the suitability of the lumped conceptual, GR4J-based rainfall-runoff model for tiered flood warning and risk management in data-scarce tropical mountain catchments.

Keywords: Streamflow reconstruction, Flood risk forecasting, Rainfall-runoff modelling, Tropical mountain catchment hydrology, Fused threshold analysis

4.1 Introduction

Linkage of observational rainfall and streamflow create a supporting point in hydrology, as it provides essential tools that help understand the catchment responses, predicting streamflows, supporting water resources management, forecasting flood hazards and risks, and designing hydraulic infrastructure (Beven, 2012; V. P. Singh et al., 2018). Few decades ago, different researchers directed toward improving the hydrological models' robustness and transferability of across different climatic and geomorphic environments. Despite significant progress, many conceptual rainfall-runoff models developed about 20–50 years ago remain widely used and continue to be refined and adapted to regions outside their original applicability (Andréassian et al., 2009; Gupta et al., 1999). Among these, the conceptual lumped GR4J model, developed in the early 1980s by Claude Michel at Cemagref (*Centre national du machinisme agricole, du génie rural, des eaux et des forêts*) is widely used and continuously refined to simulate catchment-scale hydrology (Coron et al., 2017; Edijatno & Michel, 1989; Perrin et al., 2003a). This parsimonious model relies on four parameters: production storage capacity X_1 (mm), groundwater exchange coefficient X_2 (mm/day), routing storage capacity X_3 (mm), and unit hydrograph time constant X_4 (days) (Park et al., 2025). These parameters are the key processes of storage, transfer, and release that transform rainfall into streamflows (Boumenni et al., 2017; Coron et al., 2017; Perrin et al., 2003b). This model plays a particular advantageous while simulating streamflow in data-scarce environments, where semi-distributed or distributed models present limitations due to the absence of fine-scale observational rainfall and streamflow data that require more computational demands and introduce considerable parameter uncertainties (Andréassian et al., 2014a; Hrachowitz et al., 2013b; Perrin et al., 2003b). Although subjected to some limitations, GR4J has shown its capability to simulate streamflow in complex mountainous environments, including tropical catchment settings.

In the tropical West African catchments, Kodja et al., (2020) highlighted that the GR4J model can perform well even if the potential evapotranspiration (ET_o) is estimated with the Penman-Monteith method. However, under climatic and land use/land cover (LULC) change, its application provided critical insights into such hydrological processes and requires careful adaptation of hydrological settings in tropical regions. (Wanzala et al., 2022), through their comparative study of 19 East African catchments highlighted that the performance of GR4J model requires site-specific catchment considerations (Wanzala et al., 2022).

Therefore, GR4J can be tested and tailored to reflect contrasting processes of runoff generation in the two contiguous catchments: the small and steep Nyamutera, with limited storage and Gaseke with a moderately steep and prolonged baseflow supported by floodplain storage and

lateral groundwater flow. Its balance between parsimony and process representation can provide a robust framework for assessing spatiotemporal rainfall-runoff variability and hydrological responses in these geomorphically contrasting tropical catchments.

Although rainfall-runoff modeling is critical in tropical Africa, and often limited by the scarcity, discontinuity, or complete absence of streamflow records (Hrachowitz et al., 2013a; Muvundja et al., 2009), efforts to quantify hydrological variability, design hydraulic structures, and implement effective flood early-warning systems are still challenging in the African tropics, specifically in northwestern Rwanda, where long-term streamflow data are unavailable. Given the recurrent floods due to steep terrain and frequent intense rainfall, reconstructing historical discharge measurements from the available rainfall data is important to build the guidance of flood early-warning system in the region. This research gap raises the following question: *"To what extent can GR4J-based streamflow reconstruction support the development of flood early-warning thresholds and enhance flood-risk management in data-limited tropical mountain environments?"* To address this gap, a GR4J-based framework was extended and applied to reconstruct historical daily streamflow for two contiguous catchments, Nyamutera (44 km²) and Gaseke (109 km²), within the Mukungwa watershed. Specifically, this study aims to: (i) calibrate the GR4J rainfall-runoff model using rainfall and streamflow data recorded between March 2022 and May 2023; (ii) reconstruct historical daily streamflows for both rivers based on the historical rainfall record and satellite derived potential evapotranspiration from April 2010; and (iii) use the best-calibrated GR4J parameters to derive guideline thresholds for supporting a flood early-warning system.

Collectively, this research effort could establish a robust framework for reconstructing hydrological records and deriving catchment-specific flood early-warning thresholds, enhancing flood-risk management in tropical mountainous catchments.

4.2 Materials and methods

4.2.1 GR4J model framework and adaptation for the Nyamutera and Gaseke catchments

The daily rainfall-runoff transformation in this study was simulated using the GR4J-based model (Boumenni et al., 2017; Perrin et al., 2003), which represents catchment hydrological processes through two conceptual stores and four parameters. The GR4J structure used here is illustrated in Figure 4-1, with adaptations made to account for floodplain effects in the Gaseke catchment.

After interception, the total precipitation (P) and potential evapotranspiration (E) are reduced to effective precipitation (P_n) and net evapotranspiration (E_n). Here, P_n represents the net precipitation available after interception and initial evapotranspiration demand, while E_n is the remaining atmospheric demand. The production store, with capacity X_1 (mm), regulates the partitioning of P_n between soil moisture storage (S) and percolation, while En drives actual evapotranspiration losses from the store. The methodological approach for the Nyamutera catchment follows Kapoor et al. (2023) and Kuana et al. (2024), and was extended for the Gaseke catchment, which includes an approximately 168 ha (15.47 mm) floodplain, as follows. Effective rainfall (the portion of P_n infiltrating into the production store, Ps), actual evapotranspiration from the store (E_s), and percolation from the store (P_{erc}) are expressed, respectively, as:

$$P_s = \frac{X_1\left[1-\left(\frac{S}{X_1}\right)^2\right]\tanh\left(\frac{P_n}{X_1}\right)}{\left(1-\frac{S}{X_1}\right)\tanh\left(\frac{P_n}{X_1}\right)} \quad (4.1)$$

$$E_s = \frac{S\left[1-\frac{S}{X_1}\right]\tanh\left(\frac{E_n}{X_1}\right)}{1+\left(1-\frac{S}{X_1}\right)\tanh\left(\frac{E_n}{X_1}\right)} \quad (4.2)$$

$$P_{erc} = S\{1-\left[\left(1+\frac{4}{9}\frac{S}{X_1}\right)^4\right]^{-1/4}\} \quad (4.3)$$

The residual rainfall bypassing the production store is directed to quick response pathways. The net rainfall that bypasses the production store (P_n-P_s) is divided into two unit hydrographs: UH1, which routes 90% of the effective rainfall with a time base of X_4 (days), and UH2 that routes the reminder 10% with a time base of $2X_4$ (Birhanu et al., 2018). Both routed rapid and delayed runoff responses (P_r) are expressed as follows:

$$P_r = 0.9(P_n - P_s), \text{and } P_d = 0.1(P_n - P_s) \quad (4.4)$$

Additionally, the discharge routed through UH1 enters the routing store with capacity X_3 (mm). The outflow from the routing store, together with groundwater exchange governed by parameter X_2 (mm/day), is simulated using a nonlinear relationship that links storage level (R) to discharge.

$$Q_r = R\left[1-\left(1+\frac{R}{X_3}\right)^{-1/2}\right] \quad (4.5)$$

Lateral water exchange between the routing store and the groundwater system is represented by the parameter X_2, simulated as:

$$F(X_2) = P_d * R \quad (4.6)$$

A fixed fraction (10%) of the net rainfall is routed through the direct runoff pathway using a unit hydrograph (UH2), whose time base is controlled by the routing time parameter (X4), producing the rapid runoff component (Qd). The remaining effective rainfall is routed through a nonlinear storage reservoir to generate the delayed flow component (Qr). Total simulated discharge at the catchment outlet (Q) is computed as the sum of Qd and Qr (Birhanu et al., 2018):

$$Q = Q_r + Q_d \quad (4.7)$$

For the Gaseke catchment, the model was extended with an additional floodplain store to represent the buffering effect of its 168-hectare floodplain. To express the floodplain storage in terms of catchment-wide runoff depth, the floodplain area (168 ha) was first converted to km² (1.68 km²) and compared to the total catchment area of Gaseke (108.58 km²). This yielded a fractional area of 0.01547, or 1.547% of the catchment. The floodplain is assumed to be able to store water up to an average depth of 1 m (1000 mm) over its entire area. This assumption is common in conceptual floodplain or wetland storage representations (Rose et al., 2017; Wohl, 2021). When scaled to the whole catchment, this proportion corresponds to a uniform runoff depth of 15.47 mm. In other words, the maximum floodplain storage (F_{max}), equivalent to 15.47 mm of water uniformly distributed across the catchment, provides a basis for incorporating floodplain dynamics into the rainfall-runoff model. The parameter setting of the custom GR4J-Python framework was guided by Rainfall-Runoff Model Playground (RRMPG) (RRMPG, 2025) conceptualization (RRMPG, 2025) and extended based on the catchment-specificity.

The model's extension included the actual evapotranspiration coefficient (K_a), floodplain storage (Fmax) and release (Fα) coefficients. K_a was employed rather than the crop coefficient (K_c) to convert ET_0 into ET_a to take into account the soil moisture and LULC conditions instead of crop demand. The core GR4J parameters (X_1–X_4) and their extension (Fmax, Fα, and K_a) were then calibrated against the complete observed rainfall, streamflow and ET_o time series to ensure that all flow dynamics (either high, moderate or low) are taken into consideration during streamflow reconstruction. Figure 4-1 shows the model structure, including floodplain storage and release in Gaseke catchment.

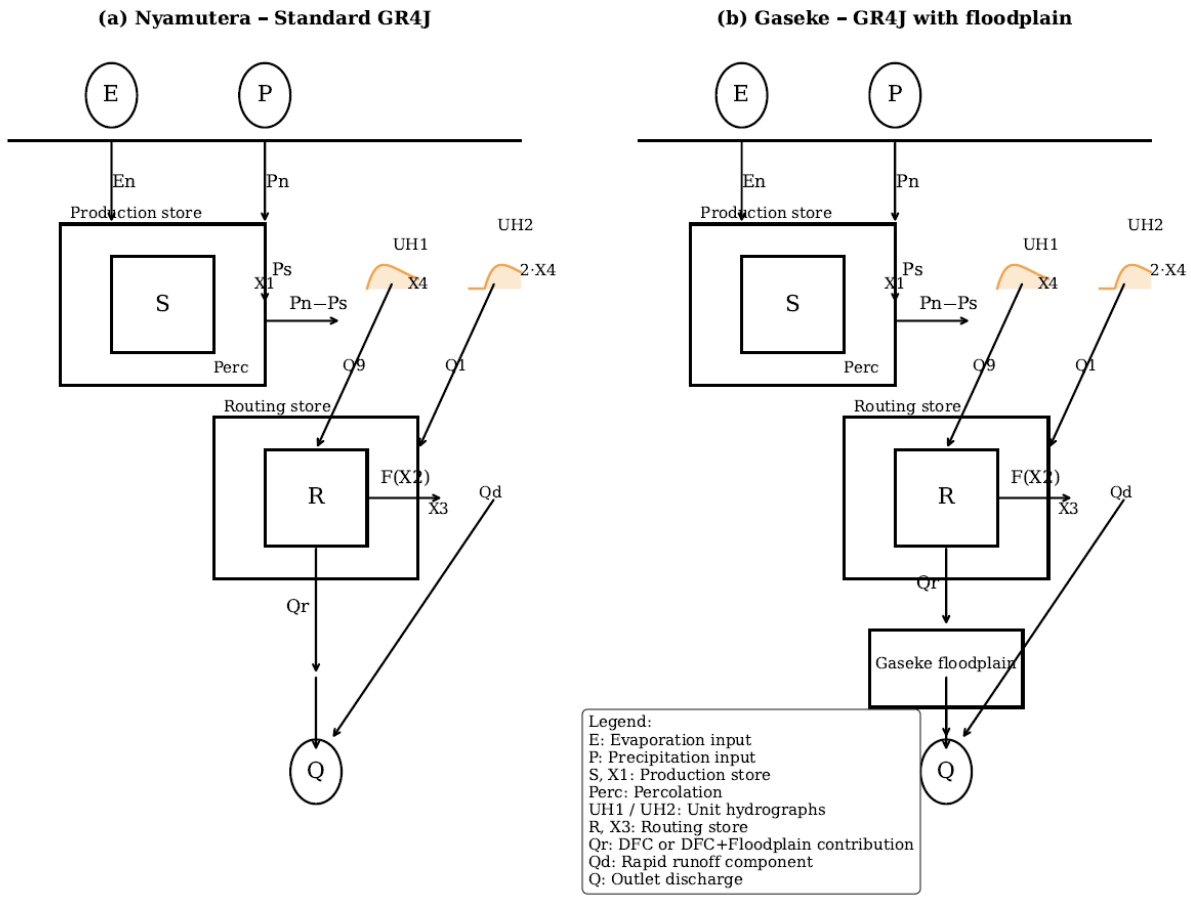

Figure 4-1 GR4J model schematic for Nyamutera (a) and Gaseke (b) catchments.

Note: The Nyamutera panel shows the standard configuration, while the Gaseke panel incorporates a floodplain. Key components are labeled: evapotranspiration (E), precipitation (P), production store (S/X1), percolation (Perc), unit hydrographs (UH1/UH2, X4/2·X4), routing store (R/X3), floodplain/outlet flow contribution (Qr), rapid runoff component (Qd), delayed flow component (DFC), and outlet discharge (Q). The legend is included only in panel (b) for clarity.

4.2.2 Setting of the composite objective function and calibration strategies

The composite objective function was set and implemented in the custom Python-based framework based on the key influential performance metrics and geomorphological characteristics of the two catchments. The weighting scheme for each core metrics (NSE, KGE, pwRMSE, and PEPD) was set to 0.25 to prevent any single metric from dominating others in the objective function. Additionally, as suggested by Mizukami et al. (2019), two parameters, including attenuation factor (Fα) and maximum floodplain storage depth (Fmax) were added. The higher values of Fα indicate slower drainage from the floodplain (Sridharan et al., 2020). By explicitly accounting for geomorphic and hydrological differences, this extension improves the realism of model simulations, enhances predictive performance, and ultimately supports more informed water-resource management and flood-risk planning.

The objective function was set as follows:

$$F = 0.25(1 - NSE) + 0.25(1 - KGE) + 0.25\frac{pwRMSE(Q_o, Q_m)}{\max(Q_o)} + 0.25\frac{PEPD(Q_o, Q_m)}{100} \quad (4.8)$$

where , F is the composite objective function, Q_o is the observed discharge, Q_m is the simulated streamflows, NSE is the Nash-Sutcliffe efficiency (Nash & Sutcliffe, 1970), KGE is the Kling-Gupta efficiency (Gupta et al., 2009; Knoben et al., 2019b), pwRMSE is the peak-weighted root mean square error, and PEPD is the percent error in peak discharge (USACE HEC, 2025).

4.2.3 Rainfall-runoff simulation and streamflow reconstruction

For both catchments, the lumped conceptual GR4J rainfall-runoff model was calibrated using a differential evolution (DE) algorithm to optimize model parameters against observed daily streamflow (S. Das & Suganthan, 2011). Parameter bounds were based on the guidelines set in the GRMPG and physical characteristics of both catchments (RRMPG, 2025). Daily precipitation records and ET_o estimated using the Penman-Monteith equation, while simulated daily discharges were evaluated against observed streamflow during calibration process (Allen et al., 2006). The calibrated GR4J-based rainfall-runoff model parameters were then applied to reconstruct flows over April 2010–February 2023 for both catchments, including floodplain storage dynamics for Gaseke.

4.2.4 Logistic regression for flood early-warning analysis

Numerous methods for defining flood early-warning thresholds have been proposed, including decision-theoretic thresholds based on the cost-loss approach (Wilks, 2001), soft fusion that combines statistical probabilities (P_{log}) with physically derived thresholds (P_{phys}) (Roulston & Smith, 2003), Bayesian fusion, which treats physical thresholds as priors (Krzysztofowicz, 1999), reliability calibration with threshold selection (Bröcker, 2008a, 2008b), multi-criteria or dynamic thresholds (Alfieri et al., 2019; Cloke & Pappenberger, 2009), and operational binding (Cloke & Pappenberger, 2009).

Table 4-1 provides an overview of early-warning threshold development methods, including their required input data, key strengths, and limitations (Biondi & De Luca, 2012; Kong et al., 2023; Kurian et al., 2020; J. Liu et al., 2024; Roohi, Ghafouri, et al., 2025; Yuan et al., 2024).

Table 4-1 Summary of methodological approaches for early-warning threshold derivation (hybrid/soft fusion, Bayesian updating, dynamic/multi-criteria thresholds, reliability calibration, decision-theoretic cost-loss, and operational binding) drawn from recent hydrological and forecast-value literature (e.g. Kurian et al., 2020; Liu et al., 2023; Biondi et al., 2012; Kong et al., 2023; Yuan et al., 2024).

Method	Input data	Strengths	Weaknesses
Decision-theoretic threshold (Cost–Loss approach)	Probabilistic forecasts (rainfall-runoff, ensemble streamflow); socio-economic cost-loss ratios; historical event-impact data	Explicitly incorporates socio-economic trade-offs; transparent and defensible	Requires reliable cost/loss estimates (often uncertain); may be politically sensitive
Soft fusion (weighted combination of P_log and P_phys)	Historical hydrological data for statistical/logistic models; outputs from physical models; weighting scheme	Leverages both physical realism and statistical adaptability; relatively simple to implement	Weight choice can be subjective; risk of double-counting uncertainty
Bayesian fusion (physical thresholds as prior)	Physical thresholds (e.g., bankfull discharge); statistical/probabilistic models; observational data for updating	Provides coherent probabilistic framework; handles uncertainty well; allows continuous updating	Computationally intensive; sensitive to choice of priors
Reliability calibration + threshold selection	Forecast–observation pairs (hindcasts); reliability diagrams	Improves forecast trustworthiness; aligns thresholds with user confidence	Requires long hindcast datasets; assumes stationarity of forecast skill
Multi-criteria / dynamic thresholds	Rainfall, streamflow, soil moisture, snowmelt, catchment conditions	More realistic (reflects varying catchment states); reduces false alarms and misses	Complex to design and explain; requires diverse datasets and calibration
Operational binding	Selected thresholds; institutional mandates and protocols; communication systems	Ensures scientific thresholds trigger concrete actions; improves accountability	Dependent on governance capacity and communication chains; science–policy gaps may undermine effectiveness

In the present study, the soft fusion approach was selected because it combines historical hydrological data (for statistical/logistic models), outputs from physical models, and a weighting scheme. The key strengths of this method results in balancing physical realism with statistical adaptability for its implementation (Solanki et al., 2025). Although the method is subjected to potential double-counting in weight choices, it can provide a clear picture of hydrological processes of these contrasting catchments, and that limitation has been taken into account during threshold identification for a better flood early-warning analysis.

To assess the potential of rainfall-based early warning for streamflow exceedances, a comparative logistic regression framework was used (Szeląg et al., 2020; Wu et al., 2024).

4.2.5 Logistic rainfall thresholds

Logistic rainfall thresholds represent statistically derived rainfall amounts associated with specified probabilities of flood occurrence. In this framework, flood events are first defined as binary outcomes [(1) flood occurred (discharge exceeds a defined threshold), and (2) flood did

not occur], indicating whether discharge exceeds a predefined flood threshold. Antecedent rainfall totals, accumulated over varying time windows, are then related to flood occurrence using logistic regression (Lee & Kim, 2021).

Rather than predicting discharge magnitude directly, the logistic model estimates the probability that a flood will occur given a particular rainfall history. From this probabilistic relationship, rainfall depths corresponding to selected exceedance probabilities (e.g., 25%, 50%, 75%, and 90%) are derived. These rainfall depths are referred to as logistic rainfall thresholds.

Physically, a logistic rainfall threshold expresses the likelihood of flooding rather than a deterministic trigger. For example, a 75% logistic threshold indicates that when antecedent rainfall exceeds this value, a flood is expected to occur in approximately three out of four similar situations. This probabilistic formulation explicitly accounts for uncertainty arising from variability in rainfall intensity, spatial distribution, soil moisture conditions, and runoff routing processes.

Logistic thresholds are particularly useful for early-warning applications because they allow warning levels to be directly linked to risk tolerance and decision-making needs (Bouttier & Marchal, 2024; Ramos Filho et al., 2021). However, when used alone, they may be sensitive to data limitations or produce physically unrealistic thresholds under conditions not well represented in the observational record.

4.2.6 Physical rainfall thresholds

Physical rainfall thresholds are derived from hydrological reasoning and event-based analysis rather than statistical fitting. They represent rainfall amounts expected to generate critical runoff responses based on catchment characteristics, storage capacity, and dominant hydrological processes (Luong et al., 2021a).

These thresholds reflect the amount of rainfall required to overcome losses due to infiltration, interception, evapotranspiration, and subsurface storage, leading to rapid runoff generation and channel response. Physical thresholds may be informed by observed rainfall-runoff relationships, soil moisture considerations, runoff coefficients, or prior flood studies conducted within the catchment (Zhai et al., 2018).

Unlike logistic thresholds, physical rainfall thresholds provide a stable and physically interpretable reference that is less sensitive to random variability or limited sample size. They are particularly valuable in data-scarce environments or when extrapolating beyond observed conditions. However, because they simplify complex hydrological processes, physical

thresholds may not fully capture event-to-event variability when applied alone (Ramos Filho et al., 2021).

4.2.7 Fused operational rainfall thresholds

To balance statistical adaptability with physical realism, this study adopts a fused operational rainfall threshold approach. Fused thresholds are computed as weighted combinations of logistic rainfall thresholds and physical rainfall thresholds, producing a single rainfall threshold suitable for operational early-warning use (Mentzafou et al., 2023).

The weighting between the two components is not fixed but dynamically adjusted according to catchment characteristics that influence flood response behavior. Smaller, steeper, and more hydrologically responsive catchments are assigned greater weight to logistic thresholds, reflecting the strong and direct linkage between rainfall and flood occurrence. In contrast, larger or more buffered catchments are assigned greater weight to physical thresholds, reflecting the moderating influence of storage, floodplains, and routing effects.

The resulting fused thresholds are expressed in rainfall units and vary with antecedent rainfall duration and exceedance probability. These thresholds combine observed system behavior with hydrological process understanding, thereby reducing the risk of unrealistic extrapolation while maintaining sensitivity to observed flood responses. As such, fused operational thresholds provide a practical and scientifically grounded basis for real-time flood early-warning decisions (Bouttier & Marchal, 2024; Ramos Filho et al., 2021).

In this study, the related custom Python framework incorporates the computation of the logistic and physical thresholds (L_T and P_T) weighted by the calibrated fusion factor (w) to find the overall rainfall threshold (F_T) as follows:

$$F_T = w * L_T + (1 - w) * P_T \quad (4.9)$$

Rainfall and streamflow time series from April 2022 to May 2023 were analyzed on an event basis, with antecedent rainfall accumulated over 1–15 days that preceded each observed flood event, including the daily rainfall of the day of the reference flood event. The iterations were stopped when the accumulated antecedent rainfall produced a receiver operating characteristic curve indicating very high discriminatory power (AUC approaching 1) for a given duration, reflecting strong separation between event and non-event conditions, while recognizing that classification errors, including false negatives, may persist depending on the threshold.

4.2.8 Integrated interpretation of logistic and physical thresholds

Together, logistic (probabilistic) thresholds, physically derived thresholds, and ROC-based skill assessment form a comprehensive early-warning framework that balances observational

learning with process understanding and objective performance evaluation. Hybrid approaches that combine multiple threshold types have been recognized as improving early warning system performance, particularly when data are limited or catchment responses are complex (Mentzafou et al., 2023).

Briefly, logistic thresholds describe how likely flooding is given rainfall history, physical thresholds describe how much rainfall the catchment can physically accommodate, fused thresholds combine both into operational warning levels, and ROC analysis evaluates how well rainfall history distinguishes flood from non-flood conditions across different antecedent periods.

4.2.9 Receiver operating characheristic analysis across antecedent rainfall windows

The predictive performance of rainfall-based flood thresholds was evaluated using receiver operating characteristic (ROC) analysis across multiple antecedent rainfall windows. ROC curves assess the ability of rainfall predictors to discriminate between flood and non-flood conditions over the full range of probability thresholds (Lee & Kim, 2021).

For each antecedent rainfall window, the true positive rate (correct flood detections) is plotted against the false positive rate (false alarms). The area under the ROC curve (AUC) provides a summary measure of discrimination skill, with values near 0.5 indicating no predictive skill and values approaching 1.0 indicating excellent flood discrimination. However, AUC is an aggregate performance metric and does not explicitly reflect the asymmetric importance of false negatives, which are often more consequential than false positives in flood early-warning and risk management contexts.

Comparing ROC curves across different antecedent rainfall windows allows identification of the rainfall memory length most relevant to flood generation in each catchment. Therefore, ROC analysis provides objective evidence for selecting appropriate rainfall accumulation periods for early-warning applications.

The custom Python-based framework was set to iteratively adjust thresholds based on flow percentiles to ensure a sufficient number of exceedances. This approach supports robust logistic regression fits by minimizing subjectivity and uncertainty (Roulston & Smith, 2003). Additionally, a dynamic catchment-specific soft-fusion weighting combining logistic regression and physical thresholds enabled to derive fused thresholds based on the catchment area, slope, and runoff variability. In other words, this soft-fusion approach combines the probabilistic estimates with physically based thresholds and weights each according to catchment characteristics to maintain and account for both statistical robustness and physical

realism (Gichamo et al., 2024; Malik et al., 2025). The set of actions was set based on 4 percentiles: 0.25, 0.5, 0.75, and 0.9 corresponding to different categories of early-warning thresholds, namely No action, Watch, Alert, and Warning, respectively. These categories were also automatically assigned. The results were evaluated and visualized through ROC curves through a multi-window discrimination (AUC) (Figure 4-5, and Tables 4-4 and 4-5).

The evaluation of the logistic regression-based early-warning system was done through confusion matrices for each antecedent rainfall window as follows: The first evaluation was based on the probability of detection (POD) to capture model responsiveness to true events, and false alarm ratio (FAR) to penalize overprediction (its value is inverted before normalization). The second evaluation was based on supplementary evaluation metrics, including the critical success index (CSI) to reflect overall detection quality; the precision to complement the POD by reducing false alarms; the specificity to evaluate the stability under non-flood conditions; the accuracy to summarize general forecast reliability; the F1-score to indicate balance between false alarms and missed events; the bias score (BS) to assess forecast reliability and bias; and finally, the Heidke skill score (HSS) to quantify true forecast skill beyond random performance (Papacharalampous et al., 2020; Schratz et al., 2019; Sukovich et al., 2014). The formulas, performance indicators, and roles of these metrics are listed in Table 4-2.

To ensure that all metrics contributed meaningfully to the interpretation, composite skill scores were systematically calculated from normalized POD, FAR (inverted), AUC, and CSI using variable weightings. Among these, CSI and AUC were prioritized by assigning them higher weights (weight sets: CSI = 0.4, AUC = 0.4, POD = 0.1, FAR = 0.1), which were determined as optimal through an iterative weighting process. This approach quantifies overall performance and enable robust comparison across antecedent rainfall windows. The resulting composite skill indices (CSI*) provided an integrated measure of model reliability and discrimination power.

Finally, thresholds were judged to get a reasonable composite skill that balances detection skill and reliability by evaluating the trade-off between POD and FAR. This ensured robust and actionable early-warning performance across antecedent rainfall windows (Casado-Rodríguez et al., 2025; Sättele et al., 2016). Table 4-2 summarizes statistical metrics used to evaluate the performance of logistic early-warning models and their hydrological intepretations.

Table 4-2 Summary of statistical metrics used to evaluate the performance of logistic early-warning models in the Nyamutera and Gaseke catchments.

Metric	Definition / Formula	Hydrological Interpretation	Range/ Ideal Value	Role in Composite Skill
Probability of	$POD = \frac{TP}{TP + FN}$	Fraction of observed events correctly	0–1; higher = better	Captures model

Detection (POD)		detected by the model (sensitivity).		responsiveness to true events.
False Alarm Ratio (FAR)	$FAR = \frac{FP}{TP + FP}$	Fraction of predicted events that did not occur (false positives).	0–1; lower = better	Penalizes overprediction; inverted before normalization.
Critical Success Index (CSI)	$CSI = \frac{TP}{TP + FP + FN}$	Balances hits, misses, and false alarms; overall event-based accuracy.	0–1; higher = better	Weighted heavily to reflect overall detection quality.
Area Under ROC Curve (AUC)	$AUC = \int_0^1 TPR(FPR)d(FPR)$	Discrimination ability across thresholds; higher indicates better separability between events and non-events.	0–1; higher = better	Emphasizes predictive discrimination independent of threshold.
Precision (Positive Predictive Value)	$Precision = \frac{TP + TN}{TP + FP}$	Likelihood that a predicted event actually occurred.	0–1; higher = better	Complements POD by reducing false alarms.
Specificity (True Negative Rate)	$Specificity = \frac{TN}{TN + FP}$	Fraction of non-events correctly identified.	0–1; higher = better	Evaluates stability under non-flood conditions.
Accuracy (ACC)	$Accuracy = \frac{TP}{TP + TN + FP + FN}$	Overall proportion of correct classifications.	0–1; higher = better	Summarizes general forecast reliability.
F1-score	$F_1 = \frac{2 * Precision * POD}{Precision + POD}$	Harmonic mean of precision and detection; balances omission and commission errors.	0–1; higher = better	Indicates balance between false alarms and missed events.
Bias Score (BS)	$BS = \frac{TP + FP}{TP + FN}$	Ratio of predicted to observed events; measures over- or underprediction tendency.	0–∞; 1 = ideal, < 1 = underprediction, > 1 = overprediction	Assesses forecast reliability and bias.
Heidke Skill Score (HSS)	$HSS = \frac{2 * (TP * TN - FP * FN)}{(TP + FN)(FN + TN) + (TP + FP)(FP + TN)}$	Measures forecast skill relative to random chance.	−∞ to 1; higher = better	Quantifies true forecast skill beyond random performance.
Composite Skill Index (CSI*)	Weighted sum of normalized POD, FAR (inverted), AUC, and CSI	Aggregated measure integrating detection, reliability, and discrimination.	0–1; higher = better	Primary criterion for selecting optimal antecedent rainfall window.

Note: TP, FP, TN, and FN represent true positive, false positive, true negative, and false negative, while TPR and FPR denote the true positive rate and false positive rate, respectively. The listed indices assess model detection ability, reliability, discrimination, and bias, Higher values of POD, CSI, AUC, Precision, Specificity, Accuracy, F1, and HSS indicate better predictive performance, whereas lower FAR values denote fewer false alarms. The Bias Score (BS) reflects the ratio of predicted to observed events, with BS = 1 representing an unbiased forecast. The Composite Skill Index (CSI) integrates normalized POD, FAR (inverted), AUC, and CSI using predefined weights to identify the most effective antecedent rainfall window for each catchment.*

4.2.10 Skill metric thresholds and evaluation criteria for early-warning performance

The evaluation of early-warning skill relied on a suite of standard forecast verification metrics, including POD, FAR, CSI, AUC, HSS, Precision, Specificity, Accuracy, F1 score, Bias Score

(BS), and a composite CSI-star metrics. Suggested thresholds for acceptable skill were based on established practice in hydrology and meteorology (Ebert et al., 2013; Guimarães Nobre et al., 2023; Jolliffe & Stephenson, 2011). For example, POD and CSI values ≥ 0.45 were considered to reflect moderate event detection, while FAR ≤ 0.30 limits false alarms without overly restricting operational usefulness. AUC ≥ 0.80 ensures good discrimination between events and non-events, whereas specificity and accuracy ≥ 0.70 guarantee reasonable performance for correctly identifying non-events and overall classification. F1 scores ≥ 0.50 balance detection and precision, and bias scores between 0.8 and 1.2 indicate the absence of systematic over- or under-prediction. Composite metrics such as CSI-star ≥ 0.50 provide an integrated measure of overall predictive skill, capturing multiple dimensions of reliability and sensitivity (P. Das et al., 2024; Duc et al., 2025; Guimarães Nobre et al., 2023). These boundaries—listed in Table 4-3—offer a practical and interpretable framework for assessing early-warning performance across catchments with contrasting geomorphology and rainfall-runoff responses.

Table 4-3 Practical thresholds for early-warning skill metrics, with rationale for operational assessment in mountainous tropical catchments.

Metric	Suggested Boundary	Rationale
POD	≥ 0.45	Ensures at least moderate detection of true events; slightly relaxed to allow rare events.
FAR	≤ 0.30	Limits false alarms without being overly restrictive; ensures practical operational use.
AUC	≥ 0.80	Good discrimination between events/non-events; feasible for real datasets.
CSI	≥ 0.45	Balances hits, misses, and false alarms; matches POD/FAR tradeoff.
Precision	≥ 0.50	At least half of predicted events should be correct.
Specificity	≥ 0.70	Ensures reasonable performance for correctly predicting non-events.
Accuracy	≥ 0.70	Overall classification must be better than random.
F1 Score	≥ 0.50	Combines precision and POD; ensures balanced detection skill.
Bias Score	0.8 – 1.2	Prevents systematic over- or under-prediction of events.
HSS	≥ 0.30	Ensures skill is above chance; aligns with standard hydrological model practice.
CSI-star	≥ 0.50	Weighted composite skill score; allows overall assessment combining CSI, AUC, POD, FAR.

In this study, the adopted fused threshold is the one that satisfies all eleven boundary conditions listed in Table 4-3.

4.3 Results

4.3.1 Catchment-specific parameter estimation and model calibration

Model performance metrics confirmed the suitability of the calibrated parameters: for Nyamutera, NSE = 0.213, KGE = 0.506, RMSE = 1.355 m³/s, $_{PW}$RMSE = 2.164 m³/s, and PEPD ≈ 0 %; for Gaseke, NSE = 0.451, KGE = 0.694, RMSE = 1.562 m³/s, pwRMSE = 2.942 m³/s, and PEPD ≈ 0 %. These performance metrics highlights the contrasting hydrological behavior of the two catchments: in Nyamutera (44 km², slope 0.41), the parameters were X_1 = 967.81 mm, X_2 ≈ 3.04 mm/day, X_3 ≈ 82.13 mm, X_4 = 1.06 days, α = 0.9, and Ka = 1.1, capturing its flashier response, while Gaseke (109 km², slope 0.37) required X_1 ≈ 2368.67 mm, X_2 ≈ 7.4×10^{-5}mm/day, X_3 ≈ 58.58 mm, X_4 = 1.44 days, α ≈ 0.9, Ka ≈ 0.8, and Fα ≈ 0.76, which are consistent with its more subdued, baseflow-dominated hydrograph. Figures 4-2 and 4-3 present the GR4J calibration hydrographs and rainfall, as well as the hydrographs of the reconstructed streamflows for Nyamutera and Gaseke catchments, respectively.

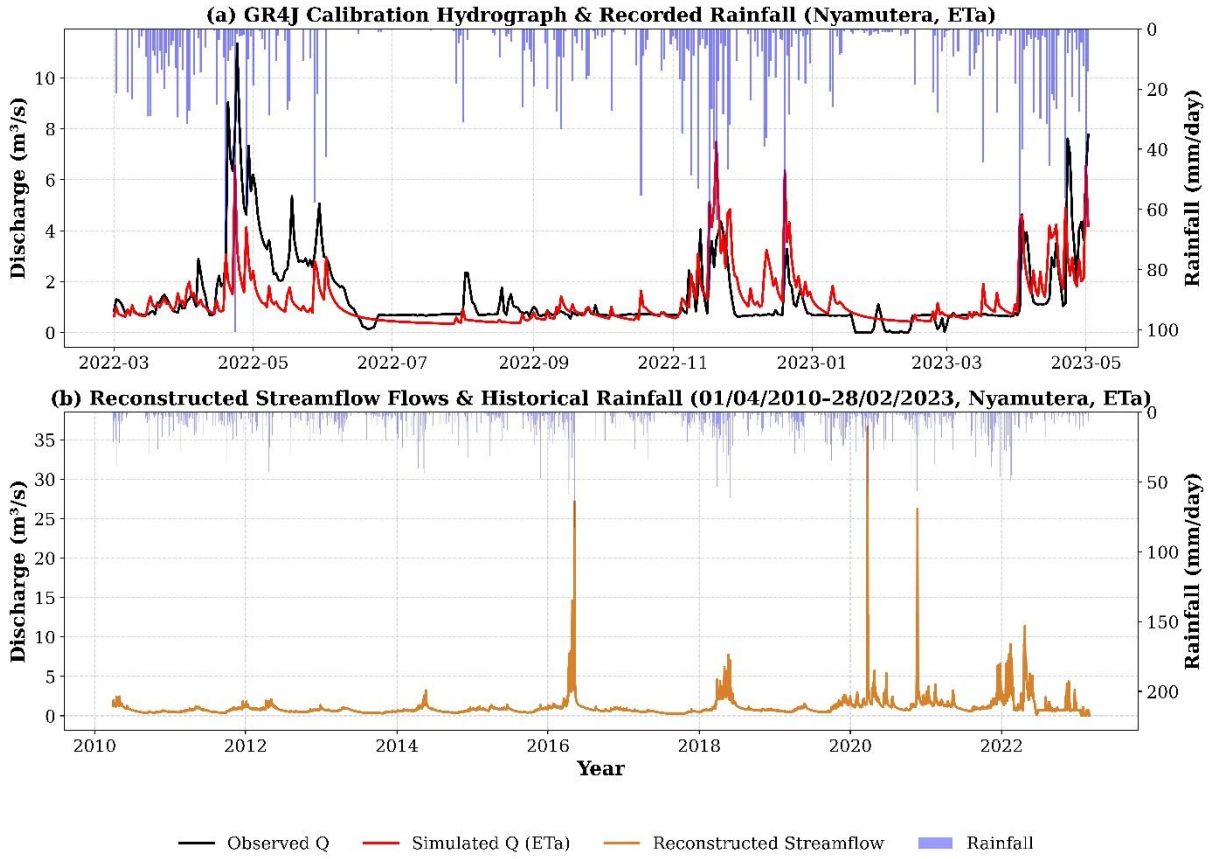

Figure 4-2 Calibrated (01March 2022-03 April 2023) and reconstructed streamflow for Nyamutera catchment (01 April 2010- 28 February 2023).

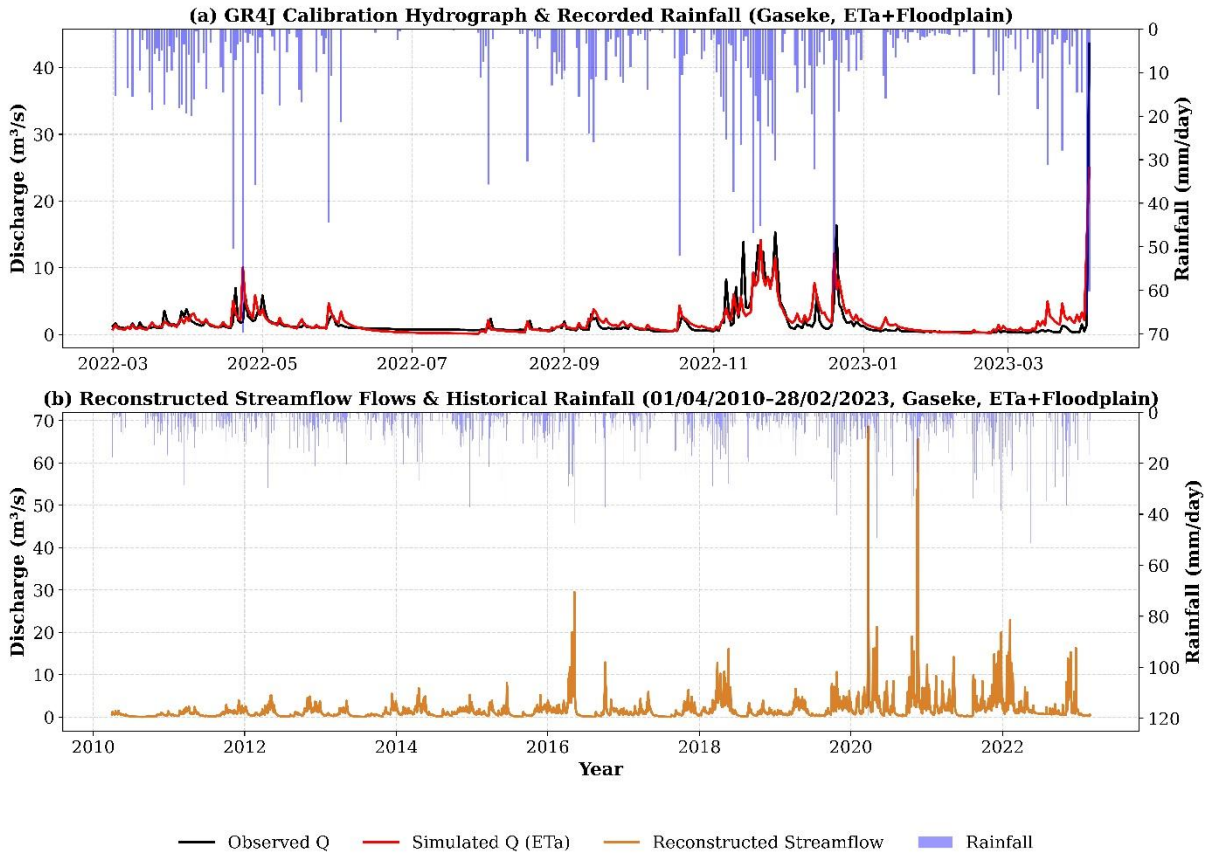

Figure 4-3 Calibrated (01March 2022-02 May 2023) and reconstructed streamflow for Gaseke catchment (01 April 2010- 28 February 2023).

4.3.2 Identified flood events during streamflow reconstruction

Using the calibrated GR4J rainfall-runoff model, streamflows were reconstructed over the full analysis period for both Nyamutera and Gaseke catchments. Flood events were identified by adopting the observed floods of 4 April 2023 and 2 May 2023 as reference thresholds for Gaseke and Nyamutera, respectively, with all simulated events having mean daily discharge greater than or equal to the reference discharges classified as flood events. For each identified event, concurrent daily rainfall and cumulative antecedent rainfall totals over multiple time windows were extracted. Tables 4-4 and 4-5 summarize the resulting reconstructed flood events for Nyamutera and Gaseke, respectively, including event timing, mean daily discharge, and associated current-day (C-day) and antecedent rainfall characteristics.

Table 4-4 Observed and reconstructed flood events from 2010 to 2023 in Nyamutera catchment.

Date	Mean daily Q (m³/s)	C-day P (mm)	5-days P (mm)	6-days P(mm)
14-04-2016	7.92	48.20	197.10	216.10
20-04-2016	8.20	43.20	133.70	168.60
28-04-2016	14.62	73.80	158.90	158.90
29-04-2016	12.68	43.10	182.70	202.00
01-05-2016	8.31	32.40	175.90	208.50

07-05-2016	11.23	62.40	92.10	114.30
08-05-2016	26.99	99.20	183.00	191.30
09-05-2016	27.13	82.60	265.60	265.60
05-03-2020	36.65	217.01	334.29	342.37
26-03-2020	9.95	21.38	346.25	355.67
27-03-2020	12.67	51.06	360.84	397.31
18-11-2020	12.94	103.43	247.06	260.46
19-11-2020	11.67	56.60	288.62	303.66
21-11-2020	26.26	143.42	408.13	428.35
22-11-2020	7.90	11.37	327.36	419.50
07-11-2022	7.83	52.40	93.70	95.50
14-11-2022	9.06	49.70	129.80	130.80
20-04-2022	9.04	16.24	43.34	50.27
23-04-2022	7.78	11.18	51.44	52.10
24-04-2022	11.35	22.75	54.99	74.19
25-04-2022	8.18	1.69	40.44	56.68
02-05-2023	7.77	40.39	120.73	121.07

Table 4-5 Observed and reconstructed flood events from 2010 to 2023 in Gaseke catchment.

Date	Mean daily Q (m^3/s)	C-day P (mm)	7-days P (mm)	8-days P(mm)	9-days P (mm)	10-days P(mm)	11-days P(mm)
25-03-2020	68.56	119.16	190.30	194.88	216.31	221.84	228.81
17-11-2020	53.65	82.35	158.05	165.09	175.49	178.08	183.75
18-11-2020	54.31	68.44	223.83	226.49	233.53	243.93	246.52
21-11-2020	65.55	93.51	336.84	350.26	359.40	362.43	365.09
03-04-2023	43.60	60.15	189.35	193.95	194.15	215.95	235.95

4.3.3 Rainfall thresholds and associated warning levels across antecedent rainfall windows

The fusion weights calculated for the logistic-physical rainfall thresholds were 0.71 for Nyamutera and 0.56 for Gaseke (Tables 4-6 and 4-7). These weights indicate the relative contribution of logistic regression versus physical thresholds in defining warning-level rainfall events.

Fused rainfall thresholds for a 90% exceedance probability increased with the length of the antecedent rainfall window in both catchments. In Nyamutera, thresholds ranged from 41 mm for a 1-day antecedent window to 449 mm for a 15-day window. In Gaseke, thresholds increased from 110 mm (1-day window) to 362 mm (15-day window). The thresholds associated with optimal early-warning skill—defined as the combination of balanced reliability and sensitivity—were observed for 5–6-day antecedent windows in Nyamutera (fused thresholds of 172–201 mm) and for 7–11-day windows in Gaseke (fused thresholds of 241–320 mm).

In Nyamutera, short antecedent rainfall windows (1–4 days) produced relatively low warning-level thresholds, while longer windows (>7 days) led to higher thresholds. In Gaseke, fused thresholds were low for very short windows (1–2 days), and logistic-only thresholds were sometimes negative. In both cases, thresholds tended to increase steadily as the antecedent rainfall duration grew.

Across both catchments, the data show a clear increase in fused warning thresholds with antecedent rainfall duration, consistent across exceedance probabilities (25%, 50%, 75%, 90%) and reflected in the full set of thresholds presented in Tables 4-6 and 4-7.

Table 4-6 Antecedent rainfall thresholds and corresponding exceedance probabilities for flood event classification in the Nyamutera catchment.

Antecedent days	Exceedance probability	Logistic threshold (mm)	Physical threshold (mm)	Fused threshold (mm)	Fusion weight logistic factor	Recommended /action
1	0.25	12.30	21.48	14.95	0.71	No Action
	0.50	24.64	21.48	23.73	0.71	Watch
	0.75	36.98	21.48	32.51	0.71	Alert
	0.90	49.32	21.48	41.28	0.71	Warning
2	0.25	47.78	32.00	43.22	0.71	No Action
	0.50	65.75	32.00	56.01	0.71	Watch
	0.75	83.72	32.00	68.80	0.71	Alert
	0.90	101.69	32.00	81.58	0.71	Warning
3	0.25	71.89	50.00	65.58	0.71	No Action
	0.50	90.98	50.00	79.16	0.71	Watch
	0.75	110.06	50.00	92.74	0.71	Alert
	0.90	129.15	50.00	106.32	0.71	Warning
4	0.25	112.26	80.34	103.05	0.71	No Action
	0.50	135.54	80.34	119.61	0.71	Watch
	0.75	158.81	80.34	136.17	0.71	Alert
	0.90	182.08	80.34	152.73	0.71	Warning
5	0.25	144.40	80.68	126.02	0.71	No Action
	0.50	166.06	80.68	141.42	0.71	Watch
	0.75	187.71	80.68	156.83	0.71	Alert
	0.90	209.36	80.68	172.24	0.71	Warning
6	0.25	180.68	88.96	154.22	0.71	No Action
	0.50	202.62	88.96	169.83	0.71	Watch
	0.75	224.56	88.96	185.44	0.71	Alert
	0.90	246.50	88.96	201.05	0.71	Warning
7	0.25	265.08	91.46	214.99	0.71	No Action
	0.50	295.77	91.46	236.83	0.71	Watch
	0.75	326.47	91.46	258.67	0.71	Alert
	0.90	357.16	91.46	280.51	0.71	Warning
8	0.25	391.50	92.63	305.28	0.71	No Action
	0.50	436.59	92.63	337.36	0.71	Watch

	0.75	481.68	92.63	369.44	0.71	Alert
	0.90	526.77	92.63	401.52	0.71	Warning
9	0.25	412.30	121.88	328.51	0.71	No Action
	0.50	458.29	121.88	361.23	0.71	Watch
	0.75	504.28	121.88	393.96	0.71	Alert
	0.90	550.27	121.88	426.68	0.71	Warning
10	0.25	430.04	136.61	345.38	0.71	No Action
	0.50	476.53	136.61	378.47	0.71	Watch
	0.75	523.03	136.61	411.55	0.71	Alert
	0.90	569.53	136.61	444.63	0.71	Warning
11	0.25	445.90	141.30	358.02	0.71	No Action
	0.50	492.10	141.30	390.89	0.71	Watch
	0.75	538.29	141.30	423.76	0.71	Alert
	0.90	584.49	141.30	456.63	0.71	Warning
12	0.25	458.45	141.84	367.11	0.71	No Action
	0.50	498.42	141.84	395.54	0.71	Watch
	0.75	538.38	141.84	423.98	0.71	Alert
	0.90	578.35	141.84	452.41	0.71	Warning
13	0.25	470.61	142.37	375.91	0.71	No Action
	0.50	496.62	142.37	394.42	0.71	Watch
	0.75	522.64	142.37	412.93	0.71	Alert
	0.90	548.65	142.37	431.44	0.71	Warning
14	0.25	483.72	161.87	390.86	0.71	No Action
	0.50	504.55	161.87	405.68	0.71	Watch
	0.75	525.38	161.87	420.51	0.71	Alert
	0.90	546.21	161.87	435.33	0.71	Warning
15	0.25	495.42	202.26	410.84	0.71	No Action
	0.50	513.24	202.26	423.52	0.71	Watch
	0.75	531.06	202.26	436.20	0.71	Alert
	0.90	548.88	202.26	448.88	0.71	Warning

Table 4-7 Antecedent rainfall thresholds and corresponding exceedance probabilities for flood event classification in the Gaseke catchment.

Antecedent days	Exceedance probability	Logistic threshold (mm)	Physical threshold (mm)	Fused threshold (mm)	Fusion weight logistic	Recommended/ action
1	0.25	97.71	60.15	81.31	0.56	No Action
	0.50	114.44	60.15	90.74	0.56	Watch
	0.75	131.18	60.15	100.18	0.56	Alert
	0.90	147.92	60.15	109.61	0.56	Warning
2	0.25	122.66	127.55	124.80	0.56	No Action
	0.50	141.69	127.55	135.52	0.56	Watch
	0.75	160.73	127.55	146.24	0.56	Alert
	0.90	179.76	127.55	156.97	0.56	Warning
3	0.25	146.75	131.15	139.94	0.56	No Action
	0.50	167.24	131.15	151.49	0.56	Watch
	0.75	187.73	131.15	163.03	0.56	Alert

	0.90	208.22	131.15	174.58	0.56	Warning
4	0.25	172.23	165.75	169.40	0.56	No Action
	0.50	193.71	165.75	181.50	0.56	Watch
	0.75	215.18	165.75	193.60	0.56	Alert
	0.90	236.66	165.75	205.71	0.56	Warning
5	0.25	195.09	165.95	182.37	0.56	No Action
	0.50	217.53	165.95	195.02	0.56	Watch
	0.75	239.97	165.95	207.66	0.56	Alert
	0.90	262.41	165.95	220.31	0.56	Warning
6	0.25	215.25	184.35	201.76	0.56	No Action
	0.50	237.26	184.35	214.17	0.56	Watch
	0.75	259.28	184.35	226.57	0.56	Alert
	0.90	281.29	184.35	238.97	0.56	Warning
7	0.25	233.78	189.35	214.39	0.56	No Action
	0.50	249.51	189.35	223.25	0.56	Watch
	0.75	265.23	189.35	232.11	0.56	Alert
	0.90	280.95	189.35	240.97	0.56	Warning
8	0.25	254.31	193.95	227.96	0.56	No Action
	0.50	264.28	193.95	233.58	0.56	Watch
	0.75	274.24	193.95	239.19	0.56	Alert
	0.90	284.20	193.95	244.81	0.56	Warning
9	0.25	276.82	194.15	240.73	0.56	No Action
	0.50	296.83	194.15	252.01	0.56	Watch
	0.75	316.84	194.15	263.28	0.56	Alert
	0.90	336.84	194.15	274.55	0.56	Warning
10	0.25	297.18	215.95	261.72	0.56	No Action
	0.50	319.75	215.95	274.44	0.56	Watch
	0.75	342.31	215.95	287.15	0.56	Alert
	0.90	364.88	215.95	299.87	0.56	Warning
11	0.25	313.87	235.95	279.85	0.56	No Action
	0.50	337.85	235.95	293.37	0.56	Watch
	0.75	361.84	235.95	306.89	0.56	Alert
	0.90	385.83	235.95	320.41	0.56	Warning
12	0.25	328.10	255.15	296.25	0.56	No Action
	0.50	353.55	255.15	310.60	0.56	Watch
	0.75	379.00	255.15	324.94	0.56	Alert
	0.90	404.45	255.15	339.28	0.56	Warning
13	0.25	341.11	257.35	304.55	0.56	No Action
	0.50	367.41	257.35	319.37	0.56	Watch
	0.75	393.71	257.35	334.19	0.56	Alert
	0.90	420.01	257.35	349.00	0.56	Warning
14	0.25	352.90	258.75	311.80	0.56	No Action
	0.50	378.84	258.75	326.42	0.56	Watch
	0.75	404.78	258.75	341.04	0.56	Alert
	0.90	430.72	258.75	355.65	0.56	Warning
15	0.25	363.53	259.15	317.97	0.56	No Action

	0.50	389.49	259.15	332.59	0.56	Watch
	0.75	415.45	259.15	347.22	0.56	Alert
	0.90	441.40	259.15	361.85	0.56	Warning

Note: Thresholds were estimated from logistic regression models calibrated for each antecedent rainfall duration, and categorized into four warning levels (No Action, Watch, Alert, Warning) to support operational flood early-warning decisions.

4.3.4 Comparison of early-warning skill metrics across catchments and antecedent rainfall windows

Figure 4-4 illustrates the early-warning skill across different antecedent rainfall windows for the Nyamutera and Gaseke catchments. The radar plot provides an intuitive, at-a-glance comparison of multiple skill metrics for each catchment-window combination, highlighting patterns of variation over time. It also reveals how catchment characteristics and rainfall history influence early-warning performance, offering a clear visual link between rainfall inputs and the predictability of floods in these mountainous tropical catchments.

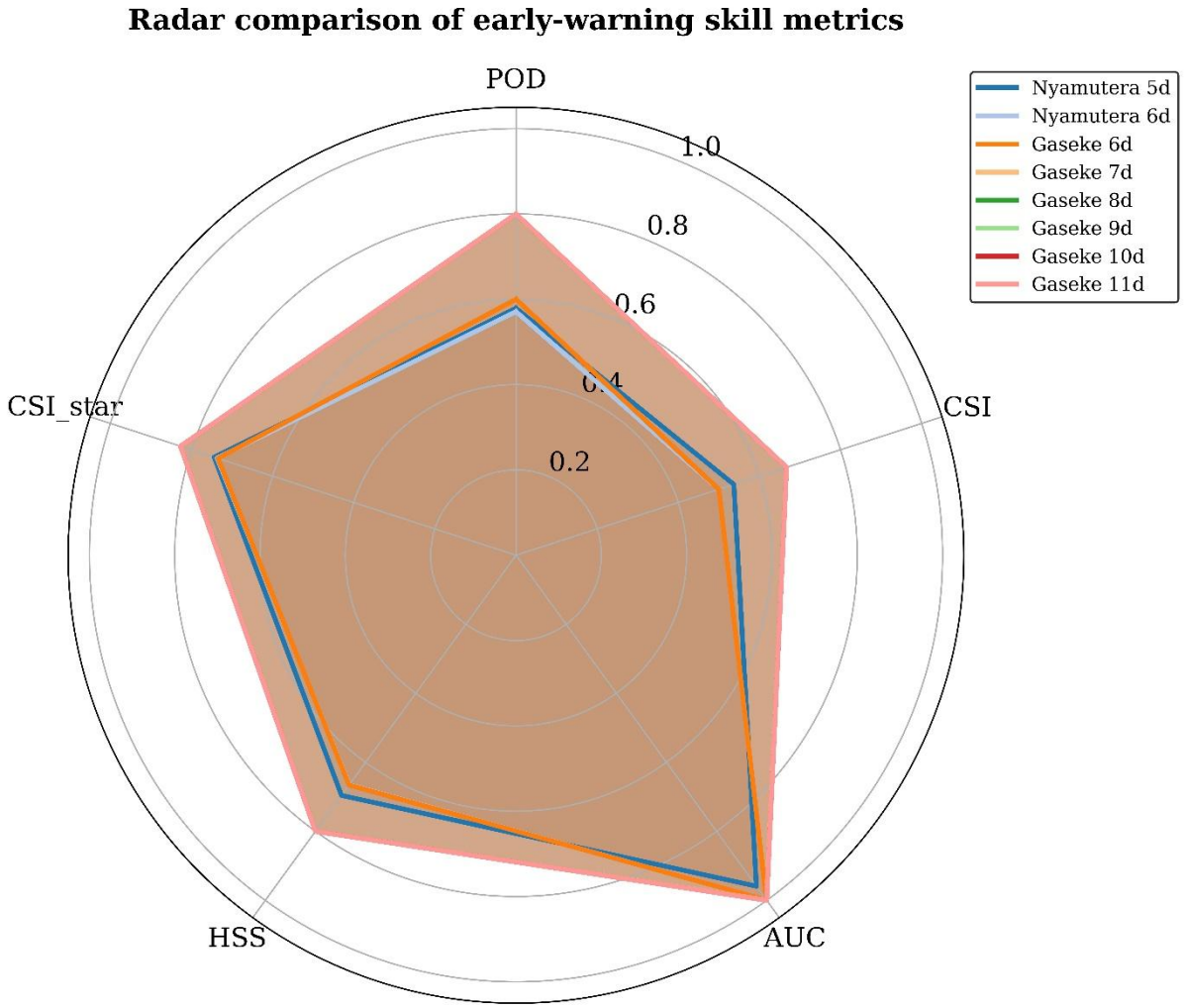

Figure 4-4 Comparison of early-warning skill metrics across antecedent rainfall windows for the Nyamutera and Gaseke catchments.

Note: Radar plot highlighting multi-metric performance consistency. Results indicate optimal operational windows of 5–6 days for Nyamutera and 7–11 days for Gaseke.

4.3.5 Catchment specific logistic early-warning model performance

The logistic regression-based early-warning model exhibited clear variations in performance depending on the length of the antecedent rainfall window and the catchment characteristics. In Nyamutera, the model performed best with 5–6 days of accumulated rainfall, reflecting the rapid hydrologic response of this steep, small catchment. Within this window, performance metrics indicated a good balance between event detection and reliability: POD ranged from 0.57 to 0.58, FAR remained low at 0.12–0.20, CSI reached 0.50–0.54, and F1-score peaked at 0.67–0.70. Heidke Skill Score (HSS) values at 0.67–0.70, and CSI-star up to 0.74 further confirmed that the model reliably distinguished flood-triggering rainfall from non-events, while overall accuracy and specificity were consistently high at approximately 1.00, and AUC reaching from 0.96 to near perfect ≈ 1, highlighting very few false alarms. These results suggest that 5–6 day rainfall accumulation captures the key flood-triggering signal in Nyamutera, providing a practical one-week early-warning horizon for operational use.

In contrast, the Gaseke catchment, characterized by larger area and more attenuated response due to its floodplain, showed optimal model performance for 7–11 day antecedent windows. Across this range, POD increased to 0.80, FAR stabilized at 0.20, CSI rose to 0.67, and F1-score reached the neat perfect ≈ 1.00, while HSS values were consistently around 0.80. Accuracy, specificity, and AUC remained near perfect (≈ 1.00), precision at 0.8, and CSI-star at 0.83, reflecting minimal false alarms and robust event detection. These results indicate that longer rainfall accumulation periods are necessary in Gaseke to capture the more gradual hydrological response, aligning the early-warning signal with the timing of flood events and supporting effective operational forecasting.

Overall, these findings highlight catchment-specific early-warning windows: 5–6 days for the steep, flashy Nyamutera and 7–11 days for the larger, attenuated Gaseke. Using these tailored windows maximizes predictive skill while minimizing false alarms, offering a practical framework for flood early-warning in contrasting tropical catchments.

Table –4-8 and Figures 4-5 and 4-6 show the thresholds and ROC curves, with AUC values, for the Nyamutera and Gaseke catchments.

Table 4-8. Performance metrics of logistic regression-based early-warning models for varying antecedent rainfall durations in the Nyamutera and Gaseke catchments.

Catchment	AD	TP	FP	FN	TN	POD	FAR	AUC	CSI	Prec	Spec	Acc	F1	BS	HSS	CSI*
Nyamutera	5	22	3	16	4735	0.58	0.12	0.96	0.54	0.88	1.00	1.00	0.70	0.66	0.70	0.74
	6	16	4	12	4743	0.57	0.2	1.00	0.50	0.80	1.00	1.00	0.67	0.71	0.67	0.74
Gaseke	6	3	1	2	4769	0.60	0.25	1.00	0.50	0.75	1.00	1.00	0.67	0.80	0.67	0.73
	7	4	1	1	4768	0.80	0.2	1.00	0.67	0.80	1.00	1.00	0.80	1.00	0.80	0.83
	8	4	1	1	4767	0.80	0.2	1.00	0.67	0.80	1.00	1.00	0.80	1.00	0.80	0.83
	9	4	1	1	4766	0.80	0.2	1.00	0.67	0.80	1.00	1.00	0.80	1.00	0.80	0.83
	10	4	1	1	4765	0.80	0.2	1.00	0.67	0.80	1.00	1.00	0.80	1.00	0.80	0.83
	11	4	1	1	4764	0.80	0.2	1.00	0.67	0.80	1.00	1.00	0.80	1.00	0.80	0.83
	15	3	0	2	4761	0.60	0	1.00	0.60	1.00	1.00	1.00	0.75	0.60	0.75	0.80

Note: AD, TP, FP, FN, and TN denote antecedent days, true positives, false positives, false negatives, and true negatives, respectively. POD (probability of detection), FAR (false alarm ratio), CSI (critical success index), Precision, Specificity, Accuracy, F1, Bias Score (BS), and Heidke Skill Score (HSS) quantify model detection skill, reliability, and bias, while AUC (area under the ROC curve) represents model discrimination power. Higher POD, CSI, AUC, Precision, Specificity, Accuracy, F1, and HSS (and lower FAR) indicate better predictive performance. CSI (CSI-star) is the choosen composite skill score (0.4–0.4–0.1–0.1 weighting scheme for CSI, AUC, POD and FAR, respectively). Optimal predictive horizons were identified at 5–6 days for Nyamutera and at 7–11 days for the Gaseke catchments.*

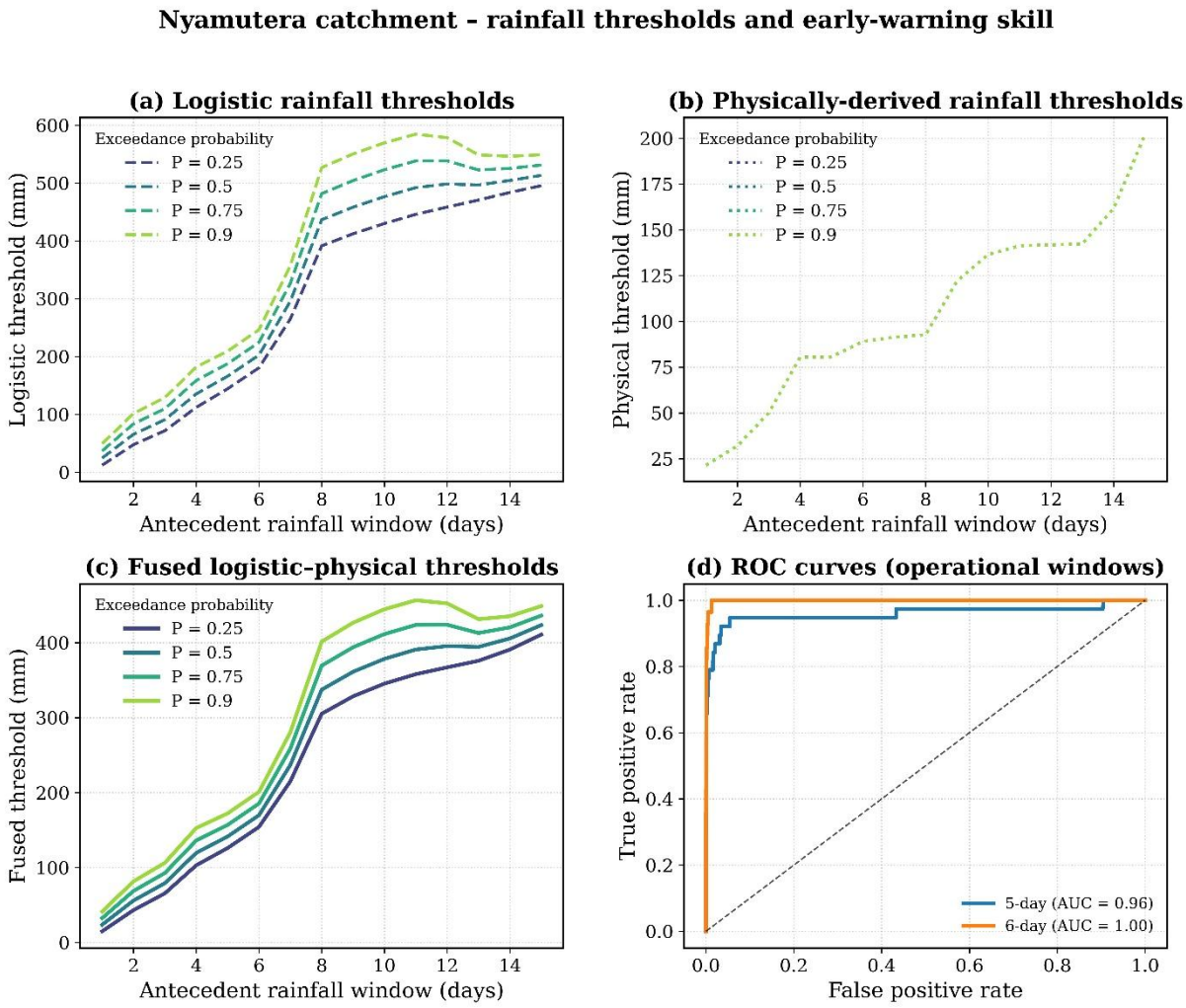

Figure 4-5 Thresholds and Receiver Operating Characteristic (ROC) curves with Area Under the Curve (AUC) for Nyamutera catchment.

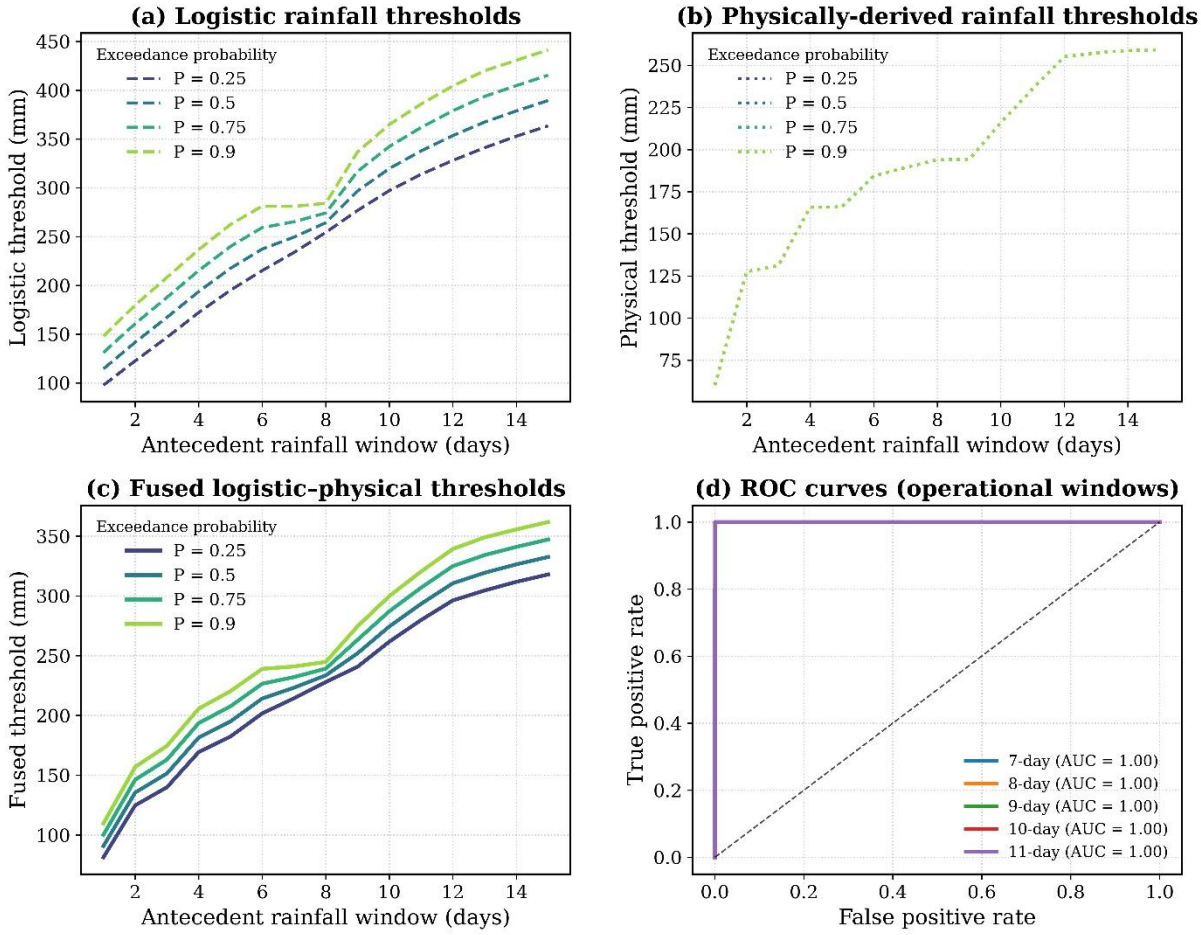

Figure 4-6 Thresholds and Receiver Operating Characteristic (ROC) curves with Area Under the Curve (AUC) for Gaseke catchment.

4.4 Discussion

4.4.1 GR4J-based rainfall-runoff model calibration and streamflow reconstruction

The obtained performance metrics highlighted contrasting hydrological behaviors across both catchments: the Nyamutera exhibited NSE = 0.213, KGE = 0.506, RMSE = 1.355 m³/s, PWRMSE = 2.164 m³/s, and PEPD ≈ 0 %, whereas Gaseke achieved NSE = 0.451, KGE = 0.694, RMSE = 1.562 m³/s, PWRMSE = 2.94 m³/s, and PEPD ≈ 0 %. These differences align with catchment characteristics. Nyamutera's steep slopes with limited storage promoted rapid runoff response, whereas Gaseke's larger area, moderate steep with a floodplain that sustains baseflow and attenuates floods. These contrasting geomorphic behaviours were also identified in the calibrated parameters: Nyamutera promotes rapid runoff due steep slope (0.41) and limited storage capacity (X1 = 968 mm), low soil retention (X2 ≈ 3.04), high initial abstraction (X3 ≈ 82 mm), and minimal baseflow (X4 = 1.06), whereas Gaseke exhibited higher storage (X1 ≈ 2369 mm), insufficient soil retention (X2 ≈ 7.4×10⁻5), lower initial abstraction

(X3 ≈ 59 mm), slightly elevated baseflow (X4 = 1.44), and notable flow adjustment (Fα ≈ 0.76). These results reflects the findings by (Park et al., 2025), who highlighted that storage capacity and soil retention (X1 and X2) are the most influential parameters on runoff response at the catchment outlet. Differences in α and Ka values also highlighted divergence in ETa dynamics between the catchments. Nyamutera, steeper and storage-limited (Ka ≈ 1.1), had ETa, which is slightly approaching ET_0, as highlighted by Allen et al., 1998 and Penna et al., 2011, who demonstrated that the ETa is higher within the upland catchments due to rapid drainage and dense vegetation.

Conversely, Gaseke, larger, moderately steep (Ka ≈ 0.8), is constrained with floodplain flow buffering, which reduced immediate evaporative fluxes (Luong et al., 2021b; Uber et al., 2018). These patterns underscore the importance of the integration of geomorphological characteristics as they play a critical role in shaping ETa, and thus could be taken into account in hydrological model calibration for tropical mountain regions.

4.4.2 Reconstructed flood events and contrasting hydrological memory in Nyamutera and Gaseke catchments

The reconstruction of streamflow using calibrated GR4J parameters identified 5 and 22 flood events in Gaseke and Nyamutera, respectively, with mean daily discharges equal to or exceeding the reference floods of 3 April and 2 May 2023 (43.60 m³/s and 7.77 m³/s, respectively). The high daily discharge of 43.60 m³/s on the day of the flood event indicates that the flow increased as the floodplain filled, temporarily sustaining the discharge. This was confirmed by an instantaneous measurement on 4 April 2023, which recorded 28.89 m³/s (stage = 2.06 m, compared to a bankfull stage of 3.28 m) one day after the flood event, showing that the flow had slightly attenuated as the flood receded. These events span multiple years and rainfall regimes, confirming that the selected reference floods represent meaningful hydrological thresholds rather than isolated extremes, and are therefore suitable benchmarks for flood-event reconstruction (Perrin et al., 2003).

In Nyamutera, the associated rainfall characteristics show substantial variability in both event rainfall and antecedent wetness, with 5–6-day cumulative totals ranging from 40 mm (5-days) and 50 mm (6 days) to 408 mm (5 days) and 428 mm (6 days). This wide spread indicates that flood generation is controlled by a combination of short-term rainfall intensity and pre-event soil moisture conditions, a behavior commonly observed in steep, storage-limited headwater catchments (Merz et al., 2006).

Several reconstructed floods were triggered by moderate daily rainfall following substantial multi-day accumulation, while others resulted from high-intensity rainfall superimposed on

already wet catchment states. This pattern highlights the dominant role of antecedent rainfall in modulating runoff response and supports the use of multi-day rainfall windows for flood early warning in fast-responding mountainous basins (Penna et al., 2011; Tramblay et al., 2010).

Consistent with this interpretation, the fused logistic-physical regression analysis identified 5–6-day antecedent rainfall windows as the most reliable predictors of flooding in Nyamutera. The 5-day window achieved the most balanced performance, combining effective detection with a low false-alarm rate and strong discrimination skill. Although the 6-day window exhibited similarly high overall accuracy, the reduced number of detected events suggests that its apparent performance advantage is partly influenced by sample-size effects rather than a genuinely superior representation of catchment processes. Importantly, the reconstructed flood events align closely with the fused rainfall thresholds derived for the 5–6-day windows, confirming the physical relevance of these accumulation periods. Events characterized by relatively modest daily rainfall but elevated antecedent totals were successfully captured, demonstrating that the early-warning framework accounts for short hydrological memory rather than relying solely on storm magnitude. Extending the accumulation window beyond 6 days increasingly incorporates rainfall that is less hydrologically effective, leading to inflated thresholds and reduced consistency. Together, these results indicate that Nyamutera's steep slopes, shallow soils, and limited storage capacity promote rapid runoff generation and short hydrological memory, making 5–6-day rainfall accumulation sufficient to represent pre-event wetness conditions (Marchi et al., 2010; Penna et al., 2011).

In contrast, Gaseke exhibits a much stronger dependence on prolonged antecedent rainfall accumulation, reflecting its larger area, gentler slopes, and extensive floodplain storage. Reconstructed flood events in Gaseke are consistently associated with high multi-day rainfall totals, and model performance improves markedly once rainfall integration exceeds one week. At shorter accumulation windows (e.g., 6 days), detection skill remains moderate, with some missed events and a higher false-alarm rate, indicating that short-term rainfall alone is insufficient to represent basin-wide saturation conditions despite the occurrence of large discharges. This delayed response is characteristic of floodplain-dominated catchments where storage and subsurface connectivity control runoff generation (McDonnell, 2003; Tromp-van Meerveld & McDonnell, 2006).

Performance stabilizes and improves substantially for 7–11-day antecedent windows, which consistently yield the highest and most balanced skill across verification metrics.

The associated cumulative rainfall totals indicate a gradual increase in variability in both event rainfall and antecedent wetness. Cumulative rainfall totals ranged from 158 mm (7 days), 165

mm (8 days), 175 mm (9 days), 178 mm (10 days), and 184 mm (11 days) to 337 mm (7 days), 350 mm (8 days), 359 mm (9 days), 362 mm (10 days), and 365 mm (11 days).

High detection rates combined with low false-alarm ratios indicate that flood initiation in Gaseke is primarily governed by cumulative wetness rather than short-term rainfall intensity, consistent with saturation-excess runoff mechanisms (Blöschl et al., 2019). The strong and stable discrimination skill across this range suggests a saturation effect, beyond which additional rainfall information provides limited predictive gain. Across reconstructed flood events, multi-day antecedent rainfall totals predominantly fall within or above the ~160–230 mm range, consistent with the stabilized warning thresholds identified earlier for this catchment.

Extending the accumulation window to 15 days increases precision but reduces sensitivity, as some flood events are missed despite the absence of false alarms. This trade-off illustrates the risk of excessive temporal smoothing, where responsiveness to critical rainfall inputs is reduced in early-warning applications (Alfieri et al., 2012).

Overall, the results indicate that optimal flood predictability in Gaseke occurs within 7–11-day rainfall windows, offering a balance between early-warning lead time, detection skill, and physical realism. The contrasting behaviors of Nyamutera and Gaseke underscore the importance of tailoring rainfall-based early-warning thresholds to catchment-specific hydrological memory, particularly in mountainous tropical regions where geomorphic controls strongly influence flood response (Blöschl et al., 2019; Merz et al., 2006).

4.4.3 Geomorphic control of antecedent rainfall memory and flood predictability

The optimal antecedent rainfall windows identified by the early-warning system reflect fundamental geomorphic and hydrological contrasts between the Nyamutera and Gaseke catchments. In Nyamutera, only short antecedent windows (5–6 days) satisfy the multi-metric skill constraints, consistent with a steep, compact basin (basin slope ≈ 0.41, relief ratio ≈ 0.08) characterized by short flowpaths and limited storage capacity. Such settings favor rapid runoff translation and event-driven flood responses, in which recent rainfall dominates flood generation and catchment memory is weak (Beven, 2012; Dunne & Black, 1970). The high discrimination ability (AUC ≈ 0.96–0.99) combined with low false alarm ratios indicates that extending the antecedent window beyond a few days provides little additional predictive benefit in this steep mountainous environment.

In contrast, Gaseke exhibits consistently superior and more stable performance for medium antecedent windows (7–11 days), with high detection rates (POD ≈ 0.8), strong agreement

beyond chance (HSS ≈ 0.8), and near-perfect discrimination (AUC ≈ 1.0). This behavior is coherent with its larger basin area (109 km²), longer and gentler flowpaths (longest flowpath slope ≈ 0.04; centroid slope ≈ 0.02), lower relief ratio, and the presence of an extensive floodplain (~168 ha), all of which promote antecedent moisture accumulation, delayed runoff propagation, and enhanced hydrological memory (Blöschl et al., 2013; Lane et al., 2011). Floodplain storage and channel-floodplain connectivity attenuate peak flows while integrating rainfall over longer periods, thereby increasing the relevance of multi-day antecedent conditions for flood triggering (Blöschl et al., 2019; Chow et al., 1988). The decline in skill at very long windows (e.g., 15 days) suggests dilution of the triggering signal by older rainfall, highlighting an upper limit to effective memory even in storage-rich systems. Overall, these results demonstrate that early-warning skill is intrinsically linked to geomorphic structure and floodplain storage, underscoring the necessity of catchment-specific antecedent window selection rather than uniform operational thresholds.

4.4.4 Geomorphic controls on flow duration structure and flood generation timescales

The combined interpretation of flow duration curves, geomorphological structure, and runoff distribution metrics reveals how catchment form governs not only flow regimes but also the timescales over which floods become predictable in mountainous tropical landscapes. In the steep and compact Nyamutera catchment, short flowpaths, high relief, and negligible floodplain storage produce a FDC characterized by weak low-flow support (Q5 ≈ 0.9 L s^{-1} km^{-2}) but relatively elevated intermediate discharges (Q50 ≈ 4.1 L s^{-1} km^{-2}; Q90 ≈ 18.4 L s^{-1} km^{-2}), reflecting rapid hillslope-channel connectivity and limited buffering capacity (Nahayo et al., 2026). This behavior is reinforced by the low Gini index (0.065), indicating that runoff volumes are distributed relatively evenly across events, with streamflow responding quickly to recent rainfall rather than accumulating storage over time (Nahayo et al., 2026). Such conditions are consistent with conceptual models of rainfall-runoff response in steep terrain where quickflow dominates and storage effects are limited (Beven, 2012; Dunne & Black, 1970). Consequently, flood occurrence in Nyamutera is best captured by short antecedent rainfall windows (5–6 days), beyond which predictive skill declines as earlier rainfall exerts little residual influence.

In contrast, the larger and more elongated Gaseke catchment exhibits a markedly different hydrological signature shaped by longer flowpaths, gentler slopes, and an extensive floodplain of approximately 168 ha. Its FDC indicates stronger low-flow support (Q5 ≈ 1.4 L s^{-1} km^{-2}) but damped intermediate flows (Q50 ≈ 3.6 L s^{-1} km^{-2}), consistent with enhanced subsurface and floodplain storage that delays runoff release (Nahayo et al., 2026). This storage-dominated

behavior is quantitatively captured by the higher Gini index (0.151), showing that a disproportionate share of total runoff is generated during a small number of events once cumulative wetness thresholds are exceeded (Nahayo et al., 2026). Such runoff concentration patterns reflect storage-release dynamics observed in floodplain-influenced basins (Blöschl et al., 2013; Lane et al., 2011). Under these conditions, flood generation becomes sensitive to antecedent moisture accumulation rather than immediate rainfall alone, explaining why longer antecedent windows (7–11 days) yield superior early-warning performance with higher detection rates and reduced false alarms. Notably, both catchments converge toward comparable high-flow extremes (Q95 ≈ 27–30 L s^{-1} km^{-2}), indicating that once storage thresholds are surpassed, floodplain-buffered systems can release volumes comparable to those of steep headwater catchments. Together, the FDCs and Lorenz-based metrics provide complementary diagnostics that link geomorphic controls, hydrological memory, and early-warning timescales, highlighting the central role of flowpath geometry and storage activation in shaping flood predictability (Blöschl et al., 2019; Nahayo et al., 2026).

4.4.5 Insights for operational early warning applications

The contrasting rainfall accumulation timescales between Nyamutera and Gaseke reveal critical implications for early-warning design. In Nyamutera, the steep slopes and limited catchment storage drive rapid runoff, with optimal logistic regression performance achieved for 5–6 day antecedent rainfall windows. Within this range, the model balanced detection and reliability effectively: POD was 0.57–0.58, FAR remained low at 0.12–0.20, CSI ranged from 0.50–0.54, and HSS reached 0.67–0.70. Shorter windows (1–4 days) required lower rainfall thresholds to capture events reliably, while longer windows (>6 days) offered little additional skill and could exaggerate the influence of infrequent rainfall extremes, potentially inflating metrics such as AUC. These results highlight the rapid hydrologic response of Nyamutera and support a 5–6 day rainfall accumulation as the most practical early-warning window for this catchment. This behavior reflects Nyamutera's short hydrological memory and fast drainage, consistent with infiltration-excess and saturation-driven runoff mechanisms in steep tropical basins (Byaruhanga et al., 2024).

The performance of the logistic regression model also revealed distinct hydrological behaviors between the two catchments. Nyamutera's consistent skill with short antecedent periods of 5–6 days reflects its rapid runoff response, driven by steep slopes, small catchment area, and limited storage. In this window, model performance was fair, with POD = 0.57–0.58, FAR = 0.12–0.20, CSI = 0.50–0.54, and HSS = 0.67–0.70, indicating reliable detection of flood-

triggering rainfall with minimal false alarms. Conversely, Gaseke's larger, less steep terrain and expansive floodplain enhance hydrological memory, resulting in improved model skill over longer antecedent windows of 7–11 days. Within this range, the model achieved POD = 0.80, FAR = 0.20, CSI = 0.67, and HSS = 0.80, demonstrating robust detection and discrimination of flood events while maintaining minimal false alarms. These contrasts highlight how catchment morphology and storage characteristics shape the optimal temporal window for early-warning rainfall accumulation (Macharia et al., 2023; Munyaneza, 2014) (Tables 1, 4-7).

Nyamutera responds to short-term rainfall intensity (Penna et al., 2011), while Gaseke integrates multi-day rainfall through subsurface and floodplain storage (Acreman & Holden, 2013b; Di Baldassarre et al., 2013; Jencso & McGlynn, 2011). Gaseke's moderate logistic fusion weight (0.56 for Gaseke against 0.71 for Nyamutera) suggest that combining statistical models with physically based rainfall thresholds enhances predictive robustness under variable conditions (Sharma et al., 2018).

For operational implementation of the present early warning tool, the forecaster should substitute the model's last day precipitation input with forecasted daily rainfall in order to simulate potential flood-generating conditions.

Collectively, integrating rainfall thresholds with model skill rankings improves operational utility and emphasizes the need for localized calibration in data-sparse, topographically complex areas like those of mountain catchments of northwestern Rwanda. Thus, optimal lead times for early-warning systems are catchment-specific, shaped by geomorphic controls and antecedent wetness. Tailoring thresholds to local hydrological behavior enhances flood predictability and operational reliability.

4.4.6 Tailored early-warning strategies for flood risk in mountainous tropics

This study offers actionable guidance for flood-risk management in tropical mountainous catchments by developing catchment-specific early-warning systems.

In Nyamutera, steep slopes and shallow soils drive rapid runoff, and detection skill improved when multi-day antecedent rainfall of 5–6 days was considered. Using a fused threshold approach weighted toward probabilistic skill (~0.71), a practical four-tier early-warning system was developed for 5–6 day rainfall totals. For a 5-day accumulation, fused thresholds ranged from 126 mm (No Action) to 172 mm (Warning), while for a 6-day accumulation, thresholds increased slightly from 154 mm to 201 mm, reflecting the increased rainfall needed to trigger events over a longer period. These thresholds were stable within the 5–6 day window, providing reliable guidance for this steep, fast-responding catchment. Shorter windows (<5 days) required

lower thresholds for event detection, whereas longer windows (>6 days) inflated thresholds due to the rarity of extreme rainfall events.

In contrast, Gaseke's larger area, gentler slopes, and extensive floodplain extend hydrological memory, necessitating longer antecedent rainfall windows of 7–11 days to capture flood-triggering events accurately. Within this range, fused thresholds for No Action ranged from 214–280 mm, Watch from 223–293 mm, Alert from 232–307 mm, and Warning from 241–320 mm, with a fusion weight of ~0.56. Shorter windows (1–6 days) produced high detection rates but also triggered frequent false alarms. The longer accumulation periods reflect the catchment's slower response and storage capacity, ensuring early-warning signals are both reliable and operationally meaningful for flood management.

This tiered configuration reflects distinct hydrological behaviors, Nyamutera's rapid-response sensitivity versus Gaseke's storage-driven predictability. The findings emphasize the need to calibrate early-warning systems to local geomorphology and antecedent wetness. Fusion of logistic and physical thresholds tailored to each basin supports a flexible, adaptive framework aligned with early-warning optimization principles (Casado-Rodríguez et al., 2025; Sättele et al., 2016), essential for reliable flood preparedness in data-scarce, topographically complex regions.

4.5 Conclusion

This study applied the extended GR4J rainfall-runoff model to reconstruct daily streamflow and develop probabilistic flood early-warning thresholds for two contiguous catchments in the Mukungwa watershed, northwest Rwanda: Nyamutera (44 km^2) and Gaseke (109 km^2). Calibration against observed rainfall and streamflow produced catchment-specific parameter sets that captured the distinct hydrological behaviors of the two basins.

Nyamutera's small size and steep slope generated a flashy hydrograph characterized by moderate storage capacity ($X1 \approx 969$ mm), limited soil retention ($X2 \approx 3.04$ mm/day), high routing store capacity ($X3 \approx 82$ mm), and moderate unit hydrograph base factor ($X4 \approx 1.06$). By contrast, Gaseke's larger area, moderate slope (0.37), and ~168 ha floodplain produced a more attenuated, baseflow-dominated response, requiring higher storage ($X1 \approx 2369$ mm), minimal soil retention ($X2 \approx 7.4 \times 10^{-5}$ mm/day), lower routing store ($X3 \approx 58.6$ mm), higher baseflow factor ($X4 \approx 1.44$), and fractional flow adjustment ($F\alpha \approx 0.76$). Actual evapotranspiration coefficients ($Ka = 1.1$ for Nyamutera; 0.8 for Gaseke) further differentiated runoff dynamics. Model performance metrics reflected these contrasts: Nyamutera achieved NSE = 0.213, KGE = 0.506, RMSE = 1.355 m^3/s, and PWRMSE = 2.164 m^3/s, while Gaseke performed better

(NSE = 0.451, KGE = 0.694, RMSE = 1.562 m³/s, PWRMSE = 2.942 m³/s), consistent with the hydrogeomorphic differences between catchments.

The study highlights catchment-specific fused rainfall thresholds, derived from logistic regression and physical exceedance probabilities, as a robust basis for flood early-warning systems in tropical mountainous regions. In Nyamutera, steep slopes and low soil storage promote rapid runoff, with optimal predictive skill observed for 5–6 day antecedent rainfall windows. Within this range, the model achieved strong performance metrics, with POD = 0.57–0.58, FAR = 0.12–0.20, CSI = 0.50–0.54, AUC ≈ 0.96–1.00, and HSS = 0.67–0.74, reflecting short-term rainfall-runoff connectivity and limited hydrological memory (Di Baldassarre et al., 2018; Penna et al., 2011; Tramblay et al., 2010). A four-tier early-warning system was established using fused thresholds weighted toward probabilistic skill (~0.71), with 5–6 day rainfall totals ranging from 126–201 mm across No Action to Warning categories, balancing detection reliability and operational practicality.

Conversely, Gaseke's broad floodplain, gentler slopes, and larger storage promote longer hydrological memory, with peak model skill at 7–11 day antecedent windows. In this window, metrics indicated robust performance (POD = 0.80, FAR = 0.20, CSI = 0.67, AUC ≈ 1.00, HSS = 0.80), consistent with slower, saturation-driven flood generation (Blöschl et al., 2019). Stabilized fused thresholds for 7–11 day rainfall totals ranged from 214–320 mm (No Action to Warning), with a fusion weight of ~0.56, allowing longer lead times and reliable early-warning alerts across this more attenuated catchment.

Despite satisfactory discrimination skill, the moderate POD and CSI values for Nyamutera indicate that the model still misses a notable proportion of flood events, pointing to limited sensitivity to certain antecedent rainfall conditions. In Gaseke, although higher POD and CSI-star values suggest improved event detection, the relatively small number of observed flood events may inflate performance metrics, introducing uncertainty in model robustness under rare-event and data-limited conditions. Nevertheless, the framework represents a foundational and transferable early-warning tool that can be consistently applied in catchments lacking operational flood forecasting systems, such as the mountainous areas of north-western Rwanda. Furthermore, although conceptually simple, models like GR4J effectively simulate catchment behavior in data-scarce environments, offering stable calibration without complex physical assumptions (Andréassian et al., 2014b; Perrin et al., 2003). These findings advocate for integrated probabilistic-physical frameworks tailored to local geomorphology and hydrological dynamics for sustainable flood-risk management.

It should be noted that streamflow reconstruction models can never fully replace long-term, real field measurements. To advance understanding, it is essential to strengthen rainfall and flow monitoring networks while continuing modeling efforts tailored to the study context.

While constrained by daily data resolution and assumptions of stationarity in rainfall-runoff behavior, this study demonstrates that catchment-specific calibration of conceptual rainfall-runoff models, such as the GR4J, combined with probabilistic and physically based thresholds, can substantially improve streamflow reconstruction and operational flood-risk assessment. The proposed framework supports adaptive early-warning systems tailored to hydrologically contrasting tropical mountainous catchments, providing a practical approach to enhance flood preparedness and hazard mitigation in data-limited regions.

Chapter 5 Synthesis and future perspectives on flood hazards and flood-risk management

5.1 Summary of the key findings

This study sought to advance understanding of flood-generating processes and flood-risk management in data-scarce, mountainous agricultural catchments of northwest Rwanda by adopting hydrogeomorphological approaches. By combining targeted field monitoring, event-based hydrological modelling, and statistical analysis, this research provides insights that extend beyond the two investigated catchments and are relevant to many tropical regions facing similar data and capacity constraints. The central research question guiding this thesis was therefore formulated as follows:

"To what extent can short-term rainfall and streamflow observations, combined with statistical and numerical analyses, help improve our understanding of the factors controlling rainfall-runoff responses and flood events in mountainous tropical catchments?"

Accordingly, this chapter synthesizes the key findings of the thesis and outlines future directions for flood hazards assessment and flood-risk management in the tropical mountainous catchments.

The study also highlights an important methodological trade-off between model simplicity and process realism, particularly in data-scarce mountainous tropical environments. While the results clearly demonstrate the influence of hydrological memory, storage, and geomorphic controls on flood generation, this does not imply that increasingly complex, fully process-based models are always the optimal solution for early-warning applications. Instead, the findings show that key hydrological processes can be effectively represented using simpler, parsimonious approaches. For example, the Rational Method can be applied in a physically process-based manner rather than relying solely on its empirical formulation, while the GR4J rainfall-runoff model—when informed by short-term rainfall and streamflow observations together with historical rainfall records—can be used to reconstruct historical streamflow records. These tools, combined with antecedent rainfall accumulation, enable the development of effective flood early-warning systems based on fundamental rainfall-runoff principles, provided that their application is guided by sound hydrological reasoning.

In regions where long-term, high-resolution hydro-meteorological and subsurface data are limited, increasing model complexity can introduce substantial parameter uncertainty and reduce operational robustness. These results therefore support a fit-for-purpose modelling philosophy, in which simplicity and interpretability are prioritized, and process understanding informs model design and threshold selection rather than driving unnecessary complexity. In this sense, awareness of key hydrological processes does not require fully process-resolving models; it enables simpler models to be applied more intelligently and effectively.

The contrasting behaviors of Nyamutera and Gaseke further illustrate that hydrological realism can be achieved by carefully integrating rainfall over time, capturing catchment memory effects without explicitly simulating all internal processes. Striking this balance between simplicity and realism is particularly relevant for operational flood early-warning systems in data-limited regions, where reliability, transparency, and transferability often outweigh the benefits of detailed mechanistic representation.

5.1.1 Value of cost-effective monitoring in data-scarce regions

A key outcome of this research is the demonstration that low-cost, strategically deployed river monitoring systems—collecting high-resolution streamflow and rainfall data—can greatly reduce information gaps in data-scarce environments. Although the observation period was relatively short, the high-resolution water-level, discharge measurements and rainfall data successfully captured key storm-event characteristics, including rapid flow rises, peak timing, and recession behaviour. Building on these observations, this study developed event-based rainfall-runoff datasets to investigate the spatiotemporal variability of hydrological responses and to assess the applicability of the Rational method, the NRCS-CN approach, and the GR4J rainfall-runoff model—from either their empirical or conceptual basis to their physical interpretation—for flood-hazards and flood-risk management in the Nyamutera (44 km²) and Gaseke (109 km²) catchments within the mountainous Mukungwa watershed of northwest Rwanda. The results highlight clear differences in runoff behaviour between the two catchments, reflecting contrasts in topography, soil properties, and storage capacity.

These results show that the absence of long-term hydrometric records does not necessarily preclude meaningful flood analysis. Instead, targeted, short-term monitoring focused on storm events can provide valuable insights into catchment response variability and flood-generating mechanisms. This approach is particularly relevant for tropical mountainous regions, where rapid hydrological responses dominate flood risk and where traditional long-term monitoring networks are often unavailable or unaffordable.

In this context, a key implication is that flood risk assessments in data-limited regions can be significantly enhanced through innovative, low-cost monitoring strategies tailored to local hydrological conditions.

5.1.2 Importance of catchment-specific hydrogeomorphic controls

The contrasting hydrological behaviour observed between the Nyamutera and Gaseke catchments underscores the dominant role of catchment-specific characteristics in shaping flood response. Nyamutera, with its steep slopes and short flowpaths, exhibited rapid runoff

responses and sharply peaked hydrographs. In contrast, Gaseke, featuring a broader floodplain and moderate slopes, showed delayed and more attenuated flood peaks.

These differences highlight that topography, soil properties, lithology, and land use exert stronger control on flood dynamics than catchment size alone. As a result, flood risk management strategies that rely on generalized assumptions or regional averages risk misrepresenting both flood magnitude and timing.

Therefore, effective flood management should consider local hydrogeomorphic conditions, rather than relying on uniform design or modeling standards across diverse landscapes (refer Chapter 2).

5.1.3 From empirical methods toward process-oriented modeling

The modeling results reveal clear limitations of purely empirical approaches—particularly the NRCS-CN method—when applied to steep tropical catchments. While such methods offer simplicity and low data requirements, they struggle to represent event-specific storage effects, routing dynamics, and runoff timing, which are critical for flood hazard assessment.

The findings highlight the need to move beyond static, runoff-generation-focused models toward process-oriented frameworks that better capture the physical controls of flood response, including travel time, channel storage, and floodplain attenuation. Lag-time analysis and Sobol' sensitivity results reveal contrasting flood controls between the two catchments. In the steep, storage-limited Nyamutera catchment, flood response is governed by a combination of channel storage and travel-time processes, with the Muskingum storage constant (K) and lag time exerting the strongest influence (mean ST = 0.45 and 0.40, respectively). The Muskingum weighting factor plays a secondary role (ST = 0.15), while initial abstraction has only a minor influence (ST = 0.05).

In contrast, flood response in the larger, floodplain-connected Gaseke catchment is dominated by lag time (mean ST = 0.67), which explains most of the model variability. Channel storage and initial abstraction play secondary roles (ST = 0.19 and 0.11), while the routing weight has a limited effect (ST = 0.06).

Overall, the NRCS-CN method proved capable of reproducing isolated aspects of flood hydrographs during calibration but struggled to simultaneously capture peak magnitude, timing, and total runoff volume, particularly during validation. These results indicate that in mountainous tropical catchments, where runoff dynamics are strongly shaped by geomorphology and storage processes, static abstraction-based methods have limited predictive reliability. This does not imply abandoning empirical methods altogether, but rather embedding

them within physically meaningful structures that reflect dominant hydrological processes. Accordingly, hydrological modeling in mountainous tropical regions should prioritize physical realism over empirical convenience, particularly when the goal is robust flood risk management rather than long-term water balance estimation (Chapter 3).

5.1.4 Limits of model transferability and the need for local calibration

Sensitivity analysis and event-based validation revealed that the relative importance of model parameters differs markedly between catchments, which constrains the transferability of calibrated models. In the steep, storage-limited Nyamutera catchment, flood response is controlled mainly by channel storage and travel-time processes, with lag time and the Muskingum storage constant exerting the strongest influence, while initial abstraction plays a relatively minor role. By contrast, in the larger, floodplain-connected Gaseke catchment, hydrograph dynamics are overwhelmingly governed by lag time, with channel storage and initial abstraction contributing secondarily and routing effects having little influence.

These contrasts highlight that "one-size-fits-all" hydrological models are poorly suited to heterogeneous tropical landscapes. Even neighboring catchments can exhibit fundamentally different flood-generating processes, meaning that parameter sets calibrated for one catchment cannot be reliably transferred to another.

Consequently, effective flood modeling and hydraulic design in mountainous tropical regions require locally adapted, event-based approaches that reflect site-specific hydrogeomorphic controls, rather than relying on the transfer of assumptions or parameters across catchments (Chapter 3).

5.1.5 Integrating statistical and numerical tools for flood hazard assessment

Key strength of this study is the integration of complementary modeling approaches, including the Rational method—from its empirical formulation to its physical interpretation—the NRCS-CN method through a custom Python-based event model, GR4J simulations, and statistical techniques such as logistic regression. Each approach contributed unique insights: the event-based models elucidated process controls, GR4J supported continuous hydrograph reconstruction, and statistical analysis quantified flood probability in relation to antecedent conditions.

This hybrid framework illustrates that combining statistical and numerical tools enhances flood hazard assessment, particularly in data-scarce regions. Rather than being competing alternatives, these methods form a coherent toolbox for understanding, predicting, and managing flood risk.

Consequently, integrated modeling frameworks offer more robust and reliable insights than reliance on any single approach, especially in complex mountainous catchments with limited data (Chapters 2–4).

5.1.6 Antecedent rainfall as a critical control on flood occurrence

Statistical analysis revealed that antecedent rainfall plays a decisive role in flood generation, with optimal accumulation windows differing between catchments (5–6 days in Nyamutera and 7–11 days in Gaseke). These differences reflect contrasting storage and drainage characteristics and explain much of the event-to-event variability observed in flood response. Incorporating antecedent rainfall information substantially improves flood predictability and provides a scientifically grounded basis for early warning systems.

Collectively, flood forecasting in tropical catchments must move beyond single-event rainfall thresholds and incorporate catchment-specific antecedent rainfall conditions (Chapter 4).

5.1.7 Practical pathways for early warning and flood-risk management

Finally, this research demonstrates how scientific modeling can be translated into actionable tools for flood risk management. Assessing the applicability of the Rational Method, from its empirical basis to its physical interpretation, enables the derivation of design runoff coefficients that inform hydraulic structure design and flood risk management (Chapter 2). GR4J-based reconstructions enabled the derivation of catchment-specific flood thresholds, directly supporting early warning and preparedness efforts (Chapter 4).

These tools are particularly valuable for regions where institutional capacity and data availability are limited. By grounding flood warnings in local hydrological behaviour, they enhance both credibility and effectiveness.

Overall, it is important to note that even in data-scarce environments, scientifically informed flood early-warning systems are achievable and can significantly strengthen community resilience and infrastructure planning.

5.2 Responses to the specific objectives of the thesis

5.2.1 To collect and provide detailed short-term rainfall and streamflow observations from two contiguous small catchments characterized by contrasting topography, soil types, and LULC conditions

This objective was successfully met through the deployment of low-cost, high-resolution rainfall and streamflow monitoring systems in the Nyamutera and Gaseke catchments. Despite the relatively short monitoring period, the collected datasets captured a wide range of storm events, including both moderate and extreme floods (Chapter 2).

The observations provided detailed insights into event-scale variability, including peak timing, hydrograph shape, recession behaviour, and runoff volumes. Importantly, the study demonstrated that strategic short-term monitoring can yield scientifically robust information, even in regions where long-term hydrometric records are unavailable.

By making these datasets available and fully documented, the study provides a valuable physically based foundation for future hydrological research and flood risk assessment in tropical mountainous environments.

5.2.2 To identify and analyze the main factors influencing rainfall-runoff response during flood events, focusing on topography, soil characteristics, and land use/land cover

This objective was achieved through a combination of event-based rainfall-runoff analysis, sensitivity assessment, and comparative evaluation of two contrasting catchments. The results clearly show that topography and hydrogeomorphological controls exert the primary influence on flood response, while soil properties and LULC act as secondary modifiers rather than dominant drivers.

In the steep and compact Nyamutera catchment, rapid runoff concentration and short flowpaths produce fast hydrograph responses, but flood generation is governed primarily by channel storage and travel time rather than by runoff initiation alone. Sobol' analysis shows that the Muskingum storage constant (K) and lag time dominate model sensitivity (mean ST = 0.45 and 0.40, respectively), indicating that flood peaks are mainly shaped by flow translation and in-channel storage processes. The Muskingum weighting factor (X) plays a secondary role (ST = 0.15), while initial abstraction (Ia) exerts only a minor influence (ST = 0.05), suggesting that threshold-controlled runoff initiation is less critical than routing dynamics in this steep, storage-limited setting.

In contrast, flood response in the larger, floodplain-connected Gaseke catchment is overwhelmingly controlled by lag time (mean ST = 0.67), reflecting the dominant role of travel time and floodplain-mediated routing in shaping peak flows. Channel storage (K) and initial abstraction (Ia) contribute more modestly (ST = 0.19 and 0.11), while the Muskingum weighting factor (X) has little influence (ST = 0.06). This pattern highlights how floodplain connectivity and longer flowpaths regulate flood peaks in Gaseke, shifting control away from in-channel storage toward basin-scale timing effects.

Soil characteristics and LULC affected infiltration and storage capacity, but their impacts were highly context-dependent and strongly mediated by topography. Overall, the analysis highlights that geomorphological structure largely governs flood dynamics and that rainfall-runoff

responses cannot be reliably interpreted without explicitly accounting for terrain-driven processes.

5.2.3 To develop statistical and numerical tools aimed at enhancing the understanding of flood hazards and risks, thereby supporting the design of more effective flood management strategies informed by rainfall-runoff dynamics and catchment characteristics

This objective was addressed by developing and applying a multi-method analytical framework that integrates numerical hydrological modeling, statistical analysis, and sensitivity assessment. Evaluating the Rational method beyond its empirical formulation, and in light of its physical assumptions, allowed the development of runoff coefficients suited to hydraulic design and flood risk assessment (Chapter 2). In parallel, GR4J-based flow reconstructions were used to establish catchment-specific flood thresholds, providing a practical basis for early warning and preparedness strategies (Chapter 4).

In addition, logistic regression analysis identified catchment-specific antecedent rainfall windows as key predictors of flood occurrence, providing a quantitative basis for early warning systems. Sensitivity analysis shows that model behavior is governed by different dominant processes in each catchment. In Nyamutera, flood response is primarily controlled by channel storage and travel-time effects, with only a minor contribution from initial abstraction, whereas in Gaseke, lag time overwhelmingly dominates model performance. These contrasts underscore the need for catchment-specific modeling strategies rather than a one-size-fits-all application of the NRCS-CN framework.

Together, these tools improved understanding of flood-generating mechanisms and translated scientific insight into practical flood hazard indicators, directly supporting risk-informed decision-making.

5.2.4 To estimate probable maximum flood events and evaluate their potential impacts on lives, properties, and hydraulic infrastructure within the study area

This objective was partially addressed through the estimation of extreme flood magnitudes using both event-based and continuous modeling approaches, which provided upper-bound flood scenarios suitable for preliminary risk screening and assessing potential stress on hydraulic infrastructure. The analyses highlighted the vulnerability of steep, rapidly responding catchments, such as Nyamutera, to high-magnitude floods, while demonstrating the moderating role of floodplain attenuation in Gaseke. Importantly, antecedent rainfall was identified as a critical control, with 5–6 days for Nyamutera and 7–11 days for Gaseke representing key windows influencing flood likelihood and magnitude.

A fully deterministic PMF estimation—requiring physically based extreme rainfall modeling, detailed inundation or dam-break simulations, and comprehensive exposure datasets—was beyond the scope of the available data and resources. Nonetheless, the study provides a conceptual and methodological foundation for future PMF and impact assessments, highlighting critical hydrological controls, data requirements, and modeling pathways.

Overall, these findings establish a basis for integrating hydrological extremes with hydraulic modeling and risk analysis, supporting improved assessment of potential impacts on lives, properties, and infrastructure in tropical mountainous catchments.

5.3 Future perspectives on flood hazards and flood-risk management

As the cost-effective river monitoring systems will still be recording data, future research should expand both the spatial and temporal coverage of hydrological monitoring in tropical mountainous catchments, combining long-term, high-resolution in situ measurements with remotely sensed rainfall and flow data. This will improve understanding of storm-event variability and strengthen model calibration in data-limited contexts.

Developing hybrid modeling approaches remains a priority. Combining empirically efficient methods, such as the NRCS-CN framework, with physically informed representations of routing, storage, and terrain-driven flow dynamics can enhance flood prediction, particularly for extreme or multi-peak events. Event-based and continuous modeling should place greater emphasis on antecedent conditions to better understand floodplain attenuation and improve catchment-specific thresholds.

Additionally, future researches should integrate antecedent hydrological conditions with sediment transport-driven river morphology changes, as both processes can alter channel-floodplain connectivity and flood attenuation dynamics.

Climate change and land-use transformations are also expected to intensify flood hazards in these regions. Future studies should incorporate scenarios of shifting rainfall extremes and altered catchment characteristics to better evaluate potential changes in flood risk. Coupling hydrological models with hydraulic and risk assessment frameworks can support anticipatory planning for lives, infrastructure, and ecosystem services.

Finally, strengthening collaboration among scientists, local authorities, and communities is essential to translate research into actionable strategies, including early-warning systems, resilient infrastructure, and adaptive management practices. By integrating monitoring, modeling, and participatory approaches, future work can deliver context-sensitive, data-informed solutions that enhance flood resilience in mountainous tropical regions.

Appendix 0-1 Field photographs illustrating conditions after the flood event of 02–03 May 2023 and during subsequent hydrological data collection.

Note: (a, e) flood events in the Nyamutera catchment; (f) flood depth; (g) destruction of the Rubagabaga small bridge; (b) downloading TD-Diver data at the Nyamutera hydrometric station; (c, d) flow measurement using a current meter; (d) surveying a cross-section of the Gaseke River.

Appendix 0-2 Comparison and ranking of commonly applied objective functions in flood modeling. Metrics are evaluated based on their capacity to capture peak discharge, hydrograph shape, and timing, with justifications tailored to flood calibration and design context.

Rank	Objective Function	Strengths	Weaknesses	Justification
1	Peak-Weighted RMSE (PWRMSE)	Balances peak accuracy with hydrograph shape	Slightly more complex to implement	Best overall metric, capturing peak magnitude, timing, and shape simultaneously
2	Percent Error in Peak Discharge (PEPD)	Directly evaluates peak discharge	Ignores timing and shape	Essential for flood studies where peak accuracy is critical
3	Peak-Weighted Variable Power (PWVP)	Flexible weighting; strong peak focus if tuned	Requires exponent selection; less intuitive	Powerful option when justified, can rival PWRMSE in peak calibration
4	Time-Weighted RMSE	Captures timing and overall shape	Underweights extreme peaks	Useful for early warning or operational flood forecasting
5	Root Mean Square Error (RMSE)	Standard, interpretable, widely used	Underweights peak flows	Balanced measure but less suited for flood extremes
6	Sum of Squared Residuals (SSR)	Strongly penalizes large deviations	Over-penalizes regardless of timing	General error metric, not peak-oriented
7	Mean Squared Residuals (MSR)	Scaled SSR; easy to compute	Same drawbacks as SSR	Suitable for general goodness-of-fit evaluation
8	Sum of Absolute Residuals (SAR)	Simple, less sensitive to outliers	Too forgiving for flood peaks	May track hydrograph shape but insufficient for flood design

Appendix 0-3 The full calibration and leave-one-out validation results.

Nyamutera/Calibration								
Storm	**Ia(mm)**	**K(s)**	**X**	**NSE**	**KGE**	**RMSE**	**PEPD(%)**	**VE(%)**
E1	0.5	5572.23	0	0.67	0.62	3.13	37.13	35.78
E2	0.5	645.25	0.5	-0.25	0.06	2.61	53.98	82.64
E3	0.5	524.39	0.5	-0.78	0.15	7.29	51.79	69.57
E4	0.5	450	0.5	-6.4	0.02	6.34	61.84	83.34
E5	0.5	500.48	0.1	-4.26	-0.44	11.96	76.49	78.5
E6	0.5	1973.55	0.33	-33.22	-0.07	6.04	58.4	84.19
E7	0.5	7677.8	0	-10.26	-0.02	5.58	68.95	78.03
E8	0.5	7327.28	0	-2.17	0.17	4	37.06	80.67
E9	0.5	6718.33	0	-8.48	-0.06	3.6	37.66	82.85
E10	0.5	2630.97	0.5	-1.1	-0.18	4.67	79.48	89.42
E11	0.5	2157.67	0.5	-0.01	-0.1	9.42	73.09	68.78
E12	9.59	7736.8	0	-0.26	0.22	7.13	17.98	60.86
E13	9.79	7731.11	0	-2.71	0.27	2.3	52.23	59.55
E14	0.5	5662.84	0	-0.34	0.4	3.51	42.38	50.97
E15	0.5	778.46	0.47	-0.36	-0.31	9.39	80.46	89.05
Gaseke/Calibration								
Storm	**Ia(mm)**	**K(s)**	**X**	**NSE**	**KGE**	**RMSE**	**PEPD(%)**	**VE(%)**
E1	8.7	15068.35	0	-5.25	-0.6	2.16	49.31	40.57
E2	0.5	11586.08	0	0.84	0.86	1.94	15.08	11.65
E3	9.62	15055.14	0	-0.21	0.5	2.64	23.02	34.24
E4	10	15068.35	0	-0.43	0.2	4.9	26.04	9.89
E5	9.13	15044.28	0	-2.17	-0.05	4.12	8.11	57.25
E6	10	15068.35	0	-19.68	-2.22	6.68	139.09	226.6
E7	10	15068.35	0	-6.26	-1.04	8.9	86.1	155.65
E8	2.99	15057.69	0.02	-1.47	0.06	1.11	2.43	14.89
E9	8.41	15068.35	0	-33.22	-2.59	4.63	171.45	150.27
E10	8.83	15068.35	0	-9.18	-1.37	7.01	138.35	159.58
E11	9.04	15065.55	0	-1.24	0.2	2.88	7.16	41.96
E12	2.41	15068.11	0	-1.66	0.05	4.3	15.17	50.09
E13	10	15068.35	0.17	-1.58	-0.08	3.86	36.03	81.21
E14	1.71	15064.64	0	0.76	0.86	2.71	28.63	7.71
E15	8.47	15066.77	0	0.89	0.74	3.63	10.14	22.55
E16	7.97	15047.76	0	-1.73	0.37	4.48	54.2	51.77
E17	0.5	11000.3	0	-0.8	0.47	7.44	28.7	50.19
E18	5.02	15043.76	0	-1.01	0.42	6.46	14.42	53.09
E19	0.5	2556.32	0	-2.86	0.2	11.54	44.15	74.07
E20	8.66	14921.68	0.4	-11.82	0.19	5.67	42.71	67
E21	0.5	3106.79	0.5	-3.62	0.2	8.17	55.51	77.16
E22	1.17	15043.42	0	0.2	0.55	9.02	17.19	33.76
E23	10	15068.35	0	-23.69	-3.89	11.74	264.64	416.31
Nyamutera/Valindation								
Storm	**Ia(mm)**	**K(s)**	**X**	**NSE**	**KGE**	**RMSE**	**PEPD(%)**	**VE(%)**
E1	9.61	742.06	0.00	0.11	0.26	5.12	36.98	54.38

E2	9.47	1786.21	0.00	-0.37	0.01	2.73	64.17	82.81
E3	10.00	1609.12	0.00	-0.83	0.10	7.39	60.34	71.54
E4	8.51	2283.74	0.00	-6.13	-0.18	6.22	61.84	79.28
E5	8.58	2283.74	0.00	-4.41	-0.64	12.13	78.87	78.87
E6	10.00	1379.43	0.00	-33.85	-0.09	6.09	58.40	85.11
E7	10.00	1379.43	0.00	-12.12	-0.13	6.03	63.38	83.84
E8	10.00	1537.21	0.00	-2.57	0.08	4.25	1.58	83.47
E9	10.00	1537.21	0.00	-9.33	-0.14	3.76	0.07	84.53
E10	10.00	1379.43	0.00	-1.14	-0.19	4.72	80.98	89.79
E11	10.00	1609.12	0.00	0.01	-0.16	9.30	85.04	72.58
E12	10.00	1437.29	0.00	-0.45	-0.07	7.62	23.25	62.60
E13	10.00	1564.56	0.00	-3.02	0.17	2.40	39.25	63.06
E14	10.00	1517.50	0.00	-0.46	0.35	3.68	10.13	53.68
E15	10.00	1379.43	0.00	-0.35	-0.32	9.38	84.29	89.33
Gaseke/Validation								
Storm	**Ia(mm)**	**K(s)**	**X**	**NSE**	**KGE**	**RMSE**	**PEPD(%)**	**VE(%)**
E1	10	15028.37	0	-5.27	-0.61	2.16	49.52	40.64
E2	10	15067.66	0	0.71	0.66	2.56	36.67	21.07
E3	10	15067.66	0	-0.21	0.50	2.64	23.05	34.24
E4	10	15067.02	0	-0.43	0.20	4.90	26.04	9.89
E5	10	15067.66	0	-2.17	-0.05	4.11	8.04	57.19
E6	10	15057.56	0	-19.69	-2.22	6.68	139.12	226.67
E7	10	15067.66	0	-6.26	-1.04	8.90	86.10	155.66
E8	10	15023.32	0	-1.45	0.06	1.11	0.82	14.95
E9	10	15028.37	0	-33.28	-2.59	4.63	171.69	150.44
E10	10	15067.66	0	-9.18	-1.37	7.01	138.35	159.58
E11	10	15061.06	0	-1.24	0.20	2.88	7.18	41.97
E12	10	15067.66	0	-1.66	0.05	4.30	15.17	50.09
E13	10	15067.17	0	-2.10	-0.19	4.23	34.56	98.67
E14	10	15060.26	0	0.77	0.82	2.68	34.69	13.96
E15	10	15062.20	0	0.89	0.73	3.62	14.52	25.82
E16	10	15067.66	0	-1.73	0.37	4.48	54.20	51.76
E17	10	15067.66	0	-1.14	0.35	8.09	45.81	54.92
E18	10	15067.66	0	-1.15	0.42	6.68	20.67	55.97
E19	10	15067.66	0	-2.65	0.09	11.23	62.81	70.31
E20	10	15060.26	0	-11.14	0.01	5.51	42.71	63.04
E21	10	15067.66	0	-3.23	0.07	7.82	73.96	70.97
E22	10	15067.66	0	0.09	0.40	9.66	42.55	53.05
E23	10	15067.30	0	-23.69	-3.90	11.74	264.65	416.31

Abdel-Fattah, M., Saber, M., Kantoush, S. A., Khalil, M. F., Sumi, T., & Sefelnasr, A. M. (2017). A Hydrological and Geomorphometric Approach to Understanding the Generation of Wadi Flash Floods. *Water*, *9*(7), 553. https://doi.org/10.3390/w9070553

Abdi, I., & Meddi, M. (2021). Study on the applicability of the SCS-CN-based models to simulate floods in the semi-arid watersheds of northern Algeria. *Acta Geophysica*, *69*(1), 217–230. https://doi.org/10.1007/s11600-020-00511-3

Abebe, W. B., Tilahun, S. A., Moges, M. M., Wondie, A., Derseh, M. G., Nigatu, T. A., Mhiret, D. A., Steenhuis, T. S., Camp, M. V., Walraevens, K., & McClain, M. E. (2020). Hydrological Foundation as a Basis for a Holistic Environmental Flow Assessment of Tropical Highland Rivers in Ethiopia. *Water*, *12*(2), 547. https://doi.org/10.3390/w12020547

Acreman, M., & Holden, J. (2013a). How Wetlands Affect Floods. *Wetlands*, *33*(5), 773–786. https://doi.org/10.1007/s13157-013-0473-2

Acreman, M., & Holden, J. (2013b). How Wetlands Affect Floods. *Wetlands*, *33*(5), 773–786. https://doi.org/10.1007/s13157-013-0473-2

Adhikari, P., Hong, Y., Douglas, K. R., Kirschbaum, D. B., Gourley, J., Adler, R., & Robert Brakenridge, G. (2010). A digitized global flood inventory (1998–2008): Compilation and preliminary results. *Natural Hazards*, *55*(2), 405–422. https://doi.org/10.1007/s11069-010-9537-2

Africa-Press. (2023). *15 students dead, 33 schools destroyed by flood* [Dataset]. https://www.africa-press.net/rwanda/all-news/15-students-dead-33-schools-destroyed-by-flood

Ahlheim, K.-H., Schirmer, H., & Bibliographisches Institut Mannheim (Eds.). (1989). *Wie funktioniert das? Wetter und Klima*. Meyers Lexikonverl.

Ahmadisharaf, E., Kalyanapu, A. J., Lillywhite, J. R., & Tonn, G. L. (2018). A probabilistic framework to evaluate the uncertainty of design hydrograph: Case study of Swannanoa River watershed. *Hydrological Sciences Journal*, *63*(12), 1776–1790. https://doi.org/10.1080/02626667.2018.1525616

Ajmal, M., Waseem, M., Ahn, J.-H., & Kim, T.-W. (2015). Improved Runoff Estimation Using Event-Based Rainfall-Runoff Models. *Water Resources Management*, *29*(6), 1995–2010. https://doi.org/10.1007/s11269-015-0924-z

Alderman, K., Turner, L. R., & Tong, S. (2012). Floods and human health: A systematic review. *Environment International*, *47*, 37–47. https://doi.org/10.1016/j.envint.2012.06.003

Alfieri, L., Salamon, P., Pappenberger, F., Wetterhall, F., & Thielen, J. (2012). Operational early warning systems for water-related hazards in Europe. *Environmental Science & Policy*, *21*, 35–49. https://doi.org/10.1016/j.envsci.2012.01.008

Alfieri, L., Zsoter, E., Harrigan, S., Aga Hirpa, F., Lavaysse, C., Prudhomme, C., & Salamon, P. (2019). Range-dependent thresholds for global flood early warning. *Journal of Hydrology X*, *4*, 100034. https://doi.org/10.1016/j.hydroa.2019.100034

Alhumoud, J., & Almashan, N. (2019). Muskingum Method with Variable Parameter Estimation. *Mathematical Modelling of Engineering Problems*, *6*(3), 355–362. https://doi.org/10.18280/mmep.060306

Ali, S., Rahman, A., & Shaik, R. (2024). A Review of Event-Based Conceptual Rainfall-Runoff Models: A Case for Australia. *Encyclopedia*, *4*(2), 966–983. https://doi.org/10.3390/encyclopedia4020062

Allen, R. G. & Food and Agriculture Organization of the United Nations (Eds.). (1998). *Crop evapotranspiration: Guidelines for computing crop water requirements*. Food and Agriculture Organization of the United Nations.

Allen, R. G., Pruitt, W. O., Wright, J. L., Howell, T. A., Ventura, F., Snyder, R., Itenfisu, D., Steduto, P., Berengena, J., Yrisarry, J. B., Smith, M., Pereira, L. S., Raes, D., Perrier, A., Alves, I., Walter, I., & Elliott, R. (2006). A recommendation on standardized surface resistance for hourly calculation of reference ETo by the FAO56 Penman-Monteith method. *Agricultural Water Management*, *81*(1–2), 1–22. https://doi.org/10.1016/j.agwat.2005.03.007

Althoff, D., & Rodrigues, L. N. (2021). Goodness-of-fit criteria for hydrological models: Model calibration and performance assessment. *Journal of Hydrology*, *600*, 126674. https://doi.org/10.1016/j.jhydrol.2021.126674

Amoussou, E., Mahe, G., Amrouni, O., Bodian, A., Cudennec, C., Dietrich, S., Kodja, D. J., & Vissin, E. W. (2021). Preface: Hydrology of Large River Basins in Africa. *Proceedings of the International Association of Hydrological Sciences*, *384*, 1–4. https://doi.org/10.5194/piahs-384-1-2021

Andréassian, V., Bourgin, F., Oudin, L., Mathevet, T., Perrin, C., Lerat, J., Coron, L., & Berthet, L. (2014a). Seeking genericity in the selection of parameter sets: Impact on hydrological model efficiency. *Water Resources Research*, *50*(10), 8356–8366. https://doi.org/10.1002/2013WR014761

Andréassian, V., Bourgin, F., Oudin, L., Mathevet, T., Perrin, C., Lerat, J., Coron, L., & Berthet, L. (2014b). Seeking genericity in the selection of parameter sets: Impact on hydrological model efficiency. *Water Resources Research*, *50*(10), 8356–8366. https://doi.org/10.1002/2013WR014761

Andréassian, V., Perrin, C., Berthet, L., Le Moine, N., Lerat, J., Loumagne, C., Oudin, L., Mathevet, T., Ramos, M.-H., & Valéry, A. (2009). HESS Opinions "Crash tests for a standardized evaluation of hydrological models." *Hydrology and Earth System Sciences*, *13*(10), 1757–1764. https://doi.org/10.5194/hess-13-1757-2009

Arango-Carmona, M. I., Voit, P., Hürlimann, M., Aristizábal, E., & Korup, O. (2025). Hillslope torrential hazard cascades in tropical mountains. *Natural Hazards and Earth System Sciences*, *25*(9), 3641–3663. https://doi.org/10.5194/nhess-25-3641-2025

Arash, A. M., Fryirs, K., & Ralph, T. J. (2025). Using a Hydro-Morphic Classification of Catchments to Characterise and Explain High Flow and Overbank Flood Behaviour. *Geosciences*, *15*(4), 141. https://doi.org/10.3390/geosciences15040141

Arciniega-Esparza, S., Birkel, C., Chavarría-Palma, A., Arheimer, B., & Breña-Naranjo, J. A. (2022). Remote sensing-aided rainfall–runoff modeling in the tropics of Costa Rica. *Hydrology and Earth System Sciences*, *26*(4), 975–999. https://doi.org/10.5194/hess-26-975-2022

Arnaud-Fassetta, G., Astrade, L., Bardou, É., Corbonnois, J., Delahaye, D., Fort, M., Gautier, E., Jacob, N., Peiry, J.-L., Piégay, H., & Penven, M.-J. (2009). Fluvial geomorphology and flood-risk management. *Géomorphologie : relief, processus, environnement*, *15*(2), 109–128. https://doi.org/10.4000/geomorphologie.7554

Assaf, M. N., Salis, N., Manenti, S., Tamellini, L., Creaco, E., & Todeschini, S. (2025). Optimizing hydrological modelling on real urban catchment: Impact of calibration data selection and objective function. *Journal of Hydrology*, *662*, 133821. https://doi.org/10.1016/j.jhydrol.2025.133821

Awah, L. S., Belle, J. A., Nyam, Y. S., & Orimoloye, I. R. (2024). A Systematic Analysis of Systems Approach and Flood Risk Management Research: Trends, Gaps, and Opportunities. *International Journal of Disaster Risk Science*, *15*(1), 45–57. https://doi.org/10.1007/s13753-024-00544-y

BA Notes. (2023, November 22). *Effective Disaster Mitigation Approaches: Structural and Non-structural Strategies*. https://banotes.org/disaster-management/effective-disaster-mitigation-structural-nonstructural-strategies/?utm_source=chatgpt.com

Bahremand, A. (2016). HESS Opinions: Advocating process modeling and de-emphasizing parameter estimation. *Hydrology and Earth System Sciences*, *20*(4), 1433–1445. https://doi.org/10.5194/hess-20-1433-2016

Bamutaze, Y., Tenywa, M. M., Majaliwa, M. J. G., Vanacker, V., Bagoora, F., Magunda, M., Obando, J., & Wasige, J. E. (2010). Infiltration characteristics of volcanic sloping soils on Mt. Elgon, Eastern Uganda. *CATENA*, *80*(2), 122–130. https://doi.org/10.1016/j.catena.2009.09.006

Baudet, D, Hanon, M, Lemmone, E, & Theunissen, K. (1989). *Lithostratigraphie du domaine sedimentaire de la chaine kibarienne au rwanda*.

Beck, H. E., Zimmermann, N. E., McVicar, T. R., Vergopolan, N., Berg, A., & Wood, E. F. (2018). Present and future Köppen-Geiger climate classification maps at 1-km resolution. *Scientific Data*, *5*(1), 180214. https://doi.org/10.1038/sdata.2018.214

Benimana, J. C., Wali, U. G., Nhapi, I., Anyemedu, F. O., & Gumindoga, W. (2015). Rainwater harvesting potential for crop production in the Bugesera district of Rwanda. *African Journal of Agricultural Research*, *10*(19), 2020–2031. https://doi.org/10.5897/AJAR12.820

Bennett, B., Leonard, M., Deng, Y., & Westra, S. (2018). An empirical investigation into the effect of antecedent precipitation on flood volume. *Journal of Hydrology*, *567*, 435–445. https://doi.org/10.1016/j.jhydrol.2018.10.025

Berghuijs, W. R., Woods, R. A., Hutton, C. J., & Sivapalan, M. (2016). Dominant flood generating mechanisms across the United States. *Geophysical Research Letters*, *43*(9), 4382–4390. https://doi.org/10.1002/2016gl068070

Beven, K. (2006). A manifesto for the equifinality thesis. *Journal of Hydrology*, *320*(1–2), 18–36. https://doi.org/10.1016/j.jhydrol.2005.07.007

Beven, K. (2012). *Rainfall-runoff modelling: The primer* (2nd ed). Wiley-Blackwell. https://doi.org/10.1002/9781119951001

Beven, K., & Freer, J. (2001). Equifinality, data assimilation, and uncertainty estimation in mechanistic modelling of complex environmental systems using the GLUE methodology. *Journal of Hydrology*, *249*(1–4), 11–29. https://doi.org/10.1016/S0022-1694(01)00421-8

Biondi, D., & De Luca, D. L. (2012). A Bayesian approach for real-time flood forecasting. *Physics and Chemistry of the Earth, Parts A/B/C*, *42–44*, 91–97. https://doi.org/10.1016/j.pce.2011.04.004

Biondi, D., Freni, G., Iacobellis, V., Mascaro, G., & Montanari, A. (2012). Validation of hydrological models: Conceptual basis, methodological approaches and a proposal for a code of practice. *Physics and Chemistry of the Earth, Parts A/B/C*, *42–44*, 70–76. https://doi.org/10.1016/j.pce.2011.07.037

Birch, A. L., Stallard, R. F., & Barnard, H. R. (2021). Precipitation Characteristics and Land Cover Control Wet Season Runoff Source and Rainfall Partitioning in Three Humid Tropical Catchments in Central Panama. *Water Resources Research*, *57*(2), e2020WR028058. https://doi.org/10.1029/2020WR028058

Birhanu, D., Kim, H., Jang, C., & Park, S. (2018). Does the Complexity of Evapotranspiration and Hydrological Models Enhance Robustness? *Sustainability*, *10*(8), 2837. https://doi.org/10.3390/su10082837

Blöschl, G., Ardoin-Bardin, S., Bonell, M., Dorninger, M., Goodrich, D., Gutknecht, D., Matamoros, D., Merz, B., Shand, P., & Szolgay, J. (2007). At what scales do climate variability and land cover change impact on flooding and low flows? *Hydrological Processes*, *21*(9), 1241–1247. https://doi.org/10.1002/hyp.6669

Blöschl, G., Bierkens, M. F. P., Chambel, A., Cudennec, C., Destouni, G., Fiori, A., Kirchner, J. W., McDonnell, J. J., Savenije, H. H. G., Sivapalan, M., Stumpp, C., Toth, E., Volpi, E., Carr, G., Lupton, C., Salinas, J., Széles, B., Viglione, A., Aksoy, H., … Zhang, Y. (2019). Twenty-three unsolved problems in hydrology (UPH) – a community perspective. *Hydrological Sciences Journal*, *64*(10), 1141–1158. https://doi.org/10.1080/02626667.2019.1620507

Blöschl, G., & Sivapalan, M. (1995). Scale issues in hydrological modelling: A review. *Hydrological Processes*, *9*(3–4), 251–290. https://doi.org/10.1002/hyp.3360090305

Blöschl, G., Sivapalan, M., Wagener, T., Viglione, A., & Savenije, H. (Eds.). (2013). *Runoff Prediction in Ungauged Basins: Synthesis across Processes, Places and Scales* (1st ed.). Cambridge University Press. https://doi.org/10.1017/CBO9781139235761

Blöschl, G., & Zehe, E. (2005). On hydrological predictability. *Hydrological Processes*, *19*(19), 3923–3929. https://doi.org/10.1002/hyp.6075

Blume, T., Zehe, E., & Bronstert, A. (2007). Rainfall—Runoff response, event-based runoff coefficients and hydrograph separation. *Hydrological Sciences Journal*, *52*(5), 843–862. https://doi.org/10.1623/hysj.52.5.843

Bonell, M. (1993). Progress in the understanding of runoff generation dynamics in forests. *Journal of Hydrology*, *150*(2–4), 217–275. https://doi.org/10.1016/0022-1694(93)90112-M

Bonell, M. (1998). SELECTED CHALLENGES IN RUNOFF GENERATION RESEARCH IN FORESTS FROM THE HILLSLOPE TO HEADWATER DRAINAGE BASIN SCALE[1]. *JAWRA Journal of the American Water Resources Association*, *34*(4), 765–785. https://doi.org/10.1111/j.1752-1688.1998.tb01514.x

Bonneau, J., Fletcher, T. D., Costelloe, J. F., Poelsma, P. J., James, R. B., & Burns, M. J. (2018). Where does infiltrated stormwater go? Interactions with vegetation and subsurface

anthropogenic features. *Journal of Hydrology*, *567*, 121–132. https://doi.org/10.1016/j.jhydrol.2018.10.006

Borga, M., Anagnostou, E. N., Blöschl, G., & Creutin, J.-D. (2011). Flash flood forecasting, warning and risk management: The HYDRATE project. *Environmental Science & Policy*, *14*(7), 834–844. https://doi.org/10.1016/j.envsci.2011.05.017

Borga, M., Stoffel, M., Marchi, L., Marra, F., & Jakob, M. (2014). Hydrogeomorphic response to extreme rainfall in headwater systems: Flash floods and debris flows. *Journal of Hydrology*, *518*, 194–205. https://doi.org/10.1016/j.jhydrol.2014.05.022

Botter, G., Porporato, A., Daly, E., Rodriguez-Iturbe, I., & Rinaldo, A. (2007). Probabilistic characterization of base flows in river basins: Roles of soil, vegetation, and geomorphology. *Water Resources Research*, *43*(6), 2006WR005397. https://doi.org/10.1029/2006WR005397

Bouaziz, L. J. E., Fenicia, F., Thirel, G., De Boer-Euser, T., Buitink, J., Brauer, C. C., De Niel, J., Dewals, B. J., Drogue, G., Grelier, B., Melsen, L. A., Moustakas, S., Nossent, J., Pereira, F., Sprokkereef, E., Stam, J., Weerts, A. H., Willems, P., Savenije, H. H. G., & Hrachowitz, M. (2021). Behind the scenes of streamflow model performance. *Hydrology and Earth System Sciences*, *25*(2), 1069–1095. https://doi.org/10.5194/hess-25-1069-2021

Boumenni, H., Bachnou, A., & Alaa, N. E. (2017). The rainfall-runoff model GR4J optimization of parameter by genetic algorithms and Gauss-Newton method: Application for the watershed Ourika (High Atlas, Morocco). *Arabian Journal of Geosciences*, *10*(15), 343. https://doi.org/10.1007/s12517-017-3086-x

Bouttier, F., & Marchal, H. (2024). Probabilistic short-range forecasts of high-precipitation events: Optimal decision thresholds and predictability limits. *Natural Hazards and Earth System Sciences*, *24*(8), 2793–2816. https://doi.org/10.5194/nhess-24-2793-2024

Braca, G. (2008). *Stage-discharge relationships in open channels: Practices and problems*. Università di Trento. Dipartimento di ingegneria civile e ambientale.

Brierley, G., Fryirs, K., & Jain, V. (2006). Landscape connectivity: The geographic basis of geomorphic applications. *Area*, *38*(2), 165–174. https://doi.org/10.1111/j.1475-4762.2006.00671.x

Bröcker, J. (2008a). On reliability analysis of multi-categorical forecasts. *Nonlinear Processes in Geophysics*, *15*(4), 661–673. https://doi.org/10.5194/npg-15-661-2008

Bröcker, J. (2008b). Some Remarks on the Reliability of Categorical Probability Forecasts. *Monthly Weather Review*, *136*(11), 4488–4502. https://doi.org/10.1175/2008MWR2329.1

Bruijnzeel, L. A. (2004). Hydrological functions of tropical forests: Not seeing the soil for the trees? *Agriculture, Ecosystems & Environment*, *104*(1), 185–228. https://doi.org/10.1016/j.agee.2004.01.015

Bruijnzeel, L. A. (2005). Tropical montane cloud forest: A unique hydrological case. In M. Bonell & L. A. Bruijnzeel (Eds.), *Forests, Water and People in the Humid Tropics* (1st ed., pp. 462–484). Cambridge University Press. https://doi.org/10.1017/CBO9780511535666.024

Buda, A. R. (2013). 7.7 Surface-Runoff Generation and Forms of Overland Flow. In *Treatise on Geomorphology* (pp. 73–84). Elsevier. https://doi.org/10.1016/B978-0-12-374739-6.00151-2

Bullock, A., & Acreman, M. (2003). The role of wetlands in the hydrological cycle. *Hydrology and Earth System Sciences*, *7*(3), 358–389. https://doi.org/10.5194/hess-7-358-2003

Buytaert, W., Célleri, R., De Bièvre, B., Cisneros, F., Wyseure, G., Deckers, J., & Hofstede, R. (2006). Human impact on the hydrology of the Andean páramos. *Earth-Science Reviews*, *79*(1–2), 53–72. https://doi.org/10.1016/j.earscirev.2006.06.002

Buytaert, W., Celleri, R., Willems, P., Bièvre, B. D., & Wyseure, G. (2006). Spatial and temporal rainfall variability in mountainous areas: A case study from the south Ecuadorian Andes. *Journal of Hydrology*, *329*(3–4), 413–421. https://doi.org/10.1016/j.jhydrol.2006.02.031

Buytaert, W., & De Bièvre, B. (2012). Water for cities: The impact of climate change and demographic growth in the tropical Andes. *Water Resources Research*, *48*(8), 2011WR011755. https://doi.org/10.1029/2011WR011755

Byaruhanga, N., Kibirige, D., Gokool, S., & Mkhonta, G. (2024). Evolution of Flood Prediction and Forecasting Models for Flood Early Warning Systems: A Scoping Review. *Water*, *16*(13), 1763. https://doi.org/10.3390/w16131763

Cai, Z., Wang, J., Yang, Y., & Zhang, R. (2021). Influence of Vegetation Coverage on Hydraulic Characteristics of Overland Flow. *Water*, *13*(8), 1055. https://doi.org/10.3390/w13081055

Calero Mosquera, D., Hoyos Villada, F., & Torres Prieto, E. A. (2022). Runoff Curve Number (CN model) Evaluation Under Tropical Conditions. *Earth Sciences Research Journal*, *25*(4), 397–404. https://doi.org/10.15446/esrj.v25n4.95321

Casado-Rodríguez, J., Carton De Wiart, C., Grimaldi, S., Zsoter, E., Baugh, C., Bosshard, N., Mikuličková, M., Pechlivanidis, I., Prudhomme, C., & Salamon, P. (2025). Optimizing Warnings for Hydrologic Ensemble Prediction Systems for Improved Decision-Making. *Journal of Hydrometeorology*, *26*(6), 675–689. https://doi.org/10.1175/JHM-D-24-0054.1

Cavallin, A., Marchetti, M., Panizza, M., & Soldati, M. (1994). The role of geomorphology in environmental impact assessment. *Geomorphology*, *9*(2), 143–153. https://doi.org/10.1016/0169-555X(94)90072-8

Charlton, R. (2007). *Fundamentals of Fluvial Geomorphology* (0 ed.). Routledge. https://doi.org/10.4324/9780203371084

Cheng, Y., Musselman, K. N., Swenson, S., Lawrence, D., Hamman, J., Dagon, K., Kennedy, D., & Newman, A. J. (2023). Moving Land Models Toward More Actionable Science: A Novel Application of the Community Terrestrial Systems Model Across Alaska and the Yukon River Basin. *Water Resources Research*, *59*(1), e2022WR032204. https://doi.org/10.1029/2022WR032204

Chow, V. T., Maidment, D. R., & Mays, L. W. (1988). *Applied hydrology*. McGraw-Hill.

Clark, M. P., Kavetski, D., & Fenicia, F. (2011). Pursuing the method of multiple working hypotheses for hydrological modeling. *Water Resources Research*, *47*(9), 2010WR009827. https://doi.org/10.1029/2010WR009827

Clark, M. P., Schaefli, B., Schymanski, S. J., Samaniego, L., Luce, C. H., Jackson, B. M., Freer, J. E., Arnold, J. R., Moore, R. D., Istanbulluoglu, E., & Ceola, S. (2016). Improving the theoretical underpinnings of process-based hydrologic models. *Water Resources Research*, *52*(3), 2350–2365. https://doi.org/10.1002/2015WR017910

Cloke, H. L., & Pappenberger, F. (2009). Ensemble flood forecasting: A review. *Journal of Hydrology*, *375*(3–4), 613–626. https://doi.org/10.1016/j.jhydrol.2009.06.005

Collischonn, W., & Fan, F. M. (2013). Defining parameters for Eckhardt's digital baseflow filter. *Hydrological Processes*, *27*(18), 2614–2622. https://doi.org/10.1002/hyp.9391

Conitz, F., Zingraff-Hamed, A., Lupp, G., & Pauleit, S. (2021). Non-Structural Flood Management in European Rural Mountain Areas—Are Scientists Supporting Implementation? *Hydrology*, *8*(4), 167. https://doi.org/10.3390/hydrology8040167

Conway, D., & Schipper, E. L. F. (2011). Adaptation to climate change in Africa: Challenges and opportunities identified from Ethiopia. *Global Environmental Change*, *21*(1), 227–237. https://doi.org/10.1016/j.gloenvcha.2010.07.013

Cools, J., Innocenti, D., & O'Brien, S. (2016). Lessons from flood early warning systems. *Environmental Science & Policy*, *58*, 117–122. https://doi.org/10.1016/j.envsci.2016.01.006

Coron, L., Thirel, G., Delaigue, O., Perrin, C., & Andréassian, V. (2017). The suite of lumped GR hydrological models in an R package. *Environmental Modelling & Software*, *94*, 166–171. https://doi.org/10.1016/j.envsoft.2017.05.002

Cortés-Salazar, N., Vásquez, N., Mizukami, N., Mendoza, P. A., & Vargas, X. (2023). To what extent does river routing matter in hydrological modeling? *Hydrology and Earth System Sciences*, *27*(19), 3505–3524. https://doi.org/10.5194/hess-27-3505-2023

Cristiano, E., Ten Veldhuis, M.-C., & Van De Giesen, N. (2017). Spatial and temporal variability of rainfall and their effects on hydrological response in urban areas – a review. *Hydrology and Earth System Sciences*, *21*(7), 3859–3878. https://doi.org/10.5194/hess-21-3859-2017

Cui, D., Liang, S., Wang, D., & Liu, Z. (2021). A 1 km global dataset of historical (1979–2013) and future (2020–2100) Köppen–Geiger climate classification and bioclimatic variables. *Earth System Science Data*, *13*(11), 5087–5114. https://doi.org/10.5194/essd-13-5087-2021

Cyuzuzo Samba & Cecilia Macaulay. (2023). *Http://www.bbc.com/news/world-africa-65469374* [Dataset].

Dams, J., Dujardin, J., Reggers, R., Bashir, I., Canters, F., & Batelaan, O. (2013). Mapping impervious surface change from remote sensing for hydrological modeling. *Journal of Hydrology*, *485*, 84–95. https://doi.org/10.1016/j.jhydrol.2012.09.045

Danielescu, S., MacQuarrie, K. T. B., & Popa, A. (2018). SEPHYDRO: A Customizable Online Tool for Hydrograph Separation. *Groundwater*, *56*(4), 589–593. https://doi.org/10.1111/gwat.12792

Darienzo, M., Renard, B., Le Coz, J., & Lang, M. (2021). Detection of Stage-Discharge Rating Shifts Using Gaugings: A Recursive Segmentation Procedure Accounting for Observational and Model Uncertainties. *Water Resources Research*, *57*(4). https://doi.org/10.1029/2020wr028607

Das, P., Posch, A., Barber, N., Hicks, M., Duffy, K., Vandal, T., Singh, D., Werkhoven, K. V., & Ganguly, A. R. (2024). Hybrid physics-AI outperforms numerical weather prediction for extreme precipitation nowcasting. *Npj Climate and Atmospheric Science*, *7*(1), 282. https://doi.org/10.1038/s41612-024-00834-8

Das, S., & Suganthan, P. N. (2011). Differential Evolution: A Survey of the State-of-the-Art. *IEEE Transactions on Evolutionary Computation*, *15*(1), 4–31. https://doi.org/10.1109/TEVC.2010.2059031

D'Asaro, F., Grillone, G., & Hawkins, R. H. (2014). Curve Number: Empirical Evaluation and Comparison with Curve Number Handbook Tables in Sicily. *Journal of Hydrologic Engineering*, *19*(12), 04014035. https://doi.org/10.1061/(ASCE)HE.1943-5584.0000997

De Hamer, W., Love, D., Owen, R., Booij, M. J., & Hoekstra, A. Y. (2008). Potential water supply of a small reservoir and alluvial aquifer system in southern Zimbabwe. *Physics and Chemistry of the Earth, Parts A/B/C*, *33*(8–13), 633–639. https://doi.org/10.1016/j.pce.2008.06.056

De Moel, H., Van Alphen, J., & Aerts, J. C. J. H. (2009). Flood maps in Europe – methods, availability and use. *Natural Hazards and Earth System Sciences*, *9*(2), 289–301. https://doi.org/10.5194/nhess-9-289-2009

De Vente, J., & Poesen, J. (2005). Predicting soil erosion and sediment yield at the basin scale: Scale issues and semi-quantitative models. *Earth-Science Reviews*, *71*(1–2), 95–125. https://doi.org/10.1016/j.earscirev.2005.02.002

Decharme, B., & Colin, J. (2025). Influence of floodplains and groundwater dynamics on the present-day climate simulated by the CNRM climate model. *Earth System Dynamics*, *16*(3), 729–752. https://doi.org/10.5194/esd-16-729-2025

Descheemaeker, K., Nyssen, J., Poesen, J., Raes, D., Haile, M., Muys, B., & Deckers, S. (2006). Runoff on slopes with restoring vegetation: A case study from the Tigray highlands, Ethiopia. *Journal of Hydrology*, *331*(1–2), 219–241. https://doi.org/10.1016/j.jhydrol.2006.05.015

Detty, J. M., & McGuire, K. J. (2010a). Threshold changes in storm runoff generation at a till-mantled headwater catchment. *Water Resources Research*, *46*(7), 2009WR008102. https://doi.org/10.1029/2009WR008102

Detty, J. M., & McGuire, K. J. (2010b). Threshold changes in storm runoff generation at a till-mantled headwater catchment. *Water Resources Research*, *46*(7), 2009WR008102. https://doi.org/10.1029/2009WR008102

Dewitte, O., Dille, A., Depicker, A., Kubwimana, D., Maki Mateso, J.-C., Mugaruka Bibentyo, T., Uwihirwe, J., & Monsieurs, E. (2021). Constraining landslide timing in a data-scarce context: From recent to very old processes in the tropical environment of the North Tanganyika-Kivu Rift region. *Landslides*, *18*(1), 161–177. https://doi.org/10.1007/s10346-020-01452-0

Di Baldassarre, G., Kooy, M., Kemerink, J. S., & Brandimarte, L. (2013). Towards understanding the dynamic behaviour of floodplains as human-water systems. *Hydrology and Earth System Sciences*, *17*(8), 3235–3244. https://doi.org/10.5194/hess-17-3235-2013

Di Baldassarre, G., Kreibich, H., Vorogushyn, S., Aerts, J., Arnbjerg-Nielsen, K., Barendrecht, M., Bates, P., Borga, M., Botzen, W., Bubeck, P., De Marchi, B., Llasat, C., Mazzoleni, M., Molinari, D., Mondino, E., Mård, J., Petrucci, O., Scolobig, A., Viglione, A., &

Ward, P. J. (2018). Hess Opinions: An interdisciplinary research agenda to explore the unintended consequences of structural flood protection. *Hydrology and Earth System Sciences*, *22*(11), 5629–5637. https://doi.org/10.5194/hess-22-5629-2018

Di Piazza, A., Conti, F. L., Noto, L. V., Viola, F., & La Loggia, G. (2011). Comparative analysis of different techniques for spatial interpolation of rainfall data to create a serially complete monthly time series of precipitation for Sicily, Italy. *International Journal of Applied Earth Observation and Geoinformation*, *13*(3), 396–408. https://doi.org/10.1016/j.jag.2011.01.005

Dinh, T. L. A., & Aires, F. (2022). Nested leave-two-out cross-validation for the optimal crop yield model selection. *Geoscientific Model Development*, *15*(9), 3519–3535. https://doi.org/10.5194/gmd-15-3519-2022

Doocy, S., Daniels, A., Murray, S., & Kirsch, T. D. (2013). The human impact of floods: A historical review of events 1980-2009 and systematic literature review. *PLoS Currents*, *5*, ecurrents.dis.f4deb457904936b07c09daa98ee8171a. https://doi.org/10.1371/currents.dis.f4deb457904936b07c09daa98ee8171a

Dos Santos, P., & Tavares, A. (2015). Basin Flood Risk Management: A Territorial Data-Driven Approach to Support Decision-Making. *Water*, *7*(12), 480–502. https://doi.org/10.3390/w7020480

Douglas, I., Alam, K., Maghenda, M., Mcdonnell, Y., Mclean, L., & Campbell, J. (2008). Unjust waters: Climate change, flooding and the urban poor in Africa. *Environment and Urbanization*, *20*(1), 187–205. https://doi.org/10.1177/0956247808089156

Douinot, A., Iffly, J. F., Tailliez, C., Meisch, C., & Pfister, L. (2022). Flood patterns in a catchment with mixed bedrock geology and a hilly landscape: Identification of flashy runoff contributions during storm events. *Hydrology and Earth System Sciences*, *26*(19), 5185–5206. https://doi.org/10.5194/hess-26-5185-2022

Duc, T. A., Khiem, M. V., Hung, M. K., Quan, D. D., Trang, D. T., Nam, H. G., Hole, L. R., & Tien, D. D. (2025). Skill Validation of High-Impact Rainfall Forecasts over Vietnam Using the European Centre for Medium-Range Weather Forecasts (ECMWF) Integrated Forecasting System (IFS) and Dynamical Downscaling with the Weather Research and Forecasting Model. *Atmosphere*, *16*(2), 224. https://doi.org/10.3390/atmos16020224

Dufatanye Umwali, E., Chen, X., Odhiambo Ayugi, B., Mumo, R., Babaousmail, H., Mbigi, D., & Izere, D. (2024). Estimating the Effects of Climate Fluctuations on Precipitation and Temperature in East Africa. *Atmosphere*, *15*(12), 1455. https://doi.org/10.3390/atmos15121455

Dulawan, J. M. T., Imamura, Y., Konishi, T., Amaguchi, H., & Ohara, M. (2024). A systematic framework for assessing social vulnerability to flood for integrated flood risk management: A case study in Metro Manila, Philippines. *International Journal of Disaster Risk Reduction*, *112*, 104778. https://doi.org/10.1016/j.ijdrr.2024.104778

Dunne, T., & Black, R. D. (1970). An Experimental Investigation of Runoff Production in Permeable Soils. *Water Resources Research*, *6*(2), 478–490. https://doi.org/10.1029/wr006i002p00478

Dwivedi, D., Poeppl, R. E., & Wohl, E. (2025). Hydrological connectivity: A review and emerging strategies for integrating measurement, modeling, and management. *Frontiers in Water*, *7*, 1496199. https://doi.org/10.3389/frwa.2025.1496199

Ebert, E., Wilson, L., Weigel, A., Mittermaier, M., Nurmi, P., Gill, P., Göber, M., Joslyn, S., Brown, B., Fowler, T., & Watkins, A. (2013). Progress and challenges in forecast verification. *Meteorological Applications*, *20*(2), 130–139. https://doi.org/10.1002/met.1392

Eckhardt, K. (2005). How to construct recursive digital filters for baseflow separation. *Hydrological Processes*, *19*(2), 507–515. https://doi.org/10.1002/hyp.5675

Edijatno, & Michel, C. (1989). Un modèle pluie-débit journalier à trois paramètres. *La Houille Blanche*, *75*(2), 113–122. https://doi.org/10.1051/lhb/1989007

Efron, B., & Tibshirani, R. (1993). *An introduction to the bootstrap*. Chapman & Hall.

Efstratiadis, A., & Koutsoyiannis, D. (2010). One decade of multi-objective calibration approaches in hydrological modelling: A review. *Hydrological Sciences Journal*, *55*(1), 58–78. https://doi.org/10.1080/02626660903526292

Ekwule, O. R., & Agunwamba, J. C. (2024). Application of the NRCS-curve number method in humid tropical basins of southeastern Nigeria: A statistical analysis. *Environmental Systems Research*, *13*(1), 52. https://doi.org/10.1186/s40068-024-00386-z

Engida, A. N. (2010). *Hydrological and Suspended Sediment Modeling in the Lake Tana Basin, Ethiopia* [Ph.D. Thesis]. https://theses.hal.science/tel-00539152v1

Esri Land Cover (arcgis.com). (2024). *Https://livingatlas.arcgis.com/landcover/* [Dataset].

Evin, G., Le Lay, M., Fouchier, C., Penot, D., Colleoni, F., Mas, A., Garambois, P.-A., & Laurantin, O. (2024). Evaluation of hydrological models on small mountainous catchments: Impact of the meteorological forcings. *Hydrology and Earth System Sciences*, *28*(1), 261–281. https://doi.org/10.5194/hess-28-261-2024

Fan, Y., & Bras, R. L. (1998). Analytical solutions to hillslope subsurface storm flow and saturation overland flow. *Water Resources Research*, *34*(4), 921–927. https://doi.org/10.1029/97WR03516

Fan, Y., Clark, M., Lawrence, D. M., Swenson, S., Band, L. E., Brantley, S. L., Brooks, P. D., Dietrich, W. E., Flores, A., Grant, G., Kirchner, J. W., Mackay, D. S., McDonnell, J. J., Milly, P. C. D., Sullivan, P. L., Tague, C., Ajami, H., Chaney, N., Hartmann, A., … Yamazaki, D. (2019). Hillslope Hydrology in Global Change Research and Earth System Modeling. *Water Resources Research*, *55*(2), 1737–1772. https://doi.org/10.1029/2018WR023903

FAO. (2021). *Strategic Framework 2022-31*.

Farmani, M. A., Behrangi, A., Gupta, A., Tavakoly, A., Geheran, M., & Niu, G.-Y. (2025). Do land models miss key soil hydrological processes controlling soil moisture memory? *Hydrology and Earth System Sciences*, *29*(2), 547–566. https://doi.org/10.5194/hess-29-547-2025

Farran, M. M., & Elfeki, A. M. (2020). Evaluation and validity of the antecedent moisture condition (AMC) of Natural Resources Conservation Service-Curve Number (NRCS-CN) procedure in undeveloped arid basins. *Arabian Journal of Geosciences*, *13*(6), 275. https://doi.org/10.1007/s12517-020-5242-y

Fatchurohman, H., Adji, T. N., Haryono, E., & Wijayanti, P. (2018). Baseflow index assessment and master recession curve analysis for karst water management in Kakap Spring, Gunung Sewu. *IOP Conference Series: Earth and Environmental Science*, *148*, 012029. https://doi.org/10.1088/1755-1315/148/1/012029

Fathi, M. M., Al Mehedi, M. A., Smith, V., Fernandes, A. M., Hren, M. T., & Terry, D. O. (2025). Evaluation of LSTM vs. Conceptual models for hourly rainfall runoff simulations with varied training period lengths. *Scientific Reports*, *15*(1), 15820. https://doi.org/10.1038/s41598-025-96577-4

Filipova, V., Lawrence, D., & Skaugen, T. (2019). A stochastic event-based approach for flood estimation in catchments with mixed rainfall and snowmelt flood regimes. *Natural Hazards and Earth System Sciences*, *19*(1), 1–18. https://doi.org/10.5194/nhess-19-1-2019

Fleischmann, A. S., Paiva, R. C. D., Collischonn, W., Sorribas, M. V., & Pontes, P. R. M. (2016). On river-floodplain interaction and hydrograph skewness: FLOODPLAINS AND HYDROGRAPH SKEWNESS. *Water Resources Research*, *52*(10), 7615–7630. https://doi.org/10.1002/2016WR019233

François Birgand. (2012). Uncertainties on flow calculated from stage-discharge rating curves in small streams. *2012 Dallas, Texas, July 29 - August 1, 2012*. 2012 Dallas, Texas, July 29 - August 1, 2012. https://doi.org/10.13031/2013.41754

François, M., Junior, T. R. D. A., Mielke, M. S., Rousseau, A. N., Faria, D., & Mariano-Neto, E. (2024). *Interactions between Forest Cover and Watershed Hydrology: A State-of-the-Art Review*. Environmental and Earth Sciences. https://doi.org/10.20944/preprints202409.0165.v1

Froehlich, D. C. (2016). Predicting Peak Discharge from Gradually Breached Embankment Dam. *Journal of Hydrologic Engineering*, *21*(11), 04016041. https://doi.org/10.1061/(ASCE)HE.1943-5584.0001424

Fryirs, K., & Brierley, G. (2022). Assemblages of geomorphic units: A building block approach to analysis and interpretation of river character, behaviour, condition and recovery. *Earth Surface Processes and Landforms*, *47*(1), 92–108. https://doi.org/10.1002/esp.5264

Gardner, W. P., Jensco, K., H. Hoylman, Z., Livesay, R., & P. Maneta, M. (2020). A numerical investigation of bedrock groundwater recharge and exfiltration on soil mantled hillslopes. *Hydrological Processes*, *34*(15), 3311–3330. https://doi.org/10.1002/hyp.13799

Garnero, G., & Godone, D. (2014). COMPARISONS BETWEEN DIFFERENT INTERPOLATION TECHNIQUES. *The International Archives of the Photogrammetry, Remote Sensing and Spatial Information Sciences*, *XL-5/W3*, 139–144. https://doi.org/10.5194/isprsarchives-XL-5-W3-139-2013

Garzon, L. F. L., Johnson, M. F., Mount, N., & Gomez, H. (2023). Exploring the effects of catchment morphometry on overland flow response to extreme rainfall using a 2D

hydraulic-hydrological model (IBER). *Journal of Hydrology*, *627*, 130405. https://doi.org/10.1016/j.jhydrol.2023.130405

Geekiyanage, N., Gunarathna, M. H. J. P., Ranagalage, M., Jayasinghe, G. Y., Perera, M. P., & Vithanage, M. (2025). *Tank Cascade Systems of Sri Lanka: A Globally Important Agricultural Heritage System* (1st ed.). CRC Press. https://doi.org/10.1201/9781003516019

Georg, J., Berghoff, B. A., & Schindler, D. (2025). Harnessing Small RNAs as Synthetic Post-transcriptional Regulators in Bacteria. *ACS Synthetic Biology*, *14*(7), 2405–2417. https://doi.org/10.1021/acssynbio.5c00118

Gericke, O. J., & Smithers, J. C. (2014a). Review of methods used to estimate catchment response time for the purpose of peak discharge estimation. *Hydrological Sciences Journal*, *59*(11), 1935–1971. https://doi.org/10.1080/02626667.2013.866712

Gericke, O. J., & Smithers, J. C. (2014b). Review of methods used to estimate catchment response time for the purpose of peak discharge estimation. *Hydrological Sciences Journal*, *59*(11), 1935–1971. https://doi.org/10.1080/02626667.2013.866712

Gichamo, T., Nourani, V., Gökçekuş, H., & Gelete, G. (2024). Ensemble of artificial intelligence and physically based models for rainfall–runoff modeling in the upper Blue Nile Basin. *Hydrology Research*, *55*(10), 976–1000. https://doi.org/10.2166/nh.2024.189

Gnecco, I., Palla, A., & La Barbera, P. (2018). A dimensionless approach for the runoff peak assessment: Effects of the rainfall event structure. *Hydrology and Earth System Sciences*, *22*(2), 943–956. https://doi.org/10.5194/hess-22-943-2018

Goyal, M. K. (2016). *Engineering hydrology*. Asoke K. Ghosh, PHI Learning Private Limited.

GPM IMERG. (n.d.). *IMERG precipitation algorithm and the Global Precipitation Measurement (GPM) Mission* [Dataset].

Grimaldi, S., & Petroselli, A. (2015). Do we still need the Rational Formula? An alternative empirical procedure for peak discharge estimation in small and ungauged basins. *Hydrological Sciences Journal*, *60*(1), 67–77. https://doi.org/10.1080/02626667.2014.880546

Gudmundsson, L., & Seneviratne, S. I. (2015). Towards observation-based gridded runoff estimates for Europe. *Hydrology and Earth System Sciences*, *19*(6), 2859–2879. https://doi.org/10.5194/hess-19-2859-2015

Guimarães Nobre, G., Pasqui, M., Quaresima, S., Pieretto, S., & Lemos Pereira Bonifácio, R. M. (2023). Forecasting, thresholds, and triggers: Towards developing a Forecast-based Financing system for droughts in Mozambique. *Climate Services*, *30*, 100344. https://doi.org/10.1016/j.cliser.2023.100344

Gupta, H. V., Kling, H., Yilmaz, K. K., & Martinez, G. F. (2009). Decomposition of the mean squared error and NSE performance criteria: Implications for improving hydrological modelling. *Journal of Hydrology*, *377*(1–2), 80–91. https://doi.org/10.1016/j.jhydrol.2009.08.003

Gupta, H. V., Sorooshian, S., & Yapo, P. O. (1998). Toward improved calibration of hydrologic models: Multiple and noncommensurable measures of information. *Water Resources Research*, *34*(4), 751–763. https://doi.org/10.1029/97WR03495

Gupta, H. V., Sorooshian, S., & Yapo, P. O. (1999). Status of Automatic Calibration for Hydrologic Models: Comparison with Multilevel Expert Calibration. *Journal of Hydrologic Engineering*, *4*(2), 135–143. https://doi.org/10.1061/(ASCE)1084-0699(1999)4:2(135)

Habets, F., Noilhan, J., Golaz, C., Goutorbe, J. P., Lacarrère, P., Leblois, E., Ledoux, E., Martin, E., Ottlé, C., & Vidal-Madjar, D. (1999). The ISBA surface scheme in a macroscale

hydrological model applied to the Hapex-Mobilhy area. *Journal of Hydrology*, *217*(1–2), 75–96. https://doi.org/10.1016/S0022-1694(99)00019-0

Haddad, K., Rahman, A., A Zaman, M., & Shrestha, S. (2013). Applicability of Monte Carlo cross validation technique for model development and validation using generalised least squares regression. *Journal of Hydrology*, *482*, 119–128. https://doi.org/10.1016/j.jhydrol.2012.12.041

Hahirwabasenga, J., Nilsson, E., Larson, M., Bizimana, H., Wali, U. G., & Persson, M. (2024). Flooding in Sebeya catchment, Rwanda—A review of causes, impacts, and management. *International Journal of Disaster Risk Reduction*, *114*, 105012. https://doi.org/10.1016/j.ijdrr.2024.105012

Haile, A. T., Rientjes, T., Gieske, A., & Gebremichael, M. (2009). Rainfall Variability over Mountainous and Adjacent Lake Areas: The Case of Lake Tana Basin at the Source of the Blue Nile River. *Journal of Applied Meteorology and Climatology*, *48*(8), 1696–1717. https://doi.org/10.1175/2009JAMC2092.1

Hajani, E., & Rahman, A. (2018). Design rainfall estimation: Comparison between GEV and LP3 distributions and at-site and regional estimates. *Natural Hazards*, *93*(1), 67–88. https://doi.org/10.1007/s11069-018-3289-9

Halwatura, D., & Najim, M. M. M. (2013). Application of the HEC-HMS model for runoff simulation in a tropical catchment. *Environmental Modelling & Software*, *46*, 155–162. https://doi.org/10.1016/j.envsoft.2013.03.006

Han, W. S., & Burian, S. J. (2009). Determining Effective Impervious Area for Urban Hydrologic Modeling. *Journal of Hydrologic Engineering*, *14*(2), 111–120. https://doi.org/10.1061/(ASCE)1084-0699(2009)14:2(111)

Han, X., Liu, J., Srivastava, P., Liu, H., Li, X., Shen, X., & Tan, H. (2021). The Dominant Control of Relief on Soil Water Content Distribution During Wet-Dry Transitions in

Headwaters. *Water Resources Research*, *57*(11), e2021WR029587. https://doi.org/10.1029/2021WR029587

Hawkins, R. H., Ward, T. J., Grillone, G., D'Asaro, F., & Shaked, M. (2015). Standard Asymptotic Response and Expected Runoff from Curve Number Theory. *Watershed Management 2015*, 182–193. https://doi.org/10.1061/9780784479322.017

He, M., Xu, X., Wu, S., Kang, C., & Huang, B. (2025). Multi-step ahead forecasting of daily streamflow based on the transform-based deep learning model under different scenarios. *Scientific Reports*, *15*(1), 5451. https://doi.org/10.1038/s41598-025-89837-w

Henrike, B. (2012). *Natural Hazards, Risk Analysis and Emergency Preparedness: Natural Hazards, Risk Analysis and Emergency Preparedness: Applying Spatial Methods in Disaster Risk Management APPLYING SPATIAL METHODS IN DISASTER RISK MANAGEMENT APPLYING SPATIAL METHODS IN DISASTER RISK MANAGEMENT* [LSU Doctoral Dissertation]. https://repository.lsu.edu/gradschool_dissertations/2972

Herman, J. D., Reed, P. M., & Wagener, T. (2013). Time-varying sensitivity analysis clarifies the effects of watershed model formulation on model behavior. *Water Resources Research*, *49*(3), 1400–1414. https://doi.org/10.1002/wrcr.20124

Herman, J., & Usher, W. (2017). SALib: An open-source Python library for Sensitivity Analysis. *The Journal of Open Source Software*, *2*(9), 97. https://doi.org/10.21105/joss.00097

Hishamunda, S., Fashaho, A., Uwihirwe, J., Bugenimana, E. D., Mpambara Musinga, C., & Munyandamutsa, P. (2024). Controlling soil erosion and landslides through ecosystem-based adaptation interventions in the hilly landscape of western Rwanda. *Soil Advances*, *2*, 100020. https://doi.org/10.1016/j.soilad.2024.100020

Hrachowitz, M., Savenije, H. H. G., Blöschl, G., McDonnell, J. J., Sivapalan, M., Pomeroy, J. W., Arheimer, B., Blume, T., Clark, M. P., Ehret, U., Fenicia, F., Freer, J. E., Gelfan, A., Gupta, H. V., Hughes, D. A., Hut, R. W., Montanari, A., Pande, S., Tetzlaff, D., … Cudennec, C. (2013a). A decade of Predictions in Ungauged Basins (PUB)—A review. *Hydrological Sciences Journal*, *58*(6), 1198–1255. https://doi.org/10.1080/02626667.2013.803183

Hrachowitz, M., Savenije, H. H. G., Blöschl, G., McDonnell, J. J., Sivapalan, M., Pomeroy, J. W., Arheimer, B., Blume, T., Clark, M. P., Ehret, U., Fenicia, F., Freer, J. E., Gelfan, A., Gupta, H. V., Hughes, D. A., Hut, R. W., Montanari, A., Pande, S., Tetzlaff, D., … Cudennec, C. (2013b). A decade of Predictions in Ungauged Basins (PUB)—A review. *Hydrological Sciences Journal*, *58*(6), 1198–1255. https://doi.org/10.1080/02626667.2013.803183

Hrour, Y., Thomas, Z., Rousseau-Gueutin, P., Ait-Brahim, Y., & Fovet, O. (2025). Enhancing hydrological modeling with bias-corrected satellite weather data in data-scarce catchments: A comparative analysis of SWAT and GR4J models. *Frontiers in Water*, *7*, 1582589. https://doi.org/10.3389/frwa.2025.1582589

https://ng.fieldclimate.com. (2023). *Https://ng.fieldclimate.com* [Dataset]. https://ng.fieldclimate.com/dashboard

Hu, S., & Shrestha, P. (2020). Examine the impact of land use and land cover changes on peak discharges of a watershed in the midwestern United States using the HEC-HMS model. *Papers in Applied Geography*, *6*(2), 101–118. https://doi.org/10.1080/23754931.2020.1732447

Huang, Y., Bárdossy, A., & Zhang, K. (2019). Sensitivity of hydrological models to temporal and spatial resolutions of rainfall data. *Hydrology and Earth System Sciences*, *23*(6), 2647–2663. https://doi.org/10.5194/hess-23-2647-2019

Hydrological Model FAQ. (2025, August 14). https://hydroclimat.com/en/faq/hydrological-model/?utm_source=chatgpt.com

Immerzeel, W. W., Van Beek, L. P. H., & Bierkens, M. F. P. (2010). Climate Change Will Affect the Asian Water Towers. *Science*, *328*(5984), 1382–1385. https://doi.org/10.1126/science.1183188

Iradukunda, P., Mwanaumo, E. M., & Kabika, J. (2024). Modelling the future climate impacts on hydraulic infrastructure development in tropical (peri-)urban region: Case of Kigali, Rwanda. *Heliyon*, *10*(5), e27126. https://doi.org/10.1016/j.heliyon.2024.e27126

Ismail Dhaqane, A., Murshed, M. F., Mourad, K. A., & Abd Manan, T. S. B. (2023). Assessment of the Streamflow and Evapotranspiration at Wabiga Juba Basin Using a Water Evaluation and Planning (WEAP) Model. *Water*, *15*(14), 2594. https://doi.org/10.3390/w15142594

Itsukushima, R. (2021). Characteristics and Controlling Factors of the Drought Runoff Coefficient. *Water*, *13*(9), 1259. https://doi.org/10.3390/w13091259

Jacobs, L., Maes, J., Mertens, K., Sekajugo, J., Thiery, W., Van Lipzig, N., Poesen, J., Kervyn, M., & Dewitte, O. (2016). Reconstruction of a flash flood event through a multi-hazard approach: Focus on the Rwenzori Mountains, Uganda. *Natural Hazards*, *84*(2), 851–876. https://doi.org/10.1007/s11069-016-2458-y

Jacobs, S. R., Timbe, E., Weeser, B., Rufino, M. C., Butterbach-Bahl, K., & Breuer, L. (2018). Assessment of hydrological pathways in East African montane catchments under different land use. *Hydrology and Earth System Sciences*, *22*(9), 4981–5000. https://doi.org/10.5194/hess-22-4981-2018

Jain, M. K., Mishra, S. K., Suresh Babu, P., Venugopal, K., & Singh, V. P. (2006). Enhanced Runoff Curve Number Model Incorporating Storm Duration and a Nonlinear Ia-S

Relation. *Journal of Hydrologic Engineering*, *11*(6), 631–635. https://doi.org/10.1061/(ASCE)1084-0699(2006)11:6(631)

Jain Sharad Kumar & Sudheer K.P. (2008). *Fitting of Hydrologic Models: A Close Look at the Nash–Sutcliffe Index*. *13*, 981–986. https://doi.org/10.1061/ASCE1084-0699(2008)13:10(981)

James, G., Witten, D., Hastie, T., Tibshirani, R., & Taylor, J. E. (2023). *An introduction to statistical learning: With applications in Python*. Springer.

Jansson, R., Backx, H., Boulton, A. J., Dixon, M., Dudgeon, D., Hughes, F. M. R., Nakamura, K., Stanley, E. H., & Tockner, K. (2005). Stating mechanisms and refining criteria for ecologically successful river restoration: A comment on Palmer *et al* . (2005). *Journal of Applied Ecology*, *42*(2), 218–222. https://doi.org/10.1111/j.1365-2664.2005.01022.x

Jencso, K. G., & McGlynn, B. L. (2011). Hierarchical controls on runoff generation: Topographically driven hydrologic connectivity, geology, and vegetation. *Water Resources Research*, *47*(11), 2011WR010666. https://doi.org/10.1029/2011WR010666

Jencso, K. G., McGlynn, B. L., Gooseff, M. N., Wondzell, S. M., Bencala, K. E., & Marshall, L. A. (2009). Hydrologic connectivity between landscapes and streams: Transferring reach- and plot-scale understanding to the catchment scale. *Water Resources Research*, *45*(4), 2008WR007225. https://doi.org/10.1029/2008WR007225

Jeon, J.-H., Lim, K., & Engel, B. (2014). Regional Calibration of SCS-CN L-THIA Model: Application for Ungauged Basins. *Water*, *6*(5), 1339–1359. https://doi.org/10.3390/w6051339

Jha, D. N., Das, S. C. S., Srivastava, K., Kumar, V., Sahoo, A. K., Srivastava, R. S., & Das, B. K. (2022). Environmental flow estimation through a hydrology-based method in the Tamas River at Bakiya Barrage, Madhya Pradesh, India. *Aquatic Ecosystem Health & Management*, *25*(2), 70–77. https://doi.org/10.14321/aehm.025.02.70

Jie, M.-X., Chen, H., Xu, C.-Y., Zeng, Q., & Tao, X. (2016). A comparative study of different objective functions to improve the flood forecasting accuracy. *Hydrology Research*, *47*(4), 718–735. https://doi.org/10.2166/nh.2015.078

Jolliffe, I. T., & Stephenson, D. B. (Eds.). (2011). *Forecast Verification: A Practitioner's Guide in Atmospheric Science* (1st ed.). Wiley. https://doi.org/10.1002/9781119960003

Jongman, B., Winsemius, H. C., Aerts, J. C. J. H., Coughlan De Perez, E., Van Aalst, M. K., Kron, W., & Ward, P. J. (2015). Declining vulnerability to river floods and the global benefits of adaptation. *Proceedings of the National Academy of Sciences*, *112*(18). https://doi.org/10.1073/pnas.1414439112

Kameyama, T., Kumagai, T., Egusa, T., & Momiyama, H. (2025). Importance of bedrock hydrology for the rainfall–runoff process in a forested mountain catchment. *Journal of Hydrology*, 134205. https://doi.org/10.1016/j.jhydrol.2025.134205

Kang, M., & Yoo, C. (2023). Use of Nonofficial Intermittent Waterfall Occurrence Data for the Validation of an Infiltration Model for Volcanic Jeju Island, Korea. *Water*, *15*(12), 2260. https://doi.org/10.3390/w15122260

Kanishka, G., & Eldho, T. I. (2020). Streamflow estimation in ungauged basins using watershed classification and regionalization techniques. *Journal of Earth System Science*, *129*(1), 186. https://doi.org/10.1007/s12040-020-01451-8

Kapoor, A., Pathiraja, S., Marshall, L., & Chandra, R. (2023). DeepGR4J: A deep learning hybridization approach for conceptual rainfall-runoff modelling. *Environmental Modelling & Software*, *169*, 105831. https://doi.org/10.1016/j.envsoft.2023.105831

Karamage, F., Shao, H., Chen, X., Ndayisaba, F., Nahayo, L., Kayiranga, A., Omifolaji, J., Liu, T., & Zhang, C. (2016). Deforestation Effects on Soil Erosion in the Lake Kivu Basin, D.R. Congo-Rwanda. *Forests*, *7*(11), 281. https://doi.org/10.3390/f7110281

Karamage, F., Zhang, C., Fang, X., Liu, T., Ndayisaba, F., Nahayo, L., Kayiranga, A., & Nsengiyumva, J. (2017). Modeling Rainfall-Runoff Response to Land Use and Land Cover Change in Rwanda (1990–2016). *Water*, *9*(2), 147. https://doi.org/10.3390/w9020147

Karamage, F., Zhang, C., Ndayisaba, F., Shao, H., Kayiranga, A., Fang, X., Nahayo, L., Muhire Nyesheja, E., & Tian, G. (2016). Extent of Cropland and Related Soil Erosion Risk in Rwanda. *Sustainability*, *8*(7), 609. https://doi.org/10.3390/su8070609

Karamouz, M., Moridi, A., & Nazif, S. (2010a). *Urban Water Engineering and Management* (0 ed.). CRC Press. https://doi.org/10.1201/b15857

Karamouz, M., Moridi, A., & Nazif, S. (2010b). *Urban Water Engineering and Management* (0 ed.). CRC Press. https://doi.org/10.1201/b15857

Keoduangsine, S., Robert, R., & Stephen, P. G. (2014). A Review of Flood Warning Systems in Developed and Developing Countries. *International Journal of Future Computer and Communication*, *3*(3), 172–176. https://doi.org/10.7763/IJFCC.2014.V3.290

Khattab, M. I., Fadl, M. E., Megahed, H. A., Saleem, A. M., El-Saadawy, O., Drosos, M., Scopa, A., & Selim, M. K. (2025). Evaluation of the Soil Conservation Service Curve Number (SCS-CN) Method for Flash Flood Runoff Estimation in Arid Regions: A Case Study of Central Eastern Desert, Egypt. *Hydrology*, *12*(3), 54. https://doi.org/10.3390/hydrology12030054

Kidanie, Y., Grum, B., & Yemane, S. (2022a). Hydrologic and hydraulic assessment of scour problems at bridge sites in Tigray region, northern Ethiopia. *Journal of Applied Water Engineering and Research*, *10*(2), 144–156. https://doi.org/10.1080/23249676.2021.1956378

Kidanie, Y., Grum, B., & Yemane, S. (2022b). Hydrologic and hydraulic assessment of scour problems at bridge sites in Tigray region, northern Ethiopia. *Journal of Applied Water*

Engineering and Research, *10*(2), 144–156. https://doi.org/10.1080/23249676.2021.1956378

Kim, B., Lee, G., Lee, Y., Kim, S., & Noh, S. J. (2024). Assessment of the Impact of Spatial Variability on Streamflow Predictions Using High-Resolution Modeling and Parameter Estimation: Case Study of Geumho River Catchment, South Korea. *Water*, *16*(4), 591. https://doi.org/10.3390/w16040591

Kim, C., & Kim, D.-H. (2020). Effects of Rainfall Spatial Distribution on the Relationship between Rainfall Spatiotemporal Resolution and Runoff Prediction Accuracy. *Water*, *12*(3), 846. https://doi.org/10.3390/w12030846

Kim, K.-H., Andreadis, K. M., & O'Loughlin, F. (2025). Predicting annual peak daily streamflow in natural basins using quantile regression forests. *Journal of Hydrology*, *660*, 133233. https://doi.org/10.1016/j.jhydrol.2025.133233

Knapp, J. L. A., Berghuijs, W. R., Floriancic, M. G., & Kirchner, J. W. (2025). Catchment hydrological response and transport are affected differently by precipitation intensity and antecedent wetness. *Hydrology and Earth System Sciences*, *29*(15), 3673–3685. https://doi.org/10.5194/hess-29-3673-2025

Knighton, D. (2014). *Fluvial Forms and Processes* (0 ed.). Routledge. https://doi.org/10.4324/9780203784662

Knoben, W. J. M., Freer, J. E., & Woods, R. A. (2019a). Technical note: Inherent benchmark or not? Comparing Nash–Sutcliffe and Kling–Gupta efficiency scores. *Hydrology and Earth System Sciences*, *23*(10), 4323–4331. https://doi.org/10.5194/hess-23-4323-2019

Knoben, W. J. M., Freer, J. E., & Woods, R. A. (2019b). *Technical note: Inherent benchmark or not? Comparing Nash-Sutcliffe and Kling-Gupta efficiency scores*. Catchment hydrology/Modelling approaches. https://doi.org/10.5194/hess-2019-327

Kodja, D. J., Akognongbé, A. J. S., Amoussou, E., Mahé, G., Vissin, E. W., Paturel, J.-E., & Houndénou, C. (2020). Calibration of the hydrological model GR4J from potential evapotranspiration estimates by the Penman-Monteith and Oudin methods in the Ouémé watershed (West Africa). *Proceedings of the International Association of Hydrological Sciences*, *383*, 163–169. https://doi.org/10.5194/piahs-383-163-2020

Kong, X., Yang, J., Xu, K., Dong, B., & Jiang, S. (2023). A Bayesian updating framework for calibrating the hydrological parameters of road networks using taxi GPS data. *Hydrology and Earth System Sciences*, *27*(20), 3803–3822. https://doi.org/10.5194/hess-27-3803-2023

Kosugi, K., Katsura, S., Katsuyama, M., & Mizuyama, T. (2006). Water flow processes in weathered granitic bedrock and their effects on runoff generation in a small headwater catchment. *Water Resources Research*, *42*(2), 2005WR004275. https://doi.org/10.1029/2005WR004275

Koutalakis, P., & Zaimes, G. N. (2022). River Flow Measurements Utilizing UAV-Based Surface Velocimetry and Bathymetry Coupled with Sonar. *Hydrology*, *9*(8), 148. https://doi.org/10.3390/hydrology9080148

Krzysztofowicz, R. (1999). Bayesian Forecasting via Deterministic Model. *Risk Analysis*, *19*(4), 739–749. https://doi.org/10.1023/A:1007050023440

Kuana, L. A., Almeida, A. S., Mercuri, E. G. F., & Noe, S. M. (2024). Regionalization of GR4J model parameters for river flow prediction in Paraná, Brazil. *Hydrology and Earth System Sciences*, *28*(14), 3367–3390. https://doi.org/10.5194/hess-28-3367-2024

Kumar, A., Anand, A., Singh, R. V., Kumar, R., & Gohil, M. (2025). Vegetation hydrology and slope interaction under variable infiltration: A state-of-the-art review. *Journal of Infrastructure Preservation and Resilience*, *6*(1), 33. https://doi.org/10.1186/s43065-025-00152-0

Kundzewicz, Z. W., Kanae, S., Seneviratne, S. I., Handmer, J., Nicholls, N., Peduzzi, P., Mechler, R., Bouwer, L. M., Arnell, N., Mach, K., Muir-Wood, R., Brakenridge, G. R., Kron, W., Benito, G., Honda, Y., Takahashi, K., & Sherstyukov, B. (2014). Flood risk and climate change: Global and regional perspectives. *Hydrological Sciences Journal*, *59*(1), 1–28. https://doi.org/10.1080/02626667.2013.857411

Kundzewicz, Z. W., & Robson, A. J. (2004). Change detection in hydrological records—A review of the methodology / Revue méthodologique de la détection de changements dans les chroniques hydrologiques. *Hydrological Sciences Journal*, *49*(1), 7–19. https://doi.org/10.1623/hysj.49.1.7.53993

Kundzewicz, Z. W., & Takeuchi, K. (1999). Flood protection and management: Quo vadimus? *Hydrological Sciences Journal*, *44*(3), 417–432. https://doi.org/10.1080/02626669909492237

Kurian, C., Sudheer, K. P., Vema, V. K., & Sahoo, D. (2020). Effective flood forecasting at higher lead times through hybrid modelling framework. *Journal of Hydrology*, *587*, 124945. https://doi.org/10.1016/j.jhydrol.2020.124945

Ladouche B., Probst A., Viville D., Idir S., Baqué D., Loubet M., Probst J.-L., & Bariac T. (2001). Hydrograph separation using isotopic, chemical and hydrological approaches (Strengbach catchment, France). *Journal of Hydrology*. https://doi.org/10.1016/S0022-1694(00)00391-7

Lane, E. W. (1955). Design of Stable Channels. *Transactions of the American Society of Civil Engineers*, *120*(1), 1234–1260. https://doi.org/10.1061/TACEAT.0007188

Lane, S. N., Odoni, N., Landström, C., Whatmore, S. J., Ward, N., & Bradley, S. (2011). Doing flood risk science differently: An experiment in radical scientific method. *Transactions of the Institute of British Geographers*, *36*(1), 15–36. https://doi.org/10.1111/j.1475-5661.2010.00410.x

Lee, J., & Kim, B. (2021). Scenario-Based Real-Time Flood Prediction with Logistic Regression. *Water*, *13*(9), 1191. https://doi.org/10.3390/w13091191

Lee, J.-Y., & Kim, J.-S. (2021). Detecting Areas Vulnerable to Flooding Using Hydrological-Topographic Factors and Logistic Regression. *Applied Sciences*, *11*(12), 5652. https://doi.org/10.3390/app11125652

Leopold, L. B., Wolman, M. G., & Miller, J. P. (1995). *Fluvial processes in geomorphology*. Dover publ.

Letsinger, S. L., Balberg, A., Hanna, E., & Hiatt, E. K. (2021). Geohydrology: Watershed Hydrology. In *Encyclopedia of Geology* (pp. 442–456). Elsevier. https://doi.org/10.1016/B978-0-12-409548-9.12389-9

Li, C. Z., Zhang, L., Wang, H., Zhang, Y. Q., Yu, F. L., & Yan, D. H. (2012). The transferability of hydrological models under nonstationary climatic conditions. *Hydrology and Earth System Sciences*, *16*(4), 1239–1254. https://doi.org/10.5194/hess-16-1239-2012

Li, W., Liu, C., Hu, C., Niu, C., Li, R., Li, M., Xu, Y., & Tian, L. (2024). Application of a hybrid algorithm of LSTM and Transformer based on random search optimization for improving rainfall-runoff simulation. *Scientific Reports*, *14*(1), 11184. https://doi.org/10.1038/s41598-024-62127-7

Lin, P., Shi, P., Yang, T., Xu, C.-Y., Li, Z., & Wang, X. (2020). A Statistical Vertically Mixed Runoff Model for Regions Featured by Complex Runoff Generation Process. *Water*, *12*(9), 2324. https://doi.org/10.3390/w12092324

Liu, J., Koch, J., Stisen, S., Troldborg, L., & Schneider, R. J. M. (2024). A national-scale hybrid model for enhanced streamflow estimation – consolidating a physically based hydrological model with long short-term memory (LSTM) networks. *Hydrology and Earth System Sciences*, *28*(13), 2871–2893. https://doi.org/10.5194/hess-28-2871-2024

Liu, T., Li, B., Jin, L., Wang, S., Wen, J., & Wang, H. (2022). Estimation of probable maximum precipitation of a high-mountain basin in a changing climate. *Hydrology Research*, *53*(1), 221–240. https://doi.org/10.2166/nh.2021.084

Liu, Y., Chang, Y., Haag, I., Krumm, J., Sivaprasad, V., Aigner, D., Vereecken, H., & Hendricks Franssen, H.-J. (2025). Historical memory in remotely sensed soil moisture can enhance flash flood modeling for headwater catchments in Germany. *Journal of Hydrology*, *648*, 132395. https://doi.org/10.1016/j.jhydrol.2024.132395

Lombana, L., Bhattacharya, B., Alfonso, L., & Martínez-Graña, A. (2024). Hydrogeomorphological approach for flood analyses at high- detailed scale: Narrow rivers with broad complex alluvial plains. *CATENA*, *242*, 108081. https://doi.org/10.1016/j.catena.2024.108081

Lørup, J. K., Refsgaard, J. C., & Mazvimavi, D. (1998). Assessing the effect of land use change on catchment runoff by combined use of statistical tests and hydrological modelling: Case studies from Zimbabwe. *Journal of Hydrology*, *205*(3–4), 147–163. https://doi.org/10.1016/S0168-1176(97)00311-9

Luong, T. T., Pöschmann, J., Kronenberg, R., & Bernhofer, C. (2021a). Rainfall Threshold for Flash Flood Warning Based on Model Output of Soil Moisture: Case Study Wernersbach, Germany. *Water*, *13*(8), 1061. https://doi.org/10.3390/w13081061

Luong, T. T., Pöschmann, J., Kronenberg, R., & Bernhofer, C. (2021b). Rainfall Threshold for Flash Flood Warning Based on Model Output of Soil Moisture: Case Study Wernersbach, Germany. *Water*, *13*(8), 1061. https://doi.org/10.3390/w13081061

Macharia, D., Mugabo, L., Kasiti, F., Noriega, A., MacDonald, L., & Thomas, E. (2023). Streamflow and flood prediction in Rwanda using machine learning and remote sensing in support of rural first-mile transport connectivity. *Frontiers in Climate*, *5*, 1158186. https://doi.org/10.3389/fclim.2023.1158186

Maki Mateso, J.-C., Bielders, C. L., Monsieurs, E., Depicker, A., Smets, B., Tambala, T., Bagalwa Mateso, L., & Dewitte, O. (2023). Characteristics and causes of natural and human-induced landslides in a tropical mountainous region: The rift flank west of Lake Kivu (Democratic Republic of the Congo). *Natural Hazards and Earth System Sciences*, *23*(2), 643–666. https://doi.org/10.5194/nhess-23-643-2023

Malik, H., Feng, J., Abdallah, M., Zhang, J., Shao, P., & Abduljabbar, Z. A. (2025). Fusion of data-driven models with a knowledge-guided loss function for flood forecasting. *Applied Soft Computing*, *184*, 113742. https://doi.org/10.1016/j.asoc.2025.113742

Mango, L. M., Melesse, A. M., McClain, M. E., Gann, D., & Setegn, S. G. (2011). Land use and climate change impacts on the hydrology of the upper Mara River Basin, Kenya: Results of a modeling study to support better resource management. *Hydrology and Earth System Sciences*, *15*(7), 2245–2258. https://doi.org/10.5194/hess-15-2245-2011

Marchi, L., Borga, M., Preciso, E., & Gaume, E. (2010). Characterisation of selected extreme flash floods in Europe and implications for flood risk management. *Journal of Hydrology*, *394*(1–2), 118–133. https://doi.org/10.1016/j.jhydrol.2010.07.017

Masaoka, N., Kosugi, K., & Fujimoto, M. (2021). Bedrock Groundwater Catchment Area Unveils Rainfall-Runoff Processes in Headwater Basins. *Water Resources Research*, *57*(9), e2021WR029888. https://doi.org/10.1029/2021WR029888

McCarthy, K. A., & Gale, R. W. (2001). Evaluation of persistent hydrophobic organic compounds in the Columbia River Basin using semipermeable-membrane devices. *Hydrological Processes*, *15*(7), 1271–1283. https://doi.org/10.1002/hyp.213

McCuen, R. H. (2005). Accuracy Assessment of Peak Discharge Models. *Journal of Hydrologic Engineering*, *10*(1), 16–22. https://doi.org/10.1061/(ASCE)1084-0699(2005)10:1(16)

McCuen, R. H. (2017). *Hydrologic analysis and design* (Fourth edition). Pearson.

McDonnell, J. J. (2003). Where does water go when it rains? Moving beyond the variable source area concept of rainfall-runoff response. *Hydrological Processes*, *17*(9), 1869–1875. https://doi.org/10.1002/hyp.5132

McGlynn, B., & McDonnell, J. J. (2003). Quantifying the relative contributions of riparian and hillslope zones to catchment runoff. *Water Resources Research*, *39*(11), 2003WR002091. https://doi.org/10.1029/2003WR002091

McGlynn, B., McDonnell, J., Stewart, M., & Seibert, J. (2003). On the relationships between catchment scale and streamwater mean residence time. *Hydrological Processes*, *17*(1), 175–181. https://doi.org/10.1002/hyp.5085

McGuire, K. J., McDonnell, J. J., Weiler, M., Kendall, C., McGlynn, B. L., Welker, J. M., & Seibert, J. (2005). The role of topography on catchment-scale water residence time. *Water Resources Research*, *41*(5), 2004WR003657. https://doi.org/10.1029/2004WR003657

McMillan, H. (2020). Linking hydrologic signatures to hydrologic processes: A review. *Hydrological Processes*, *34*(6), 1393–1409. https://doi.org/10.1002/hyp.13632

McMillan, H. K., Clark, M. P., Bowden, W. B., Duncan, M., & Woods, R. A. (2011). Hydrological field data from a modeller's perspective: Part 1. Diagnostic tests for model structure. *Hydrological Processes*, *25*(4), 511–522. https://doi.org/10.1002/hyp.7841

McSweeney, C., New, M., Lizcano, G., & Lu, X. (2010). The UNDP Climate Change Country Profiles: Improving the Accessibility of Observed and Projected Climate Information for Studies of Climate Change in Developing Countries. *Bulletin of the American Meteorological Society*, *91*(2), 157–166. https://doi.org/10.1175/2009BAMS2826.1

Mentzafou, A., Papadopoulos, A., & Dimitriou, E. (2023). Flood generating mechanisms investigation and rainfall threshold identification for regional flood early warning.

Environmental Earth Sciences, *82*(10), 242. https://doi.org/10.1007/s12665-023-10938-8

Merz, R., & Blöschl, G. (2003). A process typology of regional floods. *Water Resources Research*, *39*(12), 2002WR001952. https://doi.org/10.1029/2002WR001952

Merz, R., & Blöschl, G. (2009). A regional analysis of event runoff coefficients with respect to climate and catchment characteristics in Austria. *Water Resources Research*, *45*(1), 2008WR007163. https://doi.org/10.1029/2008WR007163

Merz, R., Blöschl, G., & Parajka, J. (2006). Spatio-temporal variability of event runoff coefficients. *Journal of Hydrology*, *331*(3–4), 591–604. https://doi.org/10.1016/j.jhydrol.2006.06.008

Michel, C., Andréassian, V., & Perrin, C. (2005). Soil Conservation Service Curve Number method: How to mend a wrong soil moisture accounting procedure? *Water Resources Research*, *41*(2), 2004WR003191. https://doi.org/10.1029/2004WR003191

MIDIMAR. (2015). *The National Risk Atlas of Rwanda The National Risk Atlas of Rwanda*. UNON, Publishing Services Section, Nairobi, ISO 14001:2004 – certified. https://www.minema.gov.rw/fileadmin/user_upload/Minema/Publications/Laws_and_Policies/National_Risk_Atlas_of_Rwanda.pdf

Milly, P. C. D., & Shmakin, A. B. (2002). Global Modeling of Land Water and Energy Balances. Part I: The Land Dynamics (LaD) Model. *Journal of Hydrometeorology*, *3*(3), 283–299. https://doi.org/10.1175/1525-7541(2002)003%253C0283:GMOLWA%253E2.0.CO;2

Mind'je, R., Li, L., Amanambu, A. C., Nahayo, L., Nsengiyumva, J. B., Gasirabo, A., & Mindje, M. (2019). Flood susceptibility modeling and hazard perception in Rwanda. *International Journal of Disaster Risk Reduction*, *38*, 101211. https://doi.org/10.1016/j.ijdrr.2019.101211

Mind'je, R., Li, L., Kayumba, P. M., Mupenzi, C., Mindje, M., & Hao, J. (2023). Exploring a form of pixel-based information value model for flood probability assessment and geo-visualization over an East African basin: A case of Nyabarongo in Rwanda. *Environmental Earth Sciences*, *82*(17), 402. https://doi.org/10.1007/s12665-023-11088-7

Mind'je, R., Li, L., Kayumba, P., Mindje, M., Ali, S., & Umugwaneza, A. (2021). Integrated Geospatial Analysis and Hydrological Modeling for Peak Flow and Volume Simulation in Rwanda. *Water*, *13*(20), 2926. https://doi.org/10.3390/w13202926

Ministry of Environment-Rwanda. (2018, October). *Sebeya Catchment Management Plan (2018-2024)*. MoE.

Mir, Y., & Dubeau, F. (2015). Least squares fitting of the stage–discharge relationship using smooth models with curvilinear asymptotes. *Hydrological Sciences Journal*, *60*(10), 1797–1812. https://doi.org/10.1080/02626667.2014.935779

Mishra, S. K., Jain, M. K., Suresh Babu, P., Venugopal, K., & Kaliappan, S. (2008). Comparison of AMC-dependent CN-conversion Formulae. *Water Resources Management*, *22*(10), 1409–1420. https://doi.org/10.1007/s11269-007-9233-5

Mishra, S. K., Pandey, R. P., Jain, M. K., & Singh, V. P. (2008). A Rain Duration and Modified AMC-dependent SCS-CN Procedure for Long Duration Rainfall-runoff Events. *Water Resources Management*, *22*(7), 861–876. https://doi.org/10.1007/s11269-007-9196-6

Mishra, S. K., & Singh, V. P. (2003). *Soil Conservation Service Curve Number (SCS-CN) Methodology* (Vol. 42). Springer Netherlands. https://doi.org/10.1007/978-94-017-0147-1

Mizukami, N., Rakovec, O., Newman, A. J., Clark, M. P., Wood, A. W., Gupta, H. V., & Kumar, R. (2019). On the choice of calibration metrics for "high-flow" estimation using

hydrologic models. *Hydrology and Earth System Sciences*, *23*(6), 2601–2614. https://doi.org/10.5194/hess-23-2601-2019

Mohammadpour Khoie, M. M., Guo, D., & Wasko, C. (2025). Improving the consistency of hydrologic event identification. *Environmental Modelling & Software*, *191*, 106521. https://doi.org/10.1016/j.envsoft.2025.106521

Montgomery, D. R. (1994). Road surface drainage, channel initiation, and slope instability. *Water Resources Research*, *30*(6), 1925–1932. https://doi.org/10.1029/94WR00538

Montgomery, D. R. (2001). Slope Distributions, Threshold Hillslopes, and Steady-state Topography. *American Journal of Science*, *301*(4–5), 432–454. https://doi.org/10.2475/ajs.301.4-5.432

Montgomery, D. R., & Buffington, J. M. (1997). Channel-reach morphology in mountain drainage basins. *Geological Society of America Bulletin*, *109*(5), 596–611. https://doi.org/10.1130/0016-7606(1997)109%253C0596:CRMIMD%253E2.3.CO;2

Montgomery, D. R., & Dietrich, W. E. (1994). A physically based model for the topographic control on shallow landsliding. *Water Resources Research*, *30*(4), 1153–1171. https://doi.org/10.1029/93WR02979

Montgomery, D. R., & Dietrich, W. E. (2002). Runoff generation in a steep, soil-mantled landscape. *Water Resources Research*, *38*(9). https://doi.org/10.1029/2001WR000822

Montgomery, D. R., Dietrich, W. E., & Heffner, J. T. (2002). Piezometric response in shallow bedrock at CB1: Implications for runoff generation and landsliding. *Water Resources Research*, *38*(12). https://doi.org/10.1029/2002WR001429

Moriasi, D. N., Arnold, J. G., Van Liew, M. W., Bingner, R. L., Harmel, R. D., & Veith ,T. L. (2007). Model Evaluation Guidelines for Systematic Quantification of Accuracy in Watershed Simulations. *Transactions of the ASABE*, *50*(3), 885–900. https://doi.org/10.13031/2013.23153

Mrokowska, M. M., & Osuch, M. (2011). Assessing Validity of the Dead Zone Model to Characterize Transport of Contaminants in the River Wkra. In P. Rowinski (Ed.), *Experimental Methods in Hydraulic Research* (Vol. 1, pp. 235–245). Springer Berlin Heidelberg. https://doi.org/10.1007/978-3-642-17475-9_16

Muche, M. E., Hutchinson, S. L., Hutchinson, J. M. S., & Johnston, J. M. (2019). Phenology-adjusted dynamic curve number for improved hydrologic modeling. *Journal of Environmental Management*, *235*, 403–413. https://doi.org/10.1016/j.jenvman.2018.12.115

Mueller, U., Selia, S. R. R., & Tolosana-Delgado, R. (2023). Multivariate Cross-Validation and Measures of Accuracy and Precision. *Mathematical Geosciences*, *55*(5), 693–711. https://doi.org/10.1007/s11004-022-10040-y

Mugiraneza, T., Nascetti, A., & Ban, Y. (2020). Continuous Monitoring of Urban Land Cover Change Trajectories with Landsat Time Series and LandTrendr-Google Earth Engine Cloud Computing. *Remote Sensing*, *12*(18), 2883. https://doi.org/10.3390/rs12182883

Muhire, I., & Ahmed, F. (2015). Spatio-temporal trend analysis of precipitation data over Rwanda. *South African Geographical Journal*, *97*(1), 50–68. https://doi.org/10.1080/03736245.2014.924869

Mul M.L., Mutiibwa R.K., Uhlenbrook S., & Savenije H.H.G. (2008). Hydrograph separation using hydrochemical tracers in the Makanya catchment, Tanzania. *Physics and Chemistry of the Earth 33*, *Physics and Chemistry of the Earth 33*. https://doi.org/10.1016/j.pce.2007.04.015

Muñoz-Villers, L. E., & McDonnell, J. J. (2012a). Runoff generation in a steep, tropical montane cloud forest catchment on permeable volcanic substrate. *Water Resources Research*, *48*(9), 2011WR011316. https://doi.org/10.1029/2011WR011316

Muñoz-Villers, L. E., & McDonnell, J. J. (2012b). Runoff generation in a steep, tropical montane cloud forest catchment on permeable volcanic substrate. *Water Resources Research*, *48*(9), 2011WR011316. https://doi.org/10.1029/2011WR011316

Muñoz-Villers, L. E., & McDonnell, J. J. (2013). Land use change effects on runoff generation in a humid tropical montane cloud forest region. *Hydrology and Earth System Sciences*, *17*(9), 3543–3560. https://doi.org/10.5194/hess-17-3543-2013

Munyaneza, O. (2014). *Space-time variation of hydrological processes and water resources in Rwanda—Focus on the migina catchment*. Crc Press.

Munyaneza, O., Mukubwa, A., Maskey, S., Uhlenbrook, S., & Wenninger, J. (2014). Assessment of surface water resources availability using catchment modelling and the results of tracer studies in the mesoscale Migina Catchment, Rwanda. *Hydrology and Earth System Sciences*, *18*(12), 5289–5301. https://doi.org/10.5194/hess-18-5289-2014

Muvundja, F. A., Pasche, N., Bugenyi, F. W. B., Isumbisho, M., Müller, B., Namugize, J.-N., Rinta, P., Schmid, M., Stierli, R., & Wüest, A. (2009). Balancing nutrient inputs to Lake Kivu. *Journal of Great Lakes Research*, *35*(3), 406–418. https://doi.org/10.1016/j.jglr.2009.06.002

Muvundja, F. A., Walumona, J. R., Dusabe, M.-C., Alunga, G. L., Kankonda, A. B., Albrecht, C., Eisenberg, J., & Wüest, A. (2022). The Land–Water–Energy Nexus of Ruzizi River Dams (Lake Kivu Outflow, African Great Lakes Region): Status, Challenges, and Perspectives. *Frontiers in Environmental Science*, *10*, 892591. https://doi.org/10.3389/fenvs.2022.892591

Nagy, E. D., Szilagyi, J., & Torma, P. (2022). Estimation of catchment response time using a new automated event-based approach. *Journal of Hydrology*, *613*, 128355. https://doi.org/10.1016/j.jhydrol.2022.128355

Nahayo, D., Tychon, B., Rukundo, E., Dewitte, O., Wali, U. G., & Vanmaercke, M. (2026). Spatiotemporal Variability of Rainfall-Streamflow Dynamics in Mountainous Tropical Environments: Insights From Agricultural Catchments of Northwest Rwanda. *Hydrological Processes*, *40*(1), e70360. https://doi.org/10.1002/hyp.70360

Nambajimana, J. D. D., He, X., Zhou, J., Justine, M. F., Li, J., Khurram, D., Mind'je, R., & Nsabimana, G. (2019). Land Use Change Impacts on Water Erosion in Rwanda. *Sustainability*, *12*(1), 50. https://doi.org/10.3390/su12010050

NASA Prediction Of Worldwide Energy Resources. (2024). *NASA Prediction Of Worldwide Energy Resources (POWER)* (https://power.larc.nasa.gov/Data-Access-Viewer/). https://Power.Larc.Nasa.Gov/Data-Access-Viewer/

Näschen, K., Diekkrüger, B., Leemhuis, C., Steinbach, S., Seregina, L., Thonfeld, F., & Van Der Linden, R. (2018). Hydrological Modeling in Data-Scarce Catchments: The Kilombero Floodplain in Tanzania. *Water*, *10*(5), 599. https://doi.org/10.3390/w10050599

Nash, J. E., & Sutcliffe, J. V. (1970). River flow forecasting through conceptual models part I — A discussion of principles. *Journal of Hydrology*, *10*(3), 282–290. https://doi.org/10.1016/0022-1694(70)90255-6

Neal, J., Schumann, G., & Bates, P. (2012). A subgrid channel model for simulating river hydraulics and floodplain inundation over large and data sparse areas. *Water Resources Research*, *48*(11), 2012WR012514. https://doi.org/10.1029/2012WR012514

Nearing, G. S., Mocko, D. M., Peters-Lidard, C. D., Kumar, S. V., & Xia, Y. (2016). Benchmarking NLDAS-2 Soil Moisture and Evapotranspiration to Separate Uncertainty Contributions. *Journal of Hydrometeorology*, *17*(3), 745–759. https://doi.org/10.1175/JHM-D-15-0063.1

Negatu, T. A., Zimale, F. A., & Steenhuis, T. S. (2022). Establishing Stage–Discharge Rating Curves in Developing Countries: Lake Tana Basin, Ethiopia. *Hydrology*, *9*(1), 13. https://doi.org/10.3390/hydrology9010013

Nguyen, S., & Bouvier, C. (2019). Flood modelling using the distributed event-based SCS-LR model in the Mediterranean Real Collobrier catchment. *Hydrological Sciences Journal*, *64*(11), 1351–1369. https://doi.org/10.1080/02626667.2019.1639715

Nied, M., Schröter, K., Lüdtke, S., Nguyen, V. D., & Merz, B. (2017). What are the hydro-meteorological controls on flood characteristics? *Journal of Hydrology*, *545*, 310–326. https://doi.org/10.1016/j.jhydrol.2016.12.003

Niehoff, D., Fritsch, U., & Bronstert, A. (2002). Land-use impacts on storm-runoff generation: Scenarios of land-use change and simulation of hydrological response in a meso-scale catchment in SW-Germany. *Journal of Hydrology*, *267*(1–2), 80–93. https://doi.org/10.1016/S0022-1694(02)00142-7

NISR. (2023). *Fifth Rwanda Population and Housing Census, 2022*. http://www.statistics.gov.rw.

Ntwali, D., Ogwang, B. A., & Ongoma, V. (2016). The Impacts of Topography on Spatial and Temporal Rainfall Distribution over Rwanda Based on WRF Model. *Atmospheric and Climate Sciences*, *06*(02), 145–157. https://doi.org/10.4236/acs.2016.62013

Nyandwi, E., Veldkamp, A., Amer, S., Karema, C., & Umulisa, I. (2017). Schistosomiasis mansoni incidence data in Rwanda can improve prevalence assessments, by providing high-resolution hotspot and risk factors identification. *BMC Public Health*, *17*(1), 845. https://doi.org/10.1186/s12889-017-4816-4

Nyandwi, E., Veldkamp, T., & Amer, S. (2016). Regional climate sensitivity of wetland environments in Rwanda: The need for a location-specific approach. *Regional Environmental Change*, *16*(6), 1635–1647. https://doi.org/10.1007/s10113-015-0905-z

Nyssen, J., Clymans, W., Descheemaeker, K., Poesen, J., Vandecasteele, I., Vanmaercke, M., Zenebe, A., Van Camp, M., Haile, M., Haregeweyn, N., Moeyersons, J., Martens, K., Gebreyohannes, T., Deckers, J., & Walraevens, K. (2010). Impact of soil and water conservation measures on catchment hydrological response-a case in north Ethiopia. *Hydrological Processes*, *24*(13), 1880–1895. https://doi.org/10.1002/hyp.7628

Odey, G., & Cho, Y. (2025). Event-Based vs. Continuous Hydrological Modeling with HEC-HMS: A Review of Use Cases, Methodologies, and Performance Metrics. *Hydrology*, *12*(2), 39. https://doi.org/10.3390/hydrology12020039

Ogden, F. L., Crouch, T. D., Stallard, R. F., & Hall, J. S. (2013). Effect of land cover and use on dry season river runoff, runoff efficiency, and peak storm runoff in the seasonal tropics of Central Panama: SPONGE EFFECT PAPER. *Water Resources Research*, *49*(12), 8443–8462. https://doi.org/10.1002/2013WR013956

Oladokun, V., Proverbs, D., Adebimpe, O., & Adedeji, T. (2023). *Handbook of Flood Risk Management in Developing Countries* (1st ed.). Routledge. https://doi.org/10.1201/9781003160823

Olcese, G., Bates, P. D., Neal, J. C., Sampson, C. C., Wing, O. E. J., Quinn, N., & Beck, H. E. (2022). Use of Hydrological Models in Global Stochastic Flood Modeling. *Water Resources Research*, *58*(12), e2022WR032743. https://doi.org/10.1029/2022WR032743

O'Sullivan, J. J., Ahilan, S., & Bruen, M. (2012). A modified Muskingum routing approach for floodplain flows: Theory and practice. *Journal of Hydrology*, *470–471*, 239–254. https://doi.org/10.1016/j.jhydrol.2012.09.007

Pachepsky, Y. A., Martinez, G., Pan, F., Wagener, T., & Nicholson, T. (2016). *Evaluating Hydrological Model Performance using Information Theory-based Metrics*. https://doi.org/10.5194/hess-2016-46

Padiyedath Gopalan, S., Kawamura, A., Amaguchi, H., & Azhikodan, G. (2019). *A SIMPLIFIED JACKKNIFE APPROACH FOR THE PARAMETER UNCERTAINTY ANALYSIS OF AN URBAN-SPECIFIC RAINFALL-RUNOFF MODEL*. 4560–4570. https://doi.org/10.3850/38WC092019-0367

Pandey, A., Mishra, S. K., Kansal, M. L., Singh, R. D., & Singh, V. P. (Eds.). (2021). *Water Management and Water Governance: Hydrological Modeling*. Springer International Publishing. https://doi.org/10.1007/978-3-030-58051-3

Pandey, M., Umamahesh, N. V., Das, J., & Pu, J. H. (Eds.). (2025). *Hydrology and Hydrologic Modelling: Proceedings of HYDRO 2023* (Vol. 410). Springer Nature Singapore. https://doi.org/10.1007/978-981-97-7474-6

Pandeya, B., Uprety, M., Paul, J. D., Sharma, R. R., Dugar, S., & Buytaert, W. (2021). Mitigating flood risk using low-cost sensors and citizen science: A proof-of-concept study from western Nepal. *Journal of Flood Risk Management*, *14*(1). https://doi.org/10.1111/jfr3.12675

Papacharalampous, G., Tyralis, H., Koutsoyiannis, D., & Montanari, A. (2020). Quantification of predictive uncertainty in hydrological modelling by harnessing the wisdom of the crowd: A large-sample experiment at monthly timescale. *Advances in Water Resources*, *136*, 103470. https://doi.org/10.1016/j.advwatres.2019.103470

Pappenberger, F., Matgen, P., Beven, K. J., Henry, J.-B., Pfister, L., & Fraipont, P. (2006). Influence of uncertain boundary conditions and model structure on flood inundation predictions. *Advances in Water Resources*, *29*(10), 1430–1449. https://doi.org/10.1016/j.advwatres.2005.11.012

Parajka, J., Merz, R., & Blöschl, G. (2005). A comparison of regionalisation methods for catchment model parameters. *Hydrology and Earth System Sciences*, *9*(3), 157–171. https://doi.org/10.5194/hess-9-157-2005

Park, J., Sung, J. H., Seo, Y.-H., & Kim, B.-S. (2025). Applicability of the daily hydrological models (GR4J, GR5J, and GR6J) in the South Korean basins. *Scientific Reports*, *15*(1), 31912. https://doi.org/10.1038/s41598-025-16429-z

Pathiraja, S., Westra, S., & Sharma, A. (2012). Why continuous simulation? The role of antecedent moisture in design flood estimation. *Water Resources Research*, *48*(6), 2011WR010997. https://doi.org/10.1029/2011WR010997

Patil, S. D., & Stieglitz, M. (2015). Comparing spatial and temporal transferability of hydrological model parameters. *Journal of Hydrology*, *525*, 409–417. https://doi.org/10.1016/j.jhydrol.2015.04.003

Penna, D., Tromp-van Meerveld, H. J., Gobbi, A., Borga, M., & Dalla Fontana, G. (2011). The influence of soil moisture on threshold runoff generation processes in an alpine headwater catchment. *Hydrology and Earth System Sciences*, *15*(3), 689–702. https://doi.org/10.5194/hess-15-689-2011

Perrin, C., Michel, C., & Andréassian, V. (2003a). Improvement of a parsimonious model for streamflow simulation. *Journal of Hydrology*, *279*(1–4), 275–289. https://doi.org/10.1016/S0022-1694(03)00225-7

Perrin, C., Michel, C., & Andréassian, V. (2003b). Improvement of a parsimonious model for streamflow simulation. *Journal of Hydrology*, *279*(1–4), 275–289. https://doi.org/10.1016/S0022-1694(03)00225-7

Petroselli, A., Grimaldi, S., Department for Innovation in Biological, Agro-food and Forest systems (DIBAF), University of Tuscia, Piscopia, R., Freelance, Rome, Italy, Tauro, F., & Department for Innovation in Biological, Agro-food and Forest systems (DIBAF), University of Tuscia. (2019). DESIGN HYDROGRAPH ESTIMATION IN SMALL AND UNGAUGED BASINS: A COMPARATIVE ASSESSMENT OF EVENT BASED (EBA4SUB) AND CONTINUOUS (COSMO4SUB) MODELING

APPROACHES. *Acta Scientiarum Polonorum Formatio Circumiectus*, *18*(4), 113–124. https://doi.org/10.15576/ASP.FC/2019.18.4.113

Phillips, J. D. (2003). Sources of nonlinearity and complexity in geomorphic systems. *Progress in Physical Geography: Earth and Environment*, *27*(1), 1–23. https://doi.org/10.1191/0309133303pp340ra

Phiri, D., Simwanda, M., Salekin, S., Nyirenda, V., Murayama, Y., & Ranagalage, M. (2020). Sentinel-2 Data for Land Cover/Use Mapping: A Review. *Remote Sensing*, *12*(14), 2291. https://doi.org/10.3390/rs12142291

Pianosi, F., Beven, K., Freer, J., Hall, J. W., Rougier, J., Stephenson, D. B., & Wagener, T. (2016). Sensitivity analysis of environmental models: A systematic review with practical workflow. *Environmental Modelling & Software*, *79*, 214–232. https://doi.org/10.1016/j.envsoft.2016.02.008

Pohl, E., Knoche, M., Gloaguen, R., Andermann, C., & Krause, P. (2015). Sensitivity analysis and implications for surface processes from a hydrological modelling approach in the Gunt catchment, high Pamir Mountains. *Earth Surface Dynamics*, *3*(3), 333–362. https://doi.org/10.5194/esurf-3-333-2015

Ponce, V. M., & Hawkins, R. H. (1996). Runoff Curve Number: Has It Reached Maturity? *Journal of Hydrologic Engineering*, *1*(1), 11–19. https://doi.org/10.1061/(ASCE)1084-0699(1996)1:1(11)

Quesada-Román, A., Ballesteros-Cánovas, J. A., Granados-Bolaños, S., Birkel, C., & Stoffel, M. (2022). Improving regional flood risk assessment using flood frequency and dendrogeomorphic analyses in mountain catchments impacted by tropical cyclones. *Geomorphology*, *396*, 108000. https://doi.org/10.1016/j.geomorph.2021.108000

Raghunath, H. M. (2006). *Hydrology: Principles, analysis and design* (Rev. 2nd ed). New Age International (P) Ltd., Publishers.

Raj, R., Kumar, R., Aishwarya, M., Aswini, M., & Cheraku, S. (2024). An artificial neural network and SCS–CN-based model for runoff estimation: A case study of the Peddavagu watershed. *Water Practice & Technology*, *19*(7), 2734–2743. https://doi.org/10.2166/wpt.2024.167

Ramos Filho, G. M., Coelho, V. H. R., Freitas, E. D. S., Xuan, Y., & Almeida, C. D. N. (2021). An improved rainfall-threshold approach for robust prediction and warning of flood and flash flood hazards. *Natural Hazards*, *105*(3), 2409–2429. https://doi.org/10.1007/s11069-020-04405-x

Ramos, M. C., & Martínez-Casasnovas, J. A. (2010). Effects of field reorganisation on the spatial variability of runoff and erosion rates in vineyards of Northeastern Spain: VARIABILITY OF RUNOFF AND EROSION RATES. *Land Degradation & Development*, *21*(1), 1–12. https://doi.org/10.1002/ldr.958

Razavi, S., & Gupta, H. V. (2015). What do we mean by sensitivity analysis? The need for comprehensive characterization of "global" sensitivity in E arth and E nvironmental systems models. *Water Resources Research*, *51*(5), 3070–3092. https://doi.org/10.1002/2014WR016527

Rentschler, J., Salhab, M., & Jafino, B. A. (2022). Flood exposure and poverty in 188 countries. *Nature Communications*, *13*(1), 3527. https://doi.org/10.1038/s41467-022-30727-4

Rezaei-Sadr, H., & Sharifi, G. (2018). Variation of runoff source areas under different soil wetness conditions in a semi-arid mountain region, Iran. *Water SA*, *44*(2 April). https://doi.org/10.4314/wsa.v44i2.14

Rijal, M., Luo, P., Mishra, B. K., Zhou, M., & Wang, X. (2024). Global systematical and comprehensive overview of mountainous flood risk under climate change and human activities. *Science of The Total Environment*, *941*, 173672. https://doi.org/10.1016/j.scitotenv.2024.173672

Roa-García, M. C., Brown, S., Schreier, H., & Lavkulich, L. M. (2011). The role of land use and soils in regulating water flow in small headwater catchments of the Andes. *Water Resources Research*, *47*(5), 2010WR009582. https://doi.org/10.1029/2010WR009582

Rodriguez-Bachiller, A., & Glasson, J. (2004). *Expert Systems and Geographic Information Systems for Impact Assessment* (0 ed.). CRC Press. https://doi.org/10.1201/9780203578841

Roedel, W. (2000). *Physik unserer Umwelt: Die Atmosphäre* (Dritte überarbeitete und aktualiserte Auflage). Springer.

Roohi, M., Dehghani, J., Irani, M., & Mina, P. (2025). A comprehensive review of flood damage in mountainous regions: Challenges, solutions, and advanced management technologies. *Discover Geoscience*, *3*(1), 59. https://doi.org/10.1007/s44288-025-00145-2

Roohi, M., Ghafouri, H. R., Ashrafi, S. M., Motagh, M., & Haghshenas Haghighi, M. (2025). A hybrid approach for enhanced flood prediction and assessment: Leveraging physical models, deep learning and satellite remote sensing. *Big Earth Data*, *9*(3), 439–472. https://doi.org/10.1080/20964471.2025.2530850

Rose, A., Wilson, J. E., & Lavkulich, L. M. (2017). Analysis of Impervious Surface Area, and the Impacts on Soil-Based Agriculture and the Hydrologic Cycle: A Case Study in the Agricultural Land Reserve in Metro Vancouver, British Columbia, Canada. *Agricultural Sciences*, *08*(08), 837–856. https://doi.org/10.4236/as.2017.88062

Roulston, M. S., & Smith, L. A. (2003). Combining dynamical and statistical ensembles. *Tellus A: Dynamic Meteorology and Oceanography*, *55*(1), 16. https://doi.org/10.3402/tellusa.v55i1.12082

Rowiński, P. (Ed.). (2013). *Experimental and Computational Solutions of Hydraulic Problems: 32nd International School of Hydraulics*. Springer Berlin Heidelberg. https://doi.org/10.1007/978-3-642-30209-1

Royem A. A., Mui C. K., Fuka D. R., & Walter M. T. (2012). Technical Note: Proposing a Low-Tech, Affordable, Accurate Stream Stage Monitoring System. *Transactions of the ASABE*, *55*(6), 2237–2242. https://doi.org/10.13031/2013.42512

Rozalis, S., Morin, E., Yair, Y., & Price, C. (2010). Flash flood prediction using an uncalibrated hydrological model and radar rainfall data in a Mediterranean watershed under changing hydrological conditions. *Journal of Hydrology*, *394*(1–2), 245–255. https://doi.org/10.1016/j.jhydrol.2010.03.021

RRMPG. (2025). *Rainfall-Runoff Model Playground* [English]. https://rrmpg.readthedocs.io/en/latest/_modules/rrmpg/models/gr4j.html?utm_source=chatgpt.com

Rukundo, E., Liu, S., Dong, Y., Rutebuka, E., Asamoah, E. F., Xu, J., & Wu, X. (2018). Spatio-temporal dynamics of critical ecosystem services in response to agricultural expansion in Rwanda, East Africa. *Ecological Indicators*, *89*, 696–705. https://doi.org/10.1016/j.ecolind.2018.02.032

Ruticumugambi, J. A., Kaplin, B., Blondeel, H., Mukuralinda, A., Ndoli, A., Verdoodt, A., Rutebuka, J., Imanirareba, E., Uwizeyimana, V., Gatesi, J., Nkurikiye, J. B., Verbeeck, H., Verheyen, K., & Vancoillie, F. (2024). Diversity and composition of agroforestry species in two agro-ecological zones of Rwanda. *Agroforestry Systems*, *98*(6), 1421–1443. https://doi.org/10.1007/s10457-024-01011-9

Rwanda Water Resources Board. (2025). *Rwanda Water Resources Portal*. https://waterportal.rwb.rw/

Sahu, M. K., Shwetha, H. R., & Dwarakish, G. S. (2023). State-of-the-art hydrological models and application of the HEC-HMS model: A review. *Modeling Earth Systems and Environment*, *9*(3), 3029–3051. https://doi.org/10.1007/s40808-023-01704-7

Sahu, R. K., Mishra, S. K., & Eldho, T. I. (2012). Improved Storm Duration and Antecedent Moisture Condition Coupled SCS-CN Concept-Based Model. *Journal of Hydrologic Engineering*, *17*(11), 1173–1179. https://doi.org/10.1061/(ASCE)HE.1943-5584.0000443

Saltelli, A., Ratto, M., Andres, T., Campolongo, F., Cariboni, J., Gatelli, D., Saisana, M., & Tarantola, S. (2007). *Global Sensitivity Analysis. The Primer* (1st ed.). Wiley. https://doi.org/10.1002/9780470725184

Samal, D. R., Gedam, S. S., & Nagarajan, R. (2015). GIS based drainage morphometry and its influence on hydrology in*parts of*Western Ghats region, Maharashtra, India. *Geocarto International*, *30*(7), 755–778. https://doi.org/10.1080/10106049.2014.978903

Samba, C., & Macaulay, C. (2023). *Rwanda floods and landslides kill more than 130 people* [BBC News]. https://www.bbc.com/news/world-africa-65469374

Sättele, M., Bründl, M., & Straub, D. (2016). Quantifying the effectiveness of early warning systems for natural hazards. *Natural Hazards and Earth System Sciences*, *16*(1), 149–166. https://doi.org/10.5194/nhess-16-149-2016

Schneider, L. E., & McCuen, R. H. (2006). Assessing the Hydrologic Performance of Best Management Practices. *Journal of Hydrologic Engineering*, *11*(3), 278–281. https://doi.org/10.1061/(ASCE)1084-0699(2006)11:3(278)

Schratz, P., Muenchow, J., Iturritxa, E., Richter, J., & Brenning, A. (2019). Hyperparameter tuning and performance assessment of statistical and machine-learning algorithms using spatial data. *Ecological Modelling*, *406*, 109–120. https://doi.org/10.1016/j.ecolmodel.2019.06.002

Sebaziga, N. J., Ntirenganya, F., Tuyisenge, A., & Iyakaremye, V. (2020). *A Statistical Analysis of the Historical Rainfall Data Over Eastern Province in Rwanda*. https://www.meteorwanda.gov.rw › user_upload

Seibert, J., & Bergström, S. (2022). A retrospective on hydrological catchment modelling based on half a century with the HBV model. *Hydrology and Earth System Sciences*, *26*(5), 1371–1388. https://doi.org/10.5194/hess-26-1371-2022

Serrano-Notivoli, R., Martínez-Salvador, A., García-Lorenzo, R., Espín-Sánchez, D., & Conesa-García, C. (2022). Rainfall–runoff relationships at event scale in western Mediterranean ephemeral streams. *Hydrology and Earth System Sciences*, *26*(5), 1243–1260. https://doi.org/10.5194/hess-26-1243-2022

Shah, A. I., & Pan, N. D. (2024). Evaluation of probability distribution methods for flood frequency analysis in the Jhelum Basin of North-Western Himalayas, India. *Cleaner Water*, *2*, 100044. https://doi.org/10.1016/j.clwat.2024.100044

Sharma, A., Wasko, C., & Lettenmaier, D. P. (2018). If Precipitation Extremes Are Increasing, Why Aren't Floods? *Water Resources Research*, *54*(11), 8545–8551. https://doi.org/10.1029/2018WR023749

Shi, W., Huang, M., Gongadze, K., & Wu, L. (2017). A Modified SCS-CN Method Incorporating Storm Duration and Antecedent Soil Moisture Estimation for Runoff Prediction. *Water Resources Management*, *31*(5), 1713–1727. https://doi.org/10.1007/s11269-017-1610-0

Shi, W., & Wang, N. (2020). An Improved SCS-CN Method Incorporating Slope, Soil Moisture, and Storm Duration Factors for Runoff Prediction. *Water*, *12*(5), 1335. https://doi.org/10.3390/w12051335

Shin, M.-J., & Choi, Y. S. (2018). Sensitivity Analysis to Investigate the Reliability of the Grid-Based Rainfall-Runoff Model. *Water*, *10*(12), 1839. https://doi.org/10.3390/w10121839

Shin, M.-J., Guillaume, J. H. A., Croke, B. F. W., & Jakeman, A. J. (2013). Addressing ten questions about conceptual rainfall–runoff models with global sensitivity analyses in R. *Journal of Hydrology*, *503*, 135–152. https://doi.org/10.1016/j.jhydrol.2013.08.047

Shook, K. R., Whitfield, P. H., Spence, C., & Pomeroy, J. W. (2024). Estimating response times, flow velocities, and roughness coefficients of Canadian Prairie basins. *Hydrology and Earth System Sciences*, *28*(23), 5173–5192. https://doi.org/10.5194/hess-28-5173-2024

Shuster, W. D., Bonta, J., Thurston, H., Warnemuende, E., & Smith, D. R. (2005). Impacts of impervious surface on watershed hydrology: A review. *Urban Water Journal*, *2*(4), 263–275. https://doi.org/10.1080/15730620500386529

Sibomana, P., Vanmaercke, M., Depicker, A., Tychon, B., Hubert, A., & Dewitte, O. (2025). Effects of agricultural terraces on landslide occurrence: Insights from a tropical mountainous region (Rwanda, Africa). *CATENA*, *253*, 108898. https://doi.org/10.1016/j.catena.2025.108898

Sidle, R. C., Ziegler, A. D., Negishi, J. N., Nik, A. R., Siew, R., & Turkelboom, F. (2006). Erosion processes in steep terrain—Truths, myths, and uncertainties related to forest management in Southeast Asia. *Forest Ecology and Management*, *224*(1–2), 199–225. https://doi.org/10.1016/j.foreco.2005.12.019

Sieg, T., Kienzler, S., Rözer, V., Vogel, K., Rust, H., Bronstert, A., Kreibich, H., Merz, B., & Thieken, A. H. (2023). Toward an adequate level of detail in flood risk assessments. *Journal of Flood Risk Management*, *16*(3), e12889. https://doi.org/10.1111/jfr3.12889

Simulation of the water budget and the river flows of the Rhone basin. (1999). *Journal of Geophysical Research: Atmospheres*, *104*(D24), 31145–31172. https://doi.org/10.1029/1999JD901008

Singh, D. K., & Singh, N. (2019). Drying Urban lakes: A consequence of climate change, urbanization or other anthropogenic causes? An insight from northern India. *Lakes & Reservoirs: Science, Policy and Management for Sustainable Use*, *24*(2), 115–126. https://doi.org/10.1111/lre.12262

Singh, O., & Kumar, M. (2013). Flood events, fatalities and damages in India from 1978 to 2006. *Natural Hazards*, *69*(3), 1815–1834. https://doi.org/10.1007/s11069-013-0781-0

Singh, V. P., & Woolhiser, D. A. (2002). Mathematical Modeling of Watershed Hydrology. *Journal of Hydrologic Engineering*, *7*(4), 270–292. https://doi.org/10.1061/(ASCE)1084-0699(2002)7:4(270)

Singh, V. P., Yadav, S., & Yadava, R. N. (Eds.). (2018). *Hydrologic Modeling: Select Proceedings of ICWEES-2016* (Vol. 81). Springer Singapore. https://doi.org/10.1007/978-981-10-5801-1

Sivapalan, M., Blöschl, G., Zhang, L., & Vertessy, R. (2003a). Downward approach to hydrological prediction. *Hydrological Processes*, *17*(11), 2101–2111. https://doi.org/10.1002/hyp.1425

Sivapalan, M., Blöschl, G., Zhang, L., & Vertessy, R. (2003b). Downward approach to hydrological prediction. *Hydrological Processes*, *17*(11), 2101–2111. https://doi.org/10.1002/hyp.1425

Sivapalan, M., Wood, E. F., & Beven, K. J. (1990). On hydrologic similarity: 3. A dimensionless flood frequency model using a generalized geomorphologic unit hydrograph and partial area runoff generation. *Water Resources Research*, *26*(1), 43–58. https://doi.org/10.1029/wr026i001p00043

Smakhtin, V. U. (2001). Low flow hydrology: A review. *Journal of Hydrology*, *240*(3–4), 147–186. https://doi.org/10.1016/S0022-1694(00)00340-1

Smith, K., & Ward, R. C. (1998). *Floods: Physical processes and human impacts*. Wiley.

Smithers, J. (2012). Methods for design flood estimation in South Africa. *Water SA*, *38*(4), 633–646. https://doi.org/10.4314/wsa.v38i4.19

Sobol′, I. M. (2001). Global sensitivity indices for nonlinear mathematical models and their Monte Carlo estimates. *Mathematics and Computers in Simulation*, *55*(1–3), 271–280. https://doi.org/10.1016/S0378-4754(00)00270-6

Solanki, H., Vegad, U., Kushwaha, A., & Mishra, V. (2025). Improving Streamflow Prediction Using Multiple Hydrological Models and Machine Learning Methods. *Water Resources Research*, *61*(1), e2024WR038192. https://doi.org/10.1029/2024WR038192

Soulis, K. X., & Valiantzas, J. D. (2012). SCS-CN parameter determination using rainfall-runoff data in heterogeneous watersheds – the two-CN system approach. *Hydrology and Earth System Sciences*, *16*(3), 1001–1015. https://doi.org/10.5194/hess-16-1001-2012

Soulis, K. X., Valiantzas, J. D., Dercas, N., & Londra, P. A. (2009). Investigation of the direct runoff generation mechanism for the analysis of the SCS-CN method applicability to a partial area experimental watershed. *Hydrology and Earth System Sciences*, *13*(5), 605–615. https://doi.org/10.5194/hess-13-605-2009

Sridharan, B., Gurivindapalli, D., Kuiry, S. N., Mali, V. K., Nithila Devi, N., Bates, P. D., & Sen, D. (2020). Explicit Expression of Weighting Factor for Improved Estimation of Numerical Flux in Local Inertial Models. *Water Resources Research*, *56*(7), e2020WR027357. https://doi.org/10.1029/2020WR027357

Staudinger, M., Kauzlaric, M., Mas, A., Evin, G., Hingray, B., & Viviroli, D. (2025). The role of antecedent conditions in translating precipitation events into extreme floods at the

catchment scale and in a large-basin context. *Natural Hazards and Earth System Sciences*, *25*(1), 247–265. https://doi.org/10.5194/nhess-25-247-2025

Storn, R., & Price, K. (1997). Differential Evolution – A Simple and Efficient Heuristic for Global Optimization over Continuous Spaces. *Journal of Global Optimization*, *11*(4), 341–359. https://doi.org/10.1023/A:1008202821328

Subramanya, K. (2008). *Engineering hydrology* (3rd ed). Tata McGraw-Hill.

Subramanya, K. (2009). *Flow in open channels* (3rd ed). Tata McGraw-Hill.

Sukovich, E. M., Ralph, F. M., Barthold, F. E., Reynolds, D. W., & Novak, D. R. (2014). Extreme Quantitative Precipitation Forecast Performance at the Weather Prediction Center from 2001 to 2011. *Weather and Forecasting*, *29*(4), 894–911. https://doi.org/10.1175/WAF-D-13-00061.1

Sultan, D., Tsunekawa, A., Tsubo, M., Haregeweyn, N., Adgo, E., Meshesha, D. T., Fenta, A. A., Ebabu, K., Berihun, M. L., & Setargie, T. A. (2022). Evaluation of lag time and time of concentration estimation methods in small tropical watersheds in Ethiopia. *Journal of Hydrology: Regional Studies*, *40*, 101025. https://doi.org/10.1016/j.ejrh.2022.101025

Sun, R., Pan, B., & Duan, Q. (2023). A surrogate modeling method for distributed land surface hydrological models based on deep learning. *Journal of Hydrology*, *624*, 129944. https://doi.org/10.1016/j.jhydrol.2023.129944

Swamynathan, M. (2017). *Mastering Machine Learning with Python in Six Steps*. Apress. https://doi.org/10.1007/978-1-4842-2866-1

Szeląg, B., Suligowski, R., Studziński, J., & De Paola, F. (2020). Application of logistic regression to simulate the influence of rainfall genesis on storm overflow operations: A probabilistic approach. *Hydrology and Earth System Sciences*, *24*(2), 595–614. https://doi.org/10.5194/hess-24-595-2020

Tague, C. L., & Band, L. E. (2004). RHESSys: Regional Hydro-Ecologic Simulation System—An Object-Oriented Approach to Spatially Distributed Modeling of Carbon, Water, and Nutrient Cycling. *Earth Interactions*, *8*(19), 1–42. https://doi.org/10.1175/1087-3562(2004)8%253C1:RRHSSO%253E2.0.CO;2

Talei, A., & Chua, L. H. C. (2012). Influence of lag time on event-based rainfall–runoff modeling using the data driven approach. *Journal of Hydrology*, *438–439*, 223–233. https://doi.org/10.1016/j.jhydrol.2012.03.027

Tamer, M., Adego, E., & Abiyu, A. (2025). Understanding rainfall runoff dynamics across various land uses and landscape positions in North Western Ethiopia. *Scientific Reports*, *15*(1), 15287. https://doi.org/10.1038/s41598-025-98437-7

Taye, G., Vanmaercke, M., Van Wesemael, B., Tesfaye, S., Teka, D., Nyssen, J., Deckers, J., & Poesen, J. (2023a). Estimating the runoff response from hillslopes treated with soil and water conservation structures in the semi-arid Ethiopian highlands: Is the curve number method applicable? *Scientific African*, *20*, e01620. https://doi.org/10.1016/j.sciaf.2023.e01620

Taye, G., Vanmaercke, M., Van Wesemael, B., Tesfaye, S., Teka, D., Nyssen, J., Deckers, J., & Poesen, J. (2023b). Estimating the runoff response from hillslopes treated with soil and water conservation structures in the semi-arid Ethiopian highlands: Is the curve number method applicable? *Scientific African*, *20*, e01620. https://doi.org/10.1016/j.sciaf.2023.e01620

Tehrany, M. S., Pradhan, B., & Jebur, M. N. (2015). Flood susceptibility analysis and its verification using a novel ensemble support vector machine and frequency ratio method. *Stochastic Environmental Research and Risk Assessment*, *29*(4), 1149–1165. https://doi.org/10.1007/s00477-015-1021-9

Tetzlaff, D., Seibert, J., McGuire, K. J., Laudon, H., Burns, D. A., Dunn, S. M., & Soulsby, C. (2009). How does landscape structure influence catchment transit time across different geomorphic provinces? *Hydrological Processes*, *23*(6), 945–953. https://doi.org/10.1002/hyp.7240

Thanvisitthpon, N., Nakburee, A., Saguansap, P., & Mruksirisuk, P. (2024). Climate change-induced urban flooding trend analysis and land use change: A case study of flood-prone Pathumthani Province, Thailand. *Environment, Development and Sustainability*. https://doi.org/10.1007/s10668-024-05117-z

Theunissen, K, Hanon, M, & Fernandez-Alonso, M. (1991). *Carte Géologique du Rwanda*. Service Géologique, Ministère de l'Industrie et de l'Artisanat, République Rwandaise.

Tockner, K., & Stanford, J. A. (2002). Riverine flood plains: Present state and future trends. *Environmental Conservation*, *29*(3), 308–330. https://doi.org/10.1017/s037689290200022x

Todini, E. (2007). Hydrological catchment modelling: Past, present and future. *Hydrology and Earth System Sciences*, *11*(1), 468–482. https://doi.org/10.5194/hess-11-468-2007

Tramblay, Y., Bouvier, C., Martin, C., Didon-Lescot, J.-F., Todorovik, D., & Domergue, J.-M. (2010). Assessment of initial soil moisture conditions for event-based rainfall–runoff modelling. *Journal of Hydrology*, *387*(3–4), 176–187. https://doi.org/10.1016/j.jhydrol.2010.04.006

Tromp-van Meerveld, H. J., & McDonnell, J. J. (2006). Threshold relations in subsurface stormflow: 2. The fill and spill hypothesis. *Water Resources Research*, *42*(2), 2004WR003800. https://doi.org/10.1029/2004WR003800

Tufféry, S. (2017). *Modélisation prédictive et apprentissage statistique avec R* (2e éd. actualisée et augmentée). Éditions Technip.

Tuyishime, H. C., & Choi, K. S. (2025). GIS-Based Assessment of Stormwater Harvesting Potentials: A Sustainable Approach to Alleviate Water Scarcity in Rwanda's Eastern Savanna Agroecological Zone. *Water*, *17*(14), 2045. https://doi.org/10.3390/w17142045

Uber, M., Vandervaere, J.-P., Zin, I., Braud, I., Heistermann, M., Legoût, C., Molinié, G., & Nord, G. (2018). How does initial soil moisture influence the hydrological response? A case study from southern France. *Hydrology and Earth System Sciences*, *22*(12), 6127–6146. https://doi.org/10.5194/hess-22-6127-2018

UNDRR. (2022). *United Nations Office for Disaster Risk Reduction. Annual report 2022*.

UNDRR. (2023). *Global Status of Multi-Hazard Early Warning Systems*. https://preparecenter.org/wp-content/uploads/2023/12/undrr-global-status-of-mhews-2023_0.pdf?utm_source=chatgpt.com

UNEP. (2011). *Rwanda: From post-conflict to environmentally sustainable development*.

UNEP. (2022). *Too Little, Too Slow. Climate adaptation failure puts world at risk. Adaptation Gap Report 2022*. ISBN: 978-92-807-3982-4

UNHCR. (2025). *Global report on law and policy on internal displacement: Implementing national responsibility*. https://www.unhcr.org/sites/default/files/2025-02/global-report-on-law-and-policy-on-internal-displacement.pdf

UNISDR. (2012). *Disaster risk and resilience*. https://www.un.org/millenniumgoals/pdf/Think%20Pieces/3_disaster_risk_resilience.pdf

USACE HEC. (2025). *SCS Unit Hydrograph Model. U.S. Army Corps of Engineers, Hydrologic Engineering Center* [Dataset]. https://www.hec.usace.army.mil/confluence/hmsdocs/hmstrm/transform/scs-unit-hydrograph-model/

USDA NRCS. (2004). *Part 630 Hydrology: National Engineering Handbook*. https://directives.sc.egov.usda.gov/OpenNonWebContent.aspx?content=17752.wba

Uwihirwe, J., Hrachowitz, M., & Bogaard, T. A. (2020). Landslide precipitation thresholds in Rwanda. *Landslides*, *17*(10), 2469–2481. https://doi.org/10.1007/s10346-020-01457-9

Uwizeyimana, D., Mureithi, S. M., Mvuyekure, S. M., Karuku, G., & Kironchi, G. (2019). Modelling surface runoff using the soil conservation service-curve number method in a drought prone agro-ecological zone in Rwanda. *International Soil and Water Conservation Research*, *7*(1), 9–17. https://doi.org/10.1016/j.iswcr.2018.12.001

Van Kempen, G., Van Der Wiel, K., & Melsen, L. A. (2021). The impact of hydrological model structure on the simulation of extreme runoff events. *Natural Hazards and Earth System Sciences*, *21*(3), 961–976. https://doi.org/10.5194/nhess-21-961-2021

Veeck, S., Da Costa, F. F., Correia Lima, D. L., Da Paz, A. R., & Allasia Piccilli, D. G. (2020). Scale dynamics of the HIDROPIXEL high-resolution DEM-based distributed hydrologic modeling approach. *Environmental Modelling & Software*, *127*, 104695. https://doi.org/10.1016/j.envsoft.2020.104695

Verdoodt, A., & Van Ranst, E. (2006). Environmental assessment tools for multi-scale land resources information systemsA case study of Rwanda. *Agriculture, Ecosystems & Environment*, *114*(2–4), 170–184. https://doi.org/10.1016/j.agee.2005.10.006

Viessman, W., & Frost, G. L. (2003). *Introduction to hydrology* (5. ed). Pearson Education.

Viglione, A., Merz, R., & Blöschl, G. (2009). On the role of the runoff coefficient in the mapping of rainfall to flood return periods. *Hydrology and Earth System Sciences*, *13*(5), 577–593. https://doi.org/10.5194/hess-13-577-2009

Vivekanandan, N. (2018). Comparison of probability distributions in extreme value analysis of rainfall and temperature data. *Environmental Earth Sciences*, *77*(5), 201. https://doi.org/10.1007/s12665-018-7356-z

Viviroli, D., Archer, D. R., Buytaert, W., Fowler, H. J., Greenwood, G. B., Hamlet, A. F., Huang, Y., Koboltschnig, G., Litaor, M. I., López-Moreno, J. I., Lorentz, S., Schädler, B., Schreier, H., Schwaiger, K., Vuille, M., & Woods, R. (2011). Climate change and mountain water resources: Overview and recommendations for research, management and policy. *Hydrology and Earth System Sciences*, *15*(2), 471–504. https://doi.org/10.5194/hess-15-471-2011

Viviroli, D., Dürr, H. H., Messerli, B., Meybeck, M., & Weingartner, R. (2007). Mountains of the world, water towers for humanity: Typology, mapping, and global significance. *Water Resources Research*, *43*(7), 2006WR005653. https://doi.org/10.1029/2006WR005653

Viviroli, D., & Weingartner, R. (2004). The hydrological significance of mountains: From regional to global scale. *Hydrology and Earth System Sciences*, *8*(6), 1017–1030. https://doi.org/10.5194/hess-8-1017-2004

Vogel, R. M., & Fennessey, N. M. (1994). Flow-Duration Curves. I: New Interpretation and Confidence Intervals. *Journal of Water Resources Planning and Management*, *120*(4), 485–504. https://doi.org/10.1061/(ASCE)0733-9496(1994)120:4(485)

Walker, R., Mind'jeMind'je, R., Yeenee, L. N., & Habarurema. (2024). Assessing Flood Vulnerability Zones and Their Driving Factors to Guide Community-Based Resilience Planning Across Ngororero District, Rwanda. *Journal of Agriculture*, *8*(1). https://doi.org/10.53819/81018102t2386

Wamucii, C. N., Van Oel, P. R., Ligtenberg, A., Gathenya, J. M., & Teuling, A. J. (2021). Land use and climate change effects on water yield from East African forested water towers. *Hydrology and Earth System Sciences*, *25*(11), 5641–5665. https://doi.org/10.5194/hess-25-5641-2021

Wan, H., Xia, J., Zhang, L., She, D., Xiao, Y., & Zou, L. (2015). Sensitivity and Interaction Analysis Based on Sobol' Method and Its Application in a Distributed Flood Forecasting Model. *Water*, *7*(6), 2924–2951. https://doi.org/10.3390/w7062924

Wanzala, M. A., Ficchi, A., Cloke, H. L., Stephens, E. M., Badjana, H. M., & Lavers, D. A. (2022). Assessment of global reanalysis precipitation for hydrological modelling in data-scarce regions: A case study of Kenya. *Journal of Hydrology: Regional Studies*, *41*, 101105. https://doi.org/10.1016/j.ejrh.2022.101105

Wathern, P. (Ed.). (2013). *Environmental Impact Assessment: Theory and Practice* (0 ed.). Routledge. https://doi.org/10.4324/9780203409978

Weng, Q. (Ed.). (2011). *Advances in Environmental Remote Sensing: Sensors, Algorithms, and Applications* (0 ed.). CRC Press. https://doi.org/10.1201/b10599

Westerberg, I. K., Wagener, T., Coxon, G., McMillan, H. K., Castellarin, A., Montanari, A., & Freer, J. (2016). Uncertainty in hydrological signatures for gauged and ungauged catchments. *Water Resources Research*, *52*(3), 1847–1865. https://doi.org/10.1002/2015WR017635

Wilks, D. S. (2001). A skill score based on economic value for probability forecasts. *Meteorological Applications*, *8*(2), 209–219. https://doi.org/10.1017/S1350482701002092

Wohl, E. (2021). An Integrative Conceptualization of Floodplain Storage. *Reviews of Geophysics*, *59*(2), e2020RG000724. https://doi.org/10.1029/2020RG000724

Wohl, E., Lane, S. N., & Wilcox, A. C. (2015). The science and practice of river restoration. *Water Resources Research*, *51*(8), 5974–5997. https://doi.org/10.1002/2014WR016874

Wörman, A., Packman, A. I., Johansson, H., & Jonsson, K. (2002). Effect of flow-induced exchange in hyporheic zones on longitudinal transport of solutes in streams and rivers. *Water Resources Research*, *38*(1). https://doi.org/10.1029/2001WR000769

Wu, Y., Zhang, Z., Qi, X., Hu, W., & Si, S. (2024). Prediction of flood sensitivity based on Logistic Regression, eXtreme Gradient Boosting, and Random Forest modeling methods. *Water Science & Technology*, *89*(10), 2605–2624. https://doi.org/10.2166/wst.2024.146

Xie, T., Hu, C., Liu, C., Li, W., Niu, C., & Li, R. (2024). Study on long short-term memory based on vector direction of flood process for flood forecasting. *Scientific Reports*, *14*(1), 21446. https://doi.org/10.1038/s41598-024-72205-5

Yang, Q., McVicar, T. R., Van Niel, T. G., Hutchinson, M. F., Li, L., & Zhang, X. (2007). Improving a digital elevation model by reducing source data errors and optimising interpolation algorithm parameters: An example in the Loess Plateau, China. *International Journal of Applied Earth Observation and Geoinformation*, *9*(3), 235–246. https://doi.org/10.1016/j.jag.2006.08.004

Yanites, B. J., Clark, M. K., Roering, J. J., West, A. J., Zekkos, D., Baldwin, J. W., Cerovski-Darriau, C., Gallen, S. F., Horton, D. E., Kirby, E., Leshchinsky, B. A., Mason, H. B., Moon, S., Barnhart, K. R., Booth, A., Czuba, J. A., McCoy, S., McGuire, L., Pfeiffer, A., & Pierce, J. (2025). Cascading land surface hazards as a nexus in the Earth system. *Science*, *388*(6754), eadp9559. https://doi.org/10.1126/science.adp9559

Yasitli, A. N. (2021). *Assessing the effectiveness of flood management: A comparative study between Turkey and the UK* [Ph.D. Thesis].

Yazdanfar, Z., & Sharma, A. (2015). Urban drainage system planning and design – challenges with climate change and urbanization: A review. *Water Science and Technology*, *72*(2), 165–179. https://doi.org/10.2166/wst.2015.207

Ye, S., Liu, L., Li, J., Pan, H., Li, W., & Ran, Q. (2023). From rainfall to runoff: The role of soil moisture in a mountainous catchment. *Journal of Hydrology*, *625*, 130060. https://doi.org/10.1016/j.jhydrol.2023.130060

Yeshaneh, E., Eder, A., & Blöschl, G. (2014). Temporal variation of suspended sediment transport in the Koga catchment, North Western Ethiopia and environmental implications. *Hydrological Processes*, *28*(24), 5972–5984. https://doi.org/10.1002/hyp.10090

Yu, J., Chen, H., Wang, M., Bao, J., Song, W., He, X., & Shi, W. (2025). A modified curve number method for runoff prediction of different vegetation types at the slope scale in China. *Soil and Tillage Research*, *254*, 106737. https://doi.org/10.1016/j.still.2025.106737

Yuan, W., Jing, B., Xu, H., Tang, Y., & Zhang, S. (2024). A Dynamic Early Warning Model for Flash Floods Based on Rainfall Pattern Identification. *International Journal of Disaster Risk Science*, *15*(5), 769–788. https://doi.org/10.1007/s13753-024-00593-3

Zenebe, A., Vanmaercke, M., Poesen, J., Verstraeten, G., Haregeweyn, N., Haile, M., Amare, K., Deckers, J., & Nyssen, J. (2013). Spatial and temporal variability of river flows in the degraded semi-arid tropical mountains of northern Ethiopia. *Zeitschrift Für Geomorphologie*, *57*(2), 143–169. https://doi.org/10.1127/0372-8854/2012/0080

Zhai, X., Guo, L., Liu, R., & Zhang, Y. (2018). Rainfall threshold determination for flash flood warning in mountainous catchments with consideration of antecedent soil moisture and rainfall pattern. *Natural Hazards*, *94*(2), 605–625. https://doi.org/10.1007/s11069-018-3404-y

Zhan, C., Han, J., Zou, L., Sun, F., & Wang, T. (2019). Heteroscedastic and symmetric efficiency for hydrological model evaluation criteria. *Hydrology Research*, *50*(5), 1189–1201. https://doi.org/10.2166/nh.2019.121

Zhang, R., Liu, D., Xiong, L., Chen, J., Chen, H., & Yin, J. (2024). Determining the threshold of issuing flash flood warnings based on people's response process simulation.

Hydrology and Earth System Sciences, *28*(23), 5229–5247. https://doi.org/10.5194/hess-28-5229-2024

Zhao, L., Nie, X., Zheng, H., Liao, K., & Zhang, J. (2023a). The Lag Effect of Riverine Flow-Discharge and Sediment-Load Response to Antecedent Rainfall with Different Cumulative Durations in Red Hilly Area in China. *Water*, *15*(23), 4048. https://doi.org/10.3390/w15234048

Zhao, L., Nie, X., Zheng, H., Liao, K., & Zhang, J. (2023b). The Lag Effect of Riverine Flow-Discharge and Sediment-Load Response to Antecedent Rainfall with Different Cumulative Durations in Red Hilly Area in China. *Water*, *15*(23), 4048. https://doi.org/10.3390/w15234048

Zheng, Y., Coxon, G., Woods, R., Li, J., & Feng, P. (2023). A Framework for Estimating the Probability Distribution of Event Runoff Coefficient in Ungauged Catchments. *Water Resources Research*, *59*(1), e2022WR033227. https://doi.org/10.1029/2022WR033227

Zhou, Z., Zhou, Z., Xu, H., & Li, M. (2021). Surface WATER–GROUNDWATER interactions of Xiluodu Reservoir based on the dynamic evolution of seepage, temperature, and hydrochemistry due to impoundment. *Hydrological Processes*, *35*(8). https://doi.org/10.1002/hyp.14304

Zimmerman, L. S., & Byizigiro, V. (2012). *Rapid risk and capacities assessment and livelihoods profiling in Nyabihu, Musanze and Burera districts affected by floods and landslides*.

Zuecco, G., Penna, D., & Borga, M. (2018). Runoff generation in mountain catchments: Long-term hydrological monitoring in the Rio Vauz Catchment, Italy. *Cuadernos de Investigación Geográfica*, *44*(2), 397–428. https://doi.org/10.18172/cig.3327

Zwartendijk, B. W., Van Meerveld, H. J., Teuling, A. J., Ghimire, C. P., & Bruijnzeel, L. A. (2023). Rainfall-runoff responses and hillslope moisture thresholds for an upland

tropical catchment in Eastern Madagascar subject to long-term slash-and-burn practices. *Hydrological Processes*, *37*(8), e14937. https://doi.org/10.1002/hyp.14937

Curriculum Vitae

1. **Profile**

Déogratias NAHAYO

Ph.D. student at University of Liège

Faculty of Sciences, Department of Science and Environmental Management

Phone: +250788678702 / +32466059052

Email: deogratias.nahayo@doct.uliege.be/dnahayo@uliege.be /nahayod@yahoo.fr/ dnahayo@ines.ac.rw

LinkedIn: http://linkedin.com/in/deogratias-nahayo-438861182

ResearchGate: https://www.researchgate.net/profile/Deogratias-Nahayo

ORCID: https://orcid.org/0009-0009-2071-8312

Local address : Musanze-Kinigi road, Gakoro Village, Rwambogo Cell, Musanze Sector, Musanze District, Northen Province, Rwanda

Date of birth and Nationality: 26th December, 1971, Rwandan

2. **Key qualifications**

Besides his foundational training in Mathématiques-Physique during secondary school, Déogratias Nahayo holds an engineering degree in Civil Engineering (Diplôme d'Ingénieur en Génie Civil, Bacc+5) from the National University of Rwanda. He earned a Master of Science in Water Resources and Environmental Management from the same institution, in collaboration with UNESCO-IHE, the Delft Institute for Water Education, as well as a Postgraduate Certificate in Learning and Teaching in Higher Education from the University of Rwanda. His Ph.D. research focuses on hydrogeomorphological approaches to understanding flood hazards and rainfall-runoff dynamics in mountainous tropical environments, with emphasis on insights from agricultural catchments in northwest Rwanda. Additionally, he has the academic expertise in teaching civil and water engineering courses, including, Engineering Mechanics, Theory of Structures, Fluid Mechanics, Construction Project Management, Irrigation and Drainage Engineering, Engineering Hydrology, Environmental Engineering, Water Resources Engineering, and Water Resources Systems Modeling. He also has extensive expertise in writing, supervising, and executing civil engineering, hydrology, and hydraulics projects.

3. **Education**

- **Ph.D. in Sciences (Science and Environmental Management)**, University of Liège, Arlon-Campus Environnement, Belgium (2020-2025)

Thesis title: Hydrogeomorphological approaches to understanding flood hazards and flood-risk management in northwest Rwanda

- **Postgraduate Certificate in Learning and Teaching in Higher Education**, University of Rwanda, Faculty of Education (2015–2016)
- **MSc in Water Resources and Environmental Management**, National University of Rwanda, Faculty of Applied Sciences, Department of Civil Engineering, Huye, Rwanda (2006–2007).
- **Diplôme d'Ingénieur en Génie Civil** (Bac+5), National University of Rwanda, Huye (2000-2005).
- **Diplôme des humanités scientifiques (Secondary school diploma with a scientific focus),** Mathématique–Physique track, Groupe Scolaire de la Salle de Byumba and École des Sciences de Musanze (1988–1994, 1997–1998).

4. Employment records

- **May 6, 2015 – Present:** Lecturer, Civil Engineering Department, INES-Ruhengeri. Module leader of Engineering hydrology, Hydraulic structures, Water supply and Sanitation, Irrigation and drainage engineering; and Environmental Engineering.
- **May 6, 2015 – October 2020:** Coordinator of Water and Soil Resources Engineering and Management Research Cluster, INES-Ruhengeri.
- **October 2012 – May 5, 2015:** Head of Department of Civil Engineering, INES-Ruhengeri. Module leader of Fluid mechanics, Engineering mechanics and Strength of materials.
- **October 6, 2011– October 22, 2012:** Head of Department of Land Survey, INES-Ruhengeri. Module leader of Infrastructures, Quantity Surveying, Fluid Mechanics and Hydraulics.
- **April 2010 – September 2011:** Water Supply Engineer, Programme d'Alimentation en Eau Potable/Cooperation Technique Belge (CTB) in Nyaruguru, Gisagara and Huye Districts, Rwanda.
- **February 2009 – March 2010:** Institute of Agriculture and Animal Husbandry, ISAE-Busogo, Faculty of Agricultural Engineering and Environmental Sciences, Department of Soil and Agricultural Engineering (the current UR-CAVM); Lecturer of General Hydraulics, Water Supply and Sanitation, Design of Surface Irrigations, Construction Technology and Management, Rural Constructions,

Theory of Structures, Reinforced Concrete Structural Design, Design of gravity dams and Engineering Materials.

- **January 2008 – February 2009:** Procurement officer in the Ministry of Natural Resources (MINIRENA); the Ministry in charge of Water, Lands, Environment, Forests and Mines.

January 1999 – October 1999: Teacher of Mathematics and Physics, Ecole Technique Officielle de Tumba, Byumba.

5. Professional training records

- **July–August 2018 –** *Feeding the Billions: Challenges and Innovation in Food and Water Security*; *Governing Climate Change: Theory and Practice*, Vrije Universiteit Amsterdam, Netherlands.
- **June–July 2017 –** Intensive Pre-doctoral Training Course on Natural Resources Management and Conflict Resolution in the Greater Lake Region (Rwanda, DRC, Uganda), Vrije Universiteit Amsterdam, Netherlands.
- **February 2015 –** Value Chain Management (NIMPF tool), Kigali, Rwanda.
- **September 2013 –** Climate Change Mitigation and Adaptation for Water Resources, African Institute for Capacity Development, JKUAT, Juja, Nairobi, Kenya.
- **July 2013 –** Wetlands: Wise Use, Smart Plans. Meeting the Challenges for Sustainable Wetlands, Kigali, Rwanda.
- **January 2013 –** Multidimensional Application of GIS Technologies in Land Surveying and Related Fields, Musanze, Rwanda.
- **December 2012 –** Scoping for Integrated Water Resources Management (IWRM) in Rwanda, Kigali, Rwanda.
- **March 2012 –** Cadastre, Land Management and Land Information System, Musanze, Rwanda.
- **February–August 2008 –** Seven Certificates in Public Procurement, Tendering Process, Contract Management, and Project Management (Tenders financed by Rwanda, AfDB, and World Bank), Murambi, Rwanda.

6. Professional experience records

2006–2010

- Quantity Surveyor and Hydraulics Engineer for sewer design (wastewater and stormwater), Sanitary Master Plan of Kigali City – *Client: PROJEMA SIG, Swiss Company.*

- Quantity Surveyor and Irrigation Structures Designer; supervised construction of irrigation projects (earth-fill dams, irrigation networks “Runukangoma, Base”) and water supply projects (Kinazi network, 7 km) – *Client: COCA Ltd, Rwanda*
- Supervision of civil construction projects – *Client: ECONT Ltd, Rwanda*
- Developed academic programmes for Land Surveying and Civil Engineering Departments; designed laboratory equipment – *Client: INES-Ruhengeri*
- Design and supervision of Rugeramigozi irrigation systems (planning, design, construction, operation, management) – *Client: COCA Ltd, Rwanda*
- Supervision of building construction and rehabilitation of roads (Cyegera–Ntyazo, Nyanza District; Nyanza–Nyumba–Mukura, Huye District) – *Client: SOGEECO Ltd*

2010–2011

- Supervision of rural water supply projects in Gisagara, Huye, and Nyaruguru districts (273 km) – *Client: Coopération Technique Belge (CTB), PEPAPS programme*
- Supervision of construction of 3 bridges and 4 culverts in Nyaruguru District – *Client: Muganza-Kivu Tea Project*

2012–2018

- Consultancy services for survey and demarcation of national road reserves – Client: RTDA
- Projects on water quality assessment in Lava Region, rainwater harvesting in Musanze District, hydrological surveys in Virunga-Bwindi Landscape, and integrated land/water management for food security – Client: INES-Ruhengeri
- Coordination of the Survey of Hydrological Systems in the greater Virunga Landscape, around the Volcanoes National Park – Client: GVTC-ES
- Hydrological regimes and water quality monitoring of Lake Kivu influent rivers – Client: LKMP
- Review of hydrological systems of Lake Edward – Client: GVTC-ES
- Team Leader: Design, rehabilitation, upgrading, and extension of water supply networks in Musanze and Rubavu cities (304 km)
- Supervised more than 100 theses in Civil Engineering and Water/Environmental Engineering

2018–2019 (Consultancy with ECASM Ltd)

- Feasibility and technical studies for construction/rehabilitation of 8 bridges in Musanze District
- Rehabilitation study of Rafiki–Murambi road
- Supervision of drainage system construction and upgrading of murrum roads (5 km) in Kayonza town

- Supervision of Rugerero gully construction and Bukeri drainage works in Kanama Sector
- Feasibility studies for rehabilitation of 4 murrum roads in Musanze District
- Hydrological and hydraulic review of feeder roads rehabilitation (207 km) in Gatsibo, Nyagatare, and Nyaruguru districts

Head of Mission – Water Supply Projects (2011–2021)

- Extension and rehabilitation of rural water supply systems in Rutsiro, Rulindo, Nyamasheke, Ngoma, Burera districts (over 170 km total) – Clients: UNIVERS-MBC Ltd, MUAGEC Ltd, Dr S Rural Engineering Ltd
- Extension and rehabilitation of water supply networks financed by Programme Hydraulique of Ruhengeri Diocese (Kanyansyo–Kivuruga–Cyintare–Buhuga, Mataba–Gakenke, Kirambo–Busengo; total 40 km)
- Design, rehabilitation, upgrading, and extension of water supply networks in Musanze and Rubavu cities and peri-urban areas (304 km) – Client: JV SGI Ingenierie & IBC Group (January 2020– 2021)

7. Publications

- Nahayo, D., Wali, U. and Anyemedu, F. (2010) Irrigation Practices and Water Conservation Opportunities in Migina Marshlands. International Journal of Ecology and Development, 16, 100-112. ISSN 0973–7308 (Online), ISSN 0972–9984 (Print). *http://www.ceser.in/ceserp/index.php/ijed/article/view/412*
- Karume, K., Bagalwa, M., Yalire, M., Kazi, K., Bagula, E. M., Bitariho, R., Nahayo, D., Kasangaki, A., Byamukama, J. (2016). Hydrological Systems in the Greater Virunga Landscape: Water quality around Mikeno Sector. Journal of Water Resource and Protection. **DOI:** *10.4236/jwarp.2016.83032*
- Muvundja Fabrice Amisi , Masilya Pascal Mulungula, Kisekelwa Tchalondawa Kisse a, Balagizi Charles Muhigirwa, Pasche Natacha d, Hyangya Béni Lwikitcha a, Mudakikwa Ruhanamirindi Eric, Akonkwa Balagizi Désiré, Nahayo Déo, Ajode Z. Migeni, Stephanie Smith, Alfred Wüest, Ted Lawrence (2022). Current status and strategic way forward for long-term management of Lake Kivu (East Africa). DOI: *10.1016/j.jglr.2022.04.004*
- Deogratias Nahayo, Bernard Tychon, Emmanuel Rukundo, Olivier Dewitte, Umaru Garba Wali, Matthias Vanmaercke (2022). Implication of land use/land cover variabilities on rainfall-runoff response in Mukungwa and Sebeya watersheds, NW Rwanda was presented in the International Colloquium—Changes and Transition

Management: in Singular or Plural? Management of extreme events of rainfalls (2022). *https://www.spheres.uliege.be/cms/c_9613002/fr/colloque-international-changements-globaux-et-gestion-de-la-transition-au-singulier-ou-au-pluriel*

- Nahayo, D., Tychon, B., Rukundo, E., Dewitte, O., Wali, U. G., & Vanmaercke, M. (2026). Spatiotemporal Variability of Rainfall-Streamflow Dynamics in Mountainous Tropical Environments: Insights From Agricultural Catchments of Northwest Rwanda. Hydrological Processes, 40(1), e70360. *https://doi.org/10.1002/hyp.70360*

8. Technical skills

- **Civil Engineering Software:** AutoCAD, ArchiCAD
- **Programming & Data Analysis:** C^{++}, Python
- **GIS Tools:** ArcGIS, QGIS
- **Hydrological & Hydraulic Modelling:** HEC-HMS, HEC-RAS, Sephydro, EPANET, Python, SWMM

9. Languages

- **Kinyarwanda:** Mother tongue (Reading, Speaking, Writing)
- **French:** Very good (Reading, Speaking, Writing)
- **English:** Very good (Reading, Speaking, Writing)

10. Professional membership

Registered Professional Civil Engineer, Institution of Engineers Rwanda Registration Number: A974/EC/IER/2018